99162-01

The Engineering Analysis and Design of the Aircraft Dynamics Model For the FAA Target Generation Facility

Mark Peters
Michael A. Konyak

Prepared for:

Scott Doucett
ANG-E161
Simulation Branch, Laboratory Services Division

Federal Aviation Administration
William J. Hughes Technical Center
Atlantic City, NJ 08405

Under:

Air Traffic Engineering Co., LLC
1027 Route 9 South
Palermo, NJ 08223
FAA Prime Contract No. DTFAWA-10A-00020

October 2012

Acknowledgments

<div align="right">
Mark Peters

September, 1999
</div>

THIS PAGE INTENTIONALLY LEFT BLANK

Table of Contents

List of Figures

ix

List of Tables

THIS PAGE INTENTIONALLY LEFT BLANK

List of Symbols

a	Semi-minor axis of the Earth
a	Temperature lapse rate
a	Angle between intersecting segments
a^*	Speed of sound in the atmosphere
a_{IAS}	The nominal deceleration factor for an aircraft in terms of IAS
a_M	The nominal deceleration factor for an aircraft in terms of Mach
A	State matrix of a state space representation
A_{cl}	Closed loop state matrix
b	Semi-major axis of the Earth
B	Input matrix of a state space representation
B	The bearing from a station
δB_{T_A}	The airborne receiver bearing bias
δB_{T_G}	The ground based bearing bias
$\delta B_{ILS,FTE}$	The bearing deviation angle for ILS flight technical error
ΔB	The total bearing error
ΔB_I	The total bearing deviation error for localizer modeling
$\Delta B_{I,A}$	The airborne bearing deviation error for localizer modeling
$\Delta B_{I,G}$	The ground based bearing deviation error for localizer modeling
B_{cl}	Closed loop input matrix
c	Scale factor for Gauss Markov process
c_j	Thrust specific fuel consumption
C	Output matrix of a state space representation
C_L	Lift coefficient
$C_{L_{max}}$	Maximum lift coefficient
$C_{L_{nom}}$	Nominal lift coefficient of the aircraft
C_{L_i}	Integrated portion of lift coefficient signal

C_{L_p}	Proportional portion of lift coefficient signal
C_{L_o}	Zero lift lift coefficient
C_{L_α}	Lift curve slope
$C_{L_{\delta e}}$	Variation of lift coefficient with elevator deflection
C_{D_o}	Zero lift drag coefficient
C_D	Drag coefficient
C_{f_1}	BADA coefficient for determining fuel burn
C_{f_2}	BADA coefficient for determining fuel burn
C_{f_3}	BADA coefficient for determining fuel burn
C_{f_4}	BADA coefficient for determining fuel burn
$C_{M_{16}}$	Compressibility coefficient
$C_{T_{c,1}}$	BADA coefficient for determining maximum thrust
$C_{T_{c,2}}$	BADA coefficient for determining maximum thrust
$C_{T_{c,3}}$	BADA coefficient for determining maximum thrust
C_θ	Cosine of θ
d	The distance to go along a segment
d_c	Distance to a constraint
d_r	Rhumb line distance of a segment
d_{offset}	The distance the dynamic fix is placed from the leading fix
D	Drag
D	Carry through term matrix of a state space representation
D_{brake}	Braking force
D_{fix_0}	Distance the aircraft is from a fix
e_1	Error between desired indicated airspeed & actual indicated airspeed
e_{1d}	Error between absolute desired IAS & ramped desired IAS
e_{1r}	Error between ramped desired indicated airspeed & indicated airspeed
e_2	Error between desired Mach & actual Mach
e_{2d}	Error between absolute desired Mach & ramped desired Mach

e_{2r}	Error between ramped desired Mach & actual Mach
e_3	Error between desired altitude and actual altitude
e_{3d}	Error between absolute desired altitude & ramped desired altitude
e_{3r}	Error between ramped desired altitude and actual altitude
$e_{3_{ref}}$	Reference value which determines speed altitude plane location
e_s	Generic speed error used in speed altitude plane
e_4	Error between desired altitude rate and actual altitude rate
e_{4d}	Error absolute desired $\dot{h}$ & ramped desired $\dot{h}$
e_{4r}	Error between ramped desired altitude rate and actual altitude rate
e_5	Error between desired heading and actual heading
e_{3r}	Distance between the constant energy line and zero altitude error
e_{left_turn}	Left turn error between desired heading and actual heading
e_{right_turn}	Right turn error between desired heading and actual heading
e	Error vector
e^{At}	State transition matrix
E_t	Total energy
E_{td}	Desired total energy
f	Fuel burn rate
f_{min}	Minimum fuel burn rate
f	Flattening parameter for the Earth
f_{V_a}	Function for calculating $\dot{V}_a$
f_{γ_a}	Function for calculating $\dot{\gamma}_a$
f_h	Function for calculating $\dot{h}$
g	Gravitational acceleration
h	Altitude
$h_{airport}$	Airport elevation
h_{con}	Constraint altitude
h_d	Desired altitude

h_{di}	*The desired altitude of an aircraft entering Region 1 or 4 from a climb*
h_{dr}	*Ramped desired altitude*
$\dot{h}_{dr}$	*Ramped desired altitude rate*
$\dot{h}_{est}$	*Nominal average descent rate for an aircraft*
h_{error}	*The altitude error used to define the speed altitude plane*
h_{GS}	*Commanded altitude from the glideslope*
h_{target}	*Target altitude*
$\vec{H}$	*Angular momentum vector*
H_x	*Angular momentum about the x-body axis*
H_y	*Angular momentum about the y-body axis*
H_z	*Angular momentum about the z-body axis*
I_{C_L}	*State variable representing the integrated portion of the lift coefficient*
I_T	*State variable representing the integrated portion of the throttle*
I_x	*Moment of inertia about the x-body axis*
I_y	*Moment of inertia about the y-body axis*
I_z	*Moment of inertia about the z-body axis*
I_{yz}	*Product of inertia*
I_{xz}	*Product of inertia*
I_{xy}	*Product of inertia*
IAS_{error}	*The indicated airspeed error used to define the speed altitude plane*
J	*Jacobian for solving systems of equations*
k_f	*A term which determines the rate of change of ramped speed values*
k_{lag}	*A term used to characterize engine spooling lags*
k_ψ	*Feedback gain for heading capture*
K	*Induced drag factor* $\frac{1}{\pi e AR}$
$K_{\dot{h}}$	*A term used to smooth transitions into Region 7 from climbs and descents*
K_b	*Proportional gain matrix in the feedback path*
K_i	*Integral gain matrix*

K_p	Proportional gain matrix in the feedforward path
k_p	Gain feeding roll rate back to ailerons
k_ϕ	Gain feeding roll angle back to ailerons
$K_{\dot{r}_e}$	Constant for calculating $\dot{r}_e$
$K_{\dot{\varepsilon}}$	Constant for calculating $\dot{\varepsilon}$
l	Longitude
l_{dyn}	Longitude of the dynamic fix
l_e	Longitude of the aircraft's estimated position
l_{offset}	Segment transition distance
l_{turn}	Distance from a segment at which an aircraft should turn
L	Lift
$\overline{L}$	Rolling moment
L_p	Rolling moment variation with roll rate
L_{δ_a}	Rolling moment variation with elevator deflection
M	Mach number
M_{con}	Constraint Mach number
M_{nom_c}	The nominal Mach used for CAS/Mach climbs
M_{nom_d}	The nominal Mach used for Mach/CAS descents
M	Pitching moment
M_d	Desired Mach number
M_{dr}	Desired Mach number
M_{error}	The Mach error used to define the Mach speed altitude plane
M_o	Zero angle of attack pitching moment
M_α	Pitching moment variation with angle of attack
M_{δ_e}	Pitching moment variation with elevator deflection
m	Aircraft mass
m	Slope of the constant energy line
m_{IAS}	Slope of the constant energy line for IAS based flight

m_{Mach}	Slope of the constant energy line for Mach based flight
N	Yawing moment
n	Load factor
n_B	Scaled Gaussian white noise
$\hat{n}_s$	A unit vector normal to a segment
p	Roll rate
p	Pressure
p_{amb}	Ambient pressure
p_{sl}	Sea level pressure
q	Pitch rate
q	Dynamic pressure
r	Yaw rate
r_{CT}	Aircraft's lateral position from the localizer
r_{IT}	Aircraft's in track range to runway
r_e	Radius of the Earth
r_{e_l}	Radius of the Earth at a given latitude
r_l	The distance a point on the Earth's surface is from the polar axis
$\vec{r}_{lf}$	A vector from the aircraft's location to the leading fix of a segment
r_t	Aircraft radius of turn
δr_{FTE}	The lateral position error
R	Ideal gas constant
$\vec{R}_s$	A vector describing a segment along a route
$\vec{R}_e$	A vector from the center of the Earth to a point on the surface
$\vec{R}^{op}$	A vector from the center of the Earth to an aircraft
S_w	Aircraft reference or wing area
SP_{error}	Generic speed error boundary used to define speed altitude plane
S_θ	Sine of θ
t_c	Time to a constraint

t_m	Time required for a maneuver
T	Thrust
T_p	Proportional portion of thrust signal
T_i	Integrated portion of thrust signal
T	Temperature
T_{amb}	Ambient temperature
T_{max}	Maximum thrust
T_{min}	Minimum thrust
T_{sl}	Sea level temperature
u	Velocity of aircraft in the x-body direction
$u_{P_{C_L}}$	Proportional lift coefficient input signal
u_{P_T}	Proportional thrust input signal
$u_{i_{C_L}}$	Integrated lift coefficient input signal
u_{i_T}	Integrated thrust input signal
u_{FTE}	Zero mean unity variance Gaussian white noise
δv_{FTE}	The lateral position error rate
$\vec{V}$	Body frame velocity vector
V_r	Rotation speed
V_2	Climb out speed
V_a	True airspeed
V_{ap}	Approach speed
V_{stall}	Stall speed
V_{ac}	Aicraft speed with respect to the Earth's surface
V_{ad}	Desired true airspeed
V_{IAS}	Indicated airspeed
$V_{IAS_{nom_c}}$	The nominal CAS used for CAS/Mach climbs
$V_{IAS_{nom_d}}$	The nominal CAS used for Mach/CAS descents
V_{IAS_d}	Desired indicated airspeed

$V_{IAS_{dr}}$	*Desired ramped indicated airspeed*
$V_{IAS_{con}}$	*Constraint indicated airspeed*
V_{GS}	*Ground speed*
V_w	*Wind velocity*
V_x	*Aircraft speed with respect to the Earth's surface in a Northerly direction*
V_y	*Aircraft speed with respect to the Earth's surface in a Easterly direction*
V_{wx}	*Wind velocity with respect to the Earth's surface in a Northerly direction*
V_{wy}	*Wind velocity with respect to the Earth's surface in a Easterly direction*
v	*Body frame side velocity in the y-body direction*
w	*Body frame velocity in the z-body direction*
w	*Gaussian white noise*
W	*Aircraft weight*
W_{igf}	*Wind in-track gradient factor*
W_{cgf}	*Wind cross-track gradient factor*
X	*X-body force*
X_{DIS}	*X DIS position*
x	*Distance from a point on the Earth's surface to the Equatorial plane*
x'	*Mercator projection x-coordinate*
x_{ac}	*X location of the aircraft in flat Earth coordinates*
x_r	*Northerly distance of a VOR in miles from a reference point*
$\hat{x}_c$	*X-axis in the c-frame*
$\hat{x}_{DIS}$	*X-axis in the DIS frame*
$\hat{x}_e$	*X-axis in the ECEF (Earth Centered Earth Fixed) frame*
$\hat{x}_{in}$	*X-axis in an intermediate frame*
$\hat{x}_{st}$	*X-axis in the stability axis system*
$\hat{x}_s$	*X-axis in the surface or NED (North-East-Down) frame*
$\hat{x}_w$	*X-axis in the wind axis*
$\hat{x}_b$	*X-axis in the body frame*

$\hat{x}_i$	X-axis in the flat Earth inertial frame
y	Output vector
y'	Mercator projection y-coordinate
y_d	Desired output vector
Y	Y force in the y-body direction
Y_{DIS}	Aircraft position along the y-DIS axis
y_r	Easterly distance of a VOR in miles from a reference point
y_{ac}	Y location of the aircraft in flat Earth coordinates
$\hat{y}_c$	Y-axis in the geocentric reference frame
$\hat{y}_e$	Y-axis in the ECEF (Earth Centered Earth Fixed) frame
$\hat{y}_{DIS}$	Y-axis in the DIS frame
$\hat{y}_{in}$	Y-axis in an intermediate reference frame
$\hat{y}_{st}$	Y-axis in the stability reference frame
$\hat{y}_s$	Y-axis in the NED (North-East-Down) frame
$\hat{y}_w$	Y-axis in the wind reference frame
$\hat{y}_b$	Y-axis in the body reference frame
$\hat{y}_i$	Y-axis in the flat Earth inertial reference frame
Z	Z force in the z-body direction
Z_{DIS}	The position of the aircraft along the z-DIS axis
z_1	The zero of the $\dot{h}/C_L$ transfer function
$\hat{z}_c$	Z-axis of the geocentric reference frame
$\hat{z}_e$	Z-axis of the ECEF(Earth Centered Earth Fixed) reference frame
$\hat{z}_{DIS}$	Z-axis of the DIS reference frame
$\hat{z}_{in}$	Z-axis of the intermediate reference frame
$\hat{z}_{st}$	Z-axis of the stability reference frame
$\hat{z}_s$	Z-axis of the surface or NED(North East Down) reference frame
$\hat{z}_w$	Z-axis of the wind axis reference frame
$\hat{z}_b$	Z-axis of the body reference frame

$\hat{z}_i$	Z-axis of the flat Earth inertial reference frame
α	Angle of attack
β	Side-slip angle
β	Damping factor for Gauss Markov process
$\beta_B(s)$	Spatial damping factor for localizer error modeling
δ	Distance from a radial
δ_a	Aileron deflection
δ_e	Elevator deflection
δ_r	Lateral offset from flight technical error
δ_ψ	Difference between ground track and heading
Δt	Time step
ε	Difference between geodetic and geocentric latitude
γ	Ratio of specific heats
γ_a	Flight path angle relative to the air mass
γ_{ap}	Approach angle
λ	Geocentric latitude
μ	Geodetic latitude
μ_e	Latitude of the aircraft's estimated position
μ_{dyn}	Geodetic latitude of the dynamic fix
ρ	Range to a nav-aid (used in navigation error modeling)
$\Delta\rho$	The total range error (used in navigation error modeling)
$\delta\rho_{VD_A}$	Airborne receiver range bias
$\delta\rho_{VD_G}$	Ground based range bias
ρ	Air density
ρ_{sl}	Sea level air density
σ_p	Standard deviation of the position in a 2nd order Gauss Markov process
σ_v	Standard deviation of the rate term in a 2nd order Gauss Markov process
σ_{pN}	North position standard deviation for GPS modeling

σ_{pE}	East position standard deviation for GPS modeling
σ_{vN}	North velocity standard deviation for GPS modeling
σ_{vE}	East velocity standard deviation for GPS modeling
ψ	Heading angle
ψ_{GT}	Ground track angle
ψ_{GT_d}	Desired ground track angle
ψ_d	Desired heading angle
ψ_r	Radial bearing or bearing of a segment
ψ_t	Intercept angle that the aircraft makes with the segment
$\Delta\psi$	The difference between the aircraft's ground track and heading
$\delta\psi_{fte}$	The heading bias from flight technical error
θ	Pitch angle
ϕ	Roll angle
ϕ_{des}	Desired roll angle
ω_n	Natural frequency
ω_p	Natural frequency of the Phugoid mode
$^i\overline{\omega}^b$	Angular velocity between the 'i' frame and the 'b' frame
$\delta\Omega_{ILS,FTE}$	The bearing deviation rate for ILS flight technical error
ζ	Damping ratio
ζ_p	Damping ratio of the Phugoid mode
$\vec{v}_{n_{tf}}$	A unit vector from the trailing fix to the next VOR/DME
$\vec{v}_{n_{lf}}$	A unit vector from the leading fix to the next VOR/DME
$\vec{v}_{p_{tf}}$	A unit vector from the trailing fix to the previous VOR/DME
$\vec{v}_{p_{lf}}$	A unit vector from the leading fix to the previous VOR/DME
τ	Time constant associated with landing altitude tracking

THIS PAGE INTENTIONALLY LEFT BLANK

1. Introduction

This document presents the analytical development of the aircraft dynamics model for the enhancement of the functional capabilities of the FAA Target Generation Facility (TGF). The work was originally conducted under Seagull Technology's contract No. DTFA03-94-C-00042 (CADSS) with the FAA. Specifically, this document discusses the detailed engineering design and software implementation of an Aircraft Dynamics Model (ADM) suitable for incorporation into the FAA TGF simulations at the FAA William J. Hughes Technical Center, Atlantic City, NJ. The model is designed to be implemented on computers located within the facility, and to work in conjunction with software models of radar, data links, and other Air Traffic Management (ATM) equipment to provide real-time simulation of aircraft operating within the National Airspace System (NAS). This introductory section provides a brief background into the project as well as discusses the scope and organization of the document.

1.1 Background

The FAA William J. Hughes Technical Center conducts research and development to investigate emerging Air Traffic Control (ATC) & ATM technologies, associated applications, and ATC processes and procedures. Inherent in these efforts is the requirement to emulate real-world operational conditions in laboratory environments. This requirement extends across the operational domains (e.g., Terminal, En Route, and Oceanic). Much of this work requires the establishment of operational test beds encompassing current operational as well as emerging prototype ATC systems. These test beds are frequently used to conduct studies that simulate the operational conditions found or desired in the associated domain. In the majority of cases, it is necessary to provide realistic representation of air traffic scenarios to evaluate the system, process, or procedure being evaluated. The Technical Center's TGF provides this capability by producing simulated primary and secondary radar targets to the system under test. To the greatest extent possible, TGF-produced targets must accurately reflect the flight dynamics of the aircraft that they represent.

Currently, the aircraft dynamics incorporated in the TGF are based on the first principles of physics and aeronautics. The models provide the performance characteristics needed to support high fidelity simulations. The TGF incorporates fuel burn models environmental (weather) effects. Additionally, the modeled aircraft are representative of commercial air traffic in the US National Air Space (NAS).

As future simulations are developed or brought to the Technical Center, higher fidelity will be required to identify NAS operational safety and performance issues. The TGF is prepared to increase its fidelity and operational connectivity required to meet the

demands by the other FAA programs and simulators. The goal of this project has been to develop and maintain a high-fidelity simulation capability to meet the needs of the FAA in operating, testing, and evaluating its NAS.

1.2 Scope

This document provides a defendable, theoretical foundation for the engineering theory, principles and algorithmic design of the Aircraft Dynamics Model. The engineering analysis starts with the first principles of aircraft flight mechanics and derives a 6-degree-of-freedom model. Simplifying assumptions are presented and the model is reduced to 4 degrees of freedom. The propagation of the aircraft on the surface of the Earth is discussed along with all the necessary reference frames to support all current conventions and interfaces. The modeling the effects of wind are included. The flight control system necessary to fly the aircraft through the fundamental maneuvers of climb, descent, turning to a heading, and speed changes is discussed. The control theory necessary to implement the flight control system is discussed in detail. The guidance system used to plan the aircraft's path and to capture and follow routes is presented. Different types of route capture methods are discussed such as the automatic and vectored route capture methods. Navigation systems and their error models are presented, including the modeling of VOR/DME, ILS, and GPS navigation. The guidance and navigation models are used by the algorithms that meet speed and altitude constraints, and so these are presented along with them. Pilot modeling and pilot flight technical error are also included. The document concludes with a section on verification and validation, the process by which the various features of the simulation are tested and verified.

1.3 Organization

Since much of the analysis is of a highly technical nature, an effort has been made to organize the document so that specific topics are easy to access. This is done to avoid the need to read the entire document to find a specific point. The document is organized into 13 sections, each of which is summarized here.

- Section 2 provides a detailed analysis of the aircraft equations of motion. The 4 degree-of-freedom aircraft model is derived from first principles. All trajectory propagation material is also covered. The numerical integration techniques are also discussed.
- Section 3 develops a linear model of the longitudinal dynamics and analyzes the longitudinal modal properties of the system. Transfer function analysis of the longitudinal dynamics is also performed
- Section 4 provides a detailed analysis of the feedback control aspects of the longitudinal control system. The section provides insight into control strategies for capturing a desired state. There are different feedback control strategies for different

flight phases; each of these control systems is discussed, and a strategy for calculating the required gains is developed.

- Section 5 deals with the design of the feedback control algorithms that stabilize the aircraft and drive it to the desired state. It also provides the algorithms for managing the control strategies and transitioning between them.
- Section 6 documents the decision process that led to the final conclusion that gain scheduling would not be necessary. By carefully choosing the reference flight condition, it is possible to choose one set of gains that will work for the aircraft's entire flight envelope.
- Section 7 discusses the lateral directional control system
- Section 8 discusses the lateral guidance system. The purpose of the lateral guidance system is to steer the aircraft to follow routes or other simulation pilot commands.
- Section 9 discusses the navigation systems and navigation error modeling The purpose of navigation error modeling is to model the variances that occur in aircraft flight paths as a result of imperfect navigation information.
- Section 10 discusses the logic used to make aircraft meet speed and altitude constraints at fixes and to meet the restrictions of terminal flight phases (take-off and landing).
- Section 11 documents the flight technical error algorithms that model the inability of the pilot or autopilot to steer the aircraft perfectly along the desired course.
- Section 12 describes verification and validation of the aircraft simulation. The section starts with testing of climbs, descents, and speed changes and continues with testing of the guidance algorithms. The navigation error and flight technical error are also tested. Finally, the terminal flight phases are tested.

THIS PAGE INTENTIONALLY LEFT BLANK

2. The Aircraft Equations of Motion

The purpose of this section is to provide a theoretical foundation for the aircraft equations of motion that are used in the TGF aircraft simulation. The foundation will start with the definition of reference frames. Once the reference frames have been defined, we will derive the equations of motion for the full six-degree-of-freedom (DOF) model. Then, we will apply several assumptions to the equations of motion to reduce the 6-DOF model to a 4-DOF model.

2.1 The Definition of the Body Frame and the Inertial Frame

As discussed in Nelson (1989), the two major reference frames used in the derivation of the aircraft equations of motion are the aircraft body-fixed reference frame (denoted with a *b* subscript) and the inertial reference frame (denoted with an *i* subscript). The aircraft body frame's origin is fixed at the aircraft's center of gravity. The body frame has its $\hat{x}_b$-axis aligned with the nose of the aircraft so that the aircraft's nose points in the positive $\hat{x}_b$ direction. The positive $\hat{y}_b$ direction points out along the aircraft's starboard wing. The $\hat{z}_b$ axis points down to complete a right handed coordinate frame. Figure 2.1 shows the body fixed reference frame.
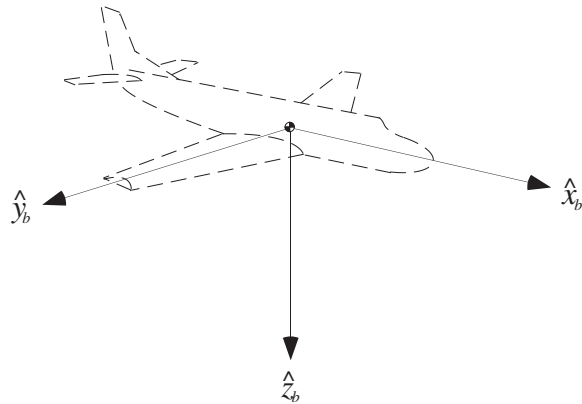
Figure 2.1. The body fixed reference frame aligned with an aircraft

The inertial reference frame is fixed on a point on the Earth's surface and is aligned so that the positive $\hat{x}_i$ axis points to true North and the positive $\hat{y}_i$ axis points to true East. The $\hat{z}_i$ axis points down and is normal to the surface of the Earth. This frame is commonly referred to as the North-East-Down, or NED frame.

The body reference frame can assume any orientation with respect to the inertial frame. Figure 2.2 illustrates the relationship between the body and inertial reference frames. The orientation of the body frame with respect to the inertial frame is usually described by an Euler sequence of rotations. The ordering of the rotations is critical to the orientation of

the body frame. It is difficult to visualize the actual sequence of rotations in a single drawing, so the sequence is illustrated with three separate drawings. Figure 2.3 shows the Euler sequence of rotations that is used to quantify the aircraft's orientation.
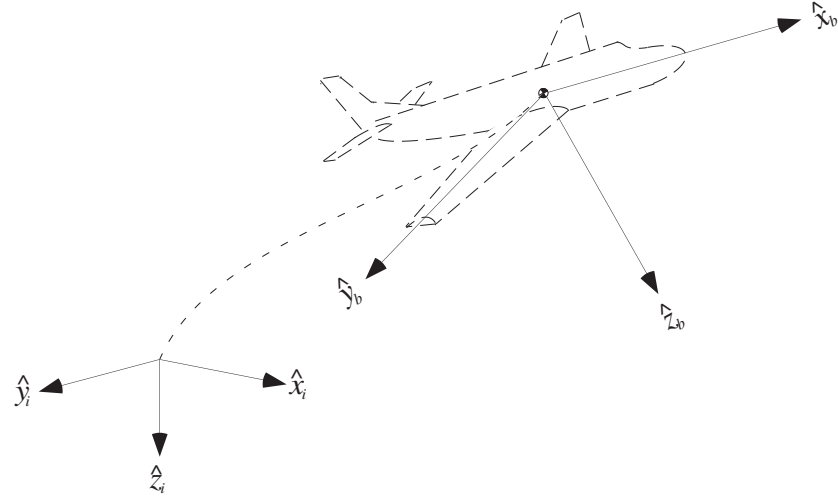
Figure 2.2. The relationship between body and inertial reference frames
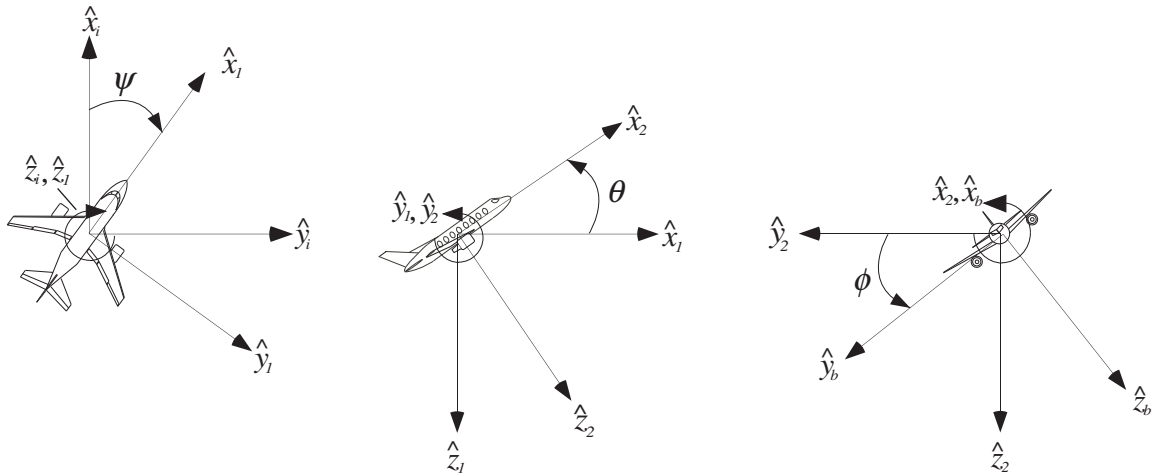
Figure 2.3. The 3-2-1 Euler sequence of rotations used to quantify the aircraft's orientation

The first rotation is through the angle ψ about the $\hat{z}_i$ axis to an intermediate reference frame, which is arbitrarily denoted with a '1' subscript. The second rotation is through the angle θ about the $\hat{y}_1$ axis to another intermediate reference frame, which is denoted with a '2' subscript. The final rotation is through the angle ϕ about the $\hat{x}_2$ axis to the body frame. The angles ψ, θ, and ϕ are referred to as the heading, pitch, and roll angles, respectively.

The conversion between the inertial frame and the body frame of the aircraft is accomplished using direction cosine matrices. The first cosine matrix establishes the relationship between the inertial frame and the first intermediate reference frame. Equations (2.1), (2.2), and (2.3) quantify the relationship between the individual rotations. The nomenclature C_θ and S_θ are simplified notation for $cos\theta$ and $sin\theta$. This is done for all trigonometric manipulations to simplify the ultimate expression. From the rotation sequence shown in Figure 2.3, one can write the following direction cosine matrices shown in Equations (2.1) through (2.3).

$$\begin{bmatrix} \hat{x}_1 \\ \hat{y}_1 \\ \hat{z}_1 \end{bmatrix} = \begin{bmatrix} C_\psi & S_\psi & 0 \\ -S_\psi & C_\psi & 0 \\ 0 & 0 & 1 \end{bmatrix} \begin{bmatrix} \hat{x}_i \\ \hat{y}_i \\ \hat{z}_i \end{bmatrix} \tag{2.1}$$

$$\begin{bmatrix} \hat{x}_2 \\ \hat{y}_2 \\ \hat{z}_2 \end{bmatrix} = \begin{bmatrix} C_\theta & 0 & -S_\theta \\ 0 & 1 & 0 \\ S_\theta & 0 & C_\theta \end{bmatrix} \begin{bmatrix} \hat{x}_1 \\ \hat{y}_1 \\ \hat{z}_1 \end{bmatrix} \tag{2.2}$$

$$\begin{bmatrix} \hat{x}_b \\ \hat{y}_b \\ \hat{z}_b \end{bmatrix} = \begin{bmatrix} 1 & 0 & 0 \\ 0 & C_\phi & S_\phi \\ 0 & -S_\phi & C_\phi \end{bmatrix} \begin{bmatrix} \hat{x}_2 \\ \hat{y}_2 \\ \hat{z}_2 \end{bmatrix} \tag{2.3}$$

The product of these three direction cosine matrices results in the complete conversion between the inertial frame and the body frame as shown in Equation (2.5).

$$\begin{bmatrix} \hat{x}_b \\ \hat{y}_b \\ \hat{z}_b \end{bmatrix} = \begin{bmatrix} 1 & 0 & 0 \\ 0 & C_\phi & S_\phi \\ 0 & -S_\phi & C_\phi \end{bmatrix} \begin{bmatrix} C_\theta & 0 & -S_\theta \\ 0 & 1 & 0 \\ S_\theta & 0 & C_\theta \end{bmatrix} \begin{bmatrix} C_\psi & S_\psi & 0 \\ -S_\psi & C_\psi & 0 \\ 0 & 0 & 1 \end{bmatrix} \begin{bmatrix} \hat{x}_i \\ \hat{y}_i \\ \hat{z}_i \end{bmatrix} \tag{2.4}$$

$$\begin{bmatrix} \hat{x}_b \\ \hat{y}_b \\ \hat{z}_b \end{bmatrix} = \begin{bmatrix} C_\theta C_\psi & C_\theta S_\psi & -S_\theta \\ -C_\phi S_\psi + S_\phi S_\theta C_\psi & C_\phi C_\psi + S_\phi S_\theta S_\psi & S_\phi C_\theta \\ S_\phi S_\psi + C_\phi S_\theta C_\psi & -S_\phi C_\psi + C_\phi S_\theta S_\psi & C_\phi C_\theta \end{bmatrix} \begin{bmatrix} \hat{x}_i \\ \hat{y}_i \\ \hat{z}_i \end{bmatrix} \tag{2.5}$$

The inverse of Equation (2.5) is shown in Equation (2.6).

$$\begin{bmatrix} \hat{x}_i \\ \hat{y}_i \\ \hat{z}_i \end{bmatrix} = \begin{bmatrix} C_\theta C_\psi & -C_\phi S_\psi + S_\phi S_\theta C_\psi & S_\phi S_\psi + C_\phi S_\theta C_\psi \\ C_\theta S_\psi & C_\phi C_\psi + S_\phi S_\theta S_\psi & -S_\phi C_\psi + C_\phi S_\theta S_\psi \\ -S_\theta & S_\phi C_\theta & C_\phi C_\theta \end{bmatrix} \begin{bmatrix} \hat{x}_b \\ \hat{y}_b \\ \hat{z}_b \end{bmatrix} \qquad (2.6)$$

2.2 Definition of Flight Mechanics Nomenclature

Next, certain flight mechanics nomenclature must be defined. This nomenclature consists of the various linear and angular velocities associated with the motion of the aircraft as well as the forces and moments that are applied. Figure 2.4 provides an illustration of the nomenclature as it applies to the aircraft.
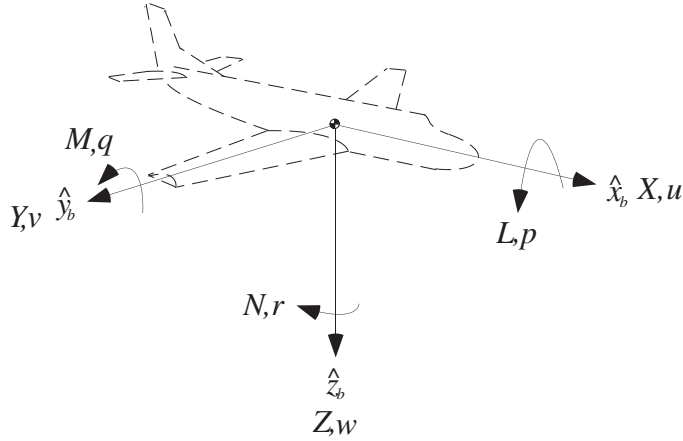
Figure 2.4. The forces, moments, velocity components and angular rates of an aircraft

Table 2.1 summarizes the nomenclature definition so that the mathematical symbols can be associated with the proper terminology. The reader will note that the term L is used to notate the rolling moment. Further along in the text, L will also be used for lift. This is an unfortunate consequence of the merging of two engineering disciplines, dynamics and control and aerodynamics. To avoid confusion, this document will notate the rolling moment using $\bar{L}$ instead of L, which is reserved for lift.

Table 2.1. Definition of flight mechanics nomenclature

	Roll Axis $\hat{x}_b$	Pitch Axis $\hat{y}_b$	Yaw Axis $\hat{z}_b$
Angular rates	p	q	r
Velocity components	u	v	w
Aerodynamic Force Components	X	Y	Z
Aerodynamic Moment Components	$\bar{L}$	M	N
Moments of Inertia	I_x	I_y	I_z
Products of Inertia	I_{yz}	I_{xz}	I_{xy}

It is important to note that the forces defined in Table 2.1 are aligned with the body frame. These forces do not directly coincide with the more commonly known aerodynamic forces of lift and drag. The forces of lift and drag are defined with respect to another reference frame, the wind frame, discussed in the following section.

2.3 The Wind and Stability Reference Frames

We need to derive two additional reference frames to resolve the relationship between the commonly known aerodynamic forces of lift and drag and the body forces of the 6-DOF model. These reference frames are the *stability frame* and the *wind frame* as defined by Stevens & Lewis (1992). The wind frame is used to describe the motion of the air mass relative to the aircraft body frame and allows us to describe the aerodynamic forces on the aircraft.

These stability and wind frames characterize the angle of attack, α, and the side-slip angle, β. These aerodynamic angles are defined by means of coordinate rotations from the body frame. The first rotation, about the $\hat{y}_b$ axis, defines the stability frame and the angle is the angle of attack, α. With no sideslip, α is the angle between the aircraft $\hat{x}_b$ axis and the aircraft velocity vector relative to the surrounding air mass. The angle of attack is positive if the rotation about the $\hat{y}_b$ axis was negative. This 'backwards' definition is the unfortunate result of merging the disciplines of aerodynamics and classical kinematics.

The second rotation leads to the wind frame, and the side-slip angle is the angle between the stability frame and the wind frame. An aircraft has sideslip if its velocity vector relative to the air mass is not in the plane defined by $\hat{x}_b$ - $\hat{z}_b$. The rotation is about the z-axis of the stability frame, $\hat{z}_{st}$, and β is defined as positive if the rotation about the $\hat{z}_{st}$ axis is positive. The wind frame's x-axis, $\hat{x}_w$, is aligned with the aircraft's velocity vector, which is the vector sum of the body frame velocities, $\mathbf{V} = u\hat{x}_b + v\hat{y}_b + w\hat{z}_b$. The other axes, $\hat{y}_w$ and $\hat{z}_w$, are orthogonal to $\hat{x}_w$ and to each other. Figure 2.5 illustrates the orientation of the x-axes of the stability and wind frames with respect to the body frame.

Equations (2.7) - (2.9) show the direction cosine matrices that define the transformations between the coordinate frames.

$$
\begin{bmatrix} \hat{x}_{st} \\ \hat{y}_{st} \\ \hat{z}_{st} \end{bmatrix} = \begin{bmatrix} C_\alpha & 0 & S_\alpha \\ 0 & 1 & 0 \\ -S_\alpha & 0 & C_\alpha \end{bmatrix} \begin{bmatrix} \hat{x}_b \\ \hat{y}_b \\ \hat{z}_b \end{bmatrix} \tag{2.7}
$$
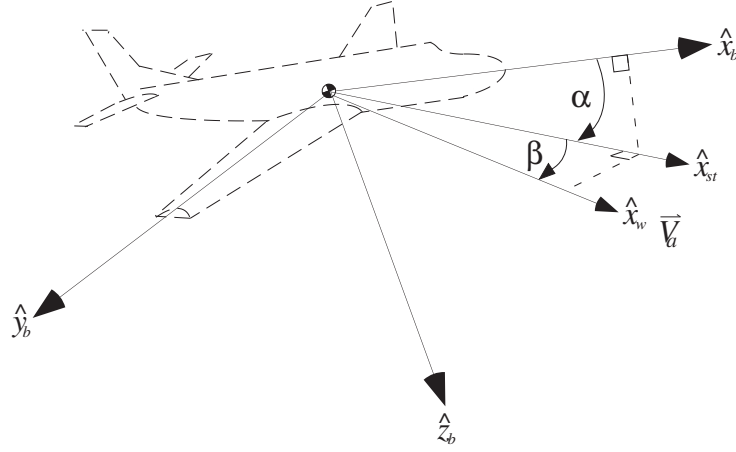
Figure 2.5. Illustration of the stability and wind coordinate systems

$$
\begin{bmatrix} \hat{x}_w \\ \hat{y}_w \\ \hat{z}_w \end{bmatrix} = \begin{bmatrix} C_\beta & S_\beta & 0 \\ -S_\beta & C_\beta & 0 \\ 0 & 0 & 1 \end{bmatrix} \begin{bmatrix} \hat{x}_{st} \\ \hat{y}_{st} \\ \hat{z}_{st} \end{bmatrix}
\tag{2.8}
$$

$$
\begin{bmatrix} \hat{x}_w \\ \hat{y}_w \\ \hat{z}_w \end{bmatrix} = \begin{bmatrix} C_\beta C_\alpha & S_\beta & C_\beta S_\alpha \\ -S_\beta C_\alpha & C_\beta & -S_\beta S_\alpha \\ -S_\alpha & 0 & C_\alpha \end{bmatrix} \begin{bmatrix} \hat{x}_b \\ \hat{y}_b \\ \hat{z}_b \end{bmatrix}
\tag{2.9}
$$

Using the direction cosine matrices, we can derive expressions for the angles, α and β. We start with the definition of true airspeed. The true airspeed of an aircraft, V_a, is defined as the magnitude of the aircraft's velocity relative to the air mass surrounding the aircraft. By definition, the only component of this velocity is along the $\hat{x}_w$ axis of the wind frame. That is to say the total aircraft velocity is aligned with the $\hat{x}_w$ axis. Written in equation form, $\mathbf{V} = V_a \hat{x}_w$. Using the inverse of the direction cosine matrix in equation (2.9), we can define the body frame velocities in terms of the true airspeed and the angles α and β.

$$
\begin{bmatrix} u\hat{x}_b \\ v\hat{y}_b \\ w\hat{z}_b \end{bmatrix} = \begin{bmatrix} C_\beta C_\alpha & -S_\beta C_\alpha & -S_\alpha \\ S_\beta & C_\beta & 0 \\ C_\beta S_\alpha & -S_\beta S_\alpha & C_\alpha \end{bmatrix} \begin{bmatrix} V_a \hat{x}_w \\ 0 \\ 0 \end{bmatrix}
\tag{2.10}
$$

The three resulting scalar equations are shown below in Equations (2.11)-(2.13).

$$u = V_a C_\beta C_\alpha \qquad (2.11)$$

$$v = V_a S_\beta \qquad (2.12)$$

$$w = V_a C_\beta S_\alpha \qquad (2.13)$$

Rearranging Equation (2.12) gives us an expression for side-slip.

$$\beta = sin^{-1} \frac{v}{V_a} \qquad (2.14)$$

Taking the quotient of *w/u,* we can derive an expression for angle of attack as shown in Equations (2.15)-(2.16).

$$\frac{w}{u} = \frac{V_a C_\beta S_\alpha}{V_a C_\beta C_\alpha} = \frac{S_\alpha}{C_\alpha} = tan\,\alpha \qquad (2.15)$$

$$\alpha = tan^{-1} \frac{w}{u} \approx \frac{w}{u} \qquad (2.16)$$

Assuming that the angle of attack is small, it can be approximated as just the ratio *w/u.* Often, this expression is used to substitute α for *w*.

Using the wind reference frame, we can resolve the relationship between the commonly known aerodynamic forces of lift, drag and thrust (*L, D,* and *T*, respectively), and the body forces of the 6 DOF model. We can see from the direction cosine matrix (2.9) that if we model the aerodynamic forces on an aircraft in terms of lift, drag, and thrust, equations (2.17) through (2.21) are expressions for *X, Y,* and *Z* forces in the body frame. The aircraft weight is not included because it is not an aerodynamic force.

$$\sum \mathbf{F}_a = T\hat{x}_b - L\hat{z}_w - D\hat{x}_w \qquad (2.17)$$

$$\begin{bmatrix} X\hat{x}_b \\ Y\hat{y}_b \\ Z\hat{z}_b \end{bmatrix} = \begin{bmatrix} C_\beta C_\alpha & -S_\beta C_\alpha & -S_\alpha \\ S_\beta & C_\beta & 0 \\ C_\beta S_\alpha & -S_\beta S_\alpha & C_\alpha \end{bmatrix} \begin{bmatrix} -D\hat{x}_w \\ 0\hat{y}_w \\ -L\hat{z}_w \end{bmatrix} + \begin{bmatrix} T\hat{x}_b \\ 0\hat{y}_b \\ 0\hat{z}_b \end{bmatrix} \qquad (2.18)$$

$$X = T - DC_\beta C_\alpha + LS_\alpha \qquad (2.19)$$

$$Y = -DS_\beta \tag{2.20}$$

$$Z = -DC_\beta S_\alpha - LC_\alpha \tag{2.21}$$

Note that the actual forces and moments of the full 6 DOF model include much more than simply lift, drag, and thrust. Unsteady aerodynamics play a large role in the determination of the complete force and moment model.

There is one more term that must be formally defined: the flight path angle, γ. The flight path angle is the angle that a velocity vector makes with the horizontal. If the velocity vector is expressed in surface coordinates, the vertical component is simply the vector magnitude multiplied by the sine of the flight path angle. We can develop an expression for the flight path angle relative to the air, γ_a, by transforming the air speed vector to the surface frame. This is accomplished via a sequence of rotations between the wind frame and the surface frame.

$$\begin{bmatrix} \mathbf{V_{a_x}} \\ \mathbf{V_{a_y}} \\ V_a \sin \gamma_a \end{bmatrix} = \begin{bmatrix} 1 & 0 & 0 \\ 0 & C_\phi & S_\phi \\ 0 & -S_\phi & C_\phi \end{bmatrix} \begin{bmatrix} C_\theta & 0 & -S_\theta \\ 0 & 1 & 0 \\ S_\theta & 0 & C_\theta \end{bmatrix} \begin{bmatrix} C_\psi & S_\psi & 0 \\ -S_\psi & C_\psi & 0 \\ 0 & 0 & 1 \end{bmatrix} \begin{bmatrix} C_\beta C_\alpha & -S_\beta C_\alpha & -S_\alpha \\ S_\beta & C_\beta & 0 \\ C_\beta S_\alpha & -S_\beta S_\alpha & C_\alpha \end{bmatrix} \begin{bmatrix} V_a \hat{x}_w \\ 0 \\ 0 \end{bmatrix}$$

Working with the third row equation, the air speed falls out and we can solve for γ_a.

$$\gamma_a = sin^{-1} \left(C_\alpha C_\beta S_\theta - \left(S_\phi S_\beta + C_\phi S_\alpha C_\beta \right) C_\theta \right) \tag{2.22}$$

The 'a' subscript on the flight path angle denotes that it is an aerodynamic flight path angle. This is to say that it is the aircraft's flight path angle relative to the air mass. The aircraft's flight path angle relative to the ground is generally different because of the influence of winds.

We can see from Equation (2.22) that if both α and β are zero, the Euler angle θ reduces to γ_a.

2.4   The Derivation of the Six Degree of Freedom Equations of Motion

Once the reference frames and nomenclature are defined, the derivation of the equations of motion is straightforward. The linear equations of motion are derived by summing the forces to the time rate of change of linear momentum ($mass \times acceleration$). The acceleration of the aircraft's velocity is determined using the basic kinematic equation, which states that the total acceleration of the aircraft with respect to the inertial frame is

equal to the derivative of the velocity vector with respect to the body frame plus the cross product of the angular velocity between the inertial and body frames and the velocity vector. The basic kinematic equation is shown in Equation (2.23)

$$\mathbf{a}_i = \frac{d\mathbf{V}}{dt} = \left(\frac{\partial \mathbf{V}}{\partial t}\right)_b + \boldsymbol{\omega} \times \mathbf{V} \qquad (2.23)$$

where

- $\mathbf{a}_i$ is the acceleration of the aircraft with respect to the inertial frame
- $\dfrac{d\mathbf{V}}{dt}$ is the total time derivative of the velocity vector
- $\left(\dfrac{\partial \mathbf{V}}{\partial t}\right)_b$ is the derivative of the velocity vector as seen in the body frame
- $\boldsymbol{\omega}$ is the angular velocity of the body frame relative to the inertial frame: $\boldsymbol{\omega} = p\hat{x}_b + q\hat{y}_b + r\hat{z}_b$
- $\mathbf{V}$ is the velocity vector in the body frame: $\mathbf{V} = u\hat{x}_b + v\hat{y}_b + w\hat{z}_b$.

The expression for the aircraft's acceleration is shown in Equation (2.24) and simplified in Equation (2.25).

$$\frac{d\mathbf{V}}{dt} = \dot{u}\hat{x}_b + \dot{v}\hat{y}_b + \dot{w}\hat{z}_b + \left(p\hat{x}_b + q\hat{y}_b + r\hat{z}_b\right) \times \left(u\hat{x}_b + v\hat{y}_b + w\hat{z}_b\right) \qquad (2.24)$$

$$\frac{d\mathbf{V}}{dt} = \left(\dot{u} + qw - rv\right)\hat{x}_b + \left(\dot{v} + ru - pw\right)\hat{y}_b + \left(\dot{w} + pv - qu\right)\hat{z}_b \qquad (2.25)$$

To complete the equations of motion, we must equate the acceleration terms to the applied forces according to Newton's second law ($F=ma$). Table 2.1 summarizes the aerodynamic forces applied to the aircraft; however, the aircraft weight must also be considered. The aircraft's weight always acts downward in the $\hat{z}_i$ direction. Using the direction cosine matrix, the aircraft's weight (mg) can be represented in body frame coordinates.

$$mg\hat{z}_i = -mgS_\theta \hat{x}_b + mgC_\theta S_\phi \hat{y}_b + mgC_\theta C_\phi \hat{z}_b \qquad (2.26)$$

where
- m is the aircraft's mass
- g is the gravitational acceleration.

Summing the forces and equating the force terms yields the final expression.

$$\left(X - mgS_\theta \right) \hat{x}_b + \left(Y + mgC_\theta S_\phi \right) \hat{y}_b + \left(Z + mgC_\theta C_\phi \right) \hat{z}_b$$
$$= m\left(\dot{u} + qw - rv \right) \hat{x}_b + m\left(\dot{v} + ru - pw \right) \hat{y}_b + m\left(\dot{w} + pv - qu \right) \hat{z}_b \tag{2.27}$$

Equation (2.27) can be broken down into its individual components to yield the three force equations of motion.

$$X - mgS_\theta = m\left(\dot{u} + qw - rv \right) \tag{2.28}$$

$$Y + mgC_\theta S_\phi = m\left(\dot{v} + ru - pw \right) \tag{2.29}$$

$$Z + mgC_\theta C_\phi = m\left(\dot{w} + pv - qu \right) \tag{2.30}$$

The moment equations are equal to the time rate of change of angular momentum. The angular momentum of the aircraft is equal to the inertia matrix multiplied by the angular velocities. The expression for angular momentum is shown in Equation (2.31) where the symbol H is used to denote the angular momentum.

$$\begin{bmatrix} H_x \\ H_y \\ H_z \end{bmatrix} = \begin{bmatrix} I_x & 0 & -I_{xz} \\ 0 & I_y & 0 \\ -I_{zx} & 0 & I_z \end{bmatrix} \begin{bmatrix} p\hat{x}_b \\ q\hat{y}_b \\ r\hat{z}_b \end{bmatrix} \tag{2.31}$$

Because aircraft are symmetric, two products of inertia, I_{yz} and I_{xy}, are zero and therefore are eliminated from the angular momentum expression. Equation (2.31) can be expanded to three scalar equations.

$$H_x = I_x p\hat{x}_b - I_{xz} r\hat{z}_b \tag{2.32}$$

$$H_y = I_y q\hat{y}_b \tag{2.33}$$

$$H_z = -I_{zx} p\hat{x}_b + I_z r\hat{z}_b \tag{2.34}$$

The time rate of change of each of these expressions is calculated using the 'Basic Kinematic Equation' of the form shown in Equation (2.35).

$$\frac{d\mathbf{H}}{dt} = \left(\frac{\partial \mathbf{H}}{\partial t}\right)_b + \boldsymbol{\omega} \times \mathbf{H} \tag{2.35}$$

When the kinematic expressions are summed to their respective moments, the three moment equations are derived. The three moment equations are shown in Equations (2.36)-(2.38). For convenience

Table 2.2 summarizes the fundamental kinematic and dynamic equations of motion.

$$\bar{L} = I_x \dot{p} - I_{xz}(\dot{r} + pq) + qr(I_z - I_y) \tag{2.36}$$

$$M = I_y \dot{q} + rp(I_x - I_z) + I_{xz}(p^2 - r^2) \tag{2.37}$$

$$N = -I_{xz}\dot{p} + I_z\dot{r} + pq(I_y - I_x) + I_{xz}qr \tag{2.38}$$

So far we have developed the full 6-DOF equations of motion, which are quite involved. The next step in developing a 6-DOF model, well beyond the scope of this discussion, would be to derive expressions for the forces and moments that act on the aircraft. For a complete discussion, refer to Nelson (1989). The forces and moments that are used in the 6 DOF model are quite different from the simplified subset presented in Equations (2.19) through (2.21). The true forces and moments are complicated expressions that require estimates of unsteady aerodynamic data to handle properly. Our next task is to simplify the 6-DOF equations of motion to 4-DOF equations using some simplifying assumptions.

However, first we will briefly discuss the modal characteristics of the 6-DOF model so we better understand which characteristics are most likely going to influence trajectory propagation.

2.5   The modal Properties of the Six Degree of Freedom Model

Before simplifying the equations of motion to 4-DOF, it is useful to discuss the five modes of motion associated with the 6-DOF model. Three of the modes are second order and two of the modes are first order making up an 8th order system. These modes are:

Table 2.2. Summary of kinematic and dynamic equations of motion

Grouping	Equations	
Force Equations	$X - mgS_\theta = m(\dot{u} + qw - rv)$	(2.28)
	$Y + mgC_\theta S_\phi = m(\dot{v} + ru - pw)$	(2.29)
	$Z + mgC_\theta C_\phi = m(\dot{w} + pv - qu)$	(2.30)
Moment Equations	$\overline{L} = I_x \dot{p} - I_{xz}(\dot{r} + pq) + qr(I_z - I_y)$	(2.36)
	$M = I_y \dot{q} + rp(I_x - I_z) + I_{xz}(p^2 - r^2)$	(2.37)
	$N = -I_{xz}\dot{p} + I_z\dot{r} + pq(I_y - I_x) + I_{xz}qr$	(2.38)
Body Angular Velocities in terms of Euler angles and Euler rates	$p = \dot{\phi} - \dot{\psi}\, S_\theta$	(2.39)
	$q = \dot{\theta}\, C_\phi + \dot{\psi}\, C_\theta\, S_\phi$	(2.40)
	$r = \dot{\psi}\, C_\theta\, C_\phi - \dot{\theta}\, S_\phi$	(2.41)
Euler rates in terms of Euler angles and body angular velocities	$\dot{\theta} = qC_\phi - rS_\phi$	(2.42)
	$\dot{\phi} = p + qS_\phi T_\theta + rC_\phi T_\theta$	(2.43)
	$\dot{\psi} = (qS_\phi + rC_\phi)\sec\theta$	(2.44)

- Short Period (Longitudinal plane)
- Phugoid   (Longitudinal plane)
- Dutch Roll (Lateral-Directional plane)
- Roll (Lateral-Directional plane)
- Spiral (Lateral-Directional plane).

The longitudinal dynamics control the forward speed and altitude of the aircraft. There are two second-order oscillatory modes comprising the longitudinal dynamics. These modes are referred to as the short period and the Phugoid mode.

The lateral-directional dynamics consist of one second-order mode and two first-order modes. These modes control the turning dynamics of the aircraft within the lateral plane.

2.5.1 The Short Period Mode

The short period mode is named because it is the faster of the two modes. It is the mode that defines the aircraft's pitching about its center of gravity. The short period mode controls the dynamics between elevator deflection and the aircraft's resulting lift coefficient. Generally, the short period mode is over ten times faster than the Phugoid mode.

2.5.2 The Phugoid Mode

The Phugoid mode is the slower of the two longitudinal modes. We can think of the Phugoid mode as a gradual interchange between potential and kinetic energy about some equilibrium altitude and airspeed. The Phugoid mode is characterized by changes in pitch attitude, altitude, and velocity at a nearly constant lift coefficient. Usually, the Phugoid is over ten times slower than the short period mode and therefore the Phugoid will have the dominant influence over the aircraft's trajectory. This is illustrated in Figure 2.7.
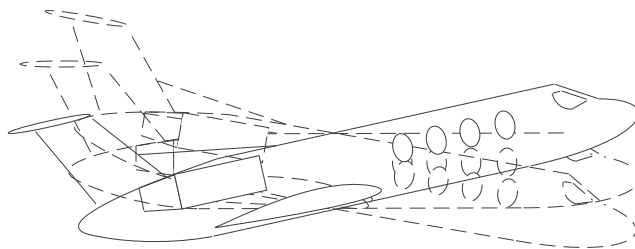
Figure 2.6. Illustration of the Short Period mode causing oscillations about the aircraft's center of gravity
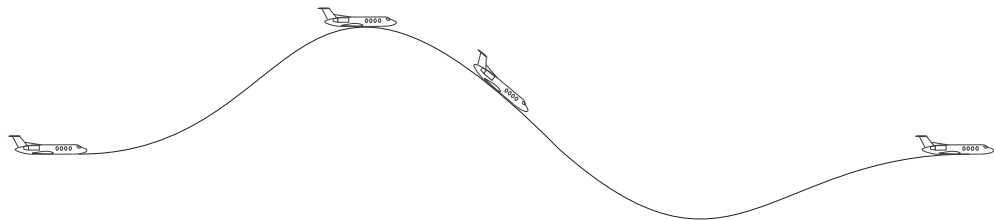
Figure 2.7. Illustration of the Phugoid mode

2.5.3 The Dutch Roll Mode

The Dutch Roll mode is the only oscillatory mode of the lateral directional dynamics and is a combination of yawing and rolling oscillations. The Dutch Roll gets its name from its resemblance to the weaving motion of an ice skater. The Dutch Roll mode is mostly an annoyance to the pilot and passengers. The pilot can easily damp out the motion of the Dutch roll. The Dutch roll is illustrated in Figure 2.8.
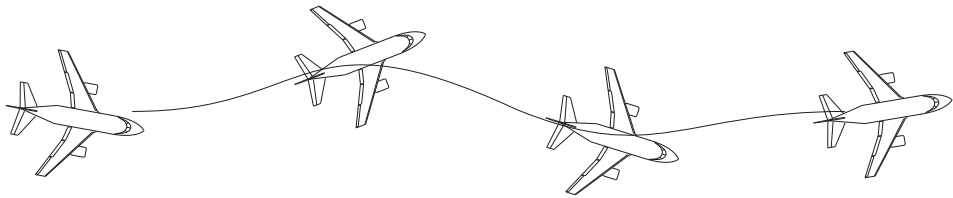
Figure 2.8. Illustration of the Dutch Roll mode

2.5.4   The Roll Mode

The roll mode characterizes how fast an aircraft can achieve a steady state roll rate after an aileron deflection. It is a first-order mode and therefore does not oscillate. The roll mode can influence the trajectory of an aircraft by causing a delay between the time a turn is commanded and when a steady state turn rate is achieved. The Roll mode is illustrated in Figure 2.9.
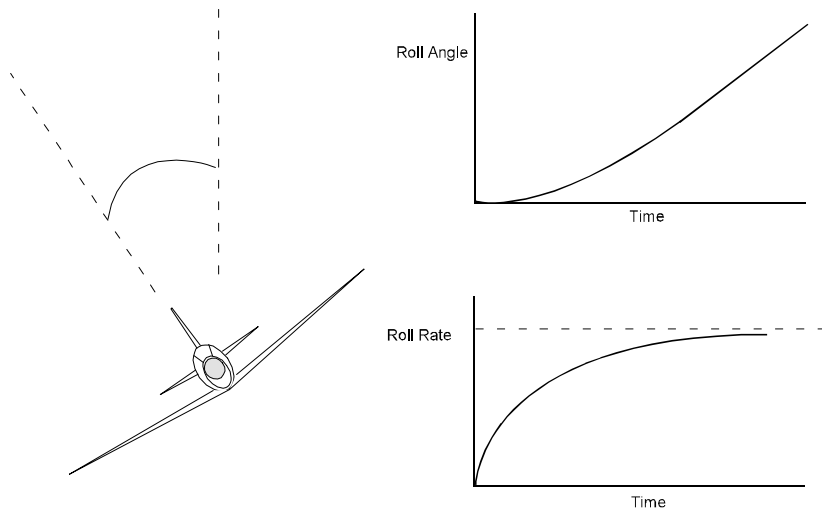
Figure 2.9. Illustration of the Roll mode

2.5.5   The Spiral Mode

The spiral mode characterizes an aircraft's spiral stability about the vertical axis. This mode controls whether or not an aircraft returns to level flight after a small perturbation in roll angle. When this mode is unstable, the aircraft will have a tendency to depart from level flight and enter a spiral dive.
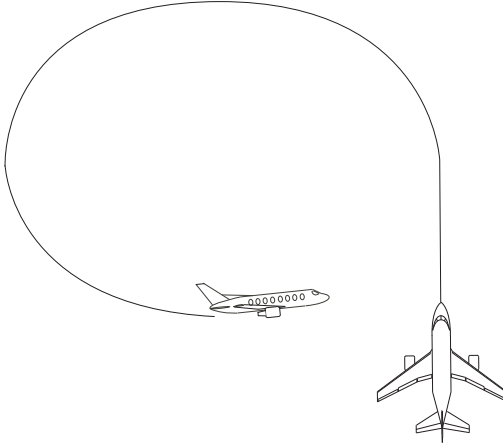
Figure 2.10. Illustration of an unstable Spiral mode

If the mode is stable, the aircraft remains in level flight. Usually the mode is stable. Even if the mode is not stable, the pilot will compensate to maintain straight and level flight.

2.6   Simplifying the Equations of Motion to Four Degrees of Freedom

The first step to simplifying the 6-DOF equations of motion is to make two assumptions about the aircraft in flight. These assumptions are that:

1. The aircraft's pitch dynamics, characterized by the short period mode, are fast enough to be assumed instantaneous.
2. The pilot maintains 'coordinated flight'.

We first concentrate on the implications of coordinated flight. Constraining the aircraft to coordinated flight implies that the side-slip angle is always zero. This in turn implies that there is never any side velocity, *v,* any side-force *Y,* or any yawing moment *N.* This reduces Equation (2.29), the side force equation, to Equation (2.45). The reduced Equation (2.45) is no longer a differential equation. Furthermore, the yaw rate derivative, $\dot{r}$, is neglected, reducing the yawing moment differential equation to an algebraic expression as shown in Equation (2.46). The rolling moment derivative is removed by the substitution of the rolling moment equation in for $\dot{p}$.

$$gC_\theta S_\phi = (ru - pw) \tag{2.45}$$

$$0 = -I_{xz}\frac{\overline{L} + I_{xz}(pq) - qr(I_z - I_y)}{I_x} + pq(I_y - I_x) + I_{xz}qr \tag{2.46}$$

Similarly, the side velocity, *v*, drops out of the other force equations as well.

$$X - mgS_\theta = m(\dot{u} + qw) \tag{2.47}$$

$$Z + mgC_\theta C_\phi = m(\dot{w} - qu) \tag{2.48}$$

Now, concentrate on the first assumption that the aircraft's pitch dynamics are fast enough to be neglected. This implies that the aircraft is able to command an angle of attack instantaneously. Therefore, we neglect the derivatives, $\dot{w}$ and $\dot{q}$. The terms $(p^2 - r^2)$ and rp in the pitching moment equation are second order effects and can be neglected. The pitching moments are, therefore, assumed to be in equilibrium, consistent with instantaneous angle of attack dynamics.

$$M = 0 \tag{2.49}$$

The net effect is that the Z force equation is reduced to an algebraic expression.

$$Z + mgC_\theta C_\phi = m(-qu) \tag{2.50}$$

This leads to an explicit expression for the pitch rate.

$$q = \frac{-Z - mgC_\theta C_\phi}{mu} \tag{2.51}$$

To solve for angle of attack, the pitching moment, *M,* must be expanded into its individual terms as shown in Equation (2.52). This is merely a formality because we will shortly show how we can remove angle of attack entirely.

$$M = M_o + M_\alpha \alpha + M_{\delta_e} \delta_e = 0 \tag{2.52}$$

The terms in (2.52) are:
- M_o : The zero angle of attack pitching moment
- M_α : A derivative relating pitching moment changes to changes in angle of attack
- M_{δ_e} : A derivative relating the effect of elevator deflection on angle of attack.

Solving for angle of attack yields Equation (2.53).

$$\alpha = \frac{-M_o - M_{\delta_e}\delta_e}{M_\alpha}$$

(2.53)

The steady-state angle of attack is an algebraic function of the elevator deflection, exclusively. This implies that the lift coefficient, C_L, also is very nearly an exclusive function of the elevator deflection as shown in Equations (2.54) and (2.55).

$$C_L = C_{L_o} + C_{L_\alpha}\alpha + C_{L_{\delta e}}\delta_e$$

(2.54)

$$C_L = C_{L_o} + C_{L_\alpha}\left(\frac{-M_o - M_{\delta_e}\delta_e}{M_\alpha}\right) + C_{L_{\delta e}}\delta_e$$

(2.55)

where
- C_{L_o} is the zero angle of attack lift coefficient
- C_{L_α} is the lift curve slope with respect to angle of attack
- $C_{L_{\delta e}}$ is the effect of elevator deflection on lift coefficient.

Although the angle of attack has been removed from our equations, we can still calculate it for animation purposes. Furthermore, the elevator deflection can be completely bypassed in favor of the aircraft's lift coefficient as the primary longitudinal control input. This is convenient because the terms relating lift coefficient, angle of attack and elevator deflection are not provided in commonly available aircraft models.

Using equations (2.52) and (2.54), we can derive an expression for the angle of attack that depends only on the coefficient of lift. This can be used for display purposes, and the reader is reminded that the expression assumes instantaneous angle of attack dynamics.

$$\alpha = \frac{C_L - C_{L_o} + C_{L_{\delta e}}\dfrac{M_o}{M_{\delta_e}}}{C_{L_\alpha} - C_{L_{\delta e}}\dfrac{M_\alpha}{M_{\delta_e}}}$$

(2.56)

This equation can be re-written in a simpler form, requiring only two airframe constants.

$$\alpha = \frac{C_L - C'_{L_o}}{C'_{L_\alpha}}$$

(2.57)

The primed constant in the numerator of equation (2.57) is an effective trim lift coefficient, while the primed constant in the denominator is an effective pitch sensitivity. For display purposes, suitable nominal values are 0.2 and 10, respectively, to yield the angle of attack in radians.

Returning to the model development, we assume that the angle of attack is small. This assumption combined with the previous assumption of coordinated flight implies that the wind and body frames are very nearly aligned with each other. The alignment of the wind and body frames implies the following:

1. True airspeed, V_a, and u are aligned. Therefore V_a can be substituted for u in the differential equations.
2. The lift force, defined as pointing in the $-\hat{z}_w$ direction, is now aligned with the Z force in Equation (2.30). $(Z = -L)$
3. The drag force, defined as pointing in the $-\hat{x}_w$, is aligned with the Thrust, defined as being aligned with the $\hat{x}_b$ axis. $(X = T - D)$
4. The Euler angle θ reduces to γ_a, the flight path angle.

These simplifications greatly reduce the equations of motion. Equations (2.58) through (2.60) show what remains of our differential equations.

$$T - D - mgS_\theta = m\dot{V}_a \tag{2.58}$$

$$q = \frac{L - mgC_\theta C_\phi}{mV_a} \tag{2.59}$$

$$\bar{L} = I_x \dot{p} - I_{xz}(pq) + qr(I_z - I_y) \tag{2.60}$$

These equations need to be rearranged into a useful form. We start with Equation (2.58), which can easily be rearranged as an expression for true airspeed.

$$\dot{V}_a = \frac{T - D}{m} - gS_\theta \tag{2.61}$$

Rearranging Equation (2.59) into an expression for flight path angle takes more steps. We start by relating the pitch rate, q, to the Euler angle θ by using the relations from

Table 2.2.

$$\dot{\theta} = \frac{L - mgC_\theta C_\phi}{mV_a C_\phi} - \dot{\psi}\frac{C_\theta S_\phi}{C_\phi} \qquad (2.62)$$

Using

Table 2.2 again, we can substitute for yaw rate, *r,* in terms of Euler angles in Equation (2.45).

$$\dot{\psi} = \frac{gC_\theta S_\phi}{V_a C_\theta C_\phi} + \dot{\theta}\frac{S_\phi}{C_\theta C_\phi} \tag{2.63}$$

Combining equations (2.62) and (2.63) result in the final expressions for $\dot{\theta}$ and $\dot{\psi}$.

$$\dot{\theta} = \frac{LC_\phi - mgC_\theta}{mV_a} \tag{2.64}$$

$$\dot{\psi} = \frac{LS_\phi}{mV_a C_\theta} \tag{2.65}$$

Using the fact that the flight path angle and the pitch angle are identical for this model, we substitute γ_a for θ. This protects us from confusion that might arise as a result of our simplified Euler angle expressions.

$$\dot{\gamma}_a = \frac{LC_\phi - mgC_{\gamma_a}}{mV_a} \tag{2.66}$$

$$\dot{\psi} = \frac{LS_\phi}{mV_a C_{\gamma_a}} \tag{2.67}$$

The final equation of motion to manipulate is the rolling moment equation. This equation governs the rate at which an aircraft can establish a bank angle. The rolling moment equation as written is a function of roll and pitch rates and the moments of inertia.

$$\bar{L} = I_x \dot{p} - I_{xz}(pq) + qr(I_z - I_y) \tag{2.68}$$

We choose to neglect the higher order terms and reduce the rolling moment equation to its linear form of $\bar{L} = I_x \dot{p}$. We will use standard stability and control derivatives to define the rolling moment.

$$L_p p + L_{\delta_a}\delta_a = I_x \dot{p} \tag{2.69}$$

where

- L_p is the rolling moment derivative with respect to roll rate
- L_{δ_a} is the rolling moment derivative with respect to aileron deflection
- δ_a is the aileron deflection.

The parameter, δ_a, is more accurately a linearized aileron deflection parameter. At small deflection angles it is mathematically equivalent to the aileron deflection. However, this linear form of the lateral dynamics allows us later to solve the system analytically while removing the aileron deflection parameter from the system of equations. We will take one further step to redefine our derivatives to include $1/I_x$ so that we can write our differential equation in first order form.

$$\dot{p} = L_p p + L_{\delta_a} \delta_a \qquad (2.70)$$

Table 2.3. The equations of motion for the 4-DOF model

Name	Equation	
True Airspeed Equation	$\dot{V}_a = \dfrac{T - D}{m} - gS_{\gamma_a}$	(2.61)
The Flight Path Angle Equation	$\dot{\gamma}_a = \dfrac{LC_\phi - mgC_{\gamma_a}}{mV_a}$	(2.66)
The Heading Equation	$\dot{\psi} = \dfrac{LS_\phi}{mV_a C_{\gamma_a}}$	(2.67)
The Roll Rate Equation	$\dot{p} = L_p p + L_{\delta_a} \delta_a$	(2.70)

Since we do not have much data for L_p and L_{δ_a}, we will have to use engineering judgment as to the best values for a specific aircraft. These numbers will be terms that must be 'tweakable' so that the user can tune them to suit. The final form of the equations of motion, without wind effects, is shown in Table 2.3.

An alternative derivation of the equations of motion may be found in Mukai (1992).

2.7   The Addition of Winds

The aerodynamic forces on an aircraft are created by its motion relative to the surrounding air. The air itself is in motion relative to the inertial frame. If the wind is constant, then the air mass is not accelerating and we need only consider the vector sum of the air mass and the aircraft's air speed to propagate over the earth model. If the wind is not constant, then we must consider the contributions of an accelerating frame to the equations of motion.

We make two important simplifying assumptions before implementing winds. The first is that the **wind contains no vertical component**.

$$\mathbf{V_w} = V_{wx}\hat{x}_i + V_{wy}\hat{y}_i \tag{2.71}$$

where

- V_w is the air mass velocity with respect to the inertial frame
- V_{wx} is the x component of the air mass velocity aligned with true North
- V_{wy} is the y component of the air mass velocity aligned with true East.

The second assumption is that the **wind varies only with altitude**; that is, the lateral and temporal variations are zero, $dV_w/dx = 0$, $dV_w/dy = 0$, $dV_w/dt = 0$.

The addition of winds into the system is done by creating yet another reference frame. This frame, the air mass frame, is inserted in between the inertial frame and the wind and body frames. Recall that the wind and body frames are equivalent for our simplified model. The air mass frame's orientation is aligned with the inertial frame, but moves at a constant velocity with respect to the inertial frame. The aircraft's motion as described in the previous sections is now considered to be with respect to the air mass frame and not the inertial frame. Knowing that the aircraft's velocity is aligned with the $\hat{x}_w$ axis we can determine the aircraft's speed relative to the air mass in inertial coordinates.

$$\begin{bmatrix} V_a C_{\gamma_a} C_\psi \hat{x}_i \\ V_a C_{\gamma_a} S_\psi \hat{y}_i \\ -V_a S_{\gamma_a} \hat{z}_i \end{bmatrix} = \begin{bmatrix} C_{\gamma_a} C_\psi & -C_\phi S_\psi + S_\phi S_{\gamma_a} C_\psi & S_\phi S_\psi + C_\phi S_{\gamma_a} C_\psi \\ C_{\gamma_a} S_\psi & C_\phi C_\psi + S_\phi S_{\gamma_a} S_\psi & -S_\phi C_\psi + C_\phi S_{\gamma_a} S_\psi \\ -S_{\gamma_a} & S_\phi C_{\gamma_a} & C_\phi C_{\gamma_a} \end{bmatrix} \begin{bmatrix} V_a \hat{x}_w \\ 0 \hat{y}_w \\ 0 \hat{z}_w \end{bmatrix} \tag{2.72}$$

The velocity of the air mass relative to the inertial frame is presented below. The reader will note that we assume there is no vertical component to the wind.

The total aircraft velocity with respect to the inertial frame is then the sum of the air mass velocity with respect to the inertial frame and the aircraft's velocity with respect to the air mass. The term $\mathbf{V}_i$ is the aircraft's velocity with respect to the inertial frame or the sum of the aircraft's true airspeed and the wind velocity.

$$\mathbf{V}_i = \left(V_{wx} + V_a C_{\gamma_a} C_\psi \right) \hat{x}_i + \left(V_{wy} + V_a C_{\gamma_a} S_\psi \right) \hat{y}_i - V_a S_{\gamma_a} \hat{z}_i \qquad (2.73)$$

The terms in Equation (2.73) can be rewritten to introduce the terms V_x, V_y, and $\dot{h}$.

$$\mathbf{V}_i = V_x \hat{x}_i + V_y \hat{y}_i - \dot{h} \hat{z}_i \qquad (2.74)$$

These terms are defined as follows:

- V_x is the velocity of the aircraft with respect to the inertial frame in the true North direction
- V_y is the velocity of the aircraft with respect to the inertial frame in the true East direction
- $\dot{h}$ is the altitude rate or vertical speed of the aircraft.

Later, the terms V_x and V_y are used when defining the latitude rate and longitude rate of the aircraft. Assuming that the winds are constant, Equation (2.73) is sufficient for modeling the dynamics. However, if the winds are not constant, then wind gradient terms must be added to the differential equations. Often, winds vary with altitude. If this is the case, the equations of motion must be re-derived accounting for the variations in winds with respect to altitude.

As the body frame is accelerating relative to the air mass, we introduce an inertial force due to the variation in wind speed, F_w.

$$\vec{F}_w = -m \begin{bmatrix} C_\theta & 0 & -S_\theta \\ S_\phi S_\theta & C_\phi & S_\phi C_\theta \\ C_\phi S_\theta & -S_\phi & C_\phi C_\theta \end{bmatrix} \begin{bmatrix} \dot{V}_{in} \\ \dot{V}_{cr} \\ 0 \end{bmatrix} \qquad (2.75)$$

In above equation, $\dot{V}_{in}$ and $\dot{V}_{cr}$ are the change in air mass velocity in-track and cross-track, respectively.

Now the Force Equations are updated to include, F_w.

$$X - mgS_\theta - m\dot{V}_{in}C_\theta = m(\dot{u} + qw - rv) \tag{2.76}$$

$$Y + mgC_\theta S_\phi - m\dot{V}_{in}S_\theta S_\phi - m\dot{V}_{cr}C_\phi = m(\dot{v} + ru - pw) \tag{2.77}$$

$$Z + mgC_\theta C_\phi - m\dot{V}_{in}S_\theta C_\phi + m\dot{V}_{cr}S_\phi = m(\dot{w} + pv - qu) \tag{2.78}$$

The same simplifications used to simplify Equations (2.28)-(2.30) in are applied Equations (2.76)-(2.78).

$$\frac{T - D}{m} - gS_{\gamma_a} - \dot{V}_{in}C_{\gamma_a} = \dot{V}_a \tag{2.79}$$

$$gC_{\gamma_a}S_\phi - \dot{V}_{in}S_{\gamma_a}S_\phi - \dot{V}_{cr}C_\phi = rV_a \tag{2.80}$$

$$\frac{-L}{m} + gC_{\gamma_a}C_\phi - \dot{V}_{in}S_{\gamma_a}C_\phi + \dot{V}_{cr}S_\phi = -qV_a \tag{2.81}$$

Equation (2.79) is the new True Airspeed Equation. To determine the effects on the Flight Path Angle Equation and the Heading Equation, use

Table 2.2 and Equations (2.80) & (2.81).

$$\dot{\theta} = \frac{L}{mV_a C_\phi} - \frac{gC_\theta}{V_a} + \frac{\dot{V}_{in} S_\theta}{V_a} - \frac{\dot{V}_{cr} S_\phi}{V_a C_\phi} - \dot{\psi} \frac{C_\theta S_\phi}{C_\phi} \tag{2.82}$$

$$\dot{\psi} = \frac{gS_\phi}{V_a C_\phi} - \frac{\dot{V}_{in} S_\theta S_\phi}{V_a C_\theta C_\phi} - \frac{\dot{V}_{cr}}{V_a C_\theta} + \dot{\theta} \frac{S_\phi}{C_\theta C_\phi} \tag{2.83}$$

Solving the system of equations given by Equations (2.82) & (2.83) gives the updated Flight Path Angle Equation and the Heading Equation in terms of $\dot{V}_{in}$ and $\dot{V}_{cr}$.

$$\dot{\theta} = \frac{LC_\phi}{mV_a} - \frac{gC_\theta}{V_a} + \frac{\dot{V}_{in} S_\theta}{V_a} \tag{2.84}$$

$$\dot{\psi} = \frac{LS_\phi}{mV_a C_\theta} - \frac{\dot{V}_{cr}}{V_a C_\theta} \tag{2.85}$$

To find $\dot{V}_{in}$ and $\dot{V}_{cr}$, use W_{igf} and W_{cgf}, the in-track gradient factor and the cross-track gradient factor, respectively. They are defined as follows:

$$W_{igf} = \frac{dV_{wx}}{dh} C_{\psi_a} + \frac{dV_{wy}}{dh} S_{\psi_a} \tag{2.86}$$

$$W_{cgf} = -\frac{dV_{wx}}{dh} S_{\psi_a} + \frac{dV_{wy}}{dh} C_{\psi_a} \tag{2.87}$$

W_{igf} and W_{cgf} are related to $\dot{V}_{in}$ and $\dot{V}_{cr}$ by the simple relations below:

$$\dot{V}_{in} = \frac{\partial V_{in}}{\partial h} \dot{h} = W_{igf} \dot{h} = W_{igf} V_a S_{\gamma_a} \tag{2.88}$$

$$\dot{V}_{cr} = \frac{\partial V_{cr}}{\partial h} \dot{h} = W_{cgf} \dot{h} = W_{cgf} V_a S_{\gamma_a} \tag{2.89}$$

The resulting equations of motion including wind terms are shown in Table 2.4

Table 2.4. The equations of motion including wind gradients

Equation	Name
True Airspeed Equation	$$\dot{V}_a = \frac{T-D}{m} - gS_{\gamma_a} - W_{igf}V_a S_{\gamma_a} C_{\gamma_a} \quad (2.90)$$
Flight Path Angle Equation	$$\dot{\gamma}_a = \frac{LC_\phi - mgC_{\gamma_a}}{mV_a} + W_{igf}S^2{}_{\gamma_a} \qquad (2.91)$$
Heading Equation	$$\dot{\psi} = \frac{LS_\phi}{mV_a C_{\gamma_a}} - W_{cgf}\frac{S_{\gamma_a}}{C_{\gamma_a}} \qquad (2.92)$$
Roll Rate Equation	$$\dot{p} = L_p p + L_{\delta_a}\delta_a \qquad (2.93)$$

2.8 Trajectory Propagation over an Earth Model

The kinematics of an aircraft have been determined in a coordinate system fixed to the surface of the earth. We now turn our attention to propagating the aircraft over the surface of the Earth. The equations that characterize this motion are developed in three steps. These steps are:

1. Develop a set of reference frames
2. Introduce an Earth model (the propagation equations are dependent on the selected model).
3. Develop the kinematic expressions relating the aircraft's velocity in the surface frame to changes in latitude and longitude.

2.8.1 Elliptic Earth Reference Frames

There are three major reference frames used for the analysis. These reference frames are

- DIS Coordinates - Since it is necessary that the TGF simulator conform to the DIS standard (Institute of Electrical and Electronics Engineers [IEEE], 1993) for representing aircraft trajectory propagation, and the DIS frame is an Earth-centered, Earth-fixed frame with rectangular coordinates, we choose to use it for our development. We will use a *'DIS'* subscript to describe the coordinates of this frame.
- Geodetic Coordinates - This frame (also known as Latitude-Longitude-Altitude) is commonly used in navigation. It uses angular coordinates (geodetic latitude and

longitude) and a position parameter (altitude). All are referenced to the local surface of the earth model. No tag is used to identify this frame, as context alone is sufficient.

- Surface Coordinates - A reference frame on the surface of the earth aligned such that the x-y plane is tangent to the surface with the x-axis pointing to the north and the y-axis pointing to the east. This frame is often referred to as the **North-East-Down (NED) frame**. We will use an '*s*' subscript for brevity of notation when writing equations. Surface Coordinates and Geodetic Coordinates are orthogonally aligned.

The observant reader will notice that the aircraft equations of motion were calculated assuming a flat Earth and that we here assume the development frame was the North-East-Down frame. This implies necessarily that earth rotation and the variation of the gravity vector with position over the earth were ignored in developing the aircraft equations of motion. This simplification limits our mathematical model to the flight of aircraft only. The model will not properly handle the flight of sub-orbital craft and spacecraft such as intercontinental ballistic missiles, satellites, or the space shuttle. The model is adequate for all vehicles traveling under Mach 3.

For trajectory propagation, since we cannot assume a flat Earth, the original inertial reference frame, denoted with an '*i*' subscript, is modified for the elliptic Earth. Thus, we align our newly defined 'surface' frame, with the inertial frame '*i*'. The surface frame then moves with the aircraft so as to provide a frame that is tangent to the Earth's surface for interfacing with trajectory propagation equations, and parallel to the aircraft's horizontal plane of flight for interfacing with the aircraft's flat-Earth dynamics. All velocities that were originally defined with respect to the '*i*' frame, are now taken to be with respect to the '*s*' frame.

Figure 2.11 shows the relationship between the DIS and surface frames. The DIS-frame is fixed in the center of the earth with the $\hat{z}_{DIS}$ -axis out the North pole. The Plane described by the $\hat{x}_{DIS}$ - and the $\hat{y}_{DIS}$ -axes is in the plane of the equator. The $\hat{x}_{DIS}$ axis is through zero degrees longitude, or the prime meridian. The surface (NED) frame is tangent to the surface of the earth and is centered in an object propagating along the Earth's surface. It is denoted with an '*s*' subscript for surface. The $\hat{z}_s$ axis points downward and is normal to the surface of the earth. The $\hat{x}_s$ - and $\hat{y}_s$ -axes define a plane tangent to the surface of the earth. The longitude and latitude angles describe the rotation between the two frames.
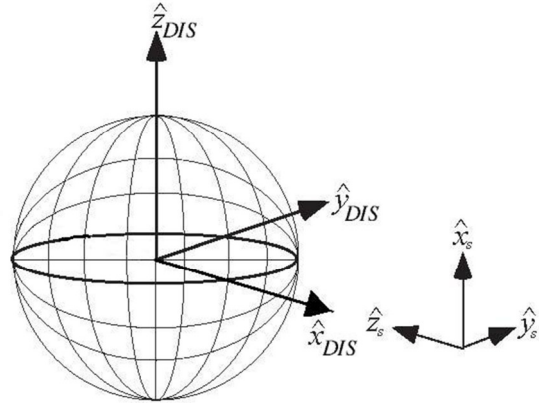
Figure 2.11. The DIS frame and the surface frame

Longitude Rotation   Latitude Rotation
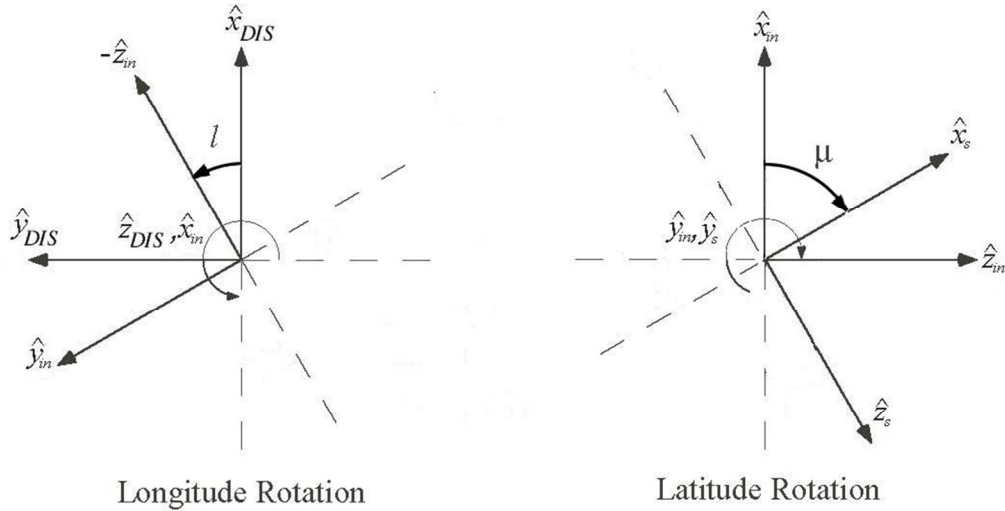
Figure 2.12. The longitude and latitude rotations

The orientation of the reference frames is such that at zero degrees longitude and latitude, the two reference frames are orthogonally aligned. Furthermore, the surface frame conforms to the orientation normally used with aircraft as shown in Figure 2.2. Figure 2.2 shows the relationship between the surface frame and the aircraft's body fixed frame. The angular rotation from the *DIS*-frame to the *s*-frame can be thought of as an Euler sequence of rotations. The ordered rotations are illustrated in Figure 2.12.

The first rotation is longitude. Longitude (ℓ) is rotated about the positive $\hat{z}_{DIS}$-axis in a right handed sense from the '*DIS*' frame to an intermediate frame noted with an '*in*'. The $\hat{z}_{DIS}$-axis coincides with the $\hat{x}_{in}$-axis in the intermediate frame. The rotation yields a direction cosine matrix in Equation (2.94).

-33-

$$
\begin{bmatrix} \hat{x}_{in} \\ \hat{y}_{in} \\ \hat{z}_{in} \end{bmatrix} = \begin{bmatrix} 0 & 0 & 1 \\ -\sin \ell & \cos \ell & 0 \\ -\cos \ell & -\sin \ell & 0 \end{bmatrix} \begin{bmatrix} \hat{x}_{DIS} \\ \hat{y}_{DIS} \\ \hat{z}_{DIS} \end{bmatrix}
\tag{2.94}
$$

The geodetic latitude (μ) is rotated about the positive $\hat{y}_{in}$-axis in a left-handed sense from the *'in'* frame to the surface frame denoted with a *'s'*. The transformation to the surface frame defined in this way, as shown in Equation (2.95), keeps geodetic latitude positive in the Northern hemisphere.

$$
\begin{bmatrix} \hat{x}_s \\ \hat{y}_s \\ \hat{z}_s \end{bmatrix} = \begin{bmatrix} \cos \mu & 0 & \sin \mu \\ 0 & 1 & 0 \\ -\sin \mu & 0 & \cos \mu \end{bmatrix} \begin{bmatrix} \hat{x}_{in} \\ \hat{y}_{in} \\ \hat{z}_{in} \end{bmatrix}
\tag{2.95}
$$

The product of these two matrices is the complete direction cosine matrix between the two reference frames.

$$
\begin{bmatrix} \hat{x}_s \\ \hat{y}_s \\ \hat{z}_s \end{bmatrix} = \begin{bmatrix} \cos \mu & 0 & \sin \mu \\ 0 & 1 & 0 \\ -\sin \mu & 0 & \cos \mu \end{bmatrix} \begin{bmatrix} 0 & 0 & 1 \\ -\sin \ell & \cos \ell & 0 \\ -\cos \ell & -\sin \ell & 0 \end{bmatrix} \begin{bmatrix} \hat{x}_{DIS} \\ \hat{y}_{DIS} \\ \hat{z}_{DIS} \end{bmatrix}
\tag{2.96}
$$

$$
\begin{bmatrix} \hat{x}_s \\ \hat{y}_s \\ \hat{z}_s \end{bmatrix} = \begin{bmatrix} -\sin \mu \cos \ell & -\sin \mu \sin \ell & \cos \mu \\ -\sin \ell & \cos \ell & 0 \\ -\cos \mu \cos \ell & -\cos \mu \sin \ell & -\sin \mu \end{bmatrix} \begin{bmatrix} \hat{x}_{DIS} \\ \hat{y}_{DIS} \\ \hat{z}_{DIS} \end{bmatrix}
\tag{2.97}
$$

The inverse of a rotation matrix is simply its transpose, and so the transformation of a vector from the NED-frame to the DIS-frame is easily obtained. As an example, the velocity in DIS coordinates is given by…

$$
\mathbf{V}_{DIS} = \begin{bmatrix} -\sin \mu \cos \ell & -\sin \ell & -\cos \mu \cos \ell \\ -\sin \mu \sin \ell & \cos \ell & -\cos \mu \sin \ell \\ \cos \mu & 0 & -\sin \mu \end{bmatrix} \mathbf{V}_s
\tag{2.98}
$$

The rotation matrix of equation (2.97) can transform a vector described in the DIS coordinate system to the North-East-Down coordinate system. The unfortunate consequence of this format is that the geodetic latitude and longitude of the origin of the vector are unknown to the vector described in DIS coordinates, and so equation (2.97) is not very useful. This problem is resolved in section **2.8.4** below.

2.8.2 The Earth Model and its Kinematic Parameters

The TGF Aircraft Dynamics Model uses the WGS-84 earth model, as defined by National Imagery and Mapping Agency (NIMA, 1997). The WGS-84 earth model is a spheroidal earth model as shown in Figure 2.13 where:

- a is the equatorial radius, or the semi-major axis of the spheroid, which is 6378137.0 meters, or 2.092565×10^7 *ft*
- b is the semi-minor axis given by *b = a(1-f)* where *f* is the *Earth Flattening Parameter* . (*1/f* = 298.257223563)

A polar cross section of the spheroidal earth is depicted in Figure 2.13. It illustrates the flattening of the spheroid at the poles as well as a graphical representation of three commonly used latitude definitions: geocentric latitude, λ, parametric latitude, θ, and geodetic latitude, μ. The side view illustrates how the cross-section of the flattened earth can be represented as a rotation from a circle. The angle subtended in this rotation is the arcsine of the eccentricity, e, of the meridional ellipse. The point O is the center of the earth. B is the North Pole. The semi-major (equatorial) axis, OA, of the meridional ellipse has length a, the semi-minor (polar) axis, OB has length b. From the diagram we can see that $b = a \cos(\arcsin(e))$. The eccentricity of the ellipse is defined as…

$$e^2 = 1 - \frac{b^2}{a^2}$$
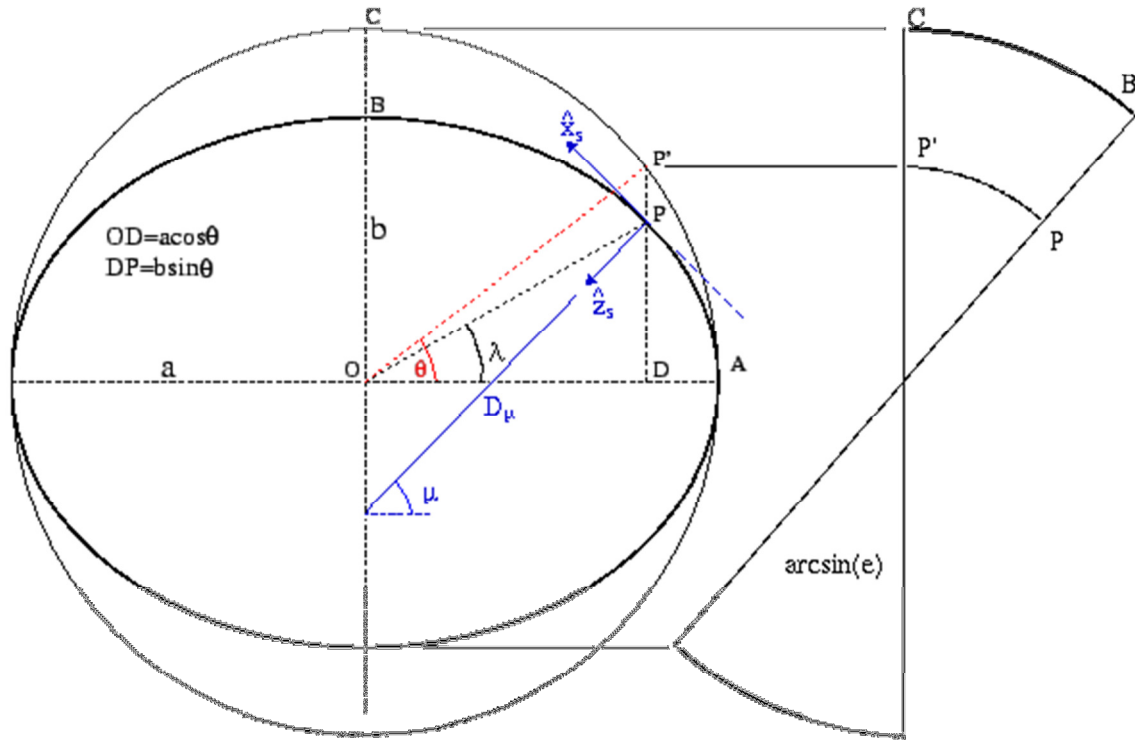
Figure 2.13. The Spheroidal Earth model
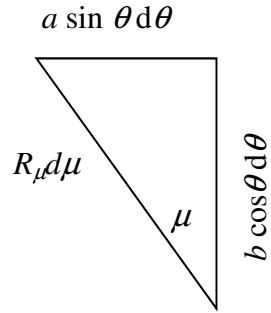
Figure 2.14. Triangle Representing Slope of Meridional Ellipse and Incremental Latitude Change

Mathematically, it is most convenient to describe the geometry of the ellipse via the parametric latitude, θ. A point P on the ellipse has coordinates ($a \cos \theta$, $b \sin \theta$). The point P' is the point on the circumscribing circle (of radius a) the same distance from the polar axis as P. The latitude used in navigation is the geodetic latitude, μ, which is defined as the angle between the northerly horizon at P and the polar axis. This definition yields a relationship between the parametric and geodetic latitudes: the tangent of the geodetic latitude is the negative inverse of the slope of the spheroid at P (i.e., the change

in equatorial displacement divided by the change in the poleward displacement). This is illustrated in Figure 2.14. R_μ is the radius of curvature of the meridional arc at P.

$$\tan \mu = -\frac{d(a\cos\theta)}{d(b\sin\theta)} = -\frac{-a\sin\theta d\theta}{b\cos\theta d\theta}$$

$$\tan \mu = \frac{a}{b}\tan\theta \tag{2.99}$$
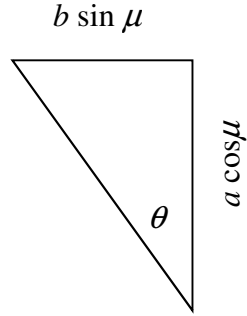
Figure 2.15. Alternate Triangle of Relationship Between Geodetic and Parametric Latitude on the Meridional Ellipse

It should be noted that equation (2.99) applies only to points on the spheroid. From inspection of equation (2.99) we can create another triangle (Figure 2.15). From inspection of Figure 2.15 we write…

$$\sin\theta = \frac{b\sin\mu}{\sqrt{b^2\sin^2\mu + a^2\cos^2\mu}}$$

$$\sin\theta = \frac{b\sin\mu}{a\sqrt{(1-e^2)\sin^2\mu + (1-\sin^2\mu)}}$$

$$\frac{\sin\theta}{\sin\mu} = \frac{\sqrt{1-e^2}}{\sqrt{1-e^2\sin^2\mu}} \tag{2.100}$$

Similarly,…

$$\cos\theta = \frac{a\cos\mu}{\sqrt{b^2\sin^2\mu + a^2\cos^2\mu}}$$

$$\cos\theta = \frac{a\cos\mu}{a\sqrt{\left(1-e^2\right)\sin^2\mu+\cos^2\mu}}$$

$$\frac{\cos\theta}{\cos\mu} = \frac{1}{\sqrt{1-e^2\sin^2\mu}} \tag{2.101}$$

From Figure 2.14 the displacement along the meridian is given by,

$$R_\mu d\mu = \sqrt{a^2\sin^2\theta+b^2\cos^2\theta}\,d\theta$$
$$= a\sqrt{1-e^2\cos^2\theta}\,d\theta$$
$$= a\frac{1-e^2}{\left(1-e^2\sin^2\mu\right)^{3/2}}d\mu$$

So that the radius of curvature of the meridional ellipse at P is given by,

$$R_\mu = a\frac{1-e^2}{\left(1-e^2\sin^2\mu\right)^{3/2}} \tag{2.102}$$

We here define one more parameter that becomes useful in our kinematic analysis. This parameter is labeled as D_μ in Figure 2.13 and we shall call this parameter the *Geodetic Distance to the Polar Axis*. It should not be confused with the radius of curvature at P, which is somewhat larger. By inspection,

$$D_\mu\cos\mu = a\cos\theta$$

From equation (2.101)

$$D_\mu = a\frac{1}{\sqrt{1-e^2\sin^2\mu}} \tag{2.103}$$

A similarly defined parameter, although not illustrated, is the *Geodetic Distance to the Equator*, $D_{\mu_{eq}}$.

$$D_{\mu_{eq}}\sin\mu = b\sin\theta$$

From equation (2.100)

$$D_{\mu_{eq}} = b \frac{\sqrt{1-e^2}}{\sqrt{1-e^2 \sin^2 \mu}}$$

$$D_{\mu_{eq}} = D_{\mu}\left(1-e^2\right) \qquad (2.104)$$

2.8.3 Kinematics Relating the Coordinate Frames

The velocity vector equation (2.74), has been developed from the aircraft aerodynamics in terms of the surface, or NED, coordinates. We can equate this velocity vector to the time rate of change of the position vector in the surface coordinate system. The position vector, $\mathbf{R}_{op}$, is easily expressed in terms of *DIS* coordinates. We transform $\mathbf{R}_{op}$ to surface coordinates via equation (2.97). Once this transformation is done, $\mathbf{R}_{op}$ is expressed in terms of latitude and longitude. Consequently, the time rate of change of $\mathbf{R}_{op}$ will yield a velocity vector in terms of latitude and longitude rates. With the velocity vector expressed in terms of aircraft dynamics and in terms of latitude and longitude rates, we can solve for the latitude and longitude rates for propagation over our earth model.
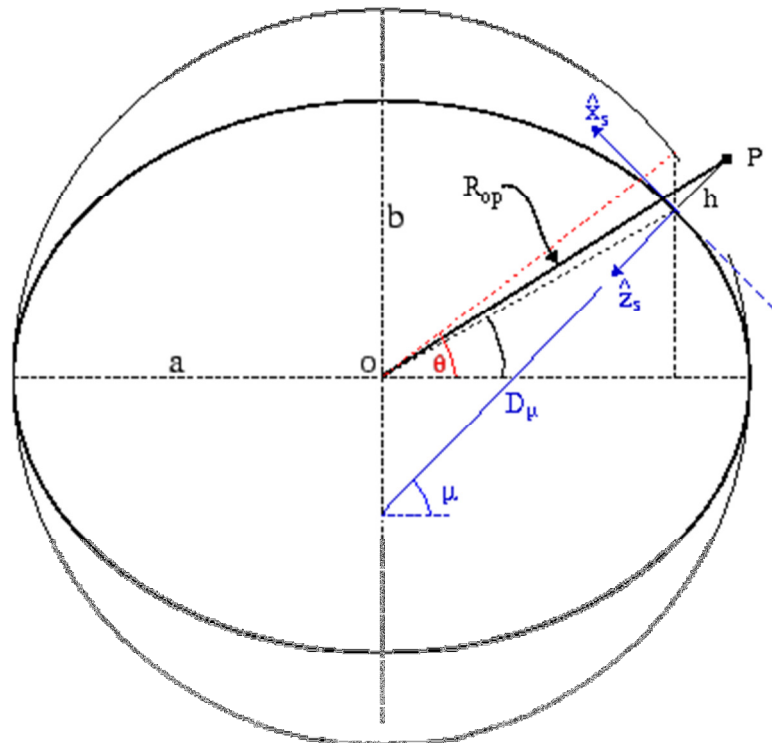
Figure 2.16 Position Vector on the Spheroid

-39-

By inspection of Figure 2.16, the component of $\mathbf{R}_{op}$ parallel to the equator from the polar axis to the point P is,

$$R_{eq} = (D_\mu + h)\cos\mu \qquad (2.105)$$

This is resolved along the $\hat{x}_{DIS}$ and $\hat{y}_{DIS}$ axes by multiplying by the cosine and sine of the longitude. Similarly, the component of $\mathbf{R}_{op}$ parallel to the polar axis from the equator to the point P is

$$z_{DIS} = \left(D_{\mu_{eq}} + h\right)\sin\mu = \left(D_\mu\left(1 - e^2\right) + h\right)\sin\mu \qquad (2.106)$$

And so the position vector in *DIS* coordinates is obtained immediately in two forms by inspection.

$$\mathbf{R}_{op}^{DIS} = \begin{bmatrix} (a\cos\theta + h\cos\mu)\cos\ell \\ (a\cos\theta + h\cos\mu)\sin\ell \\ b\sin\theta + h\sin\mu \end{bmatrix} \qquad (2.107)$$

$$\mathbf{R}_{op}^{DIS} = \begin{bmatrix} (D_\mu + h)\cos\mu\cos\ell \\ (D_\mu + h)\cos\mu\sin\ell \\ \left(D_\mu\left(1 - e^2\right) + h\right)\sin\mu \end{bmatrix} \qquad (2.108)$$

The position vector in surface coordinates is obtained by pre-multiplying by the rotation matrix in equation (2.97)

$$\mathbf{R}_{op}^s = \begin{bmatrix} -\sin\mu\cos\ell & -\sin\mu\sin\ell & \cos\mu \\ -\sin\ell & \cos\ell & 0 \\ -\cos\mu\cos\ell & -\cos\mu\sin\ell & -\sin\mu \end{bmatrix} \mathbf{R}_{op}^{DIS}$$

$$\mathbf{R}_{op}^s = \begin{bmatrix} -e^2 D_\mu \sin\mu\cos\mu \\ 0 \\ -D_\mu\left(1 - e^2\sin^2\mu\right) - h \end{bmatrix} \qquad (2.109)$$

We need to take the derivative of the position vector to get an expression for the aircraft's velocity. The derivative is defined in (2.110).

$$\frac{d\mathbf{R}_{op}^{s}}{dt} = \frac{\partial \mathbf{R}_{op}^{s}}{\partial t} + \left(\boldsymbol{\omega} \times \mathbf{R}_{op}^{s}\right) \tag{2.110}$$

$$\frac{\partial \mathbf{R}_{op}^{s}}{\partial t} = \frac{\partial}{\partial t} \begin{bmatrix} -e^{2}D_{\mu}\sin\mu\cos\mu \\ 0 \\ -D_{\mu}\left(1-e^{2}\sin^{2}\mu\right)-h \end{bmatrix}$$

$$\frac{\partial \mathbf{R}_{op}^{s}}{\partial t} = \begin{bmatrix} -e^{2}\dot{D}_{\mu}\sin\mu\cos\mu - e^{2}\dot{\mu}D_{\mu}\left(\cos^{2}\mu-\sin^{2}\mu\right) \\ 0 \\ -\dot{D}_{\mu}\left(1-e^{2}\sin^{2}\mu\right)+2e^{2}\dot{\mu}D_{\mu}\sin\mu\cos\mu-\dot{h} \end{bmatrix}$$

From equation (2.103)

$$\dot{D}_{\mu} = a\frac{e^{2}\sin\mu\cos\mu}{\left(1-e^{2}\sin^{2}\mu\right)^{3/2}}\dot{\mu} = \dot{\mu}D_{\mu}\frac{e^{2}\sin\mu\cos\mu}{\left(1-e^{2}\sin^{2}\mu\right)} \tag{2.111}$$

$$\frac{\partial \mathbf{R}_{op}^{s}}{\partial t} = \begin{bmatrix} -\dot{\mu}D_{\mu}\dfrac{e^{4}\sin^{2}\mu\cos^{2}\mu}{\left(1-e^{2}\sin^{2}\mu\right)} - e^{2}\dot{\mu}D_{\mu}\left(\cos^{2}\mu-\sin^{2}\mu\right) \\ 0 \\ \dot{\mu}e^{2}D_{\mu}\sin\mu\cos\mu-\dot{h} \end{bmatrix}$$

The angular rotation of the surface frame relative to the Earth-fixed *DIS* frame is easily defined in mixed coordinates, keeping in mind that the latitude rotation is a negative rotation about the $\hat{y}_{s}$-axis.

$$\boldsymbol{\omega} = \dot{\ell}\hat{z}_{DIS} - \dot{\mu}\hat{y}_{s}$$

Transforming the longitude rotation to surface coordinates via equation (2.97), we get…

$$\boldsymbol{\omega}^{s} = \begin{bmatrix} \dot{\ell}\cos\mu \\ -\dot{\mu} \\ -\dot{\ell}\sin\mu \end{bmatrix} \tag{2.112}$$

Expanding the cross product term,

-41-

$$\left(\boldsymbol{\omega}\times\mathbf{R}_{op}\right)^s = \begin{bmatrix} \dot{\ell}\cos\mu \\ -\dot{\mu} \\ -\dot{\ell}\sin\mu \end{bmatrix} \times \begin{bmatrix} -e^2 D_\mu \sin\mu\cos\mu \\ 0 \\ -D_\mu\left(1-e^2\sin^2\mu\right)-h \end{bmatrix}$$

$$\left(\boldsymbol{\omega}\times\mathbf{R}_{op}\right)^s = \begin{bmatrix} \dot{\mu}D_\mu\left(1-e^2\sin^2\mu\right)+\dot{\mu}h \\ \dot{\ell}\left(D_\mu+h\right)\cos\mu \\ -\dot{\mu}e^2 D_\mu\sin\mu\cos\mu \end{bmatrix}$$

we end up with the final expression for velocity in Equation (2.113).

$$\left.\frac{d\mathbf{R}_{op}}{dt}\right|^s = \begin{bmatrix} -\dot{\mu}D_\mu\dfrac{e^4\sin^2\mu\cos^2\mu}{\left(1-e^2\sin^2\mu\right)}-e^2\dot{\mu}D_\mu\left(\cos^2\mu-\sin^2\mu\right) \\ 0 \\ \dot{\mu}e^2 D_\mu\sin\mu\cos\mu-\dot{h} \end{bmatrix} + \begin{bmatrix} \dot{\mu}D_\mu\left(1-e^2\sin^2\mu\right)+\dot{\mu}h \\ \dot{\ell}\left(D_\mu+h\right)\cos\mu \\ -\dot{\mu}e^2 D_\mu\sin\mu\cos\mu \end{bmatrix}$$

$$\left.\frac{d\mathbf{R}_{op}}{dt}\right|^s = \begin{bmatrix} \dot{\mu}\left(R_\mu+h\right) \\ \dot{\ell}\left(D_\mu+h\right)\cos\mu \\ -\dot{h} \end{bmatrix} \tag{2.113}$$

From equation (2.74), the velocity of the aircraft in the surface frame is

$$\mathbf{V}^s = \begin{bmatrix} V_x \\ V_y \\ -\dot{h} \end{bmatrix} \tag{2.74}$$

We can set the x and y components of equation (2.74) equal to those of equation (2.113) and solve for the latitude and longitude rates. The z components produce an identity.

$$\begin{bmatrix} V_x \\ V_y \\ -\dot{h} \end{bmatrix} = \begin{bmatrix} \dot{\mu}\left(R_\mu+h\right) \\ \dot{\ell}\left(D_\mu+h\right)\cos\mu \\ -\dot{h} \end{bmatrix}$$

These expressions can be rearranged in terms of $\dot{\ell}$ and $\dot{\mu}$ as shown in equations (2.114).

$$\dot{\mu} = \frac{V_x}{R_\mu + h}$$

$$\dot{\ell} = \frac{V_y}{(D_\mu + h)\cos\mu}$$

(2.114)

2.8.4 Transforming DIS to Lat/Lon

There may be a future need to transform DIS coordinates to the standard position coordinates of latitude, longitude, and altitude, e.g., when TGF is integrated with external aircraft motion applications that output DIS coordinates. The equations transforming DIS to latitude-longitude position are the inverse of equation (2.108). Unfortunately, an accurate representation of the inverse of equation (2.108) is ungainly. An equivalent iterative algorithm (Borkowski, 1989) used to obtain the needed accuracy is more aesthetically appealing.

The equatorial position vector, $\mathbf{R}_{eq}$, as defined in equation (2.105), is the vector sum of the x- and y- components of the DIS coordinates of $\mathbf{R}_{op}$.

$$R_{eq} = \sqrt{x_{DIS}^2 + y_{DIS}^2}$$

The longitude is obtained from DIS coordinates immediately.

$$\ell = \arctan\left(\frac{y_{DIS}}{x_{DIS}}\right)$$

(2.115)

From equation (2.107), we have

$$R_{eq} = a\cos\theta + h\cos\mu$$

$$z_{DIS} = b\sin\theta + h\sin\mu$$

(2.116)

Eliminating h and μ, this system of equations can be shown to reduce to the form shown in Borkowski (1989) in which we need to solve for the parametric latitude, θ. Borkowski showed that this form is superior in simplicity and accuracy over the range of latitudes.

$$f(\theta) = 2\sin(\theta - \Omega) - c\sin 2\theta = 0$$

(2.117)

The parameters Ω and c are constant for each position.

$$\Omega = \tan^{-1}\left(\frac{bz_{DIS}}{aR_{eq}}\right)$$

$$c = \frac{a^2 - b^2}{\sqrt{\left(aR_{eq}\right)^2 + \left(bz_{DIS}\right)^2}}$$

(2.118)

As with the inverse of equation (2.108), an analytical solution of equation (2.117) is ungainly. An iterative approach using the Newton-Raphson method provides suitable accuracy and speedy convergence. The Newton-Raphson method requires the derivative of $f(\theta)$.

$$f'(\theta) = 2\left[\cos(\theta - \Omega) - c\cos 2\theta\right]$$

(2.119)

A suitable first approximation to the parametric latitude is provided by assuming zero altitude. This is obtained from equations (2.116).

$$\theta_0 = \tan^{-1}\left(\frac{az_{DIS}}{bR_{eq}}\right)$$

(2.120)

Subsequent values of the parametric latitude in the Newton-Raphson iterative method are defined by the following equation.

$$\theta_{n+1} = \theta_n - \frac{f(\theta_n)}{f'(\theta_n)}$$

(2.121)

To obtain one-foot accuracy requires θ settling within about 10^{-9}. Once θ is determined, the geodetic latitude, μ, is obtained from equation (2.99). This allows the use of equations (2.116) to find the altitude. By inserting the trigonometric identity,

$$\sin^2 \mu + \cos^2 \mu = 1$$

equation (2.116) can be manipulated to equation (2.122).

$$h = \left(R_{eq} - a\cos\theta\right)\cos\mu + \left(z_{DIS} - b\sin\theta\right)\sin\mu$$

(2.122)

There are simpler forms for obtaining the altitude, but Borkowski prefers equation (2.122) for its uniform accuracy over the range of latitudes.

2.9 The Derived State Variables

The equations of motion are referred to as the state equations because they are the fundamental equations that govern the aircraft's motion. Each state equation is named for the state variable for which it calculates a derivative. In our case, we have four state variables $\begin{bmatrix} V_a & \gamma_a & \psi & p \end{bmatrix}$ that are governed by the equations in Table 2.3. There are also other important values that are not state variables but rather functions of the state variables. We call these values derived state variables. There are five important derived state variables:

- V_{IAS}: The indicated Airspeed
- M: The Mach number
- ψ_{GT}: The ground track heading
- V_{GS}: The ground speed
- $\dot{\psi}$: The turn rate
- f: The fuel flow/burn rate
- W: The aircraft weight
- h: The aircraft altitude

The indicated airspeed is the speed measurement indicated on an Aneroid type airspeed indicator that is hooked to an aircraft's pitot static system. The airspeed indicator measures the difference between the static and ram-air pressures and approximates an airspeed from the pressure difference. The indicated airspeed is not a good estimate of the true airspeed. At higher altitudes the difference between indicated and true airspeed may be in error by as much as 100 kts. To simulate the reading on an airspeed indicator, Equation (2.123) is used to convert from Mach number to indicated airspeed.

$$V_{IAS} = a_0^* \sqrt{\frac{2}{\gamma-1}\left(\left\{\frac{p}{p_o}\left[\left(1+\frac{\gamma-1}{2}M^2\right)^{\frac{\gamma}{(\gamma-1)}}-1\right]+1\right\}^{\frac{(\gamma-1)}{\gamma}}-1\right)} \qquad (2.123)$$

The terms in Equation (2.123) are defined as follows:

- a^*: The speed of sound.
- γ: The ratio of specific heats for air (not to be confused with the flight path angle). $\gamma = 1.4$ under normal conditions.
- p: The ambient pressure.
- p_0: The sea-level pressure.

To convert indicated airspeed to Mach number, requires rearranging Equation (2.123). Since this algebraic manipulation is not trivial, only the result is provided here.

$$M = \sqrt{\frac{2}{\gamma-1}\left[\left(\frac{p_o}{p}\left(\left(1+\frac{\gamma-1}{2}\left(\frac{V_{IAS}}{a_0^*}\right)^2\right)^{\frac{\gamma}{\gamma-1}}-1\right)+1\right)^{\frac{\gamma-1}{\gamma}}-1\right]} \qquad (2.124)$$

The Mach number is the ratio of the true airspeed and the speed of sound as shown in Equation (2.125).

$$M = \frac{V_a}{a^*} \qquad (2.125)$$

The ground speed and the ground track heading are derived from the velocity terms first presented in Equation (2.74).

$$V_G = \sqrt{V_x^{\ 2}+V_y^{\ 2}} \qquad (2.126)$$

$$\psi_{GT} = tan^{-1}\left(\frac{V_y}{V_x}\right) \qquad (2.127)$$

The turn rate of the aircraft is calculated using the heading equation. Equation (2.65) is reprinted here for convenience.

$$\dot{\psi} = \frac{LS_\phi}{mV_a C_{\gamma_a}} \qquad (2.65)$$

There are two 'derived' state variables that are not merely functions of the integrated states. These values must be integrated; however, we separate them from the formal integration of the differential equations because they do not require the rigorous integration procedure used to numerically integrate the state equations. These two 'derived' states are altitude, h, and aircraft weight, W. The altitude is simply the integration of the altitude rate and the aircraft weight is the integration of the fuel burn rate. The method of integration is discussed in the numeric integration section.

2.10 The Airframe Model

The airframe model is adapted from Seagull Technology's AMT (Aircraft Modeling Tool), which is adapted from EUROCONTROL's Base of Aircraft Data (BADA) (Nuic, 2009). The primary purpose of the airframe model is to calculate the aerodynamic forces applied to the aircraft. These forces are lift and drag as defined in Anderson, 1989.

The lift of the aircraft is calculated using Equation (2.128).

$$L = qS_wC_L \qquad (2.128)$$

The drag of the aircraft is calculated using Equation (2.129).

$$D = qS_wC_D \qquad (2.129)$$

The terms for these equations are as follows:

- L Lift
- D Drag
- S_w Wing Reference Area
- q Dynamic pressure
- C_D Drag coefficient
- C_L Lift coefficient

To calculate the dynamic pressure Equation (2.130). is used.

$$q = \frac{1}{2}\rho V_a^{\,2} \qquad (2.130)$$

where the terms in the equation are defined as follows:

- ρ air density
- V_a true airspeed

The air density is obtained from the atmosphere model, which is discussed in Section 2.12. The lift coefficient is an input that is generated by the control laws. The drag coefficient is calculated using Equation (2.131).

$$C_D = C_{D_o} + K\left(C_L - C_{L_{min\,drag}}\right)^2 \qquad (2.131)$$

where

- C_{D_o} The zero lift drag coefficient
- $C_{L_{min\,drag}}$ The lift coefficient at minimum drag
- K The induced drag coefficient

The drag polar equation comes from classical incompressible aerodynamics. The compressibility effects of high speed flight are currently neglected.

Each aircraft in the simulation has five flap settings and a spoiler that can be deployed when needed. The flap settings are named for their respective flight phases. Each flap setting is described by its own drag polar.

- Clean configuration
- Initial climb configuration
- Take off configuration
- Approach configuration
- Landing configuration
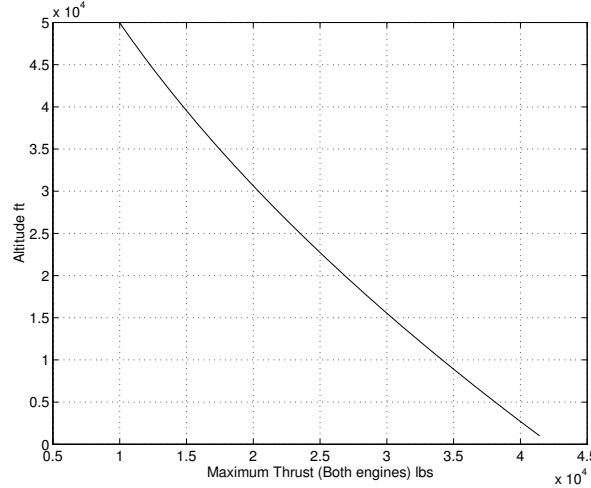
Figure 2.17. Maximum thrust vs altitude for a DC-9/MD80

2.11 The Engine Model

The engine model is responsible for providing two important parameters to the rest of the model. These parameters are the maximum thrust available and the fuel burn rate. We use the BADA parameters (Nuic, 2009) to perform these calculations. The form of the mathematical models for thrust and fuel burn depends on the aircraft's installed configuration for thrust production. The ADM uses three separate mathematical thrust/fuel burn models for three engine types: turbofan, turboprop (i.e., gas-turbine engine attached to propeller), and piston-prop (i.e., internal combustion engine attached to propeller). As an example of the implementation, we present here the thrust and fuel

burn models for the turbofan engine installation. While the models for other installations are of a similar format, the reader is referred to Nuic, 2009 for further detail.

The maximum thrust available to the turbofan-powered aircraft at any given time is a function of the local air density. Figure 2.17 shows the maximum thrust available for a DC-9 aircraft as the altitude is increased. The thrust and fuel burn models represent the air density in terms of pressure altitude. The maximum available thrust is computed using Equation (2.132).

$$T_{max} = C_{T_{c,1}} \left(1 - \frac{h}{C_{T_{c,2}}} + C_{T_{c,3}} h^2 \right) \qquad (2.132)$$

where:

- h is altitude
- T_{max} is the maximum climb thrust
- $C_{T_{c,i}}$, are the BADA coefficients fitting actual thrust performance to altitude

The fuel burn rate is calculated using the following equations.

$$\eta = C_{f_1} \left(1 + \frac{V_a}{C_{f_2}} \right) \qquad (2.133)$$

$$f = \eta T \qquad (2.134)$$

$$f_{min} = C_{f_3} \left(1 - \frac{h}{C_{f_4}} \right) \qquad (2.135)$$

where:

1. η is the thrust specific fuel consumption
2. V_a is the true airspeed
3. T is the Thrust
4. f the fuel flow rate
5. f_{min} is the minimum fuel rate
6. h is the altitude

7. C_{f_i}, are the BADA coefficients fitting actual fuel burn performance to altitude and speed

The fuel flow rate is normally calculated using Equations (2.133) and (2.134); however, there is a lower bound on the fuel burn, which is calculated using Equation (2.135). If the fuel burn calculated using Equations (2.133) and (2.134) is lower than the minimum fuel burn rate, the minimum fuel burn rate is returned as the fuel burn rate. Figure 2.18 shows the fuel burn rate for a DC-9 at maximum thrust for various airspeeds.
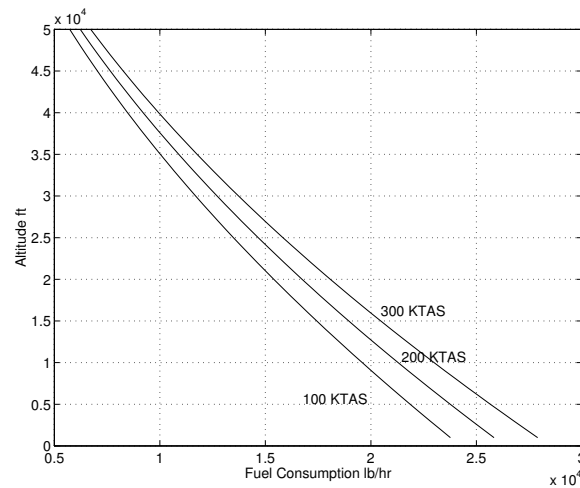
Figure 2.18. Fuel Consumption at maximum thrust (both engines) for a DC-9/MD80

2.12   The Standard Atmosphere Model

Since aircraft operate in the Earth's atmosphere and their lift and drag characteristics depend on the properties of that atmosphere, it is essential to be able to define these properties. To do this, the International Standard Atmosphere (ISA) model (International Civil Aviation Organization, 2000) is implemented. The derivation of the governing equations is omitted since they are commonly available (e.g., Anderson, 1989).

There are two separate regions to the Earth's atmosphere that we are concerned with. The first region is the gradient region where temperature drops off linearly with altitude. The gradient region spans from the Earth's surface to 11 km (~36100 ft). The second is an isothermal region where the temperature is constant. The isothermal region extends to 20 km (~65600 ft). Our model is not concerned with altitudes above 20 km. Figure 2.19 illustrates the temperature variation of the standard atmosphere.
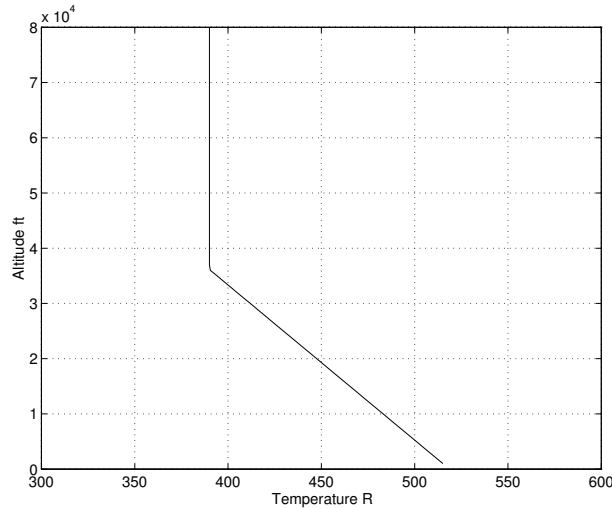
Figure 2.19. Temperature vs altitude for the standard day atmosphere

In the gradient layer (less than 11 km), the temperature of the ambient air surrounding the aircraft is calculated using Equation (2.136).

$$T_{amb} = T_{sl} - ah \tag{2.136}$$

where

- T_{sl} : The sea level temperature (15.0 °C)
- T_{amb} : The ambient temperature
- h : The altitude
- a : The temperature lapse rate in the gradient layer (6.5 °C/km)

In the isothermal layer, the temperature stays constant at -56.5 °C.

$$T_{amb} = T_{sl} - a(11km) = -56.5°C \tag{2.137}$$

The speed of sound is strictly a function of the ambient air temperature. It is calculated using the thermodynamic relation in Equation (2.138)
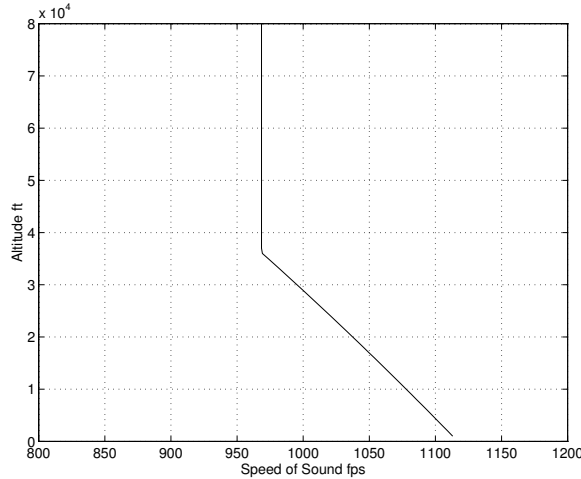
Figure 2.20. The speed of sound variation with altitude for the standard day atmosphere

$$a^* = \sqrt{\gamma RT} \qquad (2.138)$$

where

- a^* is the speed of sound, and
- γ is the ratio of specific heats for air.

$$\gamma = \frac{c_p}{c_v} \qquad (2.139)$$

where c_p is the constant pressure specific heat and c_v is the constant volume specific heat. The term R is the ideal gas constant and T is the absolute ambient air temperature. Figure 2.20 shows the relationship between the speed of sound and altitude for a standard day.

Figure 2.21 illustrates the pressure variation with altitude for the standard day. If the aircraft is in the gradient layer, the pressure ratio of the aircraft is calculated using Equation (2.140).

$$\left(\frac{p_{amb}}{p_{sl}} \right) = \left(\frac{T_{amb}}{T_{sl}} \right)^{\frac{-g}{aR}} \qquad (2.140)$$
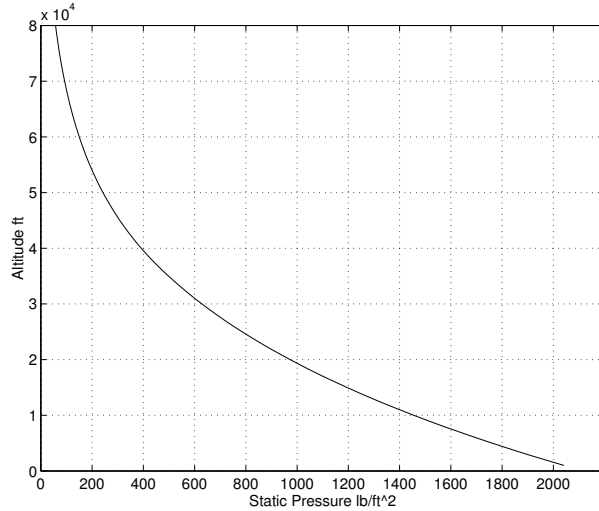
Figure 2.21. Pressure variation with altitude for the standard atmosphere

where

- p_{amb}:   The ambient pressure.
- p_{sl}: The sea level pressure.
- g :   Gravitational acceleration.
- R: Ideal gas constant.

If the aircraft is in the isothermal layer, the pressure ratio of the aircraft is calculated using Equation (2.141).

$$\left(\frac{p_{amb}}{p_{sl}} \right) = \frac{p_{iso}}{p_{sl}} e^{-\left(\frac{g}{RT_{iso}} \right)(h-11km)} \tag{2.141}$$

where the subscript 'iso' refers to conditions at the bottom of the isothermal layer (11 km).

The final equation, which calculates ambient density, is valid regardless of the atmospheric region. It is the ideal gas equation of state.

$$\rho_{amb} = \frac{p_{amb}}{RT_{amb}} \tag{2.142}$$

The relationship between density and altitude is illustrated in Figure 2.22.

-53-
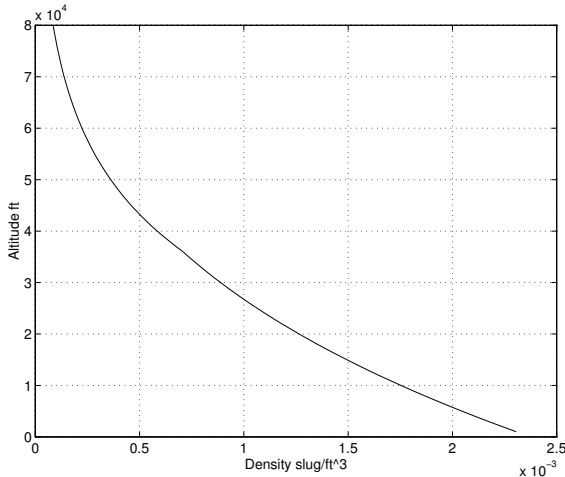
Figure 2.22. Density variation with altitude for the standard atmosphere

2.13   Integration Techniques

The TGF simulation as designed requires the real time integration of a series of nonlinear differential equations and one linear differential equation, Equation (2.93). Since nonlinear differential equations cannot be solved analytically, some type of numerical integration method must be employed. There are many techniques available, so it is important to find a technique well-suited to the needs of a particular problem. There are several items to consider when choosing a numerical algorithm. These are:

1. Accuracy required.
2. Frequency of the dynamics to be simulated.
3. The computational efficiency required.
4. The stability of the algorithm.

The most demanding integration requirements for the TGF project stem from the Phugoid mode of the longitudinal dynamics. This mode generally has a period of 30 sec, which is not very fast. Therefore, a sophisticated numerical algorithm need not be applied. Furthermore, the integrations that are not influenced by the Phugoid mode require even less computational precision. For the Phugoid influenced equations, a good second order method should suffice. For the non-Phugoid influenced equations, a first order method is quite adequate.

2.13.1   The Second Order Runge-Kutta Method

A second order Runge-Kutta method is chosen for those equations that are influenced by the Phugoid mode. This method, is simple and stable. It is self starting and does not require information from previous time steps. It is slightly more computationally expensive than other methods such as an Adams-Bashforth method, but the use of the Adams-Bashforth method did not prove as stable as the Runge-Kutta method and

required a more complex algorithm because it is not self starting. These methods are discussed in detail in Hoffman (1992), or any other numerical method text.

The second order Runge-Kutta algorithm is summarized below. Consider a state vector, $\mathbf{X}(k)$, at time step, k, and, $t(k)$, the time at step, k. These are the inputs to the numerical integrator.

$$\mathbf{X}(k) = \begin{bmatrix} x_1(k) \\ x_2(k) \\ \vdots \\ x_n(k) \end{bmatrix} \tag{2.143}$$

It is our objective to update the state vector to the next time step at $(k+1)$. To do this we must first calculate $\mathbf{K}_0$, the initial term of the Runge-Kutta integration sequence. The numerical integration routine does not actually do this. Instead, it uses a series of functions of the states and the independent variable, time, as shown in Equation(2.144). For our problem, the functions $f_1 - f_n$ are the state equations (2.61), (2.66), and (2.67).

$$\mathbf{K}_0 = \begin{bmatrix} k_{o_1} \\ k_{o_2} \\ \vdots \\ k_{o_n} \end{bmatrix} = \begin{bmatrix} f_1(x_1(k), x_2(k), \cdots x_n(k), t(k), ...) \\ f_2(x_1(k), x_2(k), \cdots x_n(k), t(k), ...) \\ \vdots \\ f_n(x_1(k), x_2(k), \cdots x_n(k), t(k), ...) \end{bmatrix} \Delta t \tag{2.144}$$

The numerical integration routine will take $\mathbf{K}_0$ and add it to the original state vector at time step (k) and then send the results back to the derivative functions. This results in $\mathbf{K}_1$.

$$\mathbf{K}_1 = \begin{bmatrix} k_{1_1} \\ k_{1_2} \\ \vdots \\ k_{1_n} \end{bmatrix} = \begin{bmatrix} f_1(x_1(k)+k_{o_1}, x_2(k)k_{o_2}, \cdots, x_n(k)+k_{o_n}+, t(k)+\Delta t, ...) \\ f_2(x_1(k)+k_{o_1}, x_2(k)k_{o_2}, \cdots, x_n(k)+k_{o_n}+, t(k)+\Delta t, ...) \\ \vdots \\ f_n(x_1(k)+k_{o_1}, x_2(k)k_{o_2}, \cdots, x_n(k)+k_{o_n}+, t(k)+\Delta t, ...) \end{bmatrix} \Delta t \tag{2.145}$$

The final step is to determine, $\mathbf{X}(k+1)$.

$$\mathbf{X}(k+1) = \begin{bmatrix} x_1(k) \\ x_2(k) \\ \vdots \\ x_n(k) \end{bmatrix} + \frac{1}{2}\left(\begin{bmatrix} k_{o_1} \\ k_{o_2} \\ \vdots \\ k_{o_n} \end{bmatrix} + \begin{bmatrix} k_{1_1} \\ k_{1_2} \\ \vdots \\ k_{1_n} \end{bmatrix}\right) \qquad (2.146)$$

The equations that are integrated using the second order Runge-Kutta technique are Equations (2.61), (2.66), and (2.67) or the true airspeed, flight path angle, and the heading angle state variable equations.

2.13.2 The First Order Euler Method

The first order Euler method is arguably the simplest numerical integration routine available. Under most conditions, it is not considered adequate for actual simulation, but rather is used only as an instructional example. However it is very inexpensive computationally, and is more than adequate for the very slow changes in altitude, position and weight changes occurring in the TGF model. Using the same $\mathbf{X}(k)$ vector defined in (2.143), the next time step, $\mathbf{X}(k+1)$, is easily calculated using Equation (2.147).

$$\mathbf{X}(k+1) = \begin{bmatrix} x_1(k) \\ x_2(k) \\ \vdots \\ x_n(k) \end{bmatrix} + \begin{bmatrix} f_1(x_1(k), x_2(k), \cdots x_n(k), t(k), \ldots) \\ f_2(x_1(k), x_2(k), \cdots x_n(k), t(k), \ldots) \\ \vdots \\ f_n(x_1(k), x_2(k), \cdots x_n(k), t(k), \ldots) \end{bmatrix} \Delta t \qquad (2.147)$$

The quantities that are integrated by this method are as follows:

- Latitude
- Longitude
- Weight
- Altitude

2.14   The Integration of the Roll Equation

The roll equation is unique in our simulation because it is the only differential equation that is linear. Because the equation is linear, no numerical integration technique need be applied. Furthermore, we can perform the loop closures of our lateral directional control logic within the analytic solution itself, eliminating the aileron deflection parameter, δ_a, via a linear control law.

2.14.1 The open loop roll rate and roll angle equations

The roll mode is governed by Equation (2.93), which is reprinted below. It is convenient to assign $\dot{\phi}$, the derivative of the roll angle, to p, the roll rate. This yields Equation (2.148). These two equations yield the second order dynamics that characterize an aircraft's roll angle in response to deflection of the ailerons.

$$\dot{p} = L_p p + L_{\delta_a} \delta_a \tag{2.93}$$

$$\dot{\phi} = p \tag{2.148}$$

It is convenient to arrange the equations into state space representation.

$$\begin{bmatrix} \dot{p} \\ \dot{\phi} \end{bmatrix} = \begin{bmatrix} L_p & 0 \\ 1 & 0 \end{bmatrix} \begin{bmatrix} p \\ \phi \end{bmatrix} + \begin{bmatrix} L_{\delta_a} \\ 0 \end{bmatrix} \delta_a \tag{2.149}$$

The system of equation (2.149) yields the lateral dynamic response to commanded ailerons. The desired system is one in which a desired roll angle is commanded and the aircraft responds accordingly, and so we move on to closing this loop.

2.14.2 The closed loop system

We here continue to describe the lateral dynamic system, equations (2.149), as a linear, time-dependent (LTD) system of equations. The system follows the common LTD vector-matrix form,

$$\dot{\mathbf{x}}(t) = \mathbf{A}\mathbf{x}(t) + \mathbf{B}\mathbf{u}(t), \tag{2.150}$$

in which the state vector, $\mathbf{x}$, contains the roll rate, p, and the roll angle, ϕ, and the control vector, $\mathbf{u}$, contains only the aileron deflection parameter, δ_a. We accordingly define a linear feedback controller that is based on the difference between the desired and actual state.

$$\mathbf{u} = \mathbf{K}\left(\mathbf{x}_{\mathrm{des}} - \mathbf{x}\right)$$

The LTD system then becomes,

$$\begin{aligned} \dot{\mathbf{x}} &= \mathbf{A}\mathbf{x} + \mathbf{B}\left\{\mathbf{K}\left(\mathbf{x}_{\mathrm{des}} - \mathbf{x}\right)\right\} \\ \dot{\mathbf{x}} &= \left(\mathbf{A} - \mathbf{B}\mathbf{K}\right)\mathbf{x} + \left(\mathbf{B}\mathbf{K}\right)\mathbf{x}_{\mathrm{des}} \end{aligned}, \tag{2.151}$$

In this case, the gain matrix is (2x1).

$$\mathbf{K} = \begin{bmatrix} k_p \\ k_\phi \end{bmatrix}$$

Expanding into the nomenclature of our lateral dynamics, the closed-loop state space system is

$$\begin{bmatrix} \dot{p} \\ \dot{\phi} \end{bmatrix} = \begin{bmatrix} L_p - L_{\delta_a} k_p & -L_{\delta_a} k_\phi \\ 1 & 0 \end{bmatrix} \begin{bmatrix} p \\ \phi \end{bmatrix} + \begin{bmatrix} L_{\delta_a} k_p & L_{\delta_a} k_\phi \\ 0 & 0 \end{bmatrix} \begin{bmatrix} p_{des} \\ \phi_{des} \end{bmatrix} \qquad (2.152)$$

where p_{des} is the desired roll rate and ϕ_{des} is the desired roll angle. We do not actually allow a command p_{des} so we can eliminate it from Equation (2.152).

$$\begin{bmatrix} \dot{p} \\ \dot{\phi} \end{bmatrix} = \begin{bmatrix} L_p - L_{\delta_a} k_p & -L_{\delta_a} k_\phi \\ 1 & 0 \end{bmatrix} \begin{bmatrix} p \\ \phi \end{bmatrix} + \begin{bmatrix} 0 & L_{\delta_a} k_\phi \\ 0 & 0 \end{bmatrix} \begin{bmatrix} 0 \\ \phi_{des} \end{bmatrix} \qquad (2.153)$$

The system we have developed is a second-order, linear system. It is completely defined by the modal properties of the standard second-order system, which we can determine by comparing the characteristic equation of equation (2.153) to that of the standard second-order system.

$$\det\left(s\mathbf{I} - \mathbf{A}_{cl}\right) = s^2 - \left(L_p - L_{\delta_a} k_p\right)s - L_{\delta_a} k_\phi = s^2 + 2\zeta\omega_n s + \omega_n^2$$

The modal properties are determined by inspection.

$$2\zeta\omega_n = -\left(L_p - L_{\delta_a} k_p\right)$$
$$\omega_n^2 = L_{\delta_a} k_\phi \qquad (2.154)$$

We can completely define the lateral dynamic response of different aircraft models by specifying the natural frequency, ω_n, and damping ratio, ζ. We have essentially replaced four parameters with two. Additionally, the aileron deflection parameter has been eliminated. The primary control parameter in its place is the desired roll angle. We rewrite the LTD system as a function of the two modal properties and the desired roll angle.

$$\begin{bmatrix} \dot{p} \\ \dot{\phi} \end{bmatrix} = \begin{bmatrix} -2\zeta\omega_n & -\omega_n^2 \\ 1 & 0 \end{bmatrix} \begin{bmatrix} p \\ \phi \end{bmatrix} + \begin{bmatrix} 0 & \omega_n^2 \\ 0 & 0 \end{bmatrix} \begin{bmatrix} 0 \\ \phi_{des} \end{bmatrix} \tag{2.155}$$

2.14.3 An Analytical Solution in the Discrete Time Interval

Our system is still in the form of equation (2.150), with the control vector, **u**, defined as the desired state vector. As stated earlier, because the system is linear, we can develop an analytical solution in the time interval of our computer simulation, thereby eliminating the need for numerical integration. The state vector is known at the beginning of the interval, the control vector is known and constant in the interval, and so we can solve equation (2.150) analytically for the state vector at the end of the interval.

If the control vector were time-dependent in the interval, the well-known (e.g., Ogata, 1990, eq. 11-41) analytical solution to equation (2.150) is given by equation (2.156).

$$\mathbf{x}(t) = e^{\mathbf{A}t}\mathbf{x}(0) + \int_0^t e^{-\mathbf{A}(t-\tau)}\mathbf{B}\mathbf{u}(\tau)d\tau \tag{2.156}$$

The state transition matrix, $e^{\mathbf{A}t}$, is defined as the inverse Laplace transform of the characteristic matrix.

$$e^{\mathbf{A}t} \equiv \mathcal{L}^{-1}\left[\left(s\mathbf{I} - \mathbf{A}\right)^{-1}\right]$$

However, since the control vector of equation (2.155) is constant in the discrete-time simulation interval from $0 \le t \le \Delta t$, we can derive a simpler solution. The control vector is one-dimensional, containing only the desired bank angle and is independent of time in the interval. Let us rewrite equation (2.155) in a shortened notation, replacing the constant closed-loop matrices with A_{cl} and B_{cl}, respectively.

$$\dot{\mathbf{x}}(t) = \mathbf{A}_{cl}\mathbf{x}(t) + \mathbf{B}_{cl}\phi_{des}$$

We transform this equation to the Laplace domain and solve for $x(s)$

$$\mathbf{x}(s) = \left(s\mathbf{I} - \mathbf{A}_{cl}\right)^{-1}\mathbf{x}_0 + \frac{1}{s}\left(s\mathbf{I} - \mathbf{A}_{cl}\right)^{-1}\mathbf{B}_{cl}\phi_{des} \tag{2.157}$$

Equation (2.157) is now a convenient and transformable function of the Laplace variable. We arrive at a solution in the time domain by taking the inverse Laplace transform. This solution is identical to the solution obtained from equation (2.156) with constant control.

$$\mathbf{x}(t) = \mathcal{L}^{-1}\left[\left(s\mathbf{I} - \mathbf{A}_{cl}\right)^{-1}\right]\mathbf{x}_0 + \mathcal{L}^{-1}\left[\frac{1}{s}\left(s\mathbf{I} - \mathbf{A}_{cl}\right)^{-1}\mathbf{B}_{cl}\right]\phi_{des} \qquad (2.158)$$

To allow for the complete range of lateral dynamic design, we choose to handle the solution differently for different values of the damping ratio, ζ. For the case of the under-damped ($\zeta < 1$) system, in which the system poles are complex conjugate pairs and the solution is oscillatory, it is convenient to keep equation (2.157) in the notation of the modal properties.

$$\mathbf{x}(s) = \begin{bmatrix} \dfrac{s}{s^2 + 2\zeta\omega_n s + \omega_n^2} & (-1)\dfrac{\omega_n^2}{s^2 + 2\zeta\omega_n s + \omega_n^2} \\[3mm] \left(\dfrac{1}{\omega_n^2}\right)\dfrac{\omega_n^2}{s^2 + 2\zeta\omega_n s + \omega_n^2} & \dfrac{s + 2\zeta\omega_n}{s^2 + 2\zeta\omega_n s + \omega_n^2} \end{bmatrix}\mathbf{x}_0 + \begin{bmatrix} \dfrac{\omega_n^2}{s^2 + 2\zeta\omega_n s + \omega_n^2} \\[3mm] \dfrac{\omega^2}{s\left(s^2 + 2\zeta\omega_n s + \omega_n^2\right)} \end{bmatrix}\phi_{des} \quad (2.159)$$

For the critically damped system ($\zeta = 1$), the characteristic equation contains a double pole at $s = -\omega_n$ and equation (2.157) can be rearranged into a more convenient form.

$$\mathbf{x}(s) = \begin{bmatrix} \dfrac{s}{\left(s + \omega_n\right)^2} & (-\omega_n^2)\dfrac{1}{\left(s + \omega_n\right)^2} \\[3mm] \dfrac{1}{\left(s + \omega_n\right)^2} & \dfrac{s + 2\omega_n}{\left(s + \omega_n\right)^2} \end{bmatrix}\mathbf{x}_0 + \begin{bmatrix} \left(\omega_n^2\right)\dfrac{1}{\left(s + \omega_n\right)^2} \\[3mm] \left(\omega^2\right)\dfrac{1}{s\left(s + \omega_n\right)^2} \end{bmatrix}\phi_{des} \qquad (2.160)$$

For the over-damped system, the system poles are real. We solve the characteristic equation for the system poles at $s = -a$ and $s = -b$, where,

$$a, b = \zeta\omega_n\left(1 \pm \sqrt{1 - \frac{1}{\zeta}}\right)$$

We can now rearrange equation (2.157) in terms of a and b.

$$\mathbf{x}(s) = \begin{bmatrix} \dfrac{s}{(s+a)(s+b)} & (-ab)\dfrac{1}{(s+a)(s+b)} \\[3mm] \dfrac{1}{(s+a)(s+b)} & \dfrac{s + (a+b)}{(s+a)(s+b)} \end{bmatrix}\mathbf{x}_0 + \begin{bmatrix} \dfrac{1}{(s+a)(s+b)} \\[3mm] \dfrac{1}{s(s+a)(s+b)} \end{bmatrix}ab\phi_{des} \quad (2.161)$$

Table 2.5 presents Laplace transforms applicable to equation (2.157), as found in commonly available Laplace transform sources. From these Laplace transforms we can

write the solutions to equations (2.158) - (2.161) in the time domain. First we write the solution for the under-damped case.

$$
\begin{bmatrix} p(t) \\ \phi(t) \end{bmatrix} = e^{-\zeta\omega_n t}
\begin{bmatrix}
-\dfrac{1}{\sqrt{1-\zeta^2}}\sin\left(\omega_n\sqrt{1-\zeta^2}\,t-\theta\right) & -\dfrac{\omega_n}{\sqrt{1-\zeta^2}}e^{-\zeta\omega t}\sin\left(\omega_n\sqrt{1-\zeta^2}\,t\right) \\[3mm]
\dfrac{1}{\omega_n\sqrt{1-\zeta^2}}\sin\left(\omega_n\sqrt{1-\zeta^2}\,t\right) & \dfrac{1}{\sqrt{1-\zeta^2}}\sin\left(\omega_n\sqrt{1-\zeta^2}\,t+\theta\right)
\end{bmatrix}
\begin{bmatrix} p(0) \\ \phi(0) \end{bmatrix}
$$

$$
+
\begin{bmatrix}
\dfrac{\omega_n}{\sqrt{1-\zeta^2}}e^{-\zeta\omega t}\sin\left(\omega_n\sqrt{1-\zeta^2}\,t\right) \\[3mm]
1-\dfrac{1}{\sqrt{1-\zeta^2}}e^{-\zeta\omega t}\sin\left(\omega_n\sqrt{1-\zeta^2}\,t+\theta\right)
\end{bmatrix}\phi_{des}
\qquad (2.162)
$$

Next we write the solution for the critically-damped case.

$$
\begin{bmatrix} p(t) \\ \phi(t) \end{bmatrix} =
\begin{bmatrix}
e^{-\omega_n t}-\omega_n t e^{-\omega_n t} & -\omega_n^2 t e^{-\omega_n t} \\[2mm]
t e^{-\omega_n t} & e^{-\omega_n t}+\omega_n t e^{-\omega_n t}
\end{bmatrix}
\begin{bmatrix} p(0) \\ \phi(0) \end{bmatrix} +
\begin{bmatrix}
\omega_n^2 t e^{-\omega_n t} \\[2mm]
1-e^{-\omega_n t}-\omega_n t e^{-\omega_n t}
\end{bmatrix}\phi_{des} \quad (2.163)
$$

And, finally, we write the solution for the over-damped case.

$$
\begin{bmatrix} p(t) \\ \phi(t) \end{bmatrix} =
\begin{bmatrix}
\dfrac{1}{b-a}\left(be^{-bt}-ae^{-at}\right) & \dfrac{-ab}{b-a}\left(e^{-at}-e^{-bt}\right) \\[3mm]
\dfrac{1}{b-a}\left(e^{-at}-e^{-bt}\right) & \dfrac{1}{b-a}\left(be^{-at}-ae^{-bt}\right)
\end{bmatrix}
\begin{bmatrix} p(0) \\ \phi(0) \end{bmatrix} +
\begin{bmatrix}
\dfrac{ab}{b-a}\left(e^{-at}-e^{-bt}\right) \\[3mm]
1+\dfrac{1}{a-b}\left(be^{-bt}-ae^{-at}\right)
\end{bmatrix}\phi_{des} \quad (2.164)
$$

Equations (2.162) - (2.164) (all of which are in the form of equation (2.158)) provide an analytical solution for the state vector at any time, *t*, when the initial value of the state vector (at *t=0*) is known. We can apply this solution across a discrete time interval, *Δt*, by setting the initial state vector, *[p(0);φ(0)]* to that at the start of the interval and solving for *[p(Δt);φ(Δt)]* using the relevant equation. The solution at the end of the interval is then a constant matrix function of the initial state and the desired bank angle.

It is important to note that the constant matrices need only be calculated once for a given aircraft and time step size. (For a varying time step, the matrices would need to be calculated each time.) Once the initial calculations are made, the relations used to update the state from one time step to another are simple. For instance, consider an aircraft with critically damped lateral dynamics defined as below.

Table 2.5. Common Laplace Transform Pairs

Laplace Domain	Time Domain
$\mathcal{L}^{-1}\left[\dfrac{\omega_n^2}{s^2 + 2\zeta\omega_n s + \omega_n^2}\right]$	$= \dfrac{\omega_n}{\sqrt{1-\zeta^2}} e^{-\zeta\omega_n t} \sin\left(\omega_n \sqrt{1-\zeta^2}\, t\right)$
$\mathcal{L}^{-1}\left[\dfrac{s}{s^2 + 2\zeta\omega_n s + \omega_n^2}\right]$	$= -\dfrac{1}{\sqrt{1-\zeta^2}} e^{-\zeta\omega_n t} \sin\left(\omega_n \sqrt{1-\zeta^2}\, t - \theta\right), \quad \theta = \tan^{-1}\dfrac{\sqrt{1-\zeta^2}}{\zeta}$
$\mathcal{L}^{-1}\left[\dfrac{s + 2\zeta\omega_n}{s^2 + 2\zeta\omega_n s + \omega_n^2}\right]$	$= \dfrac{1}{\sqrt{1-\zeta^2}} e^{-\zeta\omega_n t} \sin\left(\omega_n \sqrt{1-\zeta^2}\, t + \theta\right)$
$\mathcal{L}^{-1}\left[\dfrac{\omega_n^2}{s\left(s^2 + 2\zeta\omega_n s + \omega_n^2\right)}\right]$	$= 1 - \dfrac{1}{\sqrt{1-\zeta^2}} e^{-\zeta\omega_n t} \sin\left(\omega_n \sqrt{1-\zeta^2}\, t + \theta\right)$
$\mathcal{L}^{-1}\left[\dfrac{1}{(s+a)(s+b)}\right]$	$= \dfrac{1}{b-a}\left(e^{-at} - e^{-bt}\right)$
$\mathcal{L}^{-1}\left[\dfrac{s}{(s+a)(s+b)}\right]$	$= \dfrac{1}{b-a}\left(be^{-bt} - ae^{-at}\right)$
$\mathcal{L}^{-1}\left[\dfrac{1}{s(s+a)(s+b)}\right]$	$= \dfrac{1}{ab}\left[1 + \dfrac{1}{a-b}\left(be^{-bt} - ae^{-at}\right)\right]$
$\mathcal{L}^{-1}\left[\dfrac{s+(a+b)}{(s+a)(s+b)}\right]$	$= \dfrac{1}{b-a}\left(be^{-at} - ae^{-bt}\right)$
$\mathcal{L}^{-1}\left[\dfrac{1}{(s+a)^2}\right]$	$= te^{-at}$
$\mathcal{L}^{-1}\left[\dfrac{s}{(s+a)^2}\right]$	$= \dfrac{d}{dt}\left(te^{-at}\right) = e^{-at} - ate^{-at}$
$\mathcal{L}^{-1}\left[\dfrac{1}{s(s+a)^2}\right]$	$= \dfrac{1}{a^2}\left[1 - e^{-at} - ate^{-at}\right]$
$\mathcal{L}^{-1}\left[\dfrac{s+2a}{(s+a)^2}\right]$	$= e^{-at} + ate^{-at}$

$$\omega_n = 2\ rad/sec$$
$$\zeta = 1$$

Discretizing the system for a 0.5 sec time step, using Equation (2.163), the system becomes.

$$\begin{bmatrix} p(k+1) \\ \phi(k+1) \end{bmatrix} = \begin{bmatrix} 0.9606 & -0.0392 \\ 0.0098 & 0.9998 \end{bmatrix}\begin{bmatrix} p(k) \\ \phi(k) \end{bmatrix} + \begin{bmatrix} 0.0392 \\ 0.0002 \end{bmatrix}\phi_{des}(k) \qquad (2.165)$$

If the state vector (roll rate and angle) is zero at the beginning of the interval and the control (desired roll angle) is 30° (0.523 rad), equation (2.165) would yield a roll rate of 1.2 deg/sec and a roll angle of 0.006° at the end of the interval. Equation (2.165) is the only calculation that must be made to update between time steps.

2.15 Design of the Lateral Control System

We need to determine appropriate values for the modal properties of the lateral dynamics. While the lateral dynamic system was modeled using the stability derivatives, $L_{\delta a}$ and L_p, and the control gains, k_p and k_ϕ, it was revealed above (refer to equations (2.154)) that we need only determine appropriate values for the frequency and damping ratio of the lateral dynamics.

Let's analyze the step response to the critically system with zero initial condition. Table 16.2 of Raymer (1999) provides the specifications for the rolling performance of military aircraft per MIL-F-8785 B. From this table, we can conclude that similar commercial aircraft should be capable of achieving a 30° bank in 1.5 – 2.0 seconds. We shall assume that this time guideline refers to a settling time, T_s, of about four time constants.

$$T_s = \frac{4}{\zeta \omega_n}$$

From equation (2.163), the roll equation with zero initial condition is as follows.

$$\phi(t) = \left(1 - e^{-\omega_n t} - \omega_n t e^{-\omega_n t}\right)\phi_{des}$$

Figure 2.23 shows the response of this equation using a 30-degree desired bank angle, a natural frequency of 2 rad/sec. The reader will note that the modal properties used to create Figure 2.23 correspond to a time constant of two seconds. At a settling time of two seconds, the roll angle is within about 10% of the desired state. We can create aircraft models with faster lateral dynamics by increasing the time constant, $\zeta \omega_n$.
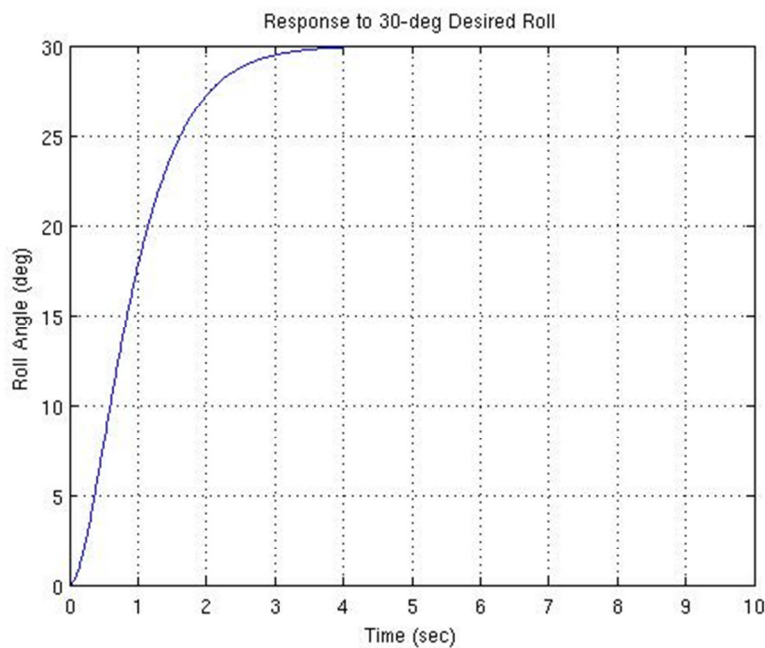
Figure 2.23. Roll mode response to a 30 degree desired bank angle

THIS PAGE INTENTIONALLY LEFT BLANK

3. The Examination of the Longitudinal Dynamics

It can be argued that the majority of the effort put forth to build a successful feedback control system is spent trying to understand the plant that is to be controlled. This certainly is the case with the nonlinear longitudinal aircraft dynamics. The insight developed is a fundamental tool used to make intelligent decisions regarding feedback control strategy. This chapter deals with the development of solid insight into the plant dynamics, in this case the longitudinal dynamics of the aircraft. To develop insight, several tasks are performed. These tasks are:

- Develop a linear model of the longitudinal dynamics
- Analysis of longitudinal modal properties
- Transfer function analysis of the longitudinal dynamics.

The linear model of the aircraft dynamics is a fundamental tool that allows for the modal analysis and the examination of the response to inputs via the transfer functions. Modal analysis of the linear model enables identification of the physical properties that affect the modal properties of the system. Finally, certain transfer functions are created from the linear model that give insight into the different feedback control strategies that can be used. It should be noted that the linear model of the longitudinal dynamics is not replacing its nonlinear parents in the dynamic simulation; it is merely being used as a learning tool.

3.1 The Linear Model of the Longitudinal Dynamics

The modeling equations for the aircraft dynamics, as presented in Table 2.3, are nonlinear with the exception of Equation (2.70). This nonlinearity limits our ability to perform an in depth study into the behavior of the system of equations and also precludes the design of a feedback control system. To overcome this limitation, a common approach in feedback control is to develop a linearized version of the system of equations.

In our linear modeling of the system of equations, we choose to separate the longitudinal dynamics from the lateral-directional dynamics. We can do this because the longitudinal modes and the lateral-directional modes are only lightly coupled (Nelson, 1989). For the longitudinal case, we constrain the aircraft to not turn.

The general form of a non-linear dynamic system is a representation of the state vector as a non-linear differential equation, and the output vector as a separate non-linear function. Both functions are generally dependent on the state, control, and time.

$$\dot{\mathbf{x}} = \mathbf{f}(\mathbf{x}, \mathbf{u}, t)$$
$$\mathbf{y} = \mathbf{g}(\mathbf{x}, \mathbf{u}, t)$$

(3.166)

In this system, **x** is the system's (in our case, the aircraft's) state vector, **u** is the system's control vector, **y** is the system's output vector. The control law is user-defined and is typically based on driving the observable output to a desired condition. While it is not typical to express a generalized control law, we can present one here to illustrate that, once the state and desired output are known, the system has a unique solution.

$$\mathbf{u} = \mathbf{u}(\mathbf{y}, \mathbf{y_d})$$

In classical control theory, a linear, time-dependent (LTD) state-space is represented by the following system.

$$\dot{\mathbf{x}}(t) = \mathbf{A}\mathbf{x}(t) + \mathbf{B}\mathbf{u}(t)$$
$$\mathbf{y}(t) = \mathbf{C}\mathbf{x}(t) + \mathbf{D}\mathbf{u}(t)$$

(3.167)

In this system, **A**, **B**, **C**, and **D** are constant matrices. The state vector is a collection of variables that completely describes the system's state at any given time. Our longitudinal state vector includes true airspeed, V_a, flight path angle, γ_a, and altitude, h. The control vector is the system's control inputs. Our longitudinal control vector includes lift coefficient, C_L and thrust, T. In discrete time, if the state and the control inputs at a given time-step are known, the state equation yields the state at the next time-step.

The output vector contains those parameters that are readily measurable by the controller. The aircraft (and, consequently, the aircraft's controller) may not know its true airspeed or its flight path angle, but it is able to measure its indicated airspeed, V_{IAS}, Mach number, M, altitude, h, and altitude rate, $\dot{h}$, and these parameters make up the output vector.

Equations (2.61) and (2.66) are the focus of the longitudinal dynamics. These two equations characterize the Phugoid mode of the aircraft. To get the appropriate altitude information, we include the vertical component of the vector equation (2.73) to our system of equations, as shown in equation (3.168). Altitude rate, $\dot{h}$, and altitude, h, are both needed for the feedback control of the longitudinal dynamics. The equations for the longitudinal dynamics are repeated here.

$$\dot{V}_a = \frac{T - D - mg\sin\gamma_a}{m}$$

(2.61)

$$\dot{\gamma}_a = \frac{L\cos\phi - mg\cos\gamma_a}{mV_a} \tag{2.66}$$

$$\dot{h} = V_a \sin\gamma_a \tag{3.168}$$

Within these equations are the terms L and D, which are functions of the state variables. However, the terms L and D are not explicitly defined in terms of the state variables. To do this we need to know the aerodynamic characteristics.

Using the airframe equations of section 2.9, we can express lift and drag and their related coefficients. As discussed in Section 2.6, we know that the lift coefficient will be treated as a control input to the system, and will not be a function of the states.

$$L = \tfrac{1}{2}\rho V_a^2 S_w C_L \tag{3.169}$$

The aircraft drag can be similarly expressed.

$$D = \tfrac{1}{2}\rho V_a^2 S_w C_D \tag{3.170}$$

where the drag coefficient, C_D, of equation (2.131) is restated here.

$$C_D = C_{D_o} + K\left(C_L - C_{L_{min\,drag}}\right)^2 \tag{2.131}$$

We need to express the total drag in terms of the drag coefficient.

$$D = \tfrac{1}{2}\rho V_a^2 S_w \left[C_{D_o} + K\left(C_L - C_{L_{min\,drag}}\right)^2\right] \tag{3.171}$$

These relations for lift and drag need to be substituted into the state equations. Equations (2.61) and (3.171) are combined to get the explicit state equation for true airspeed.

$$\dot{V}_a = \frac{T - \tfrac{1}{2}\rho V_a^2 S_w \left[C_{D_o} + K\left(C_L - C_{L_{min\,drag}}\right)^2\right] - mg\sin\gamma_a}{m} \tag{3.172}$$

Equations (2.66) and (3.169) are combined to get the explicit flight path angle equation.

$$\dot{\gamma}_a = \frac{\tfrac{1}{2}\rho V_a^2 S_w C_L \cos\phi - mg\cos\gamma_a}{mV_a} \tag{3.173}$$

We can represent Equations (3.172), (3.173), and (3.168) simply as functions of the state and control variables. This is our non-linear system.

$$\dot{V_a} = f_{V_a}(V_a, \gamma_a, h, C_L, T)$$

$$\dot{\gamma_a} = f_{\gamma_a}(V_a, \gamma_a, h, C_L, T)$$

$$\dot{h} = f_h(V_a, \gamma_a, h, C_L, T)$$

We wish to express the longitudinal dynamics as an LTD state-space, as in equation (3.167). This will facilitate an analysis of the modal properties. It will also facilitate the computation of feedback gains in Section 4.

To create a linear system from a non-linear system, we perform a Taylor series expansion about a reference condition (identified with subscript '0') and, assuming perturbations from the reference condition are small, keep only first-order terms.

$$\dot{V_a}\Big|_o + \Delta\dot{V_a} = f_{V_a}\Big|_o + \frac{\partial f_{V_a}}{\partial V_a}\Big|_o \Delta V_a + \frac{\partial f_{V_a}}{\partial \gamma_a}\Big|_o \Delta \gamma_a + \frac{\partial f_{V_a}}{\partial h}\Big|_o \Delta h + \frac{\partial f_{V_a}}{\partial T}\Big|_o \Delta T + \frac{\partial f_{V_a}}{\partial C_L}\Big|_o \Delta C_L$$

$$\dot{\gamma_a}\Big|_o + \Delta\dot{\gamma_a} = f_{\gamma_a}\Big|_o + \frac{\partial f_{\gamma_a}}{\partial V_a}\Big|_o \Delta V_a + \frac{\partial f_{\gamma_a}}{\partial \gamma_a}\Big|_o \Delta \gamma_a + \frac{\partial f_{\gamma_a}}{\partial h}\Big|_o \Delta h + \frac{\partial f_{\gamma_a}}{\partial T}\Big|_o \Delta T + \frac{\partial f_{\gamma_a}}{\partial C_L}\Big|_o \Delta C_L$$

$$\dot{h}\Big|_o + \Delta\dot{h} = f_h\Big|_o + \frac{\partial f_h}{\partial V_a}\Big|_o \Delta V_a + \frac{\partial f_h}{\partial \gamma_a}\Big|_o \Delta \gamma_a + \frac{\partial f_h}{\partial h}\Big|_o \Delta h + \frac{\partial f_h}{\partial T}\Big|_o \Delta T + \frac{\partial f_h}{\partial C_L}\Big|_o \Delta C_L$$

Similarly, the parameters of the output vector are repeated here.

$$V_{IAS} = a_0^* \sqrt{\frac{2}{\gamma-1}\left(\left\{\frac{p}{p_o}\left[\left(1+\frac{\gamma-1}{2}M^2\right)^{\frac{\gamma}{(\gamma-1)}}-1\right]+1\right\}^{\frac{(\gamma-1)}{\gamma}}-1\right)} \tag{2.119}$$

$$M = \frac{V_a}{a^*} \tag{2.121}$$

$$h = h$$

$$\dot{h} = V_a \sin \gamma_a \tag{3.168}$$

Once again, we can represent these equations as functions of the state and control variables.

$$V_{IAS} = g_{V_{IAS}}(V_a, \gamma_a, h, C_L, T)$$
$$M = g_M(V_a, \gamma_a, h, C_L, T)$$
$$h = g_h(V_a, \gamma_a, h, C_L, T)$$
$$\dot{h} = g_{\dot{h}}(V_a, \gamma_a, h, C_L, T) = f_{\dot{h}}(V_a, \gamma_a, h, C_L, T)$$

The linearized perturbation equations of the output vector are,

$$V_{IAS}\big|_o + \Delta V_{IAS} = g_{V_{IAS}}\big|_o + \frac{\partial g_{V_{IAS}}}{\partial V_a}\bigg|_o \Delta V_a + \frac{\partial g_{V_{IAS}}}{\partial \gamma_a}\bigg|_o \Delta \gamma_a + \frac{\partial g_{V_{IAS}}}{\partial h}\bigg|_o \Delta h + \frac{\partial g_{V_{IAS}}}{\partial T}\bigg|_o \Delta T + \frac{\partial g_{V_{IAS}}}{\partial C_L}\bigg|_o \Delta C_L$$

$$M\big|_o + \Delta M = g_M\big|_o + \frac{\partial g_M}{\partial V_a}\bigg|_o \Delta V_a + \frac{\partial g_M}{\partial \gamma_a}\bigg|_o \Delta \gamma_a + \frac{\partial g_M}{\partial h}\bigg|_o \Delta h + \frac{\partial g_M}{\partial T}\bigg|_o \Delta T + \frac{\partial g_M}{\partial C_L}\bigg|_o \Delta C_L$$

$$h\big|_o + \Delta h = g_h\big|_o + \frac{\partial g_h}{\partial V_a}\bigg|_o \Delta V_a + \frac{\partial g_h}{\partial \gamma_a}\bigg|_o \Delta \gamma_a + \frac{\partial g_h}{\partial h}\bigg|_o \Delta h + \frac{\partial g_h}{\partial T}\bigg|_o \Delta T + \frac{\partial g_h}{\partial C_L}\bigg|_o \Delta C_L$$

$$\dot{h}\big|_o + \Delta \dot{h} = f_h\big|_o + \frac{\partial f_{\dot{h}}}{\partial V_a}\bigg|_o \Delta V_a + \frac{\partial f_{\dot{h}}}{\partial \gamma_a}\bigg|_o \Delta \gamma_a + \frac{\partial f_{\dot{h}}}{\partial h}\bigg|_o \Delta h + \frac{\partial f_{\dot{h}}}{\partial T}\bigg|_o \Delta T + \frac{\partial f_{\dot{h}}}{\partial C_L}\bigg|_o \Delta C_L$$

A partial derivative of a system equation is called a stability derivative if it is with respect to a state variable and a control derivative if it is with respect to a control variable. The stability and control derivatives for the longitudinal model are organized in tabular form and presented in Table 3.6, Table 3.7, and Table 3.8. It is important to note that these derivatives are derived specifically for the 4 DOF model that we have constructed. These derivatives are similar, but not interchangeable with the classic stability and control derivatives of the full 6 DOF equations of motion such as those found in Nelson (1989) or Stevens and Lewis (1992).

By inspection, we see that the partial derivatives of $g_{V_{IAS}}$, g_M, and g_h are all zero except

for $\dfrac{\partial g_{V_{IAS}}}{\partial V_a}$, $\dfrac{\partial g_M}{\partial V_a}$ and $\dfrac{\partial g_h}{\partial h}$. From equations (2.119) and (2.121),

$$\frac{\partial g_M}{\partial V_a} = \frac{\partial}{\partial V_a}\left(\frac{V_a}{a^*}\right) = \frac{1}{a^*} \tag{3.174}$$

$$\frac{\partial g_{V_{IAS}}}{\partial V_a} = \frac{\partial}{\partial V_a}\left(a_0^*\sqrt{\frac{2}{\gamma-1}\left(\left\{\frac{p}{p_o}\left[\left(1+\frac{\gamma-1}{2}M^2\right)^{\frac{\gamma}{(\gamma-1)}}-1\right]+1\right\}^{\frac{(\gamma-1)}{\gamma}}-1\right)}\right)$$

$$\frac{\partial g_{V_{IAS}}}{\partial V_a} = \frac{\dfrac{a_0^*}{a^*}\dfrac{p}{p_o}M\left(1+\dfrac{\gamma-1}{2}M^2\right)^{\frac{1}{(\gamma-1)}}\left\{\dfrac{p}{p_o}\left[\left(1+\dfrac{\gamma-1}{2}M^2\right)^{\frac{\gamma}{(\gamma-1)}}-1\right]+1\right\}^{\frac{-1}{\gamma}}}{\sqrt{\dfrac{2}{\gamma-1}\left(\left\{\dfrac{p}{p_o}\left[\left(1+\dfrac{\gamma-1}{2}M^2\right)^{\frac{\gamma}{(\gamma-1)}}-1\right]+1\right\}^{\frac{(\gamma-1)}{\gamma}}-1\right)}} \tag{3.175}$$

$$\frac{\partial g_h}{\partial h} = 1$$

The LTD state-space representation of the linearized longitudinal dynamics (per equation (3.167)) is shown in equations (3.176) and (3.177).

$$\begin{bmatrix}\Delta\dot{V}_a\\ \Delta\dot{\gamma}_a\\ \Delta\dot{h}\end{bmatrix} = \begin{bmatrix}\dfrac{\partial f_{V_a}}{\partial V_a} & \dfrac{\partial f_{V_a}}{\partial \gamma_a} & \dfrac{\partial f_{V_a}}{\partial h}\\[2mm] \dfrac{\partial f_{\gamma_a}}{\partial V_a} & \dfrac{\partial f_{\gamma_a}}{\partial \gamma_a} & \dfrac{\partial f_{\gamma_a}}{\partial h}\\[2mm] \dfrac{\partial f_h}{\partial V_a} & \dfrac{\partial f_h}{\partial \gamma_a} & \dfrac{\partial f_h}{\partial h}\end{bmatrix}\begin{bmatrix}\Delta V_a\\ \Delta\gamma_a\\ \Delta h\end{bmatrix} + \begin{bmatrix}\dfrac{\partial f_{V_a}}{\partial C_L} & \dfrac{\partial f_{V_a}}{\partial T}\\[2mm] \dfrac{\partial f_{\gamma_a}}{\partial C_L} & \dfrac{\partial f_{\gamma_a}}{\partial T}\\[2mm] \dfrac{\partial f_h}{\partial C_L} & \dfrac{\partial f_h}{\partial T}\end{bmatrix}\begin{bmatrix}\Delta C_L\\ \Delta T\end{bmatrix} \tag{3.176}$$

$$\begin{bmatrix}\Delta V_{IAS}\\ \Delta M\\ \Delta h\\ \Delta\dot{h}\end{bmatrix} = \begin{bmatrix}\dfrac{\partial V_{IAS}}{\partial V_a} & 0 & 0\\[2mm] \dfrac{\partial M}{\partial V_a} & 0 & 0\\[2mm] 0 & 0 & 1\\[2mm] \dfrac{\partial f_h}{\partial V_a} & \dfrac{\partial f_h}{\partial \gamma_a} & \dfrac{\partial f_h}{\partial h}\end{bmatrix}\begin{bmatrix}\Delta V_a\\ \Delta\gamma_a\\ \Delta h\end{bmatrix} + \begin{bmatrix}0 & 0\\ 0 & 0\\ 0 & 0\\ \dfrac{\partial f_h}{\partial C_L} & \dfrac{\partial f_h}{\partial T}\end{bmatrix}\begin{bmatrix}\Delta C_L\\ \Delta T\end{bmatrix} \tag{3.177}$$

All of the derivatives in these constant matrices are evaluated at the reference condition; the notation indicating that explicitly has been removed. Numerous derivatives are zero for all cases. These derivatives are:

$$\frac{\partial f_{V_a}}{\partial h} = \frac{\partial f_{\gamma_a}}{\partial T} = \frac{\partial f_{\gamma_a}}{\partial h} = \frac{\partial f_h}{\partial h} = \frac{\partial f_h}{\partial C_L} = \frac{\partial f_h}{\partial T} = 0$$

Table 3.6. Stability and control derivatives of f_{V_a}

State/Input	Derivative of f_{V_a}	
V_a	$\dfrac{\partial f_{V_a}}{\partial V_a} = \dfrac{-\rho V_a S_w \left[C_{D_o} + K \left(C_L - C_{L_{min\,drag}} \right)^2 \right]}{m}$	(3.178)
γ_a	$\dfrac{\partial f_{V_a}}{\partial \gamma_a} = -g \cos \gamma_a$	(3.179)
h	$\dfrac{\partial f_{V_a}}{\partial h} = 0$	(3.180)
C_L	$\dfrac{\partial f_{V_a}}{\partial C_L} = \dfrac{-\rho V_a^2 S_w K \left(C_L - C_{L_{min\,drag}} \right)}{m}$	(3.181)
T	$\dfrac{\partial f_{V_a}}{\partial T} = \dfrac{1}{m}$	(3.182)

Table 3.7. Stability and control derivatives of f_{γ_a}

State/Input	Derivative of f_{γ_a}	
V_a	$\dfrac{\partial f_{\gamma_a}}{\partial V_a} = \dfrac{\rho S_{ref} C_L}{2m} + \dfrac{g}{V_a^2} \cos \gamma_a$	(3.183)
γ_a	$\dfrac{\partial f_{\gamma_a}}{\partial \gamma_a} = \dfrac{g}{V_a} \sin \gamma_a$	(3.184)
h	$\dfrac{\partial f_{\gamma_a}}{\partial h} = 0$	(3.185)
C_L	$\dfrac{\partial f_{\gamma_a}}{\partial C_L} = \dfrac{\rho V_a S_{ref}}{2m}$	(3.186)
T	$\dfrac{\partial f_{\gamma_a}}{\partial T} = 0$	(3.187)

Table 3.8. Stability and control derivatives of f_h

State/Input	Derivative of f_h	
V_a	$\dfrac{\partial f_h}{\partial V_a} = \sin \gamma_a$	(3.188)
γ_a	$\dfrac{\partial f_h}{\partial \gamma_a} = V_a \cos \gamma_a$	(3.189)
h	$\partial f_h / \partial h = 0$	(3.190)
C_L	$\partial f_h / \partial C_L = 0$	(3.191)
T	$\partial f_h / \partial T = 0$	(3.192)

Furthermore, if we assume that the aircraft's reference condition is level flight ($\gamma_a = 0$), we can set other derivatives to zero.

$$\frac{\partial f_{\gamma_a}}{\partial \gamma_a} = \frac{\partial f_h}{\partial V_a} = 0$$

Modifying our state equations results in Equations (3.193) and (3.194). These equations represent the final form of the linearized model.

$$
\begin{bmatrix} \Delta \dot{V}_a \\ \Delta \dot{\gamma}_a \\ \Delta \dot{h} \end{bmatrix} =
\begin{bmatrix}
\dfrac{\partial f_{V_a}}{\partial V_a} & \dfrac{\partial f_{V_a}}{\partial \gamma_a} & 0 \\
\dfrac{\partial f_{\gamma_a}}{\partial V_a} & 0 & 0 \\
0 & \dfrac{\partial f_h}{\partial \gamma_a} & 0
\end{bmatrix}
\begin{bmatrix} \Delta V_a \\ \Delta \gamma_a \\ \Delta h \end{bmatrix} +
\begin{bmatrix}
\dfrac{\partial f_{V_a}}{\partial C_L} & \dfrac{\partial f_{V_a}}{\partial T} \\
\dfrac{\partial f_{\gamma_a}}{\partial C_L} & 0 \\
0 & 0
\end{bmatrix}
\begin{bmatrix} \Delta C_L \\ \Delta T \end{bmatrix}
\tag{3.193}
$$

$$
\begin{bmatrix} \Delta V_{IAS} \\ \Delta M \\ \Delta h \\ \Delta \dot{h} \end{bmatrix} =
\begin{bmatrix}
\dfrac{\partial V_{IAS}}{\partial V_a} & 0 & 0 \\
\dfrac{\partial M}{\partial V_a} & 0 & 0 \\
0 & 0 & 1 \\
0 & \left(\dfrac{\partial f_h}{\partial \gamma_a} \right) & 0
\end{bmatrix}
\begin{bmatrix} \Delta V_a \\ \Delta \gamma_a \\ \Delta h \end{bmatrix} +
\begin{bmatrix}
0 & 0 \\
0 & 0 \\
0 & 0 \\
0 & 0
\end{bmatrix}
\begin{bmatrix} \Delta C_L \\ \Delta T \end{bmatrix}
\tag{3.194}
$$

It is useful to compare the simulation results of the linear model to the results from the nonlinear model. The expected result is that the linear model will agree with the nonlinear model for very small perturbations from the reference condition. As the

perturbations from the equilibrium condition become larger, the linear model will not follow the nonlinear dynamics. This behavior is seen in Figure 3.24 and Figure 3.25. Both figures show the time histories of the three longitudinal states along with the altitude rate as calculated by the linear and nonlinear models. Figure 3.24 shows the models' response to a small perturbation or change in the nominal or reference lift coefficient. As can be seen from the time histories of Figure 3.24, the match between the two models is good. However, as the perturbation or change in the nominal or reference lift coefficient becomes larger, the linear model fails to reflect accurately the behavior of the nonlinear dynamics.

This is the limitation of using linear models. To account for this limitation, many linear models, all referenced about different reference conditions, are used to accurately model the aircraft's performance throughout the entire flight envelope.
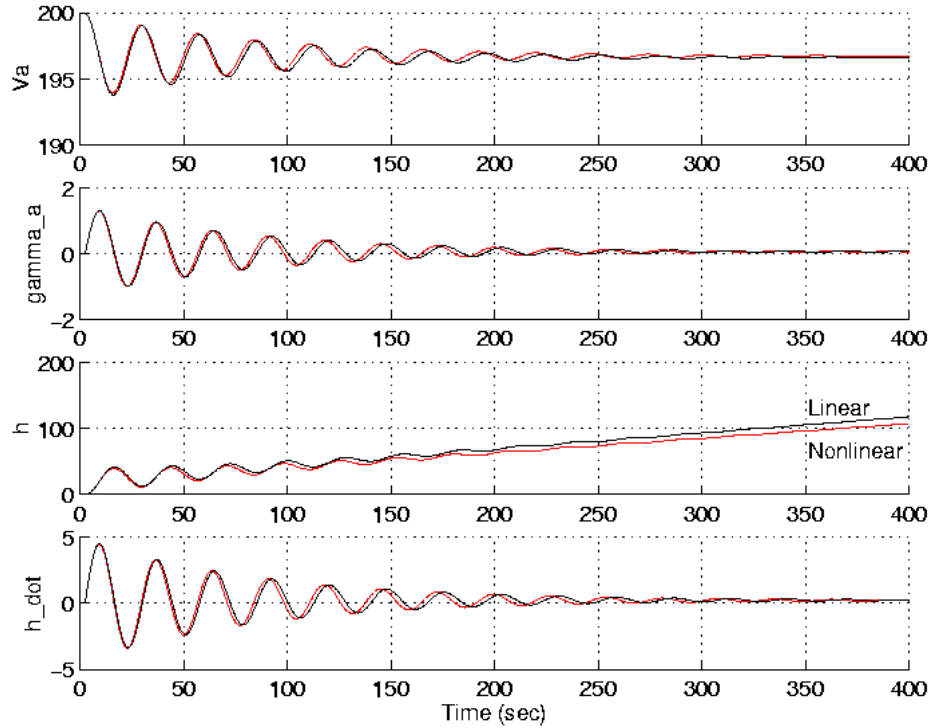
Figure 3.24. Comparison of linear and nonlinear models with a 0.01 perturbation from the reference lift coefficient
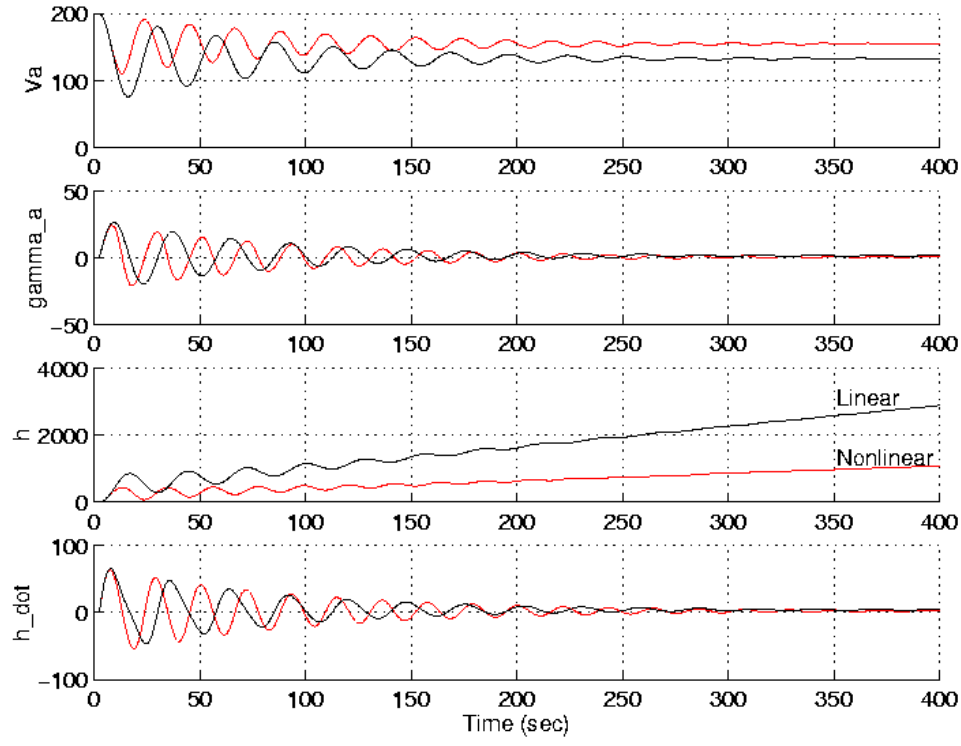
Figure 3.25. Comparison of linear and nonlinear models with a 0.2 perturbation from the reference lift coefficient

3.2 The Analysis of Longitudinal Aircraft Modal Properties

3.2.1 The Characteristic Polynomial of an LTD System

To solve the system of equations (3.167), we use a Laplace transformation, remembering that the matrices are constant. There is no loss in generality in assuming the initial conditions are zero.

$$
\begin{aligned}
s\mathbf{x}(s) - \mathbf{x}(t_0) &= s\mathbf{x}(s) = \mathbf{A}\mathbf{x}(s) + \mathbf{B}\mathbf{u}(s) \\
\mathbf{y}(s) &= \mathbf{C}\mathbf{x}(s) + \mathbf{D}\mathbf{u}(s)
\end{aligned}
\tag{3.195}
$$

The state and output vectors can be expressed in terms of the control vector.

$$
\begin{aligned}
\mathbf{x}(s) &= (s\mathbf{I} - \mathbf{A})^{-1}\mathbf{B}\mathbf{u}(s) \\
\mathbf{y}(s) &= \left[\mathbf{C}(s\mathbf{I} - \mathbf{A})^{-1}\mathbf{B} + \mathbf{D} \right]\mathbf{u}(s)
\end{aligned}
\tag{3.196}
$$

Equations (3.196) express the open loop dynamics in terms of a known control input. The polynomial given by $\det(s\mathbf{I} - \mathbf{A})$ is known as the characteristic polynomial of the LTD

system. It is of the same order as the state vector. Analysis of the characteristic polynomial reveals the modal properties of the system.

3.2.2 Modal Properties of the Longitudinal Dynamics

The main limitation of linear models is that they are valid only for a limited range around the reference conditions that were used to create them. To model an entire flight envelope of an aircraft, many linear models, each having its own set of reference conditions, must be developed. Immediately, one can then see the advantage to having a linear model that is a function of as few reference values as possible. For instance, if the aircraft's linear model varied only with true airspeed, it would make for a simple one dimensional set of linear models, each with a different true airspeed reference. However, we can see through observation that the linear model of the longitudinal dynamics for a given aircraft is fundamentally a function of three varying parameters. These are:

- V_a: The aircraft's true airspeed
- ρ: The air density
- m: The mass of the aircraft

The fact that there are three terms immediately presents an inconvenience. Any set of linear models must be three-dimensional. For instance, even a modest number of variations, say 10 true airspeeds, 10 masses, and 10 different air densities, would yield 1000 reference conditions and hence 1000 linear models. It is, therefore, very desirable to eliminate a varying parameter if possible. Elimination of a varying parameter is the attempt of this section.

Consider the state space representation of the system as shown in Equation (3.193). This system of equations contains three state equations, the first two of which characterize the Phugoid longitudinal mode (the ΔV_a and $\Delta \gamma_a$ equations). The third state equation, the Δh equation, contributes only to the calculation of altitude and does not affect the Phugoid mode.

$$
\begin{bmatrix} \Delta \dot{V}_a \\ \Delta \dot{\gamma}_a \\ \Delta \dot{h} \end{bmatrix} = \begin{bmatrix} \dfrac{\partial f_{V_a}}{\partial V_a} & \dfrac{\partial f_{V_a}}{\partial \gamma_a} & 0 \\ \dfrac{\partial f_{\gamma_a}}{\partial V_a} & 0 & 0 \\ 0 & \dfrac{\partial f_h}{\partial \gamma_a} & 0 \end{bmatrix} \begin{bmatrix} \Delta V_a \\ \Delta \gamma_a \\ \Delta h \end{bmatrix} + \begin{bmatrix} \dfrac{\partial f_{V_a}}{\partial C_L} & \dfrac{\partial f_{V_a}}{\partial T} \\ \dfrac{\partial f_{\gamma_a}}{\partial C_L} & 0 \\ 0 & 0 \end{bmatrix} \begin{bmatrix} \Delta C_L \\ \Delta T \end{bmatrix}
\tag{3.193}
$$

Because the Δh equation does not contribute to the Phugoid dynamics, we choose to ignore it in the following analysis. Ignoring the Δh equation reduces the state equations to Equation (3.197).

$$
\begin{bmatrix} \Delta \dot{V}_a \\ \Delta \dot{\gamma}_a \end{bmatrix} = \begin{bmatrix} \dfrac{\partial f_{V_a}}{\partial V_a} & \dfrac{\partial f_{V_a}}{\partial \gamma_a} \\ \dfrac{\partial f_{\gamma_a}}{\partial V_a} & 0 \end{bmatrix} \begin{bmatrix} \Delta V_a \\ \Delta \gamma_a \end{bmatrix} + \begin{bmatrix} \dfrac{\partial f_{V_a}}{\partial C_L} & \dfrac{\partial f_{V_a}}{\partial T} \\ \dfrac{\partial f_{\gamma_a}}{\partial C_L} & 0 \end{bmatrix} \begin{bmatrix} \Delta C_L \\ \Delta T \end{bmatrix} \tag{3.197}
$$

The characteristic polynomial can be written immediately by inspection.

$$
s^2 - \frac{\partial f_{V_a}}{\partial V_a} s - \frac{\partial f_{V_a}}{\partial \gamma_a} \frac{\partial f_{\gamma_a}}{\partial V_a} \tag{3.198}
$$

When we substitute for the actual derivatives we see that the characteristic polynomial expands to the following.

$$
s^2 + \frac{\rho V_a S_w \left(C_{D_0} + K \left(C_L - C_{L_{ref}} \right)^2 \right)}{m} s + g \cos \gamma_a \left(\frac{\rho S_{ref} C_L}{2m} + \frac{g}{V_a^2} \cos \gamma_a \right) \tag{3.199}
$$

We know from classical control theory that the natural frequency and damping ratio are represented in the characteristic polynomial as $s^2 + 2\zeta \omega_n s + \omega_n^2$. Therefore, we can assign the last term to equal the square of the Phugoid frequency, ω_p.

$$
\omega_p = \sqrt{g \cos \gamma_a \left(\frac{\rho S_{ref} C_L}{2m} + \frac{g}{V_a^2} \cos \gamma_a \right)} \tag{3.200}
$$

We can gain insight from this equation. First, if the flight path angle is small, the relation can be reduced to Equation (3.201).

$$
\omega_p = \sqrt{\left(\frac{\rho g S_{ref} C_L}{2m} + \frac{g^2}{V_a^2} \right)} \tag{3.201}
$$

The ratio g^2/V_a^2 is likely to dominate this term at low speeds and be small at high speeds. It is a function of true airspeed squared, which is proportional to dynamic pressure. Consider the other term. It is inversely proportional to the mass. This suggests that as the mass goes down, the frequency goes up. This is true providing that the lift coefficient does not change. However, it is likely that the lift coefficient will change with mass because the pilot will always tend to trim the aircraft for a given flight condition. If we assume that lift equals weight or is close to equaling weight for the vast number of flight conditions we can write the relation for mass as seen in Equation (3.202).

$$qS_{ref}C_L = mg \tag{3.202}$$

Using (3.202) we can substitute for C_L in Equation (3.201) resulting the Phugoid expression in Equation (3.203).

$$\omega_p = \sqrt{\left(\frac{\rho g S_{ref}}{2m} \left(\frac{mg}{qS_{ref}} \right) + \frac{g^2}{V_a^2} \right)} \tag{3.203}$$

Canceling terms leaves (3.204).

$$\omega_p = \sqrt{\left(\frac{\rho g^2}{2q} + \frac{g^2}{V_a^2} \right)} \tag{3.204}$$

Finally, noting that the dynamic pressure is a function of density and true airspeed,

$$\omega_p = \sqrt{\left(\frac{\rho g^2}{2 \frac{\rho V_a^2}{2}} + \frac{g^2}{V_a^2} \right)} \tag{3.205}$$

we can see that the Phugoid frequency for the trimmed aircraft is entirely a function of true airspeed as shown in Equation (3.206).

$$\omega_p = \sqrt{\left(\frac{2g^2}{V_a^2} \right)} = \sqrt{2} \frac{g}{V_a} \tag{3.206}$$

This is an interesting result because it suggests that the frequency of the Phugoid is not a function of the weight of the aircraft or the altitude at which the aircraft is flying.

Moving to the damping ratio of the Phugoid mode, we can express the damping ratio using the middle term of the characteristic polynomial if we divide by $2\omega_p$ as shown in Equation (3.207).

$$\zeta_p = \sqrt{\left(\frac{V_a^2}{2g^2}\right)} \frac{\rho V_a S_w \left(C_{D_0} + K\left(C_L - C_{L_{ref}}\right)^2\right)}{2m}$$

(3.207)

Unfortunately, there is no simplification that reduces the damping ratio to a single function of any parameter that we have so far defined. This expression for damping implies that the only way to schedule gains to control the Phugoid is to have three-dimensional tables consisting of aircraft weight, true airspeed and altitude (air density). This creates a large computational burden and requires the storage of many scheduled feedback gains. It is desirable to somehow reduce the schedule to a two-dimensional table. One solution is to substitute dynamic pressure for the density and true airspeed. This substitution effectively assumes that changes in speed and altitude (density) can be interchangeable. However, we can see that density and speed work independently of each other. While it may be acceptable to schedule vs. dynamic pressure, it is only an approximation. It is better if another quantity can be found.

Working towards a simplified expression for damping, we revisit Equation (3.207). Assuming a trimmed aircraft, we can substitute Equation (3.202) into Equation (3.208) for weight, mg. After some algebraic manipulation, the final result is shown in Equation (3.209).

$$\zeta_p = \frac{V_a}{\sqrt{2}g} \frac{\rho V_a S_w \left(C_{D_0} + K\left(C_L - C_{L_{ref}}\right)^2\right)}{2m}$$

$$\zeta_p = \frac{\rho V_a^2}{2} \frac{S_w \left(C_{D_0} + K\left(C_L - C_{L_{ref}}\right)^2\right)}{\sqrt{2}mg}$$

$$\zeta_p = \frac{q S_w \left(C_{D_0} + K\left(C_L - C_{L_{ref}}\right)^2\right)}{\sqrt{2}q S_w C_L}$$

$$\zeta_p = \frac{\left(C_{D_0} + K\left(C_L - C_{L_{ref}}\right)^2\right)}{\sqrt{2}C_L}$$

$$\zeta_p = \frac{1}{\sqrt{2}\left(\frac{L}{D}\right)} \tag{3.209}$$

We see that the damping is a function of the lift to drag ratio of the aircraft. An alternative derivation is contained in Nelson (1989), which comes to the same basic conclusion. Unfortunately, it is impossible for the control logic or any sophisticated instrument to actually measure the lift to drag ratio of the aircraft. However, the lift to drag ratio is always a function of the lift coefficient at a given time. So, while the lift to drag ratio can not be known, we can approximately measure the trim lift coefficient at any given time in the flight and know that the lift coefficient corresponds to a particular location on the drag polar and hence a particular L/D. Therefore, the conclusion is that the modal properties for the aircraft are uniquely described by the trim lift coefficient and the true airspeed. However this does not consider the control derivatives.

There are three control derivatives to be considered as shown in Equations (3.210) - (3.212).

$$\frac{\partial f_{\gamma_a}}{\partial C_L} = \frac{\rho V_a S_{ref}}{2m} \tag{3.210}$$

$$\frac{\partial f_{V_a}}{\partial C_L} = \frac{-\rho V_a^2 S_w K C_L}{m} \tag{3.211}$$

$$\frac{\partial f_{V_a}}{\partial T} = \frac{1}{m} \tag{3.212}$$

Consider the expression for the lift coefficient in Equation (3.213). If the lift coefficient and the true airspeed are known, it is possible to solve for the ratio between the air density and the aircraft's mass. This can be seen in Equation (3.214).

$$C_L = \frac{2mg}{\rho S_w V_a^2} \tag{3.213}$$

$$\frac{\rho}{m} = \frac{2g}{C_L S_w V_a^2} \tag{3.214}$$

While it is not possible to solve for the mass and density directly, we can solve for the ratio, which is then all that is needed to define two of the control derivatives as shown in Equations (3.215) and (3.216).

$$\frac{\partial f_{\gamma_a}}{\partial C_L} = \left(\frac{\rho}{m}\right)\frac{V_a S_{ref}}{2} \tag{3.215}$$

$$\frac{\partial f_{V_a}}{\partial C_L} = -V_a^2 S_w K C_L \left(\frac{\rho}{m}\right) \tag{3.216}$$

The final control derivative, the $\partial f_{V_a}/\partial T$ derivative, is obviously a function of mass only. Therefore, it is not completely possible to define the whole system using two parameters. However, having only one term that is a function of mass is far more convenient than having the mass term throughout the model. All gain calculations can be done using a nominal mass and varying true airspeed and trim lift coefficient. To accommodate different aircraft masses only one term need be changed.

3.3   Transfer Function Analysis of the Longitudinal Dynamics

In Section 3.2 we investigated the modal property variation of the longitudinal dynamics. The modal property analysis, by defining the damping and frequency of the mode, defined the characteristic polynomial of the system. The purpose of this section is to outline the transfer functions that are most likely to dominate the longitudinal dynamics.

A transfer function is an isolation of the affects of an input (or driving) function on an output (or response) function. Because the transfer functions include the zeros of the system as well as the poles (the roots of the characteristic polynomial), the transfer functions provide a more thorough understanding of the dynamic system. The limitation of a transfer function analysis (in addition to the analysis limitations already imposed by linearizing the system) is that it focuses attention on the isolated effects of a single input on a single output. For this reason, we use transfer function analysis only to reveal trends in linear feedback control.

The output equation of the system (3.196) can be expressed in transfer function form.

$$\mathbf{y}(s) = \mathbf{G}(s)\mathbf{u}(s) \tag{3.217}$$

where

$$\mathbf{G}(s) = \left[\mathbf{C}(s\mathbf{I} - \mathbf{A})^{-1}\mathbf{B} + \mathbf{D}\right] \tag{3.218}$$

We can plug in the system matrices to obtain the transfer function matrix for our system. First we modify the output equation, equation (3.194). Notice the addition of a factor of

60 in the $\frac{\partial f_h}{\partial \gamma_a}$ term; this factor is to convert the altitude rate from ft/sec to ft/min so that the output matches the vertical speed indicator in a cockpit.

$$
\begin{bmatrix} \Delta V_{IAS} \\ \Delta M \\ \Delta h \\ \Delta \dot{h} \end{bmatrix} = \begin{bmatrix} \dfrac{\partial V_{IAS}}{\partial V_a} & 0 & 0 \\ \dfrac{\partial M}{\partial V_a} & 0 & 0 \\ 0 & 0 & 1 \\ 0 & 60\left(\dfrac{\partial f_h}{\partial \gamma_a}\right) & 0 \end{bmatrix} \begin{bmatrix} \Delta V_a \\ \Delta \gamma_a \\ \Delta h \end{bmatrix} + \begin{bmatrix} 0 & 0 \\ 0 & 0 \\ 0 & 0 \\ 0 & 0 \end{bmatrix} \begin{bmatrix} \Delta C_L \\ \Delta T \end{bmatrix}
\tag{3.219}
$$

Our transfer function matrix is obtained by plugging the system matrices of equations (3.193) and (3.219) into equation (3.218).

$$
\mathbf{G}(s) = \frac{1}{s\left(s^2 - \dfrac{\partial f_{V_a}}{\partial V_a}s - \dfrac{\partial f_{V_a}}{\partial \gamma_a}\dfrac{\partial f_{\gamma_a}}{\partial V_a}\right)}
\begin{bmatrix}
s^2\dfrac{\partial V_{IAS}}{\partial V_a}\dfrac{\partial f_{V_a}}{\partial C_L} + s\dfrac{\partial V_{IAS}}{\partial V_a}\dfrac{\partial f_{V_a}}{\partial \gamma_a}\dfrac{\partial f_{\gamma_a}}{\partial C_L} & s^2\dfrac{\partial V_{IAS}}{\partial V_a}\dfrac{\partial f_{V_a}}{\partial T} \\
s^2\dfrac{\partial M}{\partial V_a}\dfrac{\partial f_{V_a}}{\partial C_L} + s\dfrac{\partial M}{\partial V_a}\dfrac{\partial f_{V_a}}{\partial \gamma_a}\dfrac{\partial f_{\gamma_a}}{\partial C_L} & s^2\dfrac{\partial M}{\partial V_a}\dfrac{\partial f_{V_a}}{\partial T} \\
\dfrac{\partial f_{\gamma_a}}{\partial V_a}\dfrac{\partial f_h}{\partial \gamma_a}\dfrac{\partial f_{V_a}}{\partial C_L} + \dfrac{\partial f_h}{\partial \gamma_a}\left(s - \dfrac{\partial f_{V_a}}{\partial V_a}\right)\dfrac{\partial f_{\gamma_a}}{\partial C_L} & \dfrac{\partial f_{\gamma_a}}{\partial V_a}\dfrac{\partial f_h}{\partial \gamma_a}\dfrac{\partial f_{V_a}}{\partial T} \\
60s\dfrac{\partial f_h}{\partial \gamma_a}\left[-\dfrac{\partial f_{\gamma_a}}{\partial V_a}\dfrac{\partial f_{V_a}}{\partial C_L} + \left(s - \dfrac{\partial f_{V_a}}{\partial V_a}\right)\dfrac{\partial f_{\gamma_a}}{\partial C_L}\right] & -60s\dfrac{\partial f_h}{\partial \gamma_a}\dfrac{\partial f_{\gamma_a}}{\partial V_a}\dfrac{\partial f_{V_a}}{\partial T}
\end{bmatrix}
\tag{3.220}
$$

The characteristic polynomial discussed in the previous section is also the denominator of our transfer functions. This is true for any state space system. Since the characteristic polynomial has already been investigated, there is no need to repeat the analysis here. The analysis here will focus on the numerators of the transfer functions.

Several transfer functions were selected for study to determine the acceptability of using the two control inputs (thrust and lift coefficient) for various tasks. The transfer functions that were singled out for study and discussed here are the $\dot{h}/C_L$ (g_{41}), M/C_L (g_{21}), and $\dot{h}/T$ (g_{42}) transfer functions.

3.3.1 The $\dot{h}/C_L$ Transfer Function

The $\dot{h}/C_L$ transfer function relates an aircraft's response in altitude rate to changes in the lift coefficient. The term of equation (3.220) corresponding to the $\dot{h}/C_L$ transfer function is expressed below.

$$\frac{\Delta \dot{h}}{\Delta C_L} = g_{41} = \frac{60\left(\frac{\partial f_h}{\partial \gamma_a}\right)\left(\frac{\partial f_{\gamma_a}}{\partial C_L}s + \left(\frac{\partial f_{\gamma_a}}{\partial V_a}\frac{\partial f_{V_a}}{\partial C_L} - \frac{\partial f_{V_a}}{\partial V_a}\frac{\partial f_{\gamma_a}}{\partial C_L}\right)\right)}{s^2 - \frac{\partial f_{V_a}}{\partial V_a}s - \frac{\partial f_{V_a}}{\partial \gamma_a}\frac{\partial f_{\gamma_a}}{\partial V_a}} \tag{3.221}$$

We can arrange the numerator of the transfer function to show clearly the zeros. We can see that we have one zero, which is highlighted in Equation (3.223). We represent the zero with the symbol z_1.

$$\frac{\Delta \dot{h}}{\Delta C_L} = \frac{60\left(\frac{\partial f_h}{\partial \gamma_a}\frac{\partial f_{\gamma_a}}{\partial C_L}\right)\left(s + \left(\frac{\frac{\partial f_{\gamma_a}}{\partial V_a}\frac{\partial f_{V_a}}{\partial C_L} - \frac{\partial f_{V_a}}{\partial V_a}\frac{\partial f_{\gamma_a}}{\partial C_L}}{\frac{\partial f_{\gamma_a}}{\partial C_L}}\right)\right)}{s^2 - \frac{\partial f_{V_a}}{\partial V_a}s - \frac{\partial f_{V_a}}{\partial \gamma_a}\frac{\partial f_{\gamma_a}}{\partial V_a}} \tag{3.222}$$

$$z_1 = -\left(\frac{\frac{\partial f_{\gamma_a}}{\partial V_a}\frac{\partial f_{V_a}}{\partial C_L} - \frac{\partial f_{V_a}}{\partial V_a}\frac{\partial f_{\gamma_a}}{\partial C_L}}{\frac{\partial f_{\gamma_a}}{\partial C_L}}\right) \tag{3.223}$$

We can not gain much insight from the symbolic representations of the derivatives alone, so it is necessary substitute in for the derivatives from the tables in Section 3.1. Expanding the inner terms of the zero we have:

$$z_1 = -\left(\frac{\frac{-\rho V_a^2 S_w K C_L}{m}\left(\frac{\rho S_{ref} C_L}{2m} + \frac{g}{V_a^2}\cos\gamma_a\right) + \frac{\rho V_a S_w\left(C_{D_0} + K C_L^2\right)}{m}\frac{\rho V_a S_{ref}}{2m}}{\frac{\rho V_a S_{ref}}{2m}}\right) \tag{3.224}$$

Simplifying,

$$z_1 = \left(\frac{\rho V_a S_w}{m}\right)\left(K C_L^2 - C_{D_0}\right) \tag{3.225}$$

Basically, what the zero shows us is that if the parasite drag (zero lift drag) is smaller than the induced drag, the zero of this transfer function will be positive. The cross over

point is when the aircraft is operating at its maximum lift to drag ratio. Figure 3.26 illustrates the flight regime where the zero of the $\frac{h}{C_L}$ switches sign.

The condition when a zero of a transfer function is positive is referred to as a non-minimum phase system because of such a system's tendency to immediately move in the opposite direction of the final steady state value. The $\frac{h}{C_L}$ is even more insidious because it has a negative DC gain. DC gain (the name is taken from electric circuits) is the value of the transfer function at $s = 0$. It reveals the gain of the steady-state response to the input. A negative DC gain insures that the final output will be negative of what was commanded. A simple discussion suffices to provide an intuitive understanding of what is happening.

Consider what happens when an aircraft is flying so slow that the drag is higher than it would be if it were to fly faster (see Figure 3.26). To fly slower the aircraft actually needs more thrust. However, the addition of thrust tends to accelerate the aircraft and hence lower the drag, which makes the aircraft fly faster. Likewise, if an aircraft in this condition tries to climb, the result of increasing the lift coefficient will tend to slow the aircraft. However, instead of slowing down and reducing drag, which would normally allow a climb, the aircraft sees an increase in drag. A pilot must be careful to add throttle and change lift coefficient simultaneously to control flight in this regime.
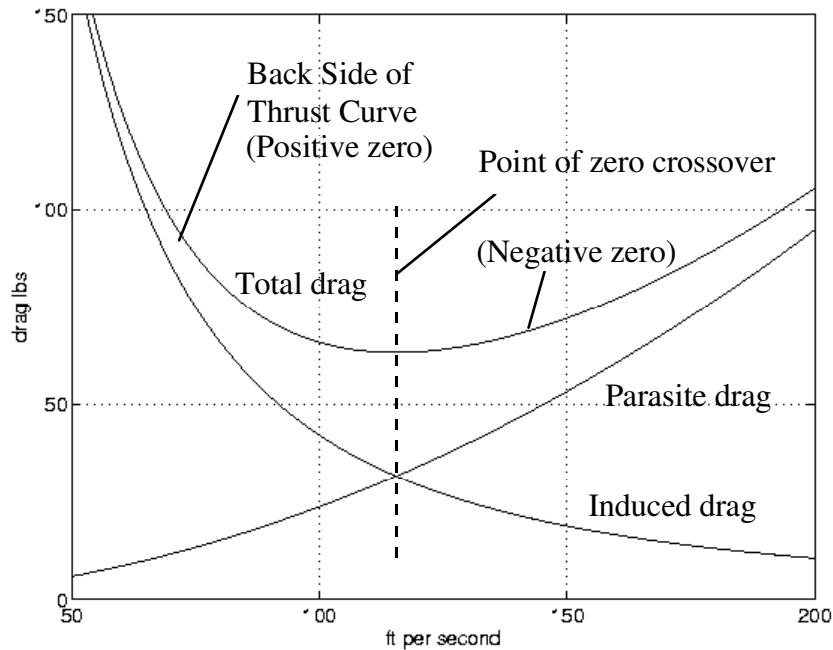
Figure 3.26. An illustration of drag vs airspeed at constant altitude, highlighting the non-minimum phase behavior of the transfer function of the linearized system.

- 75 -

Our transfer function analysis of the linearized system implies that lift coefficient control of altitude rate is stable on the front side of the thrust curve, and unstable on the backside. Based on this analysis, one might assume that control is difficult or impossible on the backside of the thrust curve. Fortunately, the linearized system and transfer function analysis fail to accurately predict the stability of our system dynamics on the backside of the thrust curve. In general, the system is not operating with constant thrust while using lift coefficient to control altitude rate. An increase in thrust is typically available to correct the non-minimum phase behavior. And, while it is not a typical maneuver to descend at idle thrust while maintaining a commanded altitude rate, such a maneuver is still possible, partly because idle thrust increases in a descent and partly because the speed is allowed to vary in such a maneuver. And lift coefficient control of altitude rate is a viable control strategy throughout the flight envelope.

3.3.2   The M/C_L Transfer function

The M/C_L transfer function characterizes the response in Mach number with changes in lift coefficient. The term of equation (3.220) corresponding to the M/C_L transfer function is shown below.

$$\frac{M}{C_L} = g_{21} = \frac{\dfrac{\partial M}{\partial V_a}\dfrac{\partial f_{V_a}}{\partial C_L}\left(s + \dfrac{\dfrac{\partial f_{V_a}}{\partial \gamma_a}\dfrac{\partial f_{\gamma_a}}{\partial C_L}}{\dfrac{\partial f_{V_a}}{\partial C_L}}\right)}{s^2 - \dfrac{\partial f_{V_a}}{\partial V_a}s - \dfrac{\partial f_{V_a}}{\partial \gamma_a}\dfrac{\partial f_{\gamma_a}}{\partial V_a}} \tag{3.226}$$

Next, the zero of the transfer function can be analyzed as shown in Equations (3.227) and (3.228).

$$\frac{-\dfrac{\partial f_{V_a}}{\partial \gamma_a}\dfrac{\partial f_{\gamma_a}}{\partial C_L}}{\dfrac{\partial f_{V_a}}{\partial C_L}} = \frac{-(-g)\dfrac{\rho V_a S_{ref}}{2m}}{\dfrac{-\rho V_a^2 S_w K C_L}{m}} \tag{3.227}$$

$$\frac{-\dfrac{\partial f_{V_a}}{\partial \gamma_a}\dfrac{\partial f_{\gamma_a}}{\partial C_L}}{\dfrac{\partial f_{V_a}}{\partial C_L}} = \frac{-g}{2V_a K C_L} \tag{3.228}$$

We can see from Equation (3.228) that the zero is always negative. This is a favorable result because it means that Mach number can always be controlled effectively by the lift coefficient. However, the control design will not necessarily be trivial. Consider the following example of a transfer function.

$$\frac{M}{C_L} = \frac{-0.0028(s+0.643)}{s^2 + 0.0088s + 0.0083} \tag{3.229}$$

The root locus of this transfer function shows us that feedback control of Mach number using the lift coefficient would be difficult. Proportional feedback tends to drive the poles unstable as seen in Figure 3.27. When the poles do converge on the real axis, one pole heads towards positive infinity and the other heads towards the zero. We can see from Figure 3.27 that it will be necessary to feedback something in addition to Mach for stability.
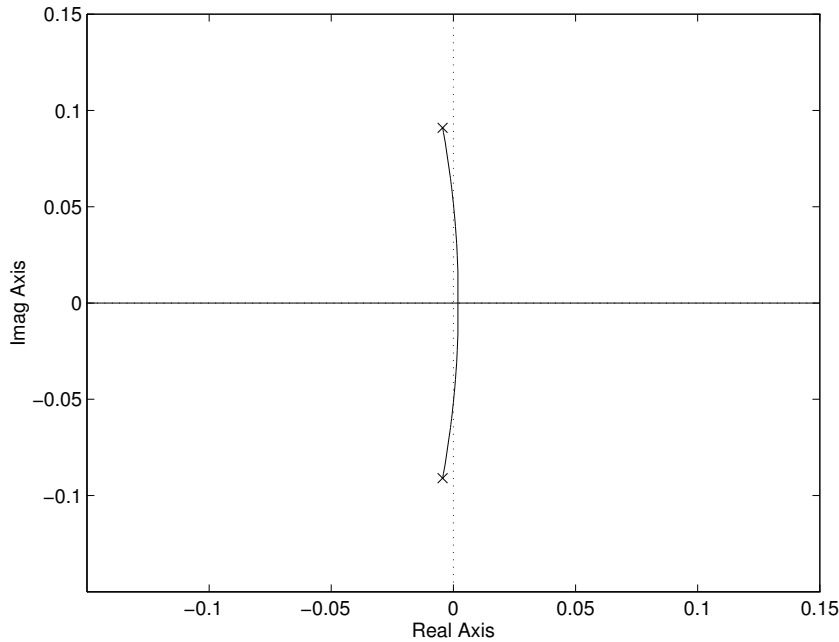
Figure 3.27. The root locus of proportional control applied to the $\frac{M}{C_L}$ transfer function

3.3.3 The $\frac{\dot{h}}{T}$ Transfer function

Consider the throttle to altitude rate transfer function. The term of equation (3.220) corresponding to the $\frac{\dot{h}}{T}$ transfer function is shown below.

$$\frac{\dot{h}}{T} = g_{42} = \frac{60\left(\dfrac{\partial f_h}{\partial \gamma_a}\right)\dfrac{\partial f_{\gamma_a}}{\partial V_a}\dfrac{\partial f_{V_a}}{\partial T}}{s^2 - \dfrac{\partial f_{V_a}}{\partial V_a}s - \dfrac{\partial f_{V_a}}{\partial \gamma_a}\dfrac{\partial f_{\gamma_a}}{\partial V_a}} \qquad (3.230)$$

This transfer function has no zeros, which makes it very well behaved. Using throttle to control altitude rate should not present a design challenge and is not affected by the back side of the thrust curve. Applying throttle while the lift coefficient is held constant will always make the aircraft climb regardless of the flight condition.

4. The Feedback Control System for Longitudinal Control

In the previous Chapters, the bulk of the analysis effort was spent on the derivation of the physical model of the aircraft. The physical model of the aircraft consisted of the dynamic equations, which model the aircraft's performance, and the kinematic equations, which characterize the aircraft's propagation over the surface of the Earth. The purpose of building such an intricate model is to insure the fidelity of modeling actual aircraft in flight. The main advantage of a high fidelity aircraft model is that it accurately models the performance and handling characteristics of an aircraft. Accordingly, the disadvantage of a high fidelity aircraft model is that it accurately models the performance and handling characteristics of the aircraft. To make the aircraft model follow a desired trajectory, the aircraft model must be 'flown' by a pilot in the same sense that the actual aircraft must be flown. Arguably, the longitudinal control system is the most complicated and sensitive part of the entire simulation. This Chapter is the first of three Chapters that cover the longitudinal control system.

The purpose of the longitudinal control system is to provide a means of automating two fundamental aircraft maneuvers. These maneuvers are:

- Altitude change and altitude capture
- Speed change and speed capture

Generally, the functionality of the longitudinal control system can be divided into two distinct classes of algorithms: feedback control and supporting functional logic. This Chapter deals with the design of the feedback control algorithms to stabilize the aircraft and drive it to the desired state. There are different feedback control algorithms for different flight phases, and each of these is discussed along with a strategy for calculating the required gains.

4.1 The General Control Law

Our general control law for the longitudinal dynamics is the same regardless of where in the flight envelope the aircraft is operating. The only real difference in controlling flight within different regions of the flight envelope is the gains that are used. The general control law framework allows for any output variable to be fed back to any input variable.

The general framework for a proportional-integral (PI) control law is shown in block diagram form in Figure 4.1. The terms in the block diagram are defined as follows:

- $\mathbf{y_d}$ is the desired output vector
- $\mathbf{y}$ is the actual output vector

- **e** is the error vector equivalent to $\mathbf{y_d}$ - $\mathbf{y}$
- $\mathbf{K_p}$ is the proportional gain matrix in the feed-forward path.
- $\mathbf{K_i}$ is the integral gain matrix (also in the feed-forward path)
- $\mathbf{K_b}$ is the proportional gain matrix in the feedback path
- $\dot{\mathbf{x}} = \mathbf{Ax} + \mathbf{Bu}$ is the linearized state equation for the longitudinal dynamics
- $\mathbf{y} = \mathbf{Cx} + \mathbf{Du}$ is the linearized output equation for the longitudinal dynamics

From experience in dealing with the longitudinal dynamics, we have seen that proportional control using the appropriate output error, **e**, is sufficient to achieve the dynamic response desired. Integral control is then added to eliminate steady-state error. The final feedback loop, the one using $\mathbf{K_b}$, is designed to allow proportional feedback control of certain output variables without affecting the zeros of the transfer functions. Gains in the feedback path affect only the modal properties of a system; gains in the feed-forward path affect the dynamics of the system while at the same time driving the state error to zero. In certain instances, it is necessary to make use of the stabilization offered by feeding back a particular output while not driving that output to any particular value.
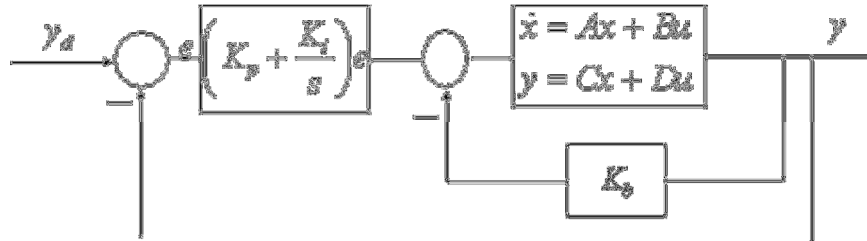
Figure 4.1. Block diagram for the longitudinal control law

The reader is reminded that the linearized system is simply a convenient approximation to the actual, non-linear system that is used for simulation. The convenience of the linear approximation is in analyzing the effects of our controller on the modal properties of the system to help us choose the controller. Once the controller is designed, we need to verify that it produces stable and realistic behavior in the actual, non-linear simulation model.

The general form of a LTD state-space is restated here.

$$\dot{\mathbf{x}}(t) = \mathbf{Ax}(t) + \mathbf{Bu}(t)$$
$$\mathbf{y}(t) = \mathbf{Cx}(t) + \mathbf{Du}(t)$$

(4.1)

Our general control law is defined in the time-domain as,

$$\mathbf{u}(t) = \mathbf{K_p}\mathbf{e}(t) + \int_0^t \mathbf{K_i}\mathbf{e}(t)\,dt - \mathbf{K_b}\mathbf{y}(t) \tag{4.2}$$

Because the general control law allows for any output variable to be fed back to any input variable, each gain matrix is of dimension (n x l), and is of the form,

$$\mathbf{K_p} = \begin{bmatrix} k_{p_{11}} & k_{p_{12}} & \cdots & k_{p_{1,l}} \\ k_{p_{21}} & \ddots & & \vdots \\ \vdots & & \ddots & \vdots \\ k_{p_{n,1}} & \cdots & \cdots & k_{p_{n,l}} \end{bmatrix} \tag{4.3}$$

where, n is the number of control variables, l is the number of output variables, and the subscript, p, refers to the proportional gain matrix. The form the integral and feedback gain matrices is the same except that subscripts i and b are substituted for the subscript p.

4.2   Manipulating an LTD State-Space with Integral Control

Integral control adds system poles to our state-space. In effect, it changes the order of our LTD system. This can be seen explicitly if we modify our LTD system to include the differential equations added by our PI controller. Let's define proportional and integral control vectors as,

$$\mathbf{u_p}(t) = \mathbf{K_p}\mathbf{e}(t) - \mathbf{K_b}\mathbf{y}(t)$$
$$\mathbf{u_i}(t) = \mathbf{K_i}\mathbf{e}(t) \tag{4.4}$$

and let's define the integrated control as,

$$\mathbf{I_u}(t) = \int_0^t \mathbf{u_i}(t)\,dt$$

Then the control vector, equation (4.2), can be written in terms of its separated proportional and integral terms.

$$\mathbf{u}(t) = \mathbf{u_p}(t) + \mathbf{I_u}(t)$$

Clearly, the derivative of the integrated control vector, $\mathbf{I_u}$, is the integral control vector, $\mathbf{u_i}$.

$$\dot{\mathbf{I}}_\mathbf{u}(t) = \mathbf{u_i}(t) \tag{4.5}$$

The state equation can be rewritten in terms of the separated control vector.

$$\dot{\mathbf{x}}(t) = \mathbf{A}\mathbf{x}(t) + \mathbf{B}\left[\mathbf{u_p}(t) + \mathbf{I_u}(t)\right]$$

$$\dot{\mathbf{x}}(t) = \mathbf{A}\mathbf{x}(t) + \mathbf{B}\mathbf{u_p}(t) + \mathbf{B}\mathbf{I_u}(t) \tag{4.6}$$

Combining equations (4.5) and (4.6) and the output equation into one LTD system gives,

$$\begin{bmatrix} \dot{\mathbf{x}}(t) \\ \dot{\mathbf{I}}_\mathbf{u}(t) \end{bmatrix} = \begin{bmatrix} \mathbf{A} & \mathbf{B} \\ \mathbf{0}_{n,m} & \mathbf{0}_n \end{bmatrix} \begin{bmatrix} \mathbf{x}(t) \\ \mathbf{I}_\mathbf{u}(t) \end{bmatrix} + \begin{bmatrix} \mathbf{B} & \mathbf{0}_{m,n} \\ \mathbf{0}_n & \mathbf{I}_n \end{bmatrix} \begin{bmatrix} \mathbf{u_p}(t) \\ \mathbf{u_i}(t) \end{bmatrix}$$

$$\mathbf{y}(t) = \begin{bmatrix} \mathbf{C} & \mathbf{D} \end{bmatrix} \begin{bmatrix} \mathbf{x}(t) \\ \mathbf{I}_\mathbf{u}(t) \end{bmatrix} + \begin{bmatrix} \mathbf{D} & \mathbf{0}_{l,n} \end{bmatrix} \begin{bmatrix} \mathbf{u_p}(t) \\ \mathbf{u_i}(t) \end{bmatrix} \tag{4.7}$$

From equation (4.4), the control law can be written as,

$$\begin{bmatrix} \mathbf{u_p}(t) \\ \mathbf{u_i}(t) \end{bmatrix} = \begin{bmatrix} \mathbf{K_p} \\ \mathbf{K_i} \end{bmatrix} \mathbf{e}(t) - \begin{bmatrix} \mathbf{K_b} \\ \mathbf{0}_{n,m} \end{bmatrix} \mathbf{y}(t) \tag{4.8}$$

- m is the number of state variables in the state vector (3 in our current example),
- n is the number of control variables in the control vector (2),
- l is the number of output variables in the output vector (4),
- $\mathbf{0}_n$ is a square, n x n matrix of zeros, and
- $\mathbf{0}_{n,m}$ is a n x m matrix of zeros.

Equations (4.7) and (4.8) represent our new LTD system with a linear, PI controller. For the purposes of analyzing the modal properties of our system, consider that the state, control, and output vectors are simply perturbations from a reference condition. Without affecting the system's characteristic polynomial, it can be assumed that our desired result is to return to that reference condition. Then the output vector, $\mathbf{y_d}$, is a vector of zeros and the error vector, $\mathbf{e}$, becomes the negative of the output vector, $\mathbf{y}$.

$$\mathbf{e} = \mathbf{y_d} - \mathbf{y} = (\mathbf{0}_l) - \mathbf{y} = -\mathbf{y}$$

Then the control law, defined by equation (4.4), can be written as,

$$\begin{bmatrix} \mathbf{u_p}(t) \\ \mathbf{u_i}(t) \end{bmatrix} = -\begin{bmatrix} \mathbf{K_p} + \mathbf{K_b} \\ \mathbf{K_i} \end{bmatrix} \mathbf{y}(t)$$

Since, in this linear approximation, there is no way to differentiate between the effects of proportional gain in the feedback path, $\mathbf{K_b}$, and proportional gain in the feed-forward path, $\mathbf{K_p}$, there is no use in considering both and so $\mathbf{K_b}$ is neglected.

$$\begin{bmatrix} \mathbf{u_p}(t) \\ \mathbf{u_i}(t) \end{bmatrix} = -\begin{bmatrix} \mathbf{K_p} \\ \mathbf{K_i} \end{bmatrix} \mathbf{y}(t) \tag{4.9}$$

Equations (4.7) still follow the format of an LTD system: the new A-matrix is square, the new state and control are still time-dependent row vectors, and the new **A**-, **B**-, **C**-, and **D**-matrices are constant. Once combined with the standard output-based feedback control law of equation (4.9), we have a complete LTD feedback control system conducive to modal analysis. It is a convenient form that adds the integral terms (and their resultant poles) to the state vector to facilitate the analysis of modal properties and calculation of gains.

4.3 An Analysis of the Effects of Feedback Control on the Modal Properties

Until this point, the analysis of this chapter is generalized to any LTD system with a PI controller defined by equation (4.2), but we now begin to tailor the analysis to our model. When we combine our LTD system of equations (4.7) with our original state, control, and output vectors and our **A**-, **B**-, **C**- and **D**-matrices as defined in Chapter 3, we get,

$$\begin{bmatrix} \begin{bmatrix} \Delta \dot{V}_a \\ \Delta \dot{\gamma}_a \\ \Delta \dot{h} \end{bmatrix} \\ \begin{bmatrix} \dot{I}_{C_L} \\ \dot{I}_T \end{bmatrix} \end{bmatrix} = \begin{bmatrix} \begin{bmatrix} \dfrac{\partial f_{V_a}}{\partial V_a} & \dfrac{\partial f_{V_a}}{\partial \gamma_a} & 0 \\ \dfrac{\partial f_{\gamma_a}}{\partial V_a} & 0 & 0 \\ 0 & \dfrac{\partial f_h}{\partial \gamma_a} & 0 \end{bmatrix} & \begin{bmatrix} \dfrac{\partial f_{V_a}}{\partial C_L} & \dfrac{\partial f_{V_a}}{\partial T} \\ \dfrac{\partial f_{\gamma_a}}{\partial C_L} & 0 \\ 0 & 0 \end{bmatrix} \\ \begin{bmatrix} 0 & 0 & 0 \\ 0 & 0 & 0 \end{bmatrix} & \begin{bmatrix} 0 & 0 \\ 0 & 0 \end{bmatrix} \end{bmatrix} \begin{bmatrix} \begin{bmatrix} \Delta V_a \\ \Delta \gamma_a \\ \Delta h \end{bmatrix} \\ \begin{bmatrix} I_{C_L} \\ I_T \end{bmatrix} \end{bmatrix} + \begin{bmatrix} \begin{bmatrix} \dfrac{\partial f_{V_a}}{\partial C_L} & \dfrac{\partial f_{V_a}}{\partial T} \\ \dfrac{\partial f_{\gamma_a}}{\partial C_L} & 0 \\ 0 & 0 \end{bmatrix} & \begin{bmatrix} 0 & 0 \\ 0 & 0 \\ 0 & 0 \end{bmatrix} \\ \begin{bmatrix} 0 & 0 \\ 0 & 0 \end{bmatrix} & \begin{bmatrix} 1 & 0 \\ 0 & 1 \end{bmatrix} \end{bmatrix} \begin{bmatrix} \begin{bmatrix} u_{p_{C_L}} \\ u_{p_T} \end{bmatrix} \\ \begin{bmatrix} u_{i_{C_L}} \\ u_{i_T} \end{bmatrix} \end{bmatrix}$$

$$\begin{bmatrix} \Delta V_{IAS} \\ \Delta M \\ \Delta h \\ \Delta \dot{h} \end{bmatrix} = \begin{bmatrix} \begin{bmatrix} \dfrac{\partial V_{IAS}}{\partial V_a} & 0 & 0 \\ \dfrac{\partial M}{\partial V_a} & 0 & 0 \\ 0 & 0 & 1 \\ 0 & 60\left(\dfrac{\partial f_h}{\partial \gamma_a}\right) & 0 \end{bmatrix} & \begin{bmatrix} 0 & 0 \\ 0 & 0 \\ 0 & 0 \\ 0 & 0 \end{bmatrix} \end{bmatrix} \begin{bmatrix} \begin{bmatrix} \Delta V_a \\ \Delta \gamma_a \\ \Delta h \end{bmatrix} \\ \begin{bmatrix} I_{C_L} \\ I_T \end{bmatrix} \end{bmatrix} + \begin{bmatrix} \begin{bmatrix} 0 & 0 \\ 0 & 0 \\ 0 & 0 \\ 0 & 0 \end{bmatrix} & \begin{bmatrix} 0 & 0 \\ 0 & 0 \\ 0 & 0 \\ 0 & 0 \end{bmatrix} \end{bmatrix} \begin{bmatrix} \begin{bmatrix} u_{p_{C_L}} \\ u_{p_T} \end{bmatrix} \\ \begin{bmatrix} u_{i_{C_L}} \\ u_{i_T} \end{bmatrix} \end{bmatrix}$$

And the general form of our LTD system is,

$$
\begin{bmatrix} \Delta \dot{V_a} \\ \Delta \dot{\gamma_a} \\ \Delta \dot{h} \\ \dot{I}_{C_L} \\ \dot{I}_T \end{bmatrix} =
\begin{bmatrix}
\dfrac{\partial f_{V_a}}{\partial V_a} & \dfrac{\partial f_{V_a}}{\partial \gamma_a} & 0 & \dfrac{\partial f_{V_a}}{\partial C_L} & \dfrac{\partial f_{V_a}}{\partial T} \\
\dfrac{\partial f_{\gamma_a}}{\partial V_a} & 0 & 0 & \dfrac{\partial f_{\gamma_a}}{\partial C_L} & 0 \\
0 & \dfrac{\partial f_h}{\partial \gamma_a} & 0 & 0 & 0 \\
0 & 0 & 0 & 0 & 0 \\
0 & 0 & 0 & 0 & 0
\end{bmatrix}
\begin{bmatrix} \Delta V_a \\ \Delta \gamma_a \\ \Delta h \\ I_{C_L} \\ I_T \end{bmatrix}
+
\begin{bmatrix}
\dfrac{\partial f_{V_a}}{\partial C_L} & \dfrac{\partial f_{V_a}}{\partial T} & 0 & 0 \\
\dfrac{\partial f_{\gamma_a}}{\partial C_L} & 0 & 0 & 0 \\
0 & 0 & 0 & 0 \\
0 & 0 & 1 & 0 \\
0 & 0 & 0 & 1
\end{bmatrix}
\begin{bmatrix} u_{p_{C_L}} \\ u_{p_T} \\ u_{i_{C_L}} \\ u_{i_T} \end{bmatrix}
$$

$$
\begin{bmatrix} \Delta V_{IAS} \\ \Delta M \\ \Delta h \\ \Delta \dot{h} \end{bmatrix} =
\begin{bmatrix}
\dfrac{\partial V_{IAS}}{\partial V_a} & 0 & 0 & 0 & 0 \\
\dfrac{\partial M}{\partial V_a} & 0 & 0 & 0 & 0 \\
0 & 0 & 1 & 0 & 0 \\
0 & 60\left(\dfrac{\partial f_h}{\partial \gamma_a}\right) & 0 & 0 & 0
\end{bmatrix}
\begin{bmatrix} \Delta V_a \\ \Delta \gamma_a \\ \Delta h \\ I_{C_L} \\ I_T \end{bmatrix}
\qquad (4.10)^{*}
$$

Following the form of the general gain matrix of equation (4.3), our proportional, integral, and feedback gain matrices are,

$$
\mathbf{K_p} = \begin{bmatrix} k_{p_{11}} & k_{p_{12}} & k_{p_{13}} & k_{p_{14}} \\ k_{p_{21}} & k_{p_{22}} & k_{p_{23}} & k_{p_{24}} \end{bmatrix} \qquad (4.11)
$$

$$
\mathbf{K_i} = \begin{bmatrix} k_{i_{11}} & k_{i_{12}} & k_{i_{13}} & k_{i_{14}} \\ k_{i_{21}} & k_{i_{22}} & k_{i_{23}} & k_{i_{24}} \end{bmatrix} \qquad (4.12)
$$

$$
\mathbf{K_b} = \begin{bmatrix} k_{b_{11}} & k_{b_{12}} & k_{b_{13}} & k_{b_{14}} \\ k_{b_{21}} & k_{b_{22}} & k_{b_{23}} & k_{b_{24}} \end{bmatrix} \qquad (4.13)
$$

Substituting into equation (4.9), we have our control law.

---

* Note that the $\dot{h}$ equation has added a factor of 60 to its $\partial f_h / \partial \gamma_a$ term. This is to convert the output from $ft/\sec$ to $ft/\min$ as would be read on a real vertical speed indicator.

$$
\begin{bmatrix} u_{P_{C_L}} \\ u_{P_T} \\ u_{i_{C_L}} \\ u_{i_T} \end{bmatrix} = - \begin{bmatrix} k_{p_{11}} & k_{p_{12}} & k_{p_{13}} & k_{p_{14}} \\ k_{p_{21}} & k_{p_{22}} & k_{p_{23}} & k_{p_{24}} \\ k_{i_{11}} & k_{i_{12}} & k_{i_{13}} & k_{i_{14}} \\ k_{i_{21}} & k_{i_{22}} & k_{i_{23}} & k_{i_{24}} \end{bmatrix} \begin{bmatrix} \Delta V_{IAS} \\ \Delta M \\ \Delta h \\ \Delta \dot{h} \end{bmatrix}
\tag{4.14}
$$

There are 16 gains in our gain matrix, each representing the effect of feedback of a particular output parameter to a particular control parameter. To gain insight into the effect each feedback gain is likely to have, we examine the root locus of each gain. Consider a Boeing 767-300 at a reference weight of 198,000 lbs in steady, level flight at 300 knots indicated airspeed (KIAS) and 30,000 feet. For this example, the LTD system of equations (4.10) becomes,

$$
\begin{bmatrix} \Delta \dot{V}_a \\ \Delta \dot{\gamma}_a \\ \Delta \dot{h} \\ \dot{I}_{C_L} \\ \dot{I}_T \end{bmatrix} = \begin{bmatrix} -0.0889 & -32.2 & 0 & -21.7 & 0.000163 \\ 0.000366 & 0 & 0 & 0.173 & 0 \\ 0 & 787 & 0 & 0 & 0 \\ 0 & 0 & 0 & 0 & 0 \\ 0 & 0 & 0 & 0 & 0 \end{bmatrix} \begin{bmatrix} \Delta V_a \\ \Delta \gamma_a \\ \Delta h \\ I_{C_L} \\ I_T \end{bmatrix} + \begin{bmatrix} -21.7 & 0.000163 & 0 & 0 \\ 0.173 & 0 & 0 & 0 \\ 0 & 0 & 0 & 0 \\ 0 & 0 & 1 & 0 \\ 0 & 0 & 0 & 1 \end{bmatrix} \begin{bmatrix} u_{P_{C_L}} \\ u_{P_T} \\ u_{i_{C_L}} \\ u_{i_T} \end{bmatrix}
$$

$$
\begin{bmatrix} \Delta V_{IAS} \\ \Delta M \\ \Delta h \\ \Delta \dot{h} \end{bmatrix} = \begin{bmatrix} 0.593 & 0 & 0 & 0 & 0 \\ 0.00100 & 0 & 0 & 0 & 0 \\ 0 & 0 & 1 & 0 & 0 \\ 0 & 47200 & 0 & 0 & 0 \end{bmatrix} \begin{bmatrix} \Delta V_a \\ \Delta \gamma_a \\ \Delta h \\ I_{C_L} \\ I_T \end{bmatrix}
$$

Figure 4.2 - Figure 4.5 show how the phugoid mode poles are moved by various types of feedback. Figure 4.2 illustrates the system's behavior with different proportional feedback to the lift coefficient. The first subplot shows the positive feedback of indicated airspeed to the lift coefficient, which we see is unstable. A moment's reflection on the nature of the system provides intuitive verification. An increase in the lift coefficient results in higher drag, which serves to slow the aircraft. This implies that lowering the lift coefficient would serve to increase speed. The second subplot verifies this and shows negative speed feedback to the lift coefficient provides for a stable control.

The third subplot shows the effect of altitude feedback to lift coefficient, which we see tends to shoot the phugoid poles up along the imaginary axis. This will increase the phugoid natural frequency while reducing the damping of the system.

The fourth subplot shows the effect of altitude rate feedback to lift coefficient. Here we see a well behaved loop. Feeding back the altitude rate tends to dampen the system. This effect can be intuitively verified by remembering that rate terms usually do increase the damping of a system.

Figure 4.3 shows the effects of integral feedback to the lift coefficient. The second subplot shows a problem with instabilities of integral speed feedback to the lift coefficient. If we choose to use negative integral speed feedback to the lift coefficient, we will need to feed some output in the feedback path to keep it stable. The fourth subplot shows that we need to be careful with low damping of integral altitude rate feedback to the lift coefficient.

Figure 4.4 shows the effect of proportional feedback to the thrust. The first subplot shows positive feedback of indicated airspeed to the thrust. The locus is well behaved and tends to increase the damping of the system. Positive feedback of indicated airspeed or Mach to the thrust is a good choice for the control of speed. The fourth subplot shows altitude rate feedback to the thrust. The altitude rate here tends to have the same effect on the Phugoid poles that altitude feedback had to the lift coefficient. Altitude rate feedback to the thrust is not a good choice for controlling altitude rate or altitude. Similarly, the third subplot shows that altitude feedback to the thrust drives the system unstable
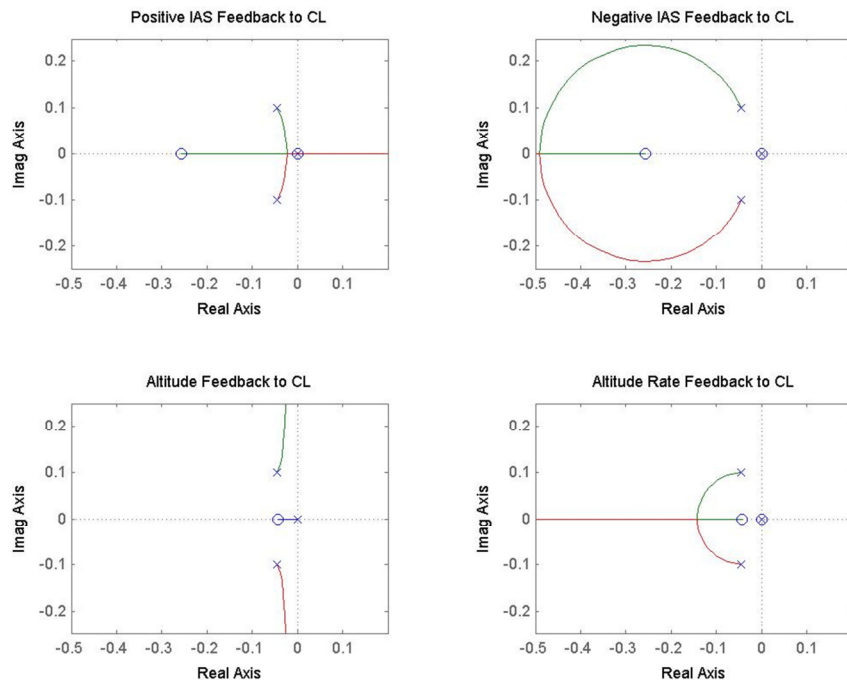
Figure 4.2. Effects of proportional feedback to the lift coefficient
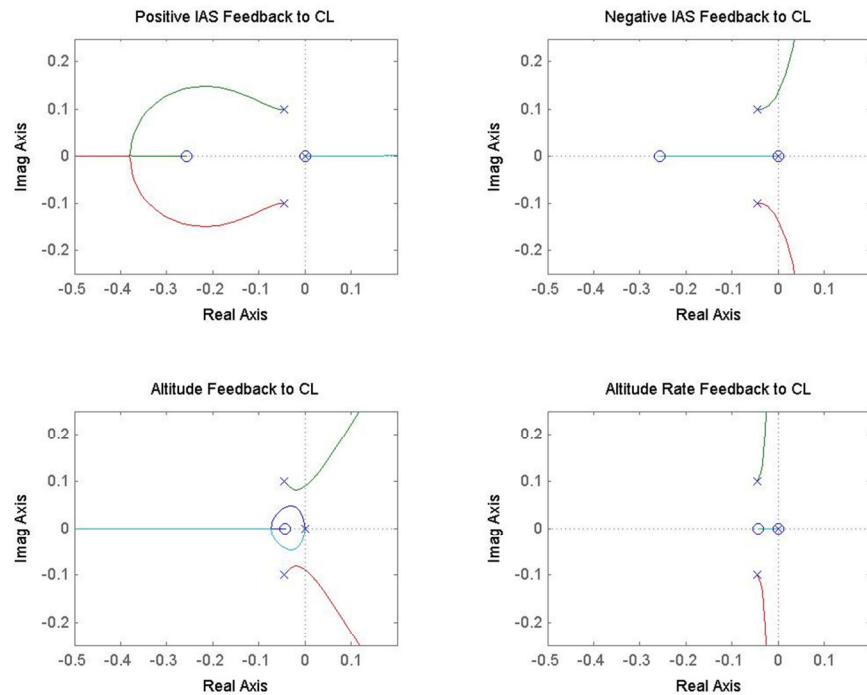
Figure 4.3. Effects of integral feedback to the lift coefficient
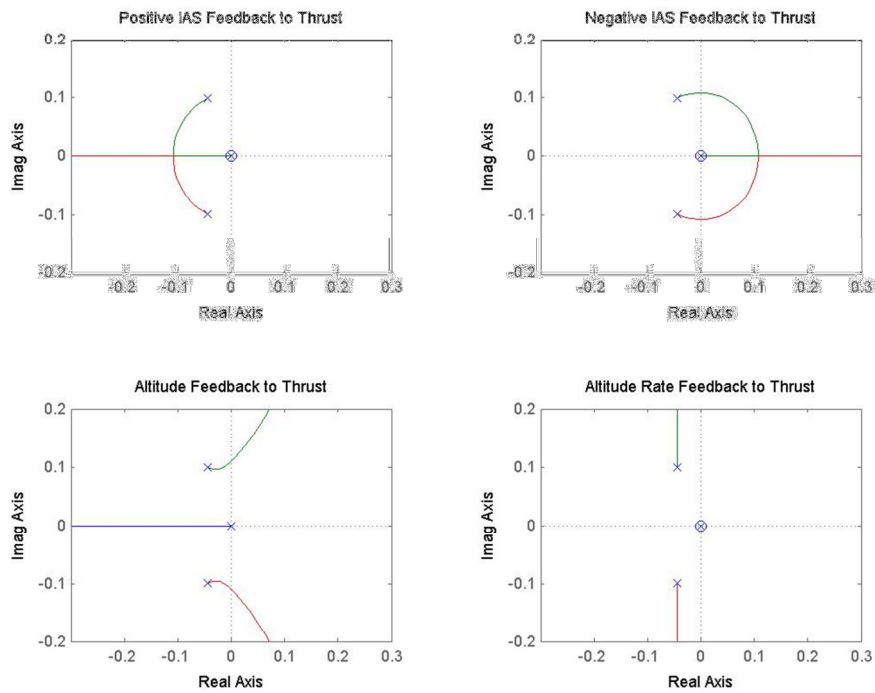
Figure 4.4 Effects of Proportional Feedback to the Thrust
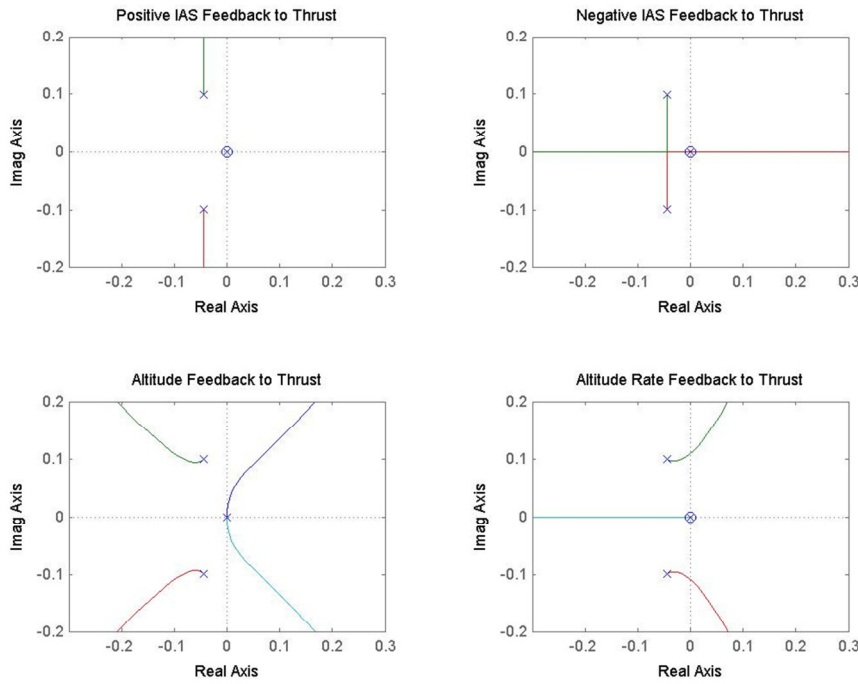
Figure 4.5 Effects of Integral Feedback to the Thrust

Figure 4.5 shows the effects of integral feedback to the thrust. The third and fourth subplots confirm that it is not wise to control altitude or altitude rate with thrust because the system becomes unstable as soon as we apply control. The first subplot shows that integral feedback of speed to the thrust tends to shoot the phugoid poles up the imaginary axis, increasing the natural frequency and lowering the damping of the response. This implies that we need to be mindful of low damping when controlling speed with the thrust.

4.4 Feedback Controller Design

In the previous section, we analyzed the effects of feedback control on the modal properties of the LTD system in order to gain insight into how feedback control would affect our nonlinear, four-degree-of-freedom model. In this section, we continue to use the LTD system to design feedback controllers for several different regions of an aircraft's flight regime. The LTD system provides a suitable approximation to the nonlinear system so that feedback controllers designed using the LTD system will produce similar results in our nonlinear model. Each controller is customized to attain the desired flight configuration using smooth transitions that are typical of commercial aircraft flight.

Let us summarize our conclusions from the analysis of the root loci of the LTD system. The primary control input in an aircraft is the control stick (i.e., the lift coefficient), so it should be the primary control in our controller as well. Figure 4.2 and Figure 4.3 show that we can successfully control speed with the lift coefficient, as long as we use negative feedback, and as long as we feed output (e.g., altitude rate) in the feedback path to keep the controller stable. Figure 4.2 and Figure 4.3 also show that we can successfully control altitude rate with the lift coefficient. Figure 4.4 and Figure 4.5 show that we can successfully control speed with the throttle (i.e., thrust). Our basic strategy will be to …

- use lift coefficient to control altitude rate during speed changes;
- use lift coefficient to control speed during altitude changes, while feeding back altitude rate to keep the system stable; and
- use thrust to control speed and lift coefficient to control altitude rate when we need to control both.

Our control law allows us to feedback all outputs to both inputs; although only a fraction of the gains are used in a given feedback system. To design our controllers, we will use our full control law, as defined by equation (4.8) and expanded here using the gain matrix definitions of equations (4.11), (4.12), and (4.13).

$$
\begin{bmatrix} u_{P_{C_L}} \\ u_{P_T} \\ u_{i_{C_L}} \\ u_{i_T} \end{bmatrix} = \begin{bmatrix} k_{p_{11}} & k_{p_{12}} & k_{p_{13}} & k_{p_{14}} \\ k_{p_{21}} & k_{p_{22}} & k_{p_{23}} & k_{p_{24}} \\ k_{i_{11}} & k_{i_{12}} & k_{i_{13}} & k_{i_{14}} \\ k_{i_{21}} & k_{i_{22}} & k_{i_{23}} & k_{i_{24}} \end{bmatrix} \begin{bmatrix} e_1 \\ e_2 \\ e_3 \\ e_4 \end{bmatrix} - \begin{bmatrix} k_{b_{11}} & k_{b_{12}} & k_{b_{13}} & k_{b_{14}} \\ k_{b_{21}} & k_{b_{22}} & k_{b_{23}} & k_{b_{24}} \\ 0 & 0 & 0 & 0 \\ 0 & 0 & 0 & 0 \end{bmatrix} \begin{bmatrix} V_{IAS} \\ M \\ h \\ \dot{h} \end{bmatrix}
\tag{4.15}
$$

The control inputs to the system split into their proportional and integrated parts. The control inputs $u_{P_{C_L}}$ and u_{P_T} are the proportional portions of the lift coefficient and thrust respectively, and $u_{i_{C_L}}$ and u_{i_T} are the integrated portions of lift coefficient and thrust.

4.4.1 Lift Coefficient Control of Altitude Rate
There are several flight regimes in which a pilot uses the control stick to capture or maintain altitude rate while allowing the speed to change. During level flight accelerations and decelerations, a pilot will preset the thrust (maximum thrust for acceleration, idle thrust for deceleration) and allow the speed to change accordingly while using the control stick to maintain level flight (i.e., a zero altitude rate). Alternatively, the pilot may wish to capture and maintain a desired, non-zero altitude rate and let the speed change as it may (i.e., during accelerations in climb or decelerations in descent).

For these regions, we need a controller that uses lift coefficient to control altitude rate but does not modulate thrust. In the truest sense, the controller is not controlling speed; however, in actuality the speed is controlled because we preset the thrust according to the desired direction of the speed change. When the speed nears the desired steady, level flight condition, we switch to a controller that simultaneously controls speed and altitude rate.

To accomplish the goals of this controller, we need simply to command an altitude rate for all time. For this reason we can simplify the output equation of the LTD system of equation (4.10) to,

$$\Delta \dot{h} = \begin{bmatrix} 0 & 60\left(\dfrac{\partial f_h}{\partial \gamma_a}\right) & 0 \end{bmatrix} \begin{bmatrix} \Delta V_a \\ \Delta \gamma_a \\ \Delta h \end{bmatrix}$$

In doing so, we can see that the dynamics of the system are governed exclusively by the $\dot{h}/C_L$ transfer function as defined in Chapter 3. Consider a DC-9 traveling at 15000 ft and 578 ft/sec and weighing 140,000lbs. The LTD system is shown below with its reduced control and output vectors. The phugoid eigenvalues for the open loop system are located at $-0.0036 \pm 0.0786i$, which corresponds to a natural frequency of 0.0787 rad/sec and a damping ratio of 0.0445. A plot of the step response of the system to a 0.1 change in lift coefficient is shown in Figure 4.6.

$$\begin{bmatrix} \Delta \dot{V}_a \\ \Delta \dot{\gamma}_a \\ \Delta \dot{h} \\ \dot{I}_{C_L} \end{bmatrix} = \begin{bmatrix} -0.0072 & -32.2 & 0 & -2.74 \\ 0.0002 & 0 & 0 & 0.1202 \\ 0 & 578.47 & 0 & 0 \\ 0 & 0 & 0 & 0 \end{bmatrix} \begin{bmatrix} \Delta V_a \\ \Delta \gamma_a \\ \Delta h \\ I_{C_L} \end{bmatrix} + \begin{bmatrix} -2.74 & 0 \\ 0.1202 & 0 \\ 0 & 0 \\ 0 & 1 \end{bmatrix} \begin{bmatrix} u_{P_{C_L}} \\ u_{i_{C_L}} \end{bmatrix} \qquad (4.16)$$

$$\Delta \dot{h} = \begin{bmatrix} 0 & 578.47 & 0 \end{bmatrix} \begin{bmatrix} \Delta V_a \\ \Delta \gamma_a \\ \Delta h \end{bmatrix}$$
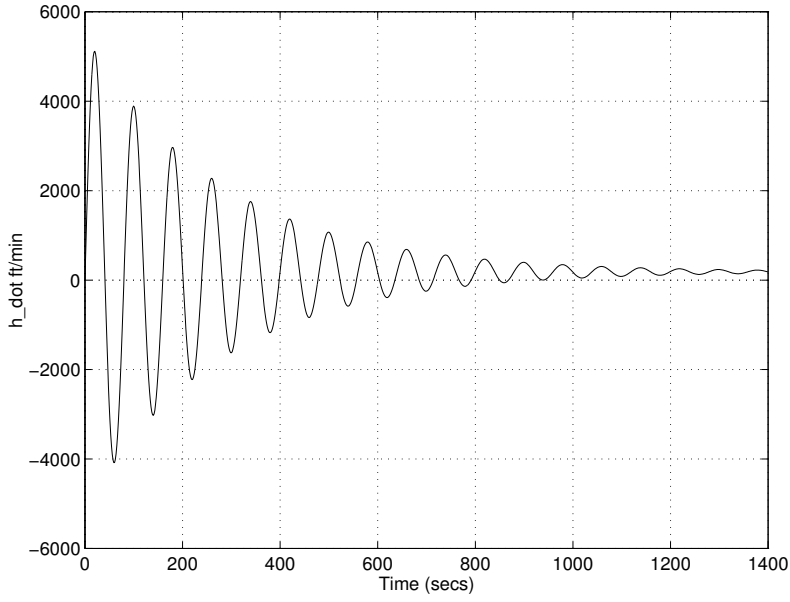
Figure 4.6. System response to a 0.1 step in lift coefficient
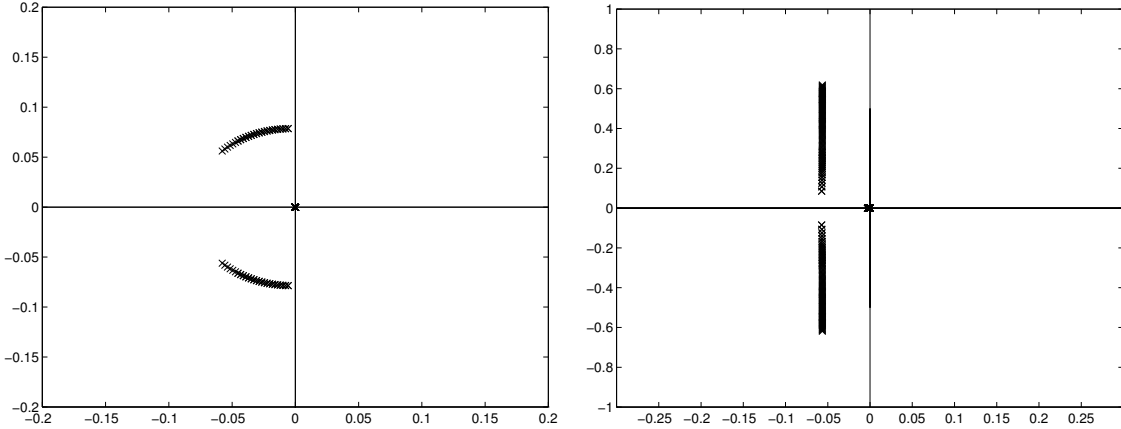
Figure 4.7. Root Loci of $k_{p_{14}}$ (left) and $k_{i_{14}}$ (right) successive loop closures

It is desired to increase the frequency and damping of the system while having zero steady state error. We start with proportional altitude rate feedback to the lift coefficient, $k_{p_{14}}$, shown in the left side of Figure 4.7. A value of $k_{p_{14}} = 2.6 \times 10^{-5}$ moves the poles to location of $-0.0578 \pm 0.0562i$ with a damping ratio of 0.7173 and a natural frequency of 0.0806rad/sec. We add integral control to guarantee zero steady state error, not frequency changes; but we must be careful about the associated decrease in damping we noticed in our preliminary analysis. As seen on the right half of Figure 4.7, we move the poles with

$k_{i_{14}} = 9.0 \times 10^{-5}$ to a location of $-0.0565 \pm 0.6152i$. In doing so, we increase the frequency of the mode to 0.6178 rad/sec but we reduce the damping to 0.0914. To correct

for the low damping we can increase the gain $k_{p_{14}}$ once again and move the Phugoid poles to the left as shown in Figure 4.8.

The final values chosen for $k_{p_{14}}$ and $k_{i_{14}}$ are 2.08×10^{-4} and 9.0×10^{-5}. The final step response is shown in Figure 4.9. Notice that the system achieves the 1000 ft/min climb rate with zero steady state error. Furthermore, the time history for the lift coefficient is well within acceptable bounds. Note however that the lift coefficient initially is rather aggressive. In the next chapter, we define limits to the amount a control input can change in a time-step so that such aggressive control action is made more realistic.

The method of successive loop closures is good for initial work and illustration of the system dynamics, but it is tedious if many gains must be chosen or specific dynamic properties are desired quickly. Furthermore, for the purpose of scheduling gains, the method of choosing gains must be automated. Automating gain scheduling is reasonably straightforward once a control scheme has been established. Since the control logic is simple, the method of pole placement can be completely analytic. This explicit method of pole placement is outlined in Brogan (1991). Its limitation is that it is cumbersome and useful only for low-order systems, however its simplicity gives added flexibility in gain selection.
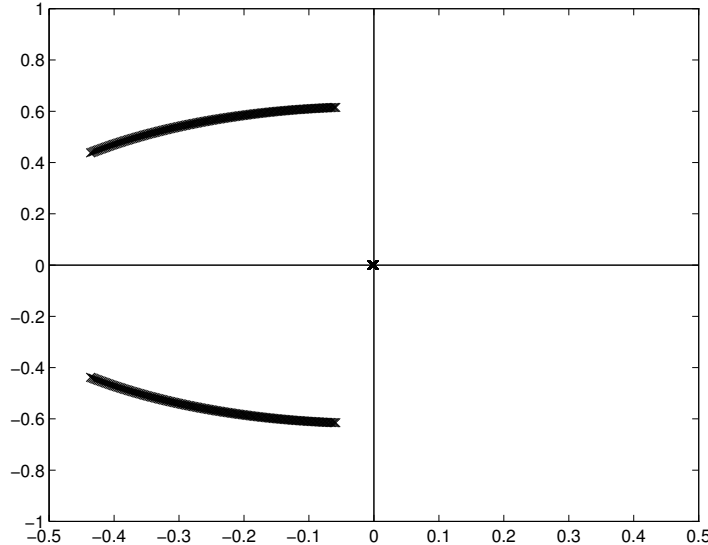
Figure 4.8. The effects of an increased proportional gain $k_{p_{14}}$
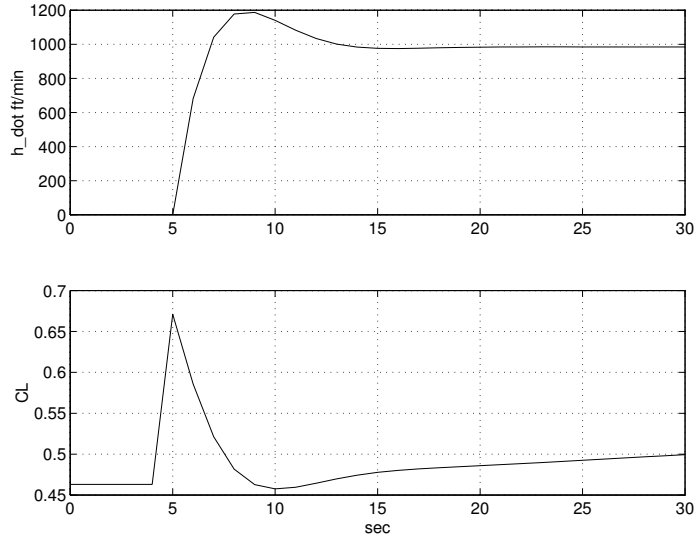
Figure 4.9. System response to a 1000 ft/min commanded rate of climb

The process starts with replacing the individual terms in the system of equations with placeholders to simplify the final expressions. Furthermore, since we are not feeding back altitude and it does not contribute to the dynamics, we can remove it from the state equation.

$$
\begin{bmatrix} \Delta \dot{V}_a \\ \Delta \dot{\gamma}_a \\ \dot{I}_{C_L} \end{bmatrix} = \begin{bmatrix} a_{11} & a_{12} & b_{11} \\ a_{21} & 0 & b_{21} \\ 0 & 0 & 0 \end{bmatrix} \begin{bmatrix} \Delta V_a \\ \Delta \gamma_a \\ I_{C_L} \end{bmatrix} + \begin{bmatrix} b_{11} & 0 \\ b_{21} & 0 \\ 0 & 1 \end{bmatrix} \begin{bmatrix} u_{p_{C_L}} \\ u_{i_{C_L}} \end{bmatrix}
$$

$$
\Delta \dot{h} = \begin{bmatrix} 0 & c_{42} & 0 \end{bmatrix} \begin{bmatrix} \Delta V_a \\ \Delta \gamma_a \\ I_{C_L} \end{bmatrix}
$$

We want to be able to control the eigenvalues of the closed loop A-matrix, which is defined as follows.

$$
\mathbf{A}_{cl} = \mathbf{A} - \mathbf{BKC}
$$

$$
\mathbf{A}_{cl} = \begin{bmatrix} a_{11} & a_{12} & b_{11} \\ a_{21} & 0 & b_{21} \\ 0 & 0 & 0 \end{bmatrix} - \begin{bmatrix} b_{11} & 0 \\ b_{21} & 0 \\ 0 & 1 \end{bmatrix} \begin{bmatrix} 0 & k_{p_{14}} \\ 0 & k_{i_{14}} \end{bmatrix} \begin{bmatrix} 0 & c_{42} & 0 \end{bmatrix}
$$

-93-

Simplifying,

$$\mathbf{A_{cl}} = \begin{bmatrix} a_{11} & a_{12} & b_{11} \\ a_{21} & 0 & b_{21} \\ 0 & 0 & 0 \end{bmatrix} - \begin{bmatrix} b_{11} & 0 \\ b_{21} & 0 \\ 0 & 1 \end{bmatrix} \begin{bmatrix} k_{p_{14}} \\ k_{i_{14}} \end{bmatrix} \begin{bmatrix} 0 & c_{42} & 0 \end{bmatrix}$$

$$\mathbf{A_{cl}} = \begin{bmatrix} a_{11} & a_{12} & b_{11} \\ a_{21} & 0 & b_{21} \\ 0 & 0 & 0 \end{bmatrix} - \begin{bmatrix} b_{11} & 0 \\ b_{21} & 0 \\ 0 & 1 \end{bmatrix} \begin{bmatrix} 0 & c_{42}k_{p_{14}} & 0 \\ 0 & c_{42}k_{i_{14}} & 0 \end{bmatrix}$$

$$\mathbf{A_{cl}} = \begin{bmatrix} a_{11} & a_{12} & b_{11} \\ a_{21} & 0 & b_{21} \\ 0 & 0 & 0 \end{bmatrix} - \begin{bmatrix} 0 & b_{11}c_{42}k_{p_{14}} & 0 \\ 0 & b_{21}c_{42}k_{p_{14}} & 0 \\ 0 & c_{42}k_{i_{14}} & 0 \end{bmatrix}$$

we have the final closed loop A-matrix in Equation (4.17).

$$\mathbf{A_{cl}} = \begin{bmatrix} a_{11} & a_{12}-b_{11}c_{42}k_{p_{14}} & b_{11} \\ a_{21} & -b_{21}c_{42}k_{p_{14}} & b_{21} \\ 0 & -c_{42}k_{i_{14}} & 0 \end{bmatrix} \tag{4.17}$$

Next, we need to calculate the characteristic polynomial for the A-matrix.

$$[s\mathbf{I} - \mathbf{A_{cl}}] = \begin{bmatrix} s-a_{11} & -a_{12}+b_{11}c_{42}k_{p_{14}} & -b_{11} \\ -a_{21} & s+b_{21}c_{42}k_{p_{14}} & -b_{21} \\ 0 & c_{42}k_{i_{14}} & s \end{bmatrix}$$

Finally, we have an expression for the characteristic polynomial shown in (4.18).

$$\begin{aligned}
\det[s\mathbf{I} - \mathbf{A_{cl}}] &= (s-a_{11})\left(s^2 + c_{42}b_{21}k_{p_{14}}s\right) + a_{21}b_{11}c_{42}k_{i_{14}} \\
&\quad + \left(-a_{12} + c_{42}b_{11}k_{p_{14}}\right)(a_{21}s) \\
&\quad + (s-a_{11})(b_{21})(c_{42}k_{i_{14}}) \\
&= s^3 + c_{42}b_{21}k_{p_{14}}s^2 - a_{11}s^2 - a_{11}c_{42}b_{21}k_{p_{14}}s + a_{21}b_{11}c_{42}k_{i_{14}} \\
&\quad - a_{12}a_{21}s + c_{42}b_{11}k_{p_{14}}a_{21}s + b_{21}c_{42}k_{i_{14}}s - a_{11}b_{21}c_{42}k_{i_{14}}
\end{aligned}$$

$$\det\left[s\mathbf{I}-\mathbf{A_{cl}}\right]=s^3+\left(c_{42}b_{21}k_{p_{14}}-a_{11}\right)s^2$$
$$+\left(c_{42}b_{11}k_{p_{14}}a_{21}+b_{21}c_{42}k_{i_{14}}-a_{11}c_{42}b_{21}k_{p_{14}}-a_{12}a_{21}\right)s \qquad (4.18)$$
$$+\left(a_{21}b_{11}c_{42}k_{i_{14}}-a_{11}b_{21}c_{42}k_{i_{14}}\right)$$

From this we can determine what gains are necessary to achieve the desired characteristic polynomial. We have the following form of the characteristic polynomial:

$$\det\left[s\mathbf{I}-\mathbf{A_{cl}}\right]=c_1 s^3+c_2 s^2+c_3 s+c_4$$

Therefore, we can set each coefficient equal to its corresponding term in Equation (4.18).

$$c_1=1$$
$$c_2=\left(c_{42}b_{21}k_{p_{14}}-a_{11}\right)$$
$$c_3=\left(b_{21}c_{42}k_{i_{14}}-a_{11}c_{42}b_{21}k_{p_{14}}-a_{12}a_{21}+c_{42}b_{11}k_{p_{14}}a_{21}\right)$$
$$c_4=\left(a_{21}c_{42}b_{11}k_{i_{14}}-a_{11}b_{21}c_{42}k_{i_{14}}\right)$$

Being able to define the coefficients in terms of the gains is helpful; however, we really want to determine the gains from the coefficients to be sure of getting the correct response. This is a problem because we have three linearly independent equations and two unknown gains. In order to solve this system, we will have to leave one of the modal properties of the third order system as an unknown. The characteristic polynomial in terms of modal properties is,

$$\det\left[s\mathbf{I}-\mathbf{A_{cl}}\right]=\left(s-p_1\right)\left(s^2+2\zeta\omega_n s+\omega_n^2\right)$$

where ζ and ω_n are the damping ratio and natural frequency of the oscillatory motion and p_1 is the system poll. We can expand this form of the characteristic polynomial and set the coefficients equal to those in the previous form.

$$2\zeta\omega_n-p_1=\left(c_{42}b_{21}k_{p_{14}}-a_{11}\right)$$
$$\omega_n^2-2\zeta\omega_n p_1=\left(b_{21}c_{42}k_{i_{14}}-a_{11}c_{42}b_{21}k_{p_{14}}-a_{12}a_{21}+c_{42}b_{11}k_{p_{14}}a_{21}\right)$$
$$-\omega_n^2 p_1=\left(a_{21}c_{42}b_{11}k_{i_{14}}-a_{11}b_{21}c_{42}k_{i_{14}}\right)$$

$$2\zeta\omega_n - p_1 = \left(b_{21}c_{42}k_{p_{14}} - a_{11}\right)$$

$$\omega_n^2 - 2\zeta\omega_n p_1 = \left(a_{21}b_{11} - a_{11}b_{21}\right)c_{42}k_{p_{14}} + b_{21}c_{42}k_{i_{14}} - a_{12}a_{21}$$

$$-\omega_n^2 p_1 = \left(a_{21}b_{11} - a_{11}b_{21}\right)c_{42}k_{i_{14}}$$

This system of equations is linear with constant coefficients and can be written in matrix form.

$$
\begin{bmatrix}
b_{21}c_{42} & 0 & 1 \\
\left(a_{21}b_{11} - a_{11}b_{21}\right)c_{42} & 0 & 2\zeta\omega_n \\
0 & \left(a_{21}b_{11} - a_{11}b_{21}\right)c_{42} & \omega_n^2
\end{bmatrix}
\begin{bmatrix}
k_{p_{14}} \\
k_{i_{14}} \\
p_1
\end{bmatrix}
=
\begin{bmatrix}
a_{11} + 2\zeta\omega_n \\
\omega_n^2 + a_{12}a_{21} \\
0
\end{bmatrix}
$$

This matrix equation is easily solved for the gains. I damping ratio of 0.9 and a natural frequency of 2.0 are suggested.

4.4.2 Lift Coefficient Control of Speed

During climbs and descents, a pilot typically maintains a constant airspeed or Mach number during the altitude change. The pilot will preset the thrust (climb thrust for climbs, idle thrust for descents) and allow the altitude rate to vary accordingly while using the control stick to maintain speed. For these regions, we need a controller that uses lift coefficient to control speed but does not modulate thrust. Since the aircraft has two measurements for speed, Mach and indicated airspeed, both speeds have to be considered in separate analyses. However, since the solutions are identical with the exception of a few changes in feedback gains, only the Mach case is discussed.

The goal of the feedback controller is to capture a given speed by adjusting the lift coefficient. This means that the system is mainly governed by the M/C_L transfer function discussed in Section 3.3.2. However, feedback of speed to the lift coefficient has a problem with low damping as illustrated in Figure 4.2. The feedback control strategy to fix the low damping problem has already been touched upon in Section 3.3.2. Our basic strategy is to build a proportional -plus- integral controller for capturing Mach, and then feedback altitude rate in the feedback path to increase the damping of the system.

We will need two of the four outputs to complete the design, so the output equation of the LTD system of equation (4.10) can be simplified to,

$$\begin{bmatrix} \Delta M \\ \Delta \dot{h} \end{bmatrix} = \begin{bmatrix} \dfrac{\partial M}{\partial V_a} & 0 & 0 \\ 0 & 60\left(\dfrac{\partial f_h}{\partial \gamma_a}\right) & 0 \end{bmatrix} \begin{bmatrix} \Delta V_a \\ \Delta \gamma_a \\ \Delta h \end{bmatrix}$$

Consider the same DC-9 traveling at 15000 ft and 578 ft/sec and weighing 140,000lbs. The open loop dynamics for the system are the same as shown in equation (4.16), and our new output equation is

$$\begin{bmatrix} \Delta M \\ \Delta \dot{h} \end{bmatrix} = \begin{bmatrix} 9.45 \times 10^5 & 0 & 0 \\ 0 & 3.47 \times 10^4 & 0 \end{bmatrix} \begin{bmatrix} \Delta V_a \\ \Delta \gamma_a \\ \Delta h \end{bmatrix}$$

Initially, the phugoid eigenvalues are located at $-0.0036 \pm 0.0786i$, which correspond to a natural frequency of 0.0787 rad/sec and a damping ratio of 0.0445 (which is very low damping). We start the loop closures by closing the feedback path $k_{b_{14}}$ as shown in Figure 4.10. Setting $k_{b_{14}} = 2.7 \times 10^{-5}$ moves the poles to $-0.0599 \pm 0.0540i$, which correspond to a natural frequency of 0.0806 rad/sec and a damping ratio of 0.7173 (a more suitable damping ratio). Applying proportional Mach feedback to the lift coefficient, we increase the frequency of the poles to 0.20 rad/sec, which we initially think is a good value as shown in Figure 4.11. The resulting feedback gain is $k_{p_{12}} = -9.5$. Note the negative value of $k_{p_{12}}$. This makes intuitive sense because an increase in speed should be the result of a lower lift coefficient. It is also consistent with our conclusions from Figure 4.2. To test the partially built controller, we attempt a command to Mach 0.7. From the simulation shown in Figure 4.12, we find out that, while we like the response, the required control effort is excessive. The lift coefficient drops nearly to -1. Realizing that too much control effort is required, we drop the frequency down to 0.1 rad/sec, which corresponds to a gain of $k_{p_{12}} = -1.5$. With this reduction in gain, the poles sit at $-0.0618 \pm 0.0904i$ with a frequency of 0.1095 rad/sec and a damping ratio of 0.5647.
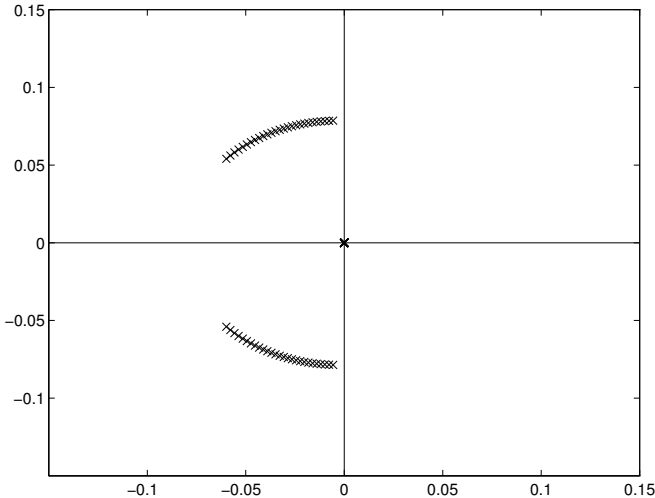
Figure 4.10. $k_{b_{14}}$ root locus for the Mach Capture controller

The next loop closure, the integral control, is tricky because the integral control tends to send the poles towards the right half plane. Integral control also pulls the integrator pole away from zero along the negative real axis. A gain of $k_{i_{12}} = -0.1$ is applied, which tends to line up the real part of the conjugate pair with the integrator pole as shown in Figure 4.13. The poles move to $-0.0412 \pm 0.0846i$ where the frequency is 0.0941 rad/sec and the damping is 0.4377. Since the damping is low, more altitude rate is applied. The altitude rate is applied until the locus starts to curve back inward and head towards the imaginary axis. The gain is set to $k_{b_{14}} = 4.2 \times 10^{-5}$ where the frequency of the system is 0.0614 rad/sec and the damping is 0.7265.
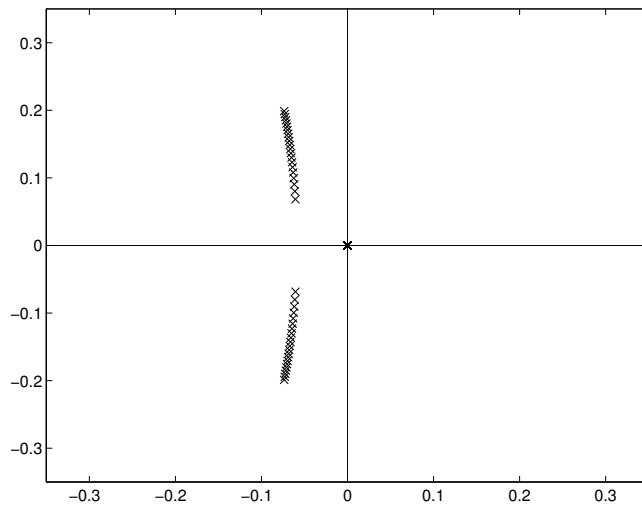
Figure 4.11. $k_{p_{12}}$ root locus for the Mach Capture controller

We also note that the integrator pole is moved to -0.0971. The complete system is simulated as shown in Figure 4.14. From Figure 4.14 we see that the controller captures a Mach of 0.7 and that the lift coefficient is not unreasonable. However, the speed of the response is low.
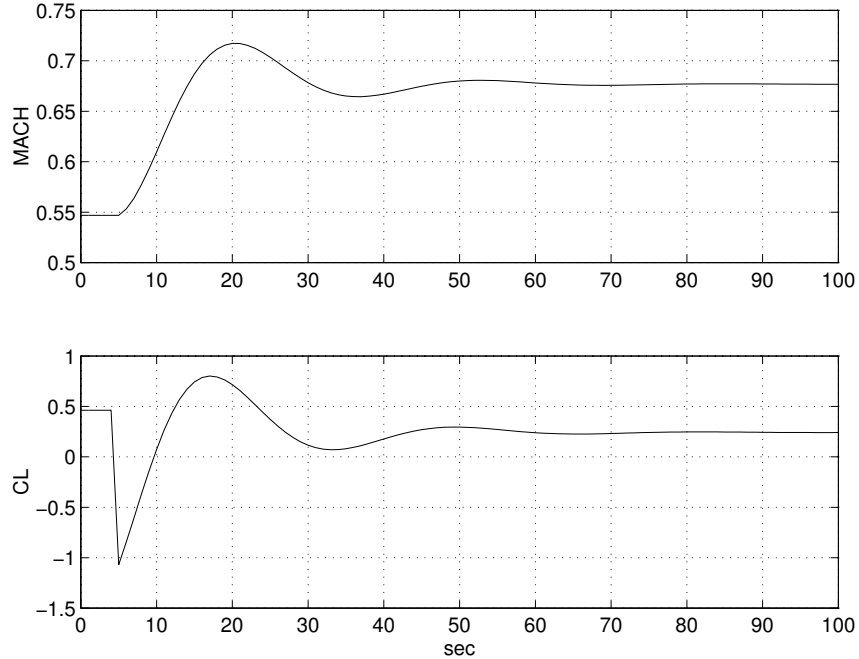
Figure 4.12. Simulated Mach Capture
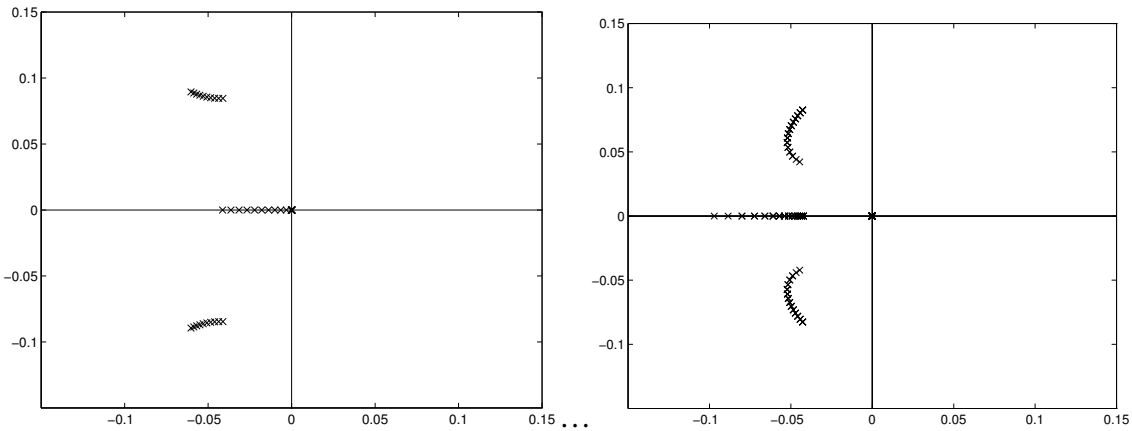
Figure 4.13. $k_{i_{12}}$ (left) and $k_{b_{14}}$ (right) root loci for Mach capture

In adding the extra gain to $k_{b_{14}}$ we diminished our frequency so we would probably want to redo the design if this set of gains were actually going to be used. However, the actual

gains used are calculated automatically by the gain scheduling algorithm where we can choose exactly the modal properties that we want.
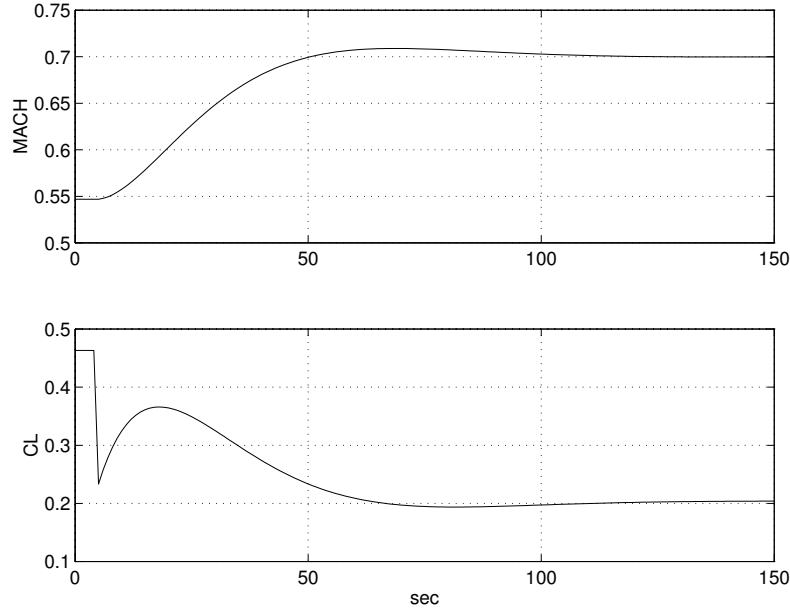
Figure 4.14. Simulation of the Completed Mach Capture

We have seen from the control law design that successive loop closures can be difficult. In this example, one can see that just about any set of modal properties could be achieved; however, the trial and error approach is certain to take a considerable amount of time. It is still valuable to manually close the loops at least once because it helps to build our understanding of the system dynamics. For instance, we now know that high system frequencies require an excessive control force. For this system, it is best to schedule natural frequencies on the order of 0.1 rad/sec and no higher. For the purpose of scheduling the actual gains, the automated method is presented next.

Taking the LTD system of equation (4.10), we remove indicated airspeed and altitude from the output equation and we remove altitude and integrated thrust from the state equation.

$$
\begin{bmatrix} \Delta \dot{V}_a \\ \Delta \dot{\gamma}_a \\ \dot{I}_{C_L} \end{bmatrix} = \begin{bmatrix} a_{11} & a_{12} & b_{11} \\ a_{21} & 0 & b_{21} \\ 0 & 0 & 0 \end{bmatrix} \begin{bmatrix} \Delta V_a \\ \Delta \gamma_a \\ I_{C_L} \end{bmatrix} + \begin{bmatrix} b_{11} & 0 \\ b_{21} & 0 \\ 0 & 1 \end{bmatrix} \begin{bmatrix} u_{p_{C_L}} \\ u_{i_{C_L}} \end{bmatrix}
$$

$$\mathbf{y} = \begin{bmatrix} M \\ \dot{h} \end{bmatrix} = \begin{bmatrix} c_{21} & 0 & 0 \\ 0 & c_{42} & 0 \end{bmatrix} \begin{bmatrix} V_a \\ \gamma_a \\ I_{C_L} \end{bmatrix}$$

The basic control law as developed earlier is,

$$C_L = \left(k_{p_{12}} + \frac{k_{i_{12}}}{s} \right) e_2 + k_{b_{14}} \dot{h}$$

where

$$e_2 = \left(M_d - M \right)$$

Note that for the purpose of determining eigenvalues, the gains $k_{p_{14}}$ and $k_{b_{14}}$ have identical effects. Therefore we substitute $k_{b_{14}}$ into the matrix location reserved for $k_{p_{14}}$ for the purposes of gain scheduling *only*. The gain matrix becomes,

$$\mathbf{K} = \begin{bmatrix} k_{p_{12}} & k_{b_{14}} \\ k_{i_{12}} & 0 \end{bmatrix}$$

The closed loop form of the equations (A-BKC) is,

$$\mathbf{A \text{-} BKC} = \begin{bmatrix} a_{11} & a_{12} & b_{11} \\ a_{21} & 0 & b_{21} \\ 0 & 0 & 0 \end{bmatrix} - \begin{bmatrix} b_{11} & 0 \\ b_{21} & 0 \\ 0 & 1 \end{bmatrix} \begin{bmatrix} k_{p_{12}} & k_{b_{14}} \\ k_{i_{12}} & 0 \end{bmatrix} \begin{bmatrix} c_{21} & 0 & 0 \\ 0 & c_{42} & 0 \end{bmatrix}$$

$$= \begin{bmatrix} a_{11} & a_{12} & b_{11} \\ a_{21} & 0 & b_{21} \\ 0 & 0 & 0 \end{bmatrix} - \begin{bmatrix} b_{11} & 0 \\ b_{21} & 0 \\ 0 & 1 \end{bmatrix} \begin{bmatrix} k_{p_{12}} c_{21} & k_{b_{14}} c_{42} & 0 \\ k_{i_{12}} c_{21} & 0 & 0 \end{bmatrix}$$

$$= \begin{bmatrix} a_{11} & a_{12} & b_{11} \\ a_{21} & 0 & b_{21} \\ 0 & 0 & 0 \end{bmatrix} - \begin{bmatrix} b_{11} k_{p_{12}} c_{21} & b_{11} k_{b_{14}} c_{42} & 0 \\ b_{21} k_{p_{12}} c_{21} & b_{21} k_{b_{14}} c_{42} & 0 \\ k_{i_{12}} c_{21} & 0 & 0 \end{bmatrix}$$

$$= \begin{bmatrix} a_{11} - b_{11}k_{p_{12}}c_{21} & a_{12} - b_{11}k_{b_{14}}c_{42} & b_{11} \\ a_{21} - b_{21}k_{p_{12}}c_{21} & -b_{21}k_{b_{14}}c_{42} & b_{21} \\ -k_{i_{12}}c_{21} & 0 & 0 \end{bmatrix}$$

The characteristic polynomial is calculated next.

$$\det[s\mathbf{I} - \mathbf{A}_{cl}] = \det \begin{bmatrix} s - a_{11} + b_{11}k_{p_{12}}c_{21} & -a_{12} + b_{11}k_{b_{14}}c_{42} & -b_{11} \\ -a_{21} + b_{21}k_{p_{12}}c_{21} & s + b_{21}k_{b_{14}}c_{42} & -b_{21} \\ +k_{i_{12}}c_{21} & 0 & s \end{bmatrix}$$

$$\det[s\mathbf{I} - \mathbf{A}_{cl}] = s\left(s - a_{11} + b_{11}k_{p_{12}}c_{21}\right)\left(s + b_{21}k_{b_{14}}c_{42}\right) + \left(-a_{12} + b_{11}k_{b_{14}}c_{42}\right)\left(-b_{21}\right)\left(+k_{i_{12}}c_{21}\right)$$
$$- \left(-b_{11}\right)\left(s + b_{21}k_{b_{14}}c_{42}\right)\left(+k_{i_{12}}c_{21}\right) - s\left(-a_{12} + b_{11}k_{b_{14}}c_{42}\right)\left(-a_{21} + b_{21}k_{p_{12}}c_{21}\right)$$

Summing like terms yields the characteristic polynomial.

$$\det[s\mathbf{I} - \mathbf{A}_{cl}] = s^3 + \left(c_{42}b_{21}k_{b_{14}}\right)s^2 - \left(a_{11} - b_{11}k_{p_{12}}c_{21}\right)s^2 - \left(\left(a_{11} - b_{11}k_{p_{12}}c_{21}\right)c_{42}b_{21}k_{b_{14}}\right)s$$
$$+ \left(a_{12}\left(-a_{21} + b_{21}k_{p_{12}}c_{21}\right)\right)s + \left(a_{12}b_{21}k_{i_{12}}c_{21}\right)$$
$$- \left(c_{42}b_{11}k_{b_{14}}\left(-a_{21} + b_{21}k_{p_{12}}c_{21}\right)\right)s - \left(c_{42}b_{11}k_{b_{14}}b_{21}k_{i_{12}}c_{21}\right)$$
$$+ \left(k_{i_{12}}b_{11}c_{21}\right)s + \left(c_{42}b_{11}b_{21}k_{b_{14}}k_{i_{12}}c_{21}\right)$$

$$\det[s\mathbf{I} - \mathbf{A}_{cl}] = s^3 + \left[\left(c_{42}b_{21}k_{b_{14}}\right) - \left(a_{11} - b_{11}k_{p_{12}}c_{21}\right)\right]s^2$$
$$+ \left[\left(a_{12}\left(-a_{21} + b_{21}k_{p_{12}}c_{21}\right)\right) - \left(\left(a_{11} - b_{11}k_{p_{12}}c_{21}\right)c_{42}b_{21}k_{b_{14}}\right)\right.$$
$$\left. - \left(c_{42}b_{11}k_{b_{14}}\left(-a_{21} + b_{21}k_{p_{12}}c_{21}\right)\right) + \left(k_{i_{12}}b_{11}c_{21}\right)\right]s$$
$$+ \left[\left(a_{12}b_{21}k_{i_{12}}c_{21}\right) - \left(c_{42}b_{11}k_{b_{14}}b_{21}k_{i_{12}}c_{21}\right) + \left(c_{42}b_{11}b_{21}k_{b_{14}}k_{i_{12}}c_{21}\right)\right]$$

The coefficients of the terms are difficult to manage so some effort is applied to simplifying them. We wish to express the characteristic polynomial in the form,

$$\det[s\mathbf{I} - \mathbf{A}] = C_1 s^3 + C_2 s + C_3 s + C_4$$

Setting the two forms equal, we can solve for the coefficients.

$$s^3: \quad C_1 = 1$$

$$s^2: \quad C_2 = \left[\left(c_{42}b_{21}k_{b_{14}}\right) - \left(a_{11} - b_{11}k_{p_{12}}c_{21}\right)\right]$$

$$C_2 = c_{42}b_{21}k_{b_{14}} + b_{11}k_{p_{12}}c_{21} - a_{11}$$

$$s^1: \quad C_3 = [\left(a_{12}\left(-a_{21} + b_{21}k_{p_{12}}c_{21}\right)\right) + \left(\left(-a_{11} + b_{11}k_{p_{12}}c_{21}\right)c_{42}b_{21}k_{b_{14}}\right)$$
$$+ \left(-a_{32}b_{11}k_{b_{14}}\left(-a_{21} + b_{21}k_{p_{12}}c_{21}\right)\right) + \left(k_{i_{12}}b_{11}c_{21}\right)]$$

$$C_3 = [-a_{12}a_{21} + a_{12}b_{21}k_{p_{12}}c_{21} - a_{11}c_{42}b_{21}k_{b_{14}} + c_{42}b_{11}b_{21}k_{p_{12}}k_{b_{14}}c_{21}$$
$$+ a_{21}c_{42}b_{11}k_{b_{14}} - c_{42}b_{11}b_{21}k_{p_{12}}k_{b_{14}}c_{21} + k_{i_{12}}b_{11}c_{21}]$$

$$C_3 = -a_{12}a_{21} + a_{12}b_{21}k_{p_{12}}c_{21} - a_{11}c_{42}b_{21}k_{b_{14}} + a_{21}c_{42}b_{11}k_{b_{14}} + k_{i_{12}}b_{11}c_{21}$$

$$s^0: \quad C_4 = \left[\left(a_{12}b_{21}k_{i_{12}}c_{21}\right) - \left(a_{32}b_{11}b_{21}k_{b_{14}}k_{i_{12}}c_{21}\right) + \left(a_{32}b_{11}b_{21}k_{b_{14}}k_{i_{12}}c_{21}\right)\right]$$

$$C_4 = a_{12}b_{21}k_{i_{12}}c_{21}$$

Assuming that the gain $k_{b_{14}}$ is known, we can solve for the other gains.

$$k_{p_{12}} = \frac{C_2 - c_{42}b_{21}k_{b_{14}} + a_{11}}{b_{11}c_{21}} \quad\quad (4.19)$$

$$k_{i_{12}} = \frac{C_4}{a_{12}b_{21}c_{21}} \quad\quad (4.20)$$

Plugging these gains back into the C_3 equation yields,

$$C_3 = -a_{12}a_{21} + a_{12}b_{21}\left(\frac{C_2 - c_{42}b_{21}k_{b_{14}} + a_{11}}{b_{11}c_{21}}\right)c_{21}$$
$$- a_{11}c_{42}b_{21}k_{b_{14}} + a_{21}c_{42}b_{11}k_{b_{14}} + \left(\frac{C_4}{a_{12}b_{21}c_{21}}\right)b_{11}c_{21}$$

Simplifying,

-103-

$$C_3 = -a_{12}a_{21} + a_{12}b_{21}\left(\frac{C_2 - c_{42}b_{21}k_{b_{14}} + a_{11}}{b_{11}c_{11}}\right)c_{21} - a_{11}c_{42}b_{21}k_{b_{14}} + a_{21}c_{42}b_{11}k_{b_{14}} + \left(\frac{C_4}{a_{12}b_{21}c_{21}}\right)b_{11}c_{21}$$

$$C_3 = -a_{12}a_{21} + \frac{a_{12}b_{21}C_2}{b_{11}} - \left(\frac{a_{12}b_{21}c_{42}b_{21}}{b_{11}}\right)k_{b_{14}} + \frac{a_{11}a_{12}b_{21}}{b_{11}} - \left(a_{11}c_{42}b_{21}\right)k_{b_{14}} + \left(a_{21}c_{42}b_{11}\right)k_{b_{14}} + \frac{C_4 b_{11}}{a_{12}b_{21}}$$

$$C_3 = \left(a_{21}c_{42}b_{11} - \frac{a_{12}b_{21}c_{42}b_{21}}{b_{11}} - a_{11}c_{42}b_{21}\right)k_{b_{14}} + \left(\frac{a_{12}b_{21}C_2}{b_{11}} - a_{12}a_{21} + \frac{a_{11}a_{12}b_{21}}{b_{11}} + \frac{C_4 b_{11}}{a_{12}b_{21}}\right)$$

and we can solve for the gain $k_{b_{14}}$.

$$k_{b_{14}} = \frac{C_3 - \left(\dfrac{a_{12}b_{21}C_2}{b_{11}} - a_{12}a_{21} + \dfrac{a_{11}a_{12}b_{21}}{b_{11}} + \dfrac{C_4 b_{11}}{a_{12}b_{21}}\right)}{\left(a_{21}c_{42}b_{11} - \dfrac{a_{12}b_{21}c_{42}b_{21}}{b_{11}} - a_{11}c_{42}b_{21}\right)} \tag{4.21}$$

Because we have three gains, we see that we were able to specify all the coefficients of the characteristic polynomial. This enables us to place the poles arbitrarily. We can choose the frequency and damping of the system poles and the location of the integrator pole. From our manual loop closing, we also have some idea of what values make good gains. We can specify the coefficients in terms of the desired modal properties and the location of the integrator pole, p, by expressing the characteristic polynomial in terms of its roots.

$$\det\left[s\mathbf{I} - \mathbf{A}\right] = C_1 s^3 + C_2 s^2 + C_3 s + C_4 = (s - p)\left(s^2 + 2\zeta\omega_p s + \omega_p^2\right)$$

$$\begin{aligned}
C_1 &= 1 \\
C_2 &= -p + 2\zeta\omega_n \\
C_3 &= -2p\zeta\omega_n + \omega_n^2 \\
C_4 &= -p\omega_n^2
\end{aligned} \tag{4.22}$$

Error! Not a valid bookmark self-reference. summarizes the gain scheduling equations used for this controller. Looking at Figure 4.14, we see that the lift coefficient is still commanded rather violently. Therefore we decide to specify slower dynamics. Using equations in **Error! Not a valid bookmark self-reference.** we can try many different modal properties quickly. After some experimentation, we choose the following modal properties:

Table 4.9. The gain scheduling equations for lift coefficient control of speed

$$C_1 = 1$$
$$C_2 = -p + 2\zeta\omega_n$$
$$C_3 = -2p\zeta\omega_n + \omega_n^2 \tag{4.22}$$
$$C_4 = -p\omega_n^2$$

$$k_{b_{14}} = \frac{C_3 - \left(\dfrac{a_{12}b_{21}C_2}{b_{11}} - a_{12}a_{21} + \dfrac{a_{11}a_{12}b_{21}}{b_{11}} + \dfrac{C_4 b_{11}}{a_{12}b_{21}} \right)}{\left(a_{21}c_{42}b_{11} - \dfrac{a_{12}b_{21}c_{42}b_{21}}{b_{11}} - a_{11}c_{42}b_{21} \right)} \tag{4.21}$$

$$k_{i_{12}} = \frac{C_4}{a_{12}b_{21}c_{21}} \tag{4.20}$$

$$k_{p_{12}} = \frac{C_2 - c_{42}b_{21}k_{b_{14}} + a_{11}}{b_{11}c_{21}} \tag{4.19}$$
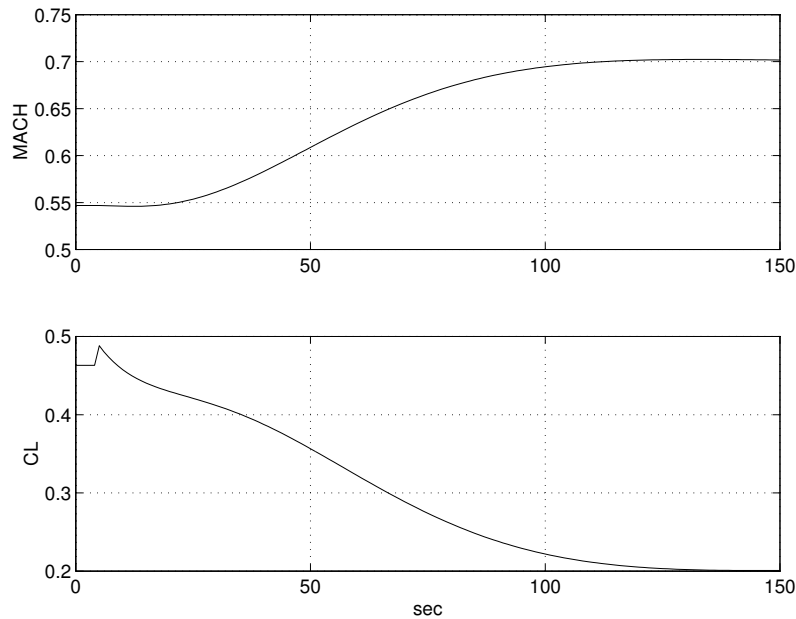
Figure 4.15. Simulation of Mach capture with slower dynamics

- $\omega_n = 0.05 rad / sec$
- $\zeta = 0.7$
- $p = -0.05$

The gains for this set of modal properties are $k_{P_{12}} = 0.1635$, $k_{i_{12}} = -0.0342$, and

$k_{b_{14}} = 0.2715 \times 10^{-4}$. Figure 4.15 shows the simulation results. With the slower dynamics, the lift coefficient no longer has its initial sharp dip; however the system takes 40 seconds longer to capture the desired Mach number. This performance penalty is acceptable because an extra 40 seconds is not much time in the course of an entire flight.

4.4.3 Controlling Speed and Altitude Rate Simultaneously

Maintaining a specified speed and a specified altitude rate simultaneously (as in steady, level flight) requires feedback control of both the thrust and lift coefficient. Because of this, the controller for this flight regime is the most complicated of our controllers. It is also the most used controller, because the aircraft spends most of its time controlling both speed and altitude (as in steady, level flight). The design goals of this controller are also the most ambitious. Here, we desire to drive both the speed of the aircraft and altitude rate to some commanded values.

Consider the same DC-9 traveling at 15000 ft and 578 ft/sec and weighing 140,000lbs. The open loop dynamics for system are the same as shown in equation (4.16); however, because of the addition of the throttle feedback control, we need to use the full state equation of the LTD system in equation (4.10). With the given flight condition, the state equation becomes,

$$
\begin{bmatrix} \begin{bmatrix} \Delta V_a \\ \Delta \gamma_a \\ \Delta h \\ I_{C_L} \\ I_T \end{bmatrix} \end{bmatrix} = \begin{bmatrix} -0.0072 & -32.2 & 0 & -2.7445 & 0.0002 \\ 0.0002 & 0 & 0 & 0.1202 & 0 \\ 0 & 578.4794 & 0 & 0 & 0 \\ 0 & 0 & 0 & 0 & 0 \\ 0 & 0 & 0 & 0 & 0 \end{bmatrix} \begin{bmatrix} \Delta V_a \\ \Delta \gamma_a \\ \Delta h \\ I_{C_L} \\ I_T \end{bmatrix}
$$

$$
+ \begin{bmatrix} -2.7445 & 0.0002 & 0 & 0 \\ 0.1202 & 0 & 0 & 0 \\ 0 & 0 & 0 & 0 \\ 0 & 0 & 1 & 0 \\ 0 & 0 & 0 & 1 \end{bmatrix} \begin{bmatrix} u_{P_{C_L}} \\ u_{P_T} \\ u_{i_{C_L}} \\ u_{i_T} \end{bmatrix}
$$

(4.23)

Since we want to be able to drive the aircraft to a particular speed and altitude rate independently of each other, we must be very careful how we arrange the feedback in the feed-forward path. Feedback to any one input cannot be used to drive two independent errors to zero simultaneously. By observing effects of feedback in Figure 4.2 and Figure 4.3, we see that the throttle is much more adept at controlling speed than altitude rate. This is because the feedback of speed to the throttle tends to increase the damping of the longitudinal mode. Similarly, the lift coefficient is a much better control of altitude rate than speed. Therefore we only allow speed feedback to the throttle and altitude rate feedback to the lift coefficient. For purposes of this demonstration, we use Mach in the feedback. The control laws that use indicated airspeed are identical in form.

Initially, the Phugoid eigenvalues are located at $-0.0036 \pm 0.0786i$, which corresponds to a natural frequency of 0.0787rad/sec and a damping ratio of 0.0445. Initially, we close the lift coefficient feedback paths in a manner very similar to what was done in Section 4.4.1. We close the proportional loop first using $k_{p_{14}}$. We increase the proportional gain to $k_{p_{14}} = 3.0 \times 10^{-5}$ as shown in Figure 4.16. This results in longitudinal mode poles at *-0.0662 ± 0.465i*. Our modal properties are ω_p = *0.081 rad* and ζ_p = *0.819*. Our damping ratio is acceptable; however, our frequency is low. We adjust the frequency when we add integral control. As shown in the second plot of Figure 4.16 , we increase the integral gain to $k_{i_{14}} = 3.7 \times 10^{-5}$. This moves the Phugoid poles to *-0.0648±0.3954i* where the modal properties are ω_p = *0.4 rad* and ζ_p = *0.1618*. While this results in an acceptable frequency, the damping ratio is too low. Therefore, we increase the proportional gain to $k_{p_{14}} = 1.34 \times 10^{-4}$ as shown in Figure 4.17. This results in longitudinal mode poles of *-0.2818 ± 0.2850i* with the corresponding modal properties of ω_p = *0.4 rad* and ζ_p = *0.7031*. The position of the integrator pole is *-0.0027*.
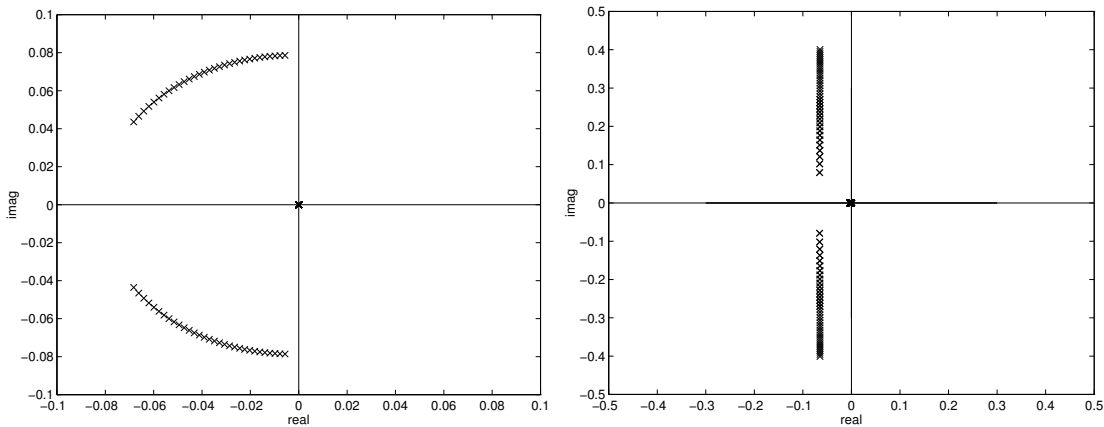
Figure 4.16. The initial $k_{p_{14}}$ (left plot) and $k_{i_{14}}$ (right plot) loop closures for region 7
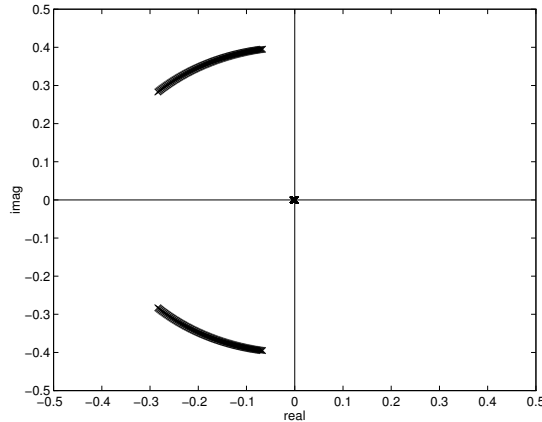
Figure 4.17. The final increase in $k_{p_{14}}$ to achieve adequate damping
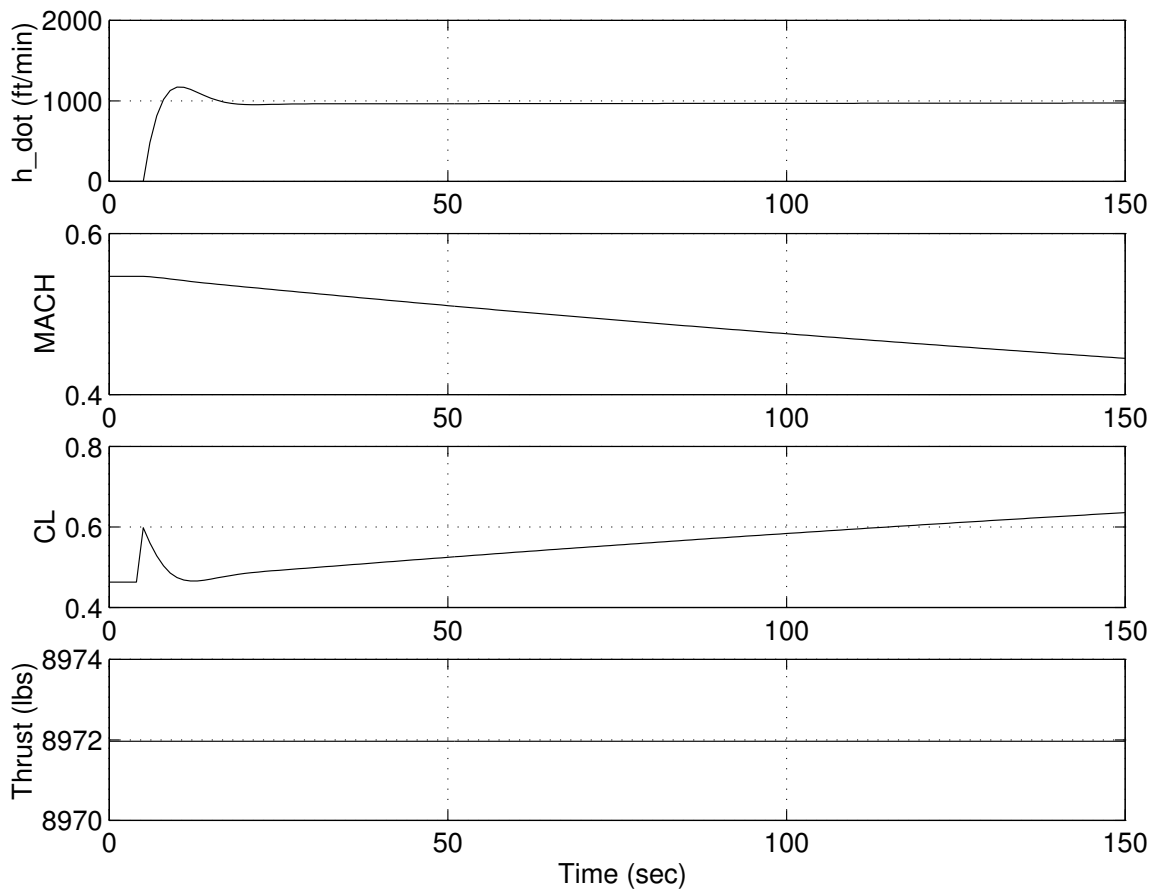
Figure 4.18. Simulation of a commanded 1000ft/min rate of climb without any feedback to thrust

At this point we can illustrate the system dynamics by commanding a 1000 ft/min climb. The simulation results (Figure 4.18) show response of altitude rate and Mach number as well as the lift coefficient and thrust inputs. We can see that we approximately achieve the 1000 ft/min climb rate; however, we have a small error of approximately 25 ft/min.

This error is due to the slow integrator pole. We ignore this small error for now. We also see that the Mach number tapers off during the climb. This is expected at the moment because there is no feedback to the throttle to maintain Mach (the thrust is constant).
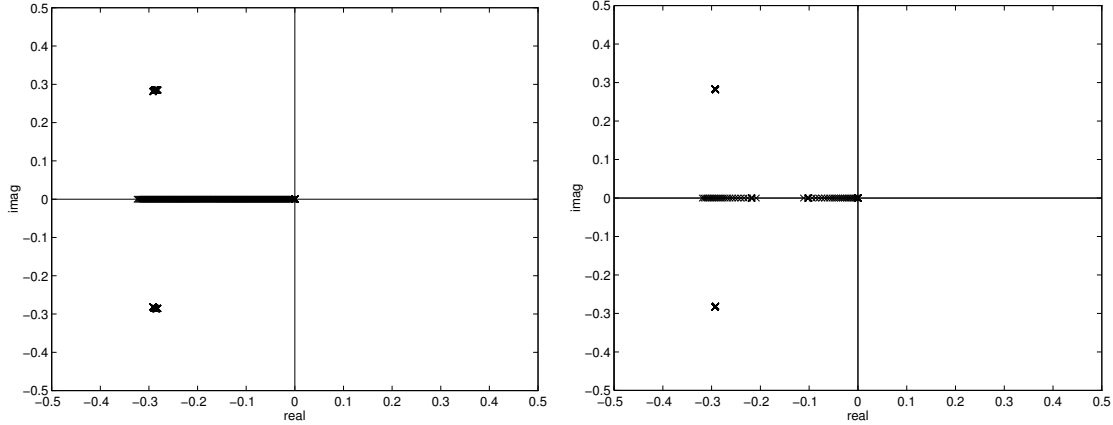
Figure 4.19. Root loci for $k_{p_{22}}$ (left plot) and $k_{i_{22}}$ (right plot)

We also see that the controller slowly increases the lift coefficient to maintain the rate of climb as the aircraft slows down. If the controller is left to continue, it will stall the aircraft. Adding feedback to thrust corrects the problem. Feedback to thrust is initiated using proportional control. We increase the gain $k_{p_{22}}$ to 1.56×10^6 as shown on the left side of Figure 4.19. The longitudinal mode is virtually unaffected by the proportional feedback to throttle. The biggest influence of the proportional feedback to the thrust is to move the integrator pole for the lift coefficient feedback farther negative. The lift coefficient's integrator pole is moved to -0.3222. This is actually desirable because it reduces the steady state error in altitude rate. The final loop closure, integrated thrust is closed next. As shown on the right hand side of Figure 4.19, the integrated feedback $k_{i_{22}}$ to thrust has virtually no effect on the longitudinal dynamics; rather, it tends to draw the two integrator poles together. If the gain is increased further, the integrator poles are drawn together and become complex conjugates. This in turn creates another longitudinal oscillation, which is slower than the dominant mode. This extra mode is undesirable, so we stop the integrated feedback at $k_{i_{22}} = 1.1 \times 10^5$. The final system is described as:

- complex conjugate poles: $-0.2927 \pm 0.2836i$
- Thrust integrator pole : -0.1020
- Lift coefficient integrator pole: -0.2179
- Modal properties: $\zeta = 0.7182 \quad \omega_n = 0.407 \mathrm{rad}/sec$
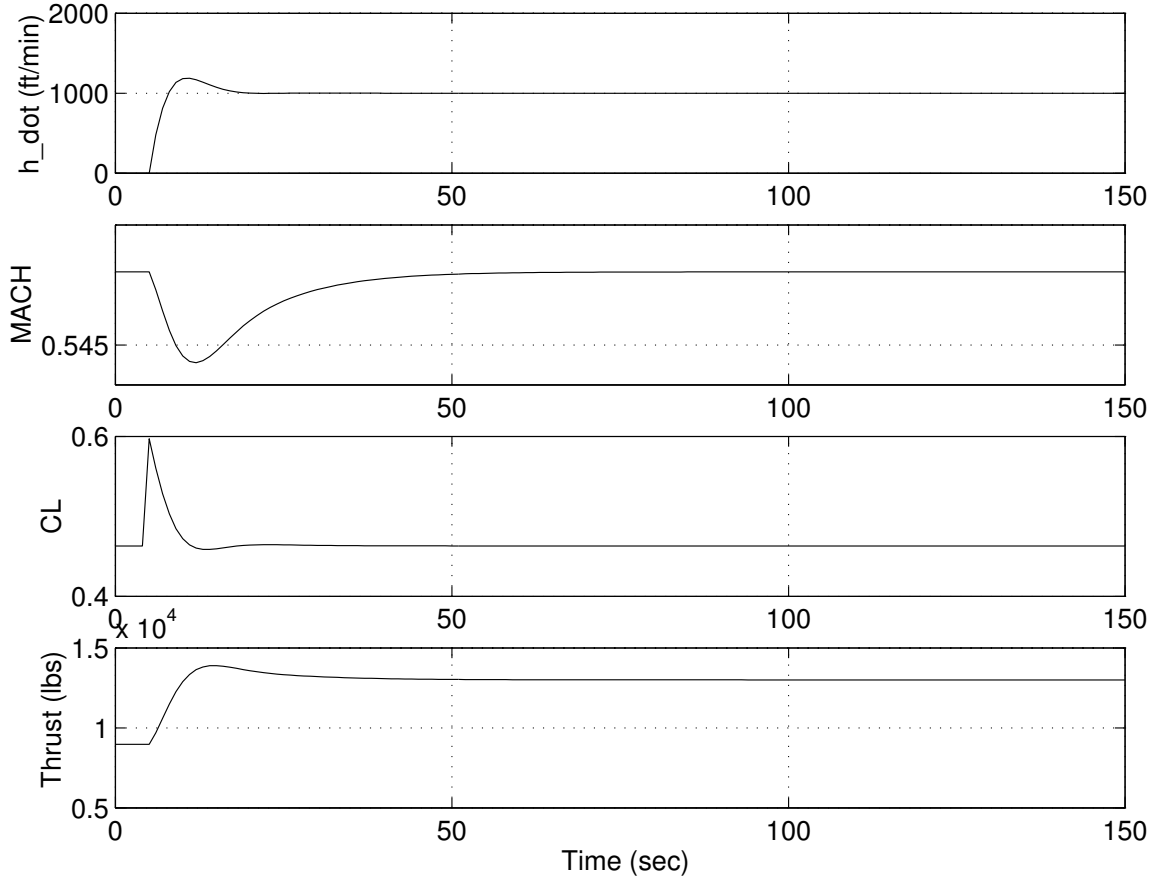
Figure 4.20. Simulation of a commanded 1000ft/min climb rate using the final controller for region 7

The final system is shown simulating a commanded altitude rate of 1000 ft/min in Figure 4.20. Note that with the addition of thrust feedback, the throttle is adjusted simultaneously to maintain the desired speed.

As with the other regions, the exercise of successive loop closures is useful but not practical for the task of scheduling many different conditions; therefore, an automated approach is developed. With the addition of throttle feedback, the problem becomes much more complex. Again, we will substitute place holders into the LTD system to make the algebra more manageable.

$$
\begin{bmatrix} \dot{V}_a \\ \dot{\gamma}_a \\ \dot{I}_{C_L} \\ \dot{I}_T \end{bmatrix} = \begin{bmatrix} a_{11} & a_{12} & b_{11} & b_{12} \\ a_{21} & 0 & b_{21} & 0 \\ 0 & 0 & 0 & 0 \\ 0 & 0 & 0 & 0 \end{bmatrix} \begin{bmatrix} V_a \\ \gamma_a \\ I_{C_L} \\ I_T \end{bmatrix} + \begin{bmatrix} b_{11} & b_{12} & 0 & 0 \\ b_{21} & 0 & 0 & 0 \\ 0 & 0 & 1 & 0 \\ 0 & 0 & 0 & 1 \end{bmatrix} \begin{bmatrix} u_{p_{C_L}} \\ u_{p_T} \\ u_{i_{C_L}} \\ u_{i_T} \end{bmatrix} \tag{4.24}
$$

$$y = \begin{bmatrix} M \\ \dot{h} \end{bmatrix} = \begin{bmatrix} c_{21} & 0 & 0 & 0 \\ 0 & c_{42} & 0 & 0 \end{bmatrix} \begin{bmatrix} V_a \\ \gamma_a \\ I_{C_L} \\ I_T \end{bmatrix}$$

We need to close the loops around the throttle and the lift coefficient. The control law is summarized as

$$C_{L_p} = k_{p_{14}} \left(\dot{h}_d - \dot{h} \right)$$
$$C_{L_i} = k_{i_{14}} \left(\dot{h}_d - \dot{h} \right)$$
$$T_p = k_{p_{22}} \left(M_d - M \right)$$
$$T_i = k_{i_{22}} \left(M_d - M \right)$$

The closed loop A-matrix, $\mathbf{A_{cl}} = \mathbf{A} - \mathbf{BKC}$ is,

$$\mathbf{A_{cl}} = \begin{bmatrix} a_{11} & a_{12} & b_{11} & b_{12} \\ a_{21} & 0 & b_{21} & 0 \\ 0 & 0 & 0 & 0 \\ 0 & 0 & 0 & 0 \end{bmatrix} - \begin{bmatrix} b_{11} & b_{12} & 0 & 0 \\ b_{21} & 0 & 0 & 0 \\ 0 & 0 & 1 & 0 \\ 0 & 0 & 0 & 1 \end{bmatrix} \begin{bmatrix} 0 & k_{p_{14}} \\ k_{p_{21}} & 0 \\ 0 & k_{i_{14}} \\ k_{i_{21}} & 0 \end{bmatrix} \begin{bmatrix} c_{11} & 0 & 0 & 0 \\ 0 & c_{42} & 0 & 0 \end{bmatrix}$$

$$\mathbf{A_{cl}} = \begin{bmatrix} a_{11} & a_{12} & b_{11} & b_{12} \\ a_{21} & 0 & b_{21} & 0 \\ 0 & 0 & 0 & 0 \\ 0 & 0 & 0 & 0 \end{bmatrix} - \begin{bmatrix} b_{11} & b_{12} & 0 & 0 \\ b_{21} & 0 & 0 & 0 \\ 0 & 0 & 1 & 0 \\ 0 & 0 & 0 & 1 \end{bmatrix} \begin{bmatrix} 0 & c_{42}k_{p_{14}} & 0 & 0 \\ c_{11}k_{p_{21}} & 0 & 0 & 0 \\ 0 & c_{42}k_{i_{14}} & 0 & 0 \\ c_{11}k_{i_{21}} & 0 & 0 & 0 \end{bmatrix}$$

$$\mathbf{A_{cl}} = \begin{bmatrix} a_{11} & a_{12} & b_{11} & b_{12} \\ a_{21} & 0 & b_{21} & 0 \\ 0 & 0 & 0 & 0 \\ 0 & 0 & 0 & 0 \end{bmatrix} - \begin{bmatrix} b_{12}c_{11}k_{p_{21}} & b_{11}c_{42}k_{p_{14}} & 0 & 0 \\ 0 & b_{21}c_{42}k_{p_{14}} & 0 & 0 \\ 0 & c_{42}k_{i_{14}} & 0 & 0 \\ c_{11}k_{i_{21}} & 0 & 0 & 0 \end{bmatrix}$$

$$\mathbf{A_{cl}} = \begin{bmatrix} a_{11} - b_{12}c_{11}k_{p_{21}} & a_{12} - b_{11}c_{42}k_{p_{14}} & b_{11} & b_{12} \\ a_{21} & -b_{21}c_{42}k_{p_{14}} & b_{21} & 0 \\ 0 & -c_{42}k_{i_{14}} & 0 & 0 \\ c_{11}k_{i_{21}} & 0 & 0 & 0 \end{bmatrix}$$

The characteristic polynomial of the closed-loop A-matrix is,

$$\det\left[s\mathbf{I}-\mathbf{A}_{cl}\right]=\det\begin{bmatrix} s-a_{11}+b_{12}c_{11}k_{p_{21}} & -a_{12}+b_{11}c_{42}k_{p_{14}} & -b_{11} & -b_{12} \\ -a_{21} & s+b_{21}c_{42}k_{p_{14}} & -b_{21} & 0 \\ 0 & c_{42}k_{i_{14}} & s & 0 \\ c_{11}k_{i_{21}} & 0 & 0 & s \end{bmatrix} \tag{4.25}$$

Simplifying Equation (4.25),

$$\det\left[s\mathbf{I}-\mathbf{A}_{cl}\right]=+\left(c_{11}k_{i_{21}}\right)\det\begin{bmatrix} -a_{12}+b_{11}c_{42}k_{p_{14}} & -b_{11} & -b_{12} \\ s+b_{21}c_{42}k_{p_{14}} & -b_{21} & 0 \\ c_{42}k_{i_{14}} & s & 0 \end{bmatrix}$$

$$-(s)\det\begin{bmatrix} s-a_{11}+b_{12}c_{11}k_{p_{21}} & -a_{12}+b_{11}c_{42}k_{p_{14}} & -b_{11} \\ -a_{21} & s+b_{21}c_{42}k_{p_{14}} & -b_{21} \\ 0 & c_{42}k_{i_{14}} & s \end{bmatrix}$$

$$\det\left[s\mathbf{I}-\mathbf{A}_{cl}\right]=\left(c_{11}k_{i_{21}}\right)\left[\left(-b_{12}s^2-b_{12}b_{21}c_{42}k_{p_{14}}s\right)-\left(b_{12}b_{21}c_{42}k_{i_{14}}\right)\right]$$

$$-(s)\begin{bmatrix} \left(s-a_{11}+b_{12}c_{11}k_{p_{21}}\right)\left(s+b_{21}c_{42}k_{p_{14}}\right)(s) \\ +(-a_{21})\left(c_{42}k_{i_{14}}\right)(-b_{11}) \\ -(-b_{21})\left(c_{42}k_{i_{14}}\right)\left(s-a_{11}+b_{12}c_{11}k_{p_{21}}\right) \\ -\left(-a_{12}+b_{11}c_{42}k_{p_{14}}\right)(-a_{21})(s) \end{bmatrix}$$

$$\det\left[s\mathbf{I}-\mathbf{A}_{cl}\right]=-b_{12}c_{11}k_{i_{21}}s^2-b_{12}b_{21}c_{42}k_{p_{14}}c_{11}k_{i_{21}}s-c_{11}k_{i_{21}}b_{12}b_{21}c_{42}k_{i_{14}}$$

$$-\left(s^2\right)\left(s-a_{11}+b_{12}c_{11}k_{p_{21}}\right)\left(s+b_{21}c_{42}k_{p_{14}}\right)$$

$$-a_{21}b_{11}c_{42}k_{i_{14}}s-b_{21}c_{42}k_{i_{14}}\left(s^2-a_{11}s+b_{12}c_{11}k_{p_{21}}s\right)$$

$$-a_{21}\left(-a_{12}+b_{11}c_{42}k_{p_{14}}\right)s^2$$

$$\det[s\mathbf{I} - \mathbf{A}_{cl}] =$$

$$-b_{12}c_{11}k_{i_{21}}s^2 - b_{12}b_{21}c_{42}k_{p_{14}}c_{11}k_{i_{21}}s - c_{11}k_{i_{21}}b_{12}b_{21}c_{42}k_{i_{14}}$$

$$-s^4 + a_{11}s^3 - b_{12}c_{11}k_{p_{21}}s^3 - b_{21}c_{42}k_{p_{14}}s^3 + a_{11}b_{21}c_{42}k_{p_{14}}s^2 - b_{12}c_{11}k_{p_{21}}b_{21}c_{42}k_{p_{14}}s^2$$

$$-a_{21}b_{11}c_{42}k_{i_{14}}s - b_{21}c_{42}k_{i_{14}}s^2 + b_{21}c_{42}k_{i_{14}}a_{11}s - b_{21}c_{42}k_{i_{14}}b_{12}c_{11}k_{p_{21}}s$$

$$+a_{21}a_{12}s^2 - a_{21}b_{11}c_{42}k_{p_{14}}s^2$$

$$\det[s\mathbf{I} - \mathbf{A}_{cl}] =$$

$$+(1)s^4$$

$$-\left(a_{11} - b_{12}c_{11}k_{p_{21}} - b_{21}c_{42}k_{p_{14}}\right)s^3$$

$$-\left(a_{11}b_{21}c_{42}k_{p_{14}} - b_{12}c_{11}k_{p_{21}}b_{21}c_{42}k_{p_{14}} - b_{21}c_{42}k_{i_{14}} + a_{21}a_{12} - a_{21}b_{11}c_{42}k_{p_{14}} - b_{12}c_{11}k_{i_{21}}\right)s^2$$

$$-\left(-b_{12}b_{21}c_{42}k_{p_{14}}c_{11}k_{i_{21}} - a_{21}b_{11}c_{42}k_{i_{14}} + b_{21}c_{42}k_{i_{14}}a_{11} - b_{21}c_{42}k_{i_{14}}b_{12}c_{11}k_{p_{21}}\right)s$$

$$-\left(-c_{11}k_{i_{21}}b_{12}b_{21}c_{42}k_{i_{14}}\right)$$

The equation is of the form,

$$\det[s\mathbf{I} - \mathbf{A}_{cl}] = C_1 s^4 + C_2 s^3 + C_3 s^2 + C_4 s + C_5 = (s - p_1)(s - p_2)(s^2 + 2\zeta\omega_n + \omega_n^2)$$

The coefficients of the characteristic polynomial, in terms of the modal properties that we specify for the design (two integrator poles, the damping ratio and natural frequency), are shown below.

$$C_1 = 1$$
$$C_2 = 2\zeta\omega_n - (p_1 + p_2)$$
$$C_3 = \omega_n^2 - 2\zeta\omega_n(p_1 + p_2) + p_1 p_2$$
$$C_4 = -\omega_n^2(p_1 + p_2) + 2\zeta\omega_n p_1 p_2$$
$$C_5 = \omega_n^2 p_1 p_2$$

The coefficients of the characteristic polynomial, in terms of the system parameters, are shown below.

$$C_1 = 1$$

$$C_2 = -\left(a_{11} - b_{12}c_{11}k_{p_{21}} - b_{21}c_{42}k_{p_{14}}\right)$$

$$C_3 = -\left(a_{11}b_{21}c_{42}k_{p_{14}} - b_{12}c_{11}k_{p_{21}}b_{21}c_{42}k_{p_{14}} - b_{21}c_{42}k_{i_{14}} + a_{21}a_{12} - a_{21}b_{11}c_{42}k_{p_{14}} - b_{12}c_{11}k_{i_{21}}\right)$$

$$C_4 = -\left(-b_{12}b_{21}c_{42}k_{p_{14}}c_{11}k_{i_{21}} - a_{21}b_{11}c_{42}k_{i_{14}} + b_{21}c_{42}k_{i_{14}}a_{11} - b_{21}c_{42}k_{i_{14}}b_{12}c_{11}k_{p_{21}}\right)$$

$$C_5 = -\left(-c_{11}k_{i_{21}}b_{12}b_{21}c_{42}k_{i_{14}}\right)$$

Since we have four gains and four coefficients, we are able to arbitrarily place the poles. Because the algebra is complex in the solution of these equations, we simplify the equations with following substitutions.

$$
\begin{aligned}
&C_2' = C_2 + a_{11} \\
&C_3' = C_3 + a_{21}a_{12} \\
&C_4' = C_4 \\
&C_5' = C_5
\end{aligned}
\qquad
\begin{aligned}
&x_1 = +b_{12}c_{11} \\
&x_2 = +b_{21}c_{42} \\
&x_3 = -a_{11}b_{21}c_{42} \\
&x_4 = b_{12}c_{11}b_{21}c_{42} \\
&x_5 = +b_{21}c_{42}
\end{aligned}
\qquad
\begin{aligned}
&x_6 = +a_{21}b_{11}c_{42} \\
&x_7 = +b_{12}c_{11} \\
&x_8 = +b_{12}b_{21}c_{42}c_{11} \\
&x_9 = +a_{21}b_{11}c_{42} - b_{21}c_{42}a_{11} \\
&x_{10} = +b_{21}c_{42}b_{12}c_{11} \\
&x_{11} = c_{11}b_{12}b_{21}c_{42}
\end{aligned}
$$

Finally, we have the following system of equations.

$$C_1 = 1$$

$$C_2' = \left(x_1 k_{p_{21}} + x_2 k_{p_{14}}\right)$$

$$C_3' = \left(x_3 k_{p_{14}} + x_4 k_{p_{21}}k_{p_{14}} + x_5 k_{i_{14}} + x_6 k_{p_{14}} + x_7 k_{i_{21}}\right)$$

$$C_4' = \left(x_8 k_{p_{14}}k_{i_{21}} + x_9 k_{i_{14}} + x_{10}k_{i_{14}}k_{p_{21}}\right)$$

$$C_5' = \left(x_{11}k_{i_{21}}k_{i_{14}}\right)$$

To obtain a solution, we use algebra to extract as much information from the system of equations as possible and then employ a simple iterative routine. This method proved to be satisfactory and is now outlined.

First, we can simplify the C_3' equation.

$$C_3' = \left((x_3 + x_6)k_{p_{14}} + x_4 k_{p_{21}}k_{p_{14}} + x_5 k_{i_{14}} + x_7 k_{i_{21}}\right)$$

adding C_2' to C_3',

$$C_3' = \left((x_3 + x_6)k_{p_{14}} + x_4 \frac{C_2' - x_2 k_{p_{14}}}{x_1} k_{p_{14}} + x_5 k_{i_{14}} + x_7 k_{i_{21}} \right)$$

$$C_3' = \left((x_3 + x_6)k_{p_{14}} + \left(\frac{x_4}{x_1}\right)\left(C_2' k_{p_{14}} - x_2 k_{p_{14}}^2\right) + x_5 \frac{C_5'}{x_{11} k_{i_{21}}} + x_7 k_{i_{21}} \right)$$

$$C_3' = \left((x_3 + x_6)k_{p_{14}} + \left(\frac{x_4}{x_1}\right)\left(C_2' k_{p_{14}} - x_2 k_{p_{14}}^2\right) + x_5 \frac{C_5'}{x_{11} k_{i_{21}}} + x_7 k_{i_{21}} \right)$$

We end up with a quadratic equation in terms of $k_{p_{14}}$ where $k_{i_{21}}$ is a term in the coefficients as shown in Equation (3.210).

$$x_2 k_{p_{14}}^2 - \left((x_3 + x_6) + C_2'\left(\frac{x_4}{x_1}\right) \right)k_{p_{14}} + \left(C_3' - x_5 \frac{C_5'}{x_{11} k_{i_{21}}} + x_7 k_{i_{21}} \right) = 0 \qquad (4.26)$$

Using C_5', C_4', and C_2' we can get $k_{i_{21}}$ in terms of $k_{p_{14}}$ as shown in Equation (3.212) .

$$C_4' = \left(x_8 k_{p_{14}}\left(\frac{C_5'}{x_{11} k_{i_{14}}}\right) + x_9 k_{i_{14}} + x_{10} k_{i_{14}}\left(\frac{C_2' - x_2 k_{p_{14}}}{x_1}\right) \right)$$

$$C_4' k_{i_{14}} = \frac{C_5' x_8 k_{p_{14}}}{x_{11}} + x_9 k_{i_{14}}^2 + \frac{x_{10}}{x_1} k_{i_{14}}^2 \left(C_2' - x_2 k_{p_{14}}\right)$$

$$C_4' k_{i_{14}} = \frac{C_5' x_8 k_{p_{14}}}{x_{11}} + x_9 k_{i_{14}}^2 + \frac{x_{10} C_2'}{x_1} k_{i_{14}}^2 - x_2 k_{p_{14}} k_{i_{14}}^2$$

$$\frac{C_5' x_8 k_{p_{14}}}{x_{11}} + x_9 k_{i_{14}}^2 + \frac{x_{10} C_2'}{x_1} k_{i_{14}}^2 - x_2 k_{p_{14}} k_{i_{14}}^2 - C_4' k_{i_{14}} = 0$$

$$\left(x_9 + \frac{x_{10} C_2'}{x_1} - x_2 k_{p_{14}} \right)k_{i_{14}}^2 - C_4' k_{i_{14}} + \frac{C_5' x_8 k_{p_{14}}}{x_{11}} = 0$$

$$k_{i_{14}} = \frac{C_4' \pm \sqrt{C_4'^2 - 4\left(x_9 + \frac{x_{10} C_2'}{x_1} - x_2 k_{p_{14}} \right)\frac{C_5' x_8 k_{p_{14}}}{x_{11}}}}{2\left(x_9 + \frac{x_{10} C_2'}{x_1} - x_2 k_{p_{14}} \right)}$$

$$k_{i_{21}} = \frac{C_5'}{x_{11}} \frac{C_4' \pm \sqrt{C_4'^2 - 4\left(x_9 + \dfrac{x_{10}C_2'}{x_1} - x_2 k_{p_{14}}\right) \dfrac{C_5' x_8 k_{p_{14}}}{x_{11}}}}{2\left(x_9 + \dfrac{x_{10}C_2'}{x_1} - x_2 k_{p_{14}}\right)} \qquad (4.27)$$

Since we know that $k_{p_{14}}$ is always positive and on the order of 10^{-4}, a simple iteration algorithm was developed that begins with an initial $k_{p_{14}}$, calculates a $k_{i_{21}}$ using Equation (3.213), and then tests the solution using Equation (3.214). Generally, the method yields two sets of workable gains. The solution chosen of the two workable sets is the solution with the lowest throttle gains. This way the throttle is modulated the least.

5. The Supporting Functional Logic of the Longitudinal Control System

In the previous chapter, we developed the feedback control algorithms that stabilize the aircraft and drive it to the desired condition. The result was our basic, linear control model, equation (4.2), which can be expressed in matrix/operator notation as,

$$u = Ke \qquad (5.28)$$

where u is the control vector (in our case, lift coefficient and thrust), e is the output error vector (which contains the indicated airspeed, Mach number, altitude, and altitude rate), and K is the constant matrix operator of proportional, integral, and feedback gains. Our goal is to squeeze standard piloting strategies into that basic, linear model and use it to control our non-linear dynamics.

But a basic, linear control model is too simple to capture the complexities of piloting an aircraft throughout its entire flight envelope. In general, a pilot will provide different control inputs for a given error vector based on the flight regime. As an illustration of the different piloting strategies used in different flight regimes, consider the following.

- During take-off, the pilot sets take-off thrust and a nominal stick location and holds them constant until the aircraft reaches its rotation speed.
- In climb, the pilot fixes the thrust at climb thrust and uses the control stick to capture either airspeed or altitude rate.
- In descent, the pilot fixes the thrust at descent thrust and uses the control stick to capture either airspeed or altitude rate. Our linear controller may be able to use the same lift coefficient controller as for climbs, but the fixed thrust value is different.
- In steady, level flight, the pilot uses the throttle to hold the airspeed at the desired value and the control stick to hold the altitude.

So there are cases in which there is no modulation of control inputs at all, cases in which only one control parameter is modulated, and cases in which they are both modulated. Since different flight regimes require different control strategies, we will need to develop a basic, linear controller for each flight regime. The purpose of this chapter is to define these different flight regimes, or **regions**, and the conditions that bound them, and to develop the algorithms for determining the desired condition within those regions.

In the previous chapter, we introduced the concept of the desired output. Because our system uses multiple regions and multiple controllers, we need to differentiate between the desired output that each mathematical controller sees and the commanded output that

the system (in the real world this would be the pilot) is trying to attain. The commanded output, $\mathbf{y_c}$, typically comes from the user interface. Each region will use supporting functional logic to select a time-varying desired output, $\mathbf{y_d}(t)$, that defines a "path" to the commanded output, $\mathbf{y_c}$. The desired output is then passed to the region's controller and the controller determines the control inputs needed to follow that path.

5.1   Control Strategies

In this section, we briefly revisit the discussions of the previous chapter on the different control strategies used for different phases of flight and explicitly state the control law used for each.

5.1.1   Altitude Rate Controller - Feeding Back Altitude Rate Only

A pilot will accomplish speed changes in level flight typically by fixing the throttle appropriately (advanced for speed increase, reduced for speed decrease) and using the control stick to maintain level flight. To insure that the aircraft stays in level flight, the pilot will rely primarily on the altimeter and the attitude indicator. In a sense, he is using feedback control on his altitude rate (with a desired rate of zero) and allowing the aircraft to accelerate (or decelerate).

Alternatively, a pilot can use the control stick to maintain a constant, non-zero altitude rate while keeping the throttle fixed. He can also follow a varying altitude rate that may be determined by a specific geometric path (i.e., following a glide slope or flight path angle).

The pilot can also use the control stick to gain a balance of airspeed acceleration and vertical speed. This amounts to dividing the changing total energy between changes in potential and kinetic energy. It is also possible to exchange potential and kinetic energy without affecting the aircraft's total energy much at all (e.g., descending and accelerating). By adjusting the control stick, the pilot can control how much energy goes to changing airspeed and how much goes to changing altitude.

All of these regimes are examples of altitude rate control. The TGF simulator can use altitude-rate-only feedback to follow a constant or time-varying altitude rate using this control strategy. All that remains is for the region (i.e., the supporting functional logic) to tell the controller the desired altitude rate, $\dot{h}_d$. For altitude-rate-only feedback, equation (5.28) becomes

$$C_L(t) = k_{p_{14}}\left(\dot{h}_d(t) - \dot{h}(t)\right) + \int k_{i_{14}}\left(\dot{h}_d(t) - \dot{h}(t)\right)dt - k_{b_{14}}\dot{h}(t) \qquad (5.29)$$

5.1.2 Speed Controller - Feeding Back Speed Only

Climbs and descents at constant airspeed are also typically accomplished without modulation of the throttle. For climbs, the throttle is advanced to the desired climb power, and for descents, the power is reduced to descent power. The control stick is then adjusted to maintain the proper airspeed while the altitude is allowed to change. The pilot uses information from the airspeed (or Mach) indicator to adjust the control stick to maintain speed. This type of control is fundamentally different from the speed change in level flight because the control stick is now controlling speed instead of altitude rate. The altitude rate is left to vary according to the throttle setting.

The TGF simulator can use speed-only feedback to accomplish altitude changes using this control strategy. All that remains is for the region (i.e., the supporting functional logic) to tell the controller the desired speed, V_{IAS}, or Mach number, M. For indicated airspeed feedback, equation (5.28) becomes

$$C_L(t) = k_{p_{11}}\left(V_{IAS_d}(t) - V_{IAS}(t)\right) + \int k_{i_{11}}\left(V_{IAS_d}(t) - V_{IAS}(t)\right) dt - k_{b_{11}} V_{IAS}(t) \qquad (5.30)$$

and for Mach feedback, equation (5.28) becomes

$$C_L(t) = k_{p_{12}}\left(M_d(t) - M(t)\right) + \int k_{i_{12}}\left(M_d(t) - M(t)\right) dt - k_{b_{12}} M(t) \qquad (5.31)$$

5.1.3 Dual Controller - Feeding Back Speed and Altitude Rate

A pilot will maintain steady, level flight typically by using the control stick to fly level and adjusting the throttle to hold the desired speed. To insure that the aircraft stays in level flight, the pilot will monitor the altimeter and the attitude indicator. To insure that the aircraft holds speed, the pilot will monitor the airspeed (or Mach) indicator.

The TGF simulator can use this strategy to maintain steady, level flight, to fly a constant vertical speed at a specified airspeed, or to follow a specific speed-altitude profile, as on approach and landing. All that remains is for the region (i.e., the supporting functional logic) to tell the controller the desired speed and altitude rate. For IAS-based control, equation (5.28) becomes

$$\begin{aligned} C_L(t) &= k_{p_{14}}\left(\dot{h}_d(t) - \dot{h}(t)\right) + \int k_{i_{14}}\left(\dot{h}_d(t) - \dot{h}(t)\right) dt - k_{b_{14}} \dot{h}(t) \\ T(t) &= k_{p_{21}}\left(V_{IAS_d}(t) - V_{IAS}(t)\right) + \int k_{i_{21}}\left(V_{IAS_d}(t) - V_{IAS}(t)\right) dt - k_{b_{21}} V_{IAS}(t) \end{aligned} \qquad (5.32)$$

and for Mach feedback, equation (5.28) becomes

$$C_L(t) = k_{p_{14}}\left(\dot{h}_d(t) - \dot{h}(t)\right) + \int k_{i_{14}}\left(\dot{h}_d(t) - \dot{h}(t)\right) dt - k_{b_{14}}\dot{h}(t)$$

$$T(t) = k_{p_{22}}\left(M_d(t) - M(t)\right) + \int k_{i_{22}}\left(M_d(t) - M(t)\right) dt - k_{b_{22}}M(t)$$

<div align="right">(5.33)</div>

5.1.4 Altitude Capture

Capturing altitude is a fundamental function that the longitudinal dynamics must perform; however, altitude is never a feedback parameter directly in the controllers designed for our ADM. Instead altitude rate is commanded in a manner such that altitude capture is obtained. Initially it was not clear that this was the best solution to the problem. In fact many direct altitude feedback strategies were tried, and the state space model still allows for altitude feedback. However, instead of direct altitude feedback, the altitude error is used to determine an appropriate value for $\dot{h}_d$, the desired altitude rate. The reason for this decision is based primarily on the need for a smooth transition between a control region that does not control altitude rate, and one that does.
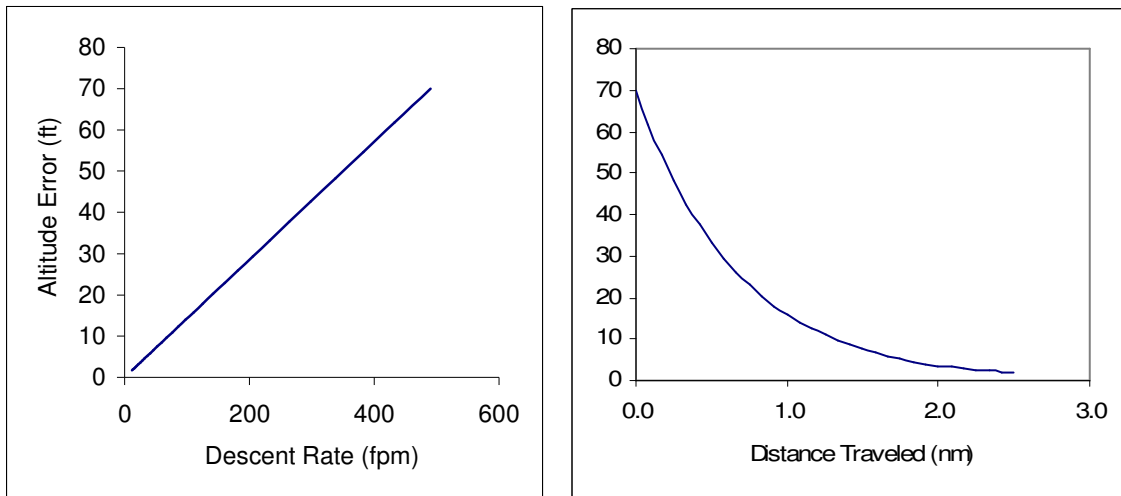
Figure 5.1: Illustration of an aircraft capturing an altitude

For regions in which the altitude is captured, the desired altitude rate is calculated by applying a gain to the difference between the desired altitude and the actual altitude.

$$\dot{h}_d = K_{\dot{h}}\left(h_d - h\right)$$

<div align="right">(5.34)</div>

We set a nominal value of $K_{\dot{h}} = 7 \; {1}/{min}$. Figure 5.1 shows how the descent rate varies over the final 70 feet and the smooth capture of the altitude when $K_{\dot{h}} = 7$.

There is still a problem to contend with at region transition. Consider an aircraft in, descent at idle throttle at a specified airspeed as shown in Figure 5.2. The aircraft

descends at whatever rate is required to maintain the commanded airspeed with an idle throttle; consequently, there is no direct control over the rate of descent. There is likely to be an undesired transient when the aircraft makes the transition to a region with controlled altitude rate. The cause of the undesirable transient is the fact that the aircraft's altitude rate upon entering the new region and the desired altitude rate derived from Equation (5.34) will not necessarily match. The mismatch causes the control law to drive the initial 'error' to zero with excessive control inputs. Figure 5.2 shows the mismatch and the sudden increase in the descent rate.

To solve this problem, the initial desired altitude rate is set equal to the aircraft's current altitude rate. The measured (current) altitude and altitude rate are used to calculate the value of $K_{\dot{h}}$ by rearranging Equation (5.34).

$$K_{\dot{h}_{initial}} = \frac{\dot{h}_{current}}{(h_d - h)_{current}} \qquad (5.35)$$
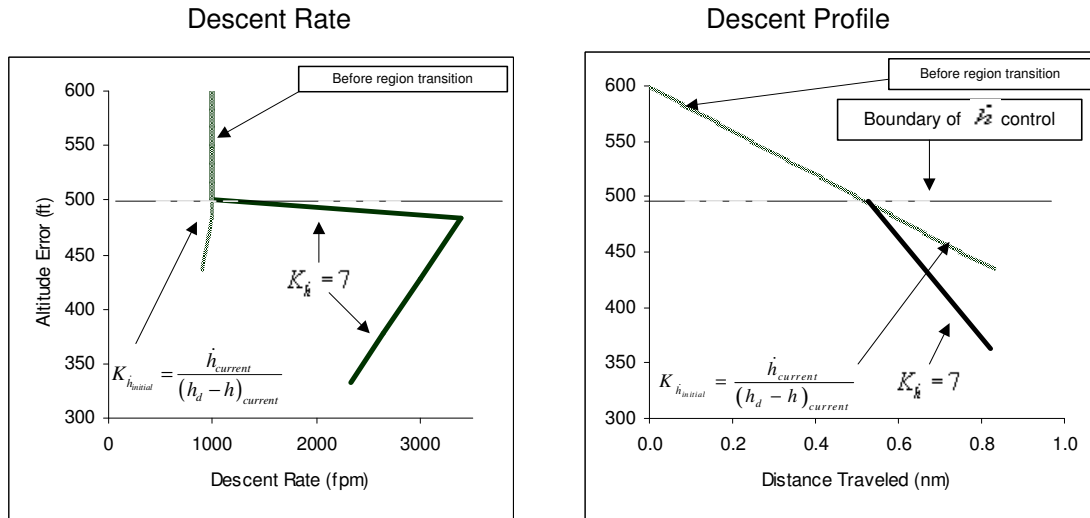
Figure 5.2: Altitude Rate During Region Transition

When the aircraft is within 70 feet of the target altitude, $K_{\dot{h}}$ is returned to its nominal value of seven regardless of the initial calculated value. Seventy feet is chosen because it yields an altitude rate near 500 fpm, a standard value for altitude capture established by Federal Air Regulations. This change in $K_{\dot{h}}$ does yield an unrealistic jump in the altitude rate just before altitude capture but it is much smaller than at region transition and it ensures that the altitude is captured in a timely manner. It also prevents the previous descent or climb from affecting the continuing cruise performance of the aircraft that

would come from preserving either an unusually low or high K_h. Figure 5.3 shows the logic for calculating K_h

5.1.5   Speed Capture

The feedback control laws were derived for small errors. In the steady, level flight control region, which uses speed control, the speed error is never more than 10 knots. This is a suitable speed to keep the control inputs from being excessive. But in the climb and descent regions, which also use speed control, it is possible for the speed error to be 100 knots or more. Our controller would produce excessive control inputs to correct this error.

To avoid these excessive control inputs, we must devise a varying desired speed profile that will produce acceptable control inputs and speed rates. A constant desired acceleration of one knot per second was chosen for its simplicity and suitability in producing an acceptable transient response. The initial desired speed upon entering a speed-controlled region is the actual speed.
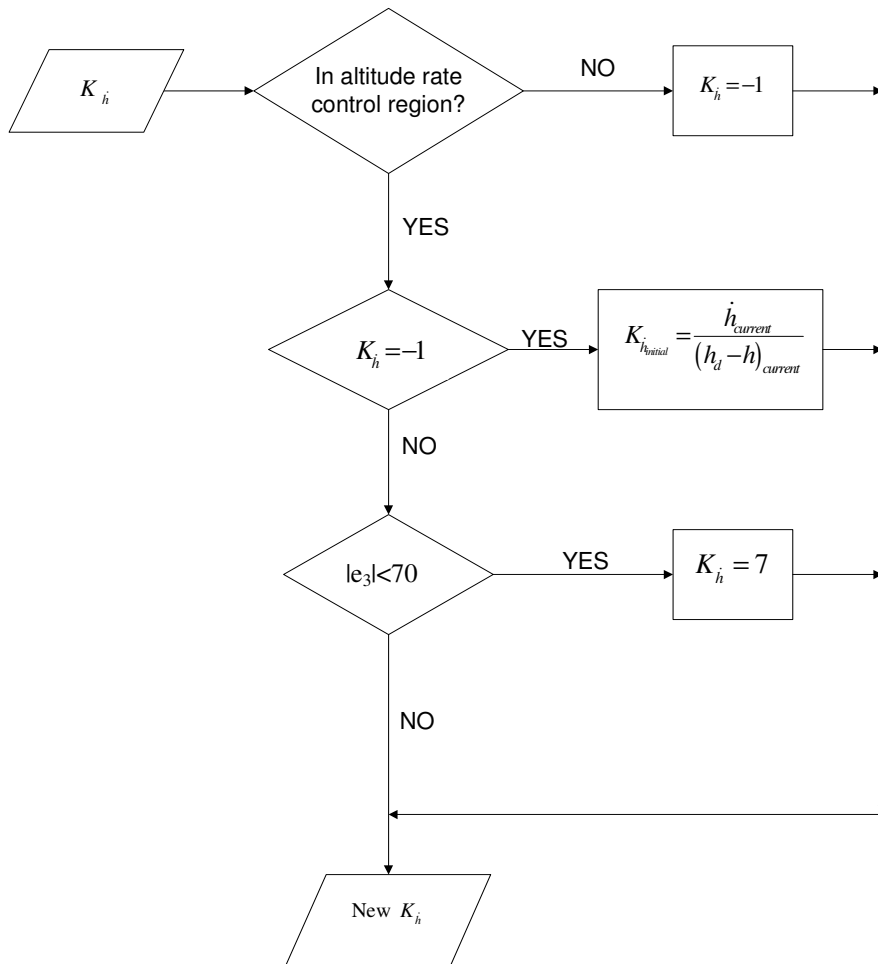
Figure 5.3. Flow diagram for calculating $K_{\dot{h}}$

$$V_{IAS_{d_0}} = V_{IAS}$$
$$V_{IAS_d} = V_{IAS_d} + \dot{V}_{IAS_d}\Delta t \qquad\qquad (5.36)$$

where

$$\dot{V}_{IAS_d} = \left(1 \quad kt\!\Big/\!sec\right) \;*\; \text{sign}\left(V_{IAS_c} - V_{IAS}\right)$$

The function, *sign(x)*, returns *+1* if *x ≥0* and *-1* otherwise. Once the indicated airspeed is within five knots of the commanded value, the desired speed is simply the commanded speed.

For Mach control, the equations for desired Mach are similar. A constant desired acceleration of 0.02 Mach per second is selected. It is equivalent to an acceleration of one knot per second at 25,000 feet altitude and 300 knots.

$$M_{d_0} = M$$
$$M_d = M_d + \dot{M}_d\Delta t \qquad\qquad (5.37)$$

where

$$\dot{M}_d = \left(0.02 \quad 1\!\Big/\!sec\right) \;*\; \text{sign}\left(M_c - M\right)$$

5.2   Dividing the Flight Envelope into Regions

Because of the need for different controllers and different supporting logic in different regimes of the flight envelope, we need to divide the flight envelope into regions. Each region's control law, supporting logic, and desired output reflect the pilot's decision logic in bringing the aircraft from its actual state to its desired state.

All of the supporting functional logic for the longitudinal control system centers on the concept of the speed-altitude plane. The speed-altitude plane was used by Mukai (1992) during the development of *Pseudocontrol*, the original control system developed for the Pseudo Aircraft Simulation (PAS) system developed for NASA Ames. The speed-altitude plane has been revisited and adapted for the TGF project and has undergone extensive modification since it was used in PAS.
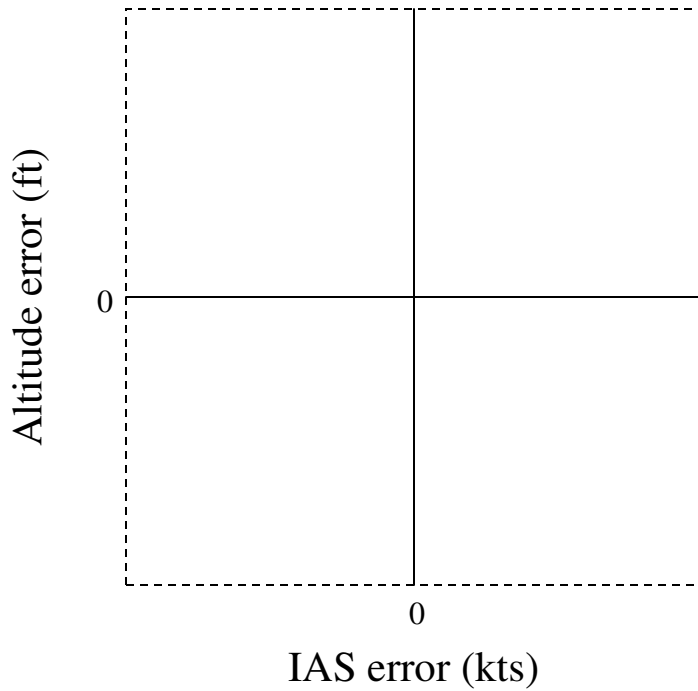
Figure 5.4. The Speed-Altitude Plane

5.2.1 The Speed-Altitude Plane

The speed-altitude plane is used to represent the aircraft's actual position relative to its commanded position, with altitude error plotted on the vertical axis and speed error plotted on the horizontal axis. It allows us to split the aircraft's en route flight envelope into different control regions. A diagram of the speed-altitude plane is shown in Figure 5.4.

The basic purpose of the speed-altitude plane is to emulate the way a pilot makes decisions about flying an aircraft. We define an area in the immediate vicinity of the commanded condition in which the aircraft is in steady, level flight. We set up speed error and altitude error bounds to define this steady, level flight region. We then need to define what to do outside of these bounds in order to bring the aircraft within them.

The speed-altitude plane provides a means of generalizing these relationships and also provides insight into what the throttle setting should be based on the aircraft's current energy level.

5.2.1.1 The Line of Constant Energy

The line of constant energy illustrates how an aircraft can have the same energy level at different speeds and altitudes. It is a means of determining whether the aircraft is low on

energy or high on energy with respect to its commanded condition; that is, does the aircraft need to add thrust or reduce thrust to attain the commanded condition. Originally, the line of constant energy was based on true energy calculations for the aircraft but as it evolved it became simply a gross representation of the aircraft's energy. This section discusses the evolution of the line of constant energy.

The total energy of an aircraft is the sum of its potential and kinetic energies.

$$E = K.E. + P.E. = mgh + \tfrac{1}{2}\, mV_a^2$$

The terms are defined as follows:

- E: The total aircraft energy
- m: The aircraft mass
- g: The gravitational acceleration
- h: The altitude
- V_a: The true airspeed

The equation can also be written in terms of the energy per unit mass.

$$e = gh + \tfrac{1}{2}\, V_a^2 \tag{5.38}$$

The energy that the aircraft would have at some commanded state can be written similarly,

$$e_c = gh_c + \tfrac{1}{2}V_{a_c}^{\,2} \tag{5.39}$$

where e_c is the total energy at the commanded state, h_c is the commanded altitude, and V_{a_c} is the commanded true airspeed. Notice that it is quite possible for $e_c = e$ without the aircraft actually being at the commanded state. That is to say, the aircraft could have the right amount of energy but be either fast and low or high and slow. This is illustrated in Figure 5.5 which shows the line of constant energy. The x- and y-axes on Figure 5.5 are the speed error and altitude error from some commanded state shown at the point (0,0).

If the aircraft's current state lies on the constant energy line, the aircraft already has enough energy to attain the commanded state. Therefore, the amount of throttle adjustment needed is minimal. However, if the aircraft lies below the constant energy line, the aircraft needs energy to attain the commanded state. Likewise, if the aircraft is above the energy line, the aircraft has excess energy and must lose energy to achieve the commanded state.

The constant energy curve is a parabola, as illustrated by the quadratic relationship between altitude and speed in equation (5.38). For practical control implementation, linear approximation to the constant energy curve in the speed-altitude plane is used, as shown in Figure 5.5. However, even this approximation is simplified because of transition problems between regions. The final form of the line of constant energy approximates the actual energy curve by forming a diagonal across the steady, level flight region, as shown in Figure 5.6.
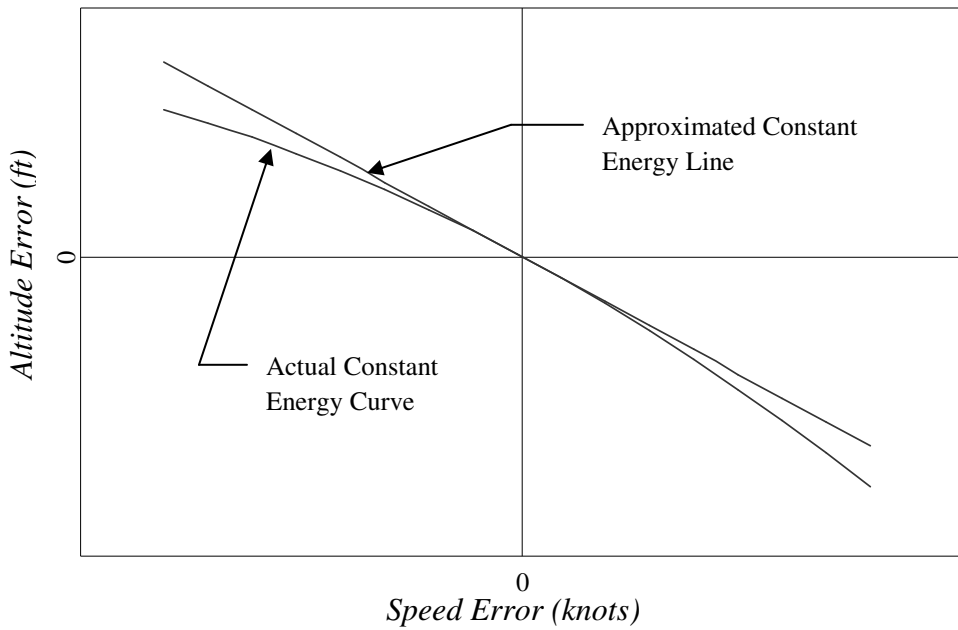
Figure 5.5. The constant energy line on the speed-altitude plane
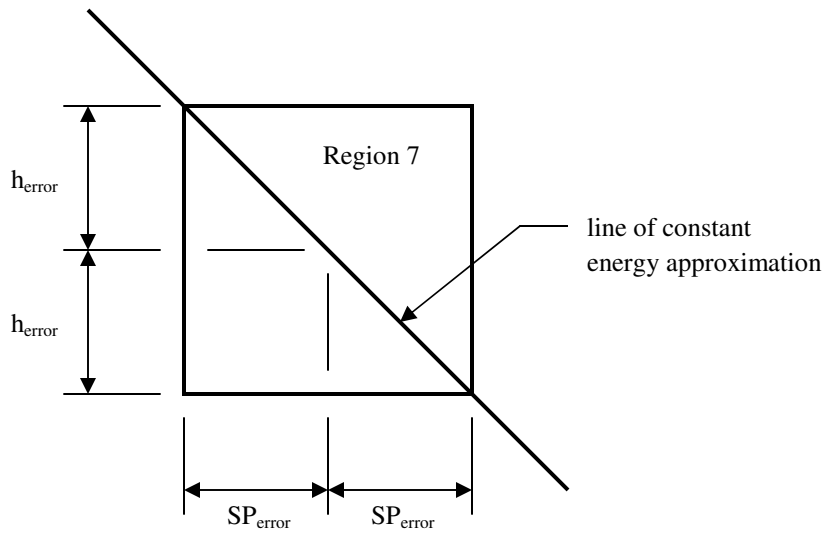
Figure 5.6. Illustration of the approximation for the constant energy line using the diagonal cut across the steady, level flight region (region 7) of the speed-altitude plane

5.2.1.2 Bounding the Speed-Altitude Plane

The speed error bound on the steady, level flight region is 10 knots. The simulation engineers chose this value because it is a bound typically used in real flight; an aircraft within ten knots of a controller-assigned speed is considered to be in compliance with that speed. The simulation engineers chose the altitude error bounds so that the slope of the diagonal of the steady, level flight region is the same as the slope of the constant energy line in the vicinity of a flight condition that is representative of en route flight: 300 knots IAS @ 25,000 ft.

At 25,000 feet altitude in the standard atmosphere, 300 knots IAS corresponds to 728 fps true airspeed (TAS) and a ten knot IAS speed difference corresponds to about a 22 fps speed difference in TAS. The slope of the constant energy curve at this point is given by the derivative of equation (5.38). Assuming that gravity is constant,

$$d\left(e\right)=d\left(gh\right)+d\left(\frac{1}{2}V_a^{\,2}\right)$$

$$de = g\ dh + V_a\ dV_a \tag{5.40}$$

Using discrete notation, and substituting in the values corresponding to our speed change and flight condition, we can calculate the corresponding altitude change that would keep the total energy constant.

- 125 -

$$\Delta e = g \; \Delta h + V_a \; \Delta V_a$$

$$(0) = \left(32.2 \; {ft}\!\big/\!{s^2}\right) \Delta h + \left(728 \; {ft}\!\big/\!{s}\right)\left(22 \; {ft}\!\big/\!{s}\right)$$

$$\Delta h = 497 \; {ft}\!\big/\!{s}$$

We choose to round to 500 feet for the altitude error.

The parameters needed to define the regions of the speed-altitude plane are the speed error, altitude error, and slope of the constant energy line. These parameters nominally are set as follows:

- h_{error}: This is the altitude error used to bound the steady, level flight region and, consequently, the slope of the constant energy line of the speed-altitude plane. The nominal value is 500 feet.
- SP_{error}: This is the speed error used to bound the steady, level flight region. It needs to be defined in terms of knots for IAS-based control and in terms of Mach number for Mach-based control.
    - IAS-based: $SP_{error} = IAS_{error} = 10 \; knots$. Aircraft are typically expected to hold their speeds within 10 knots.
    - Mach-based: $SP_{error} = M_{error} = 0.022$. This is the Mach error used to bound the steady, level flight region in the Mach speed-altitude plane. The value corresponds to a 10 knot IAS speed change at 300 knots IAS and 25,000 feet in the standard atmosphere.

5.2.1.3 The Regions of the Speed-Altitude Plane

The speed-altitude plane is divided into nine different regions. Each region has a different combination of control law and supporting functional logic. The speed error on the speed-altitude plane is either represented in knots of indicated airspeed or in Mach number. Figure 5.7 shows the regions of the speed-altitude plane in terms of indicated airspeed. The regions are enumerated below with their various functions.

- **Steady, Level Flight (Region 7):** In Region 7, the aircraft is sufficiently close to converging on a desired state. The pilot modulates the control stick and the throttle simultaneously to capture the desired state.
- **Climbing & Accelerating (Region 1):** In Region 1, the aircraft is low and slow and is, therefore, low on energy. The throttle is set to full and the pilot climbs and accelerates the aircraft, using the control stick to maintain a balance of airspeed acceleration and climb rate.
- **Level Acceleration (Region 2):** In Region 2, the aircraft is slow enough to be low on energy; therefore, the throttle is set to full. The pilot uses the control stick to capture and maintain the desired altitude while accelerating into Region 7.
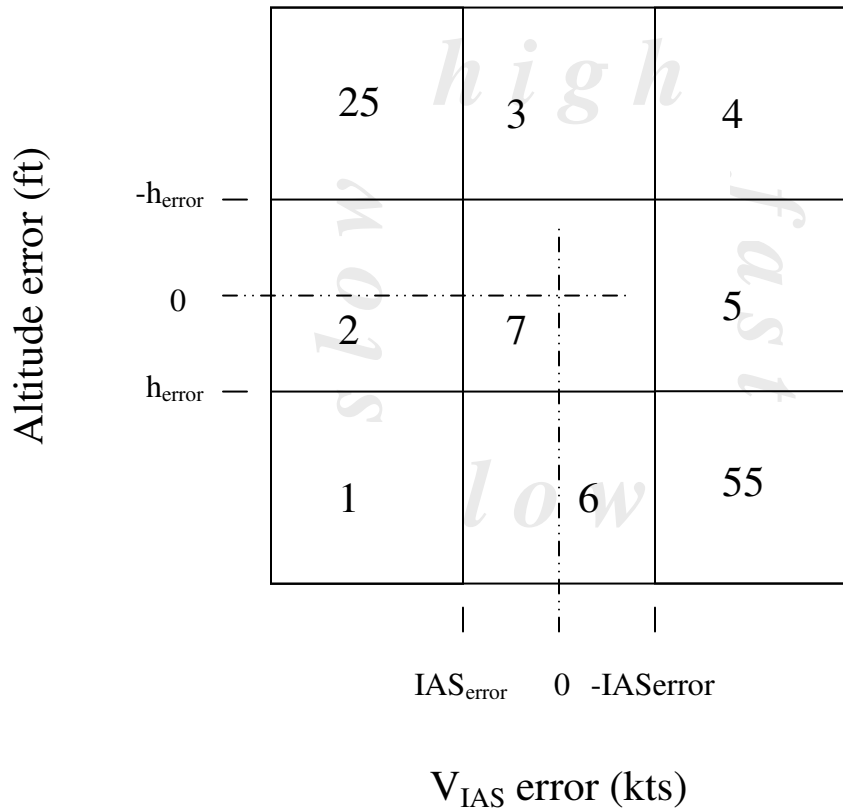
Figure 5.7. The speed-altitude plane in terms of indicated airspeed

- **Descending & Accelerating (Region 25):** This is an energy trade region, meaning that the aircraft is trading potential energy for kinetic energy. The throttle is set to idle and lift coefficient is used to capture a desired altitude rate that is a constant multiple of the altitude error.
- **Steady Descent (Region 3):** In Region 3, the aircraft is high enough to have excess energy; therefore, the throttle is set to idle. The pilot uses the control stick to capture and maintain the desired speed while descending into Region 7.
- **Descending & Decelerating (Region 4):** In Region 4, the aircraft is high and fast and is, therefore, high on energy. The throttle is set to idle and the pilot descends and decelerates the aircraft, using the control stick to maintain a balance of airspeed deceleration and descent rate that is weighted towards descending.
- **Level Deceleration (Region 5):** In Region 5, the aircraft is fast enough to have excess energy; therefore, the throttle is set to idle. The pilot uses the control stick to capture and maintain the desired altitude while decelerating into Region 7.
- **Climbing & Decelerating (Region 55):** This is an energy trade region, meaning that the aircraft is trading kinetic energy for potential energy. The throttle is set to idle and

lift coefficient is used to capture a desired altitude rate that is a constant multiple of the altitude error.

- **Steady Climb (Region 6):** In Region 6, the aircraft is low enough to be low on energy; therefore, the throttle is set to full. The pilot uses the control stick to capture and maintain the desired speed while climbing into Region 7.

The reader should notice a similarity between the basic strategy in each of the regions and the discussion of Section 4.1.1, where the basic piloting strategies for different types of maneuvers are outlined. The speed-altitude plane is a means of mechanizing the control strategy that a pilot would use depending on the aircraft's state relative to the commanded state.

5.2.1.4 Region Management in the Speed-Altitude Plane

The error between the aircraft's commanded and actual states is compared to the error bounds of the speed-altitude plane. This determines the aircraft's control region in the speed-altitude plane. The absolute errors between the aircraft's actual and commanded states, e_1 through e_4, are defined below.

$$e_1 = V_{IASc} - V_{IAS} \tag{5.41}$$

$$e_2 = M_c - M \tag{5.42}$$

$$e_3 = h_c - h \tag{5.43}$$

$$e_4 = \dot{h}_c - \dot{h} \tag{5.44}$$

The terms are defined as follows:

- V_{IASc} : The commanded indicated airspeed (kts)
- V_{IAS}: The actual indicated airspeed (kts)
- M_c: The commanded Mach number
- M: The actual Mach number
- h_c: The commanded altitude (ft)
- h: The actual altitude (ft)
- $\dot{h}_c$: The commanded altitude rate (ft/min)
- $\dot{h}$: The actual altitude rate (ft/min)

We can use Boolean expressions to define four true-false parameters that coincide with the bounds and definitions of the speed-altitude plane. These are used to aid the flow algorithm (illustrated below) that determines which region logic to use. For example, if the commanded speed is more than ten knots below the actual speed, the aircraft is defined to be *fast*. These *speed-altitude plane Booleans* are defined in Table 5.1.

LOW	$e_3 > h_{error}$
HIGH	$e_3 < -h_{error}$
SLOW	$e_s > SP_{error}$
FAST	$e_s < -SP_{error}$
LOWENERGY	$e_3 > (m*e_s)$

Table 5.1: Speed - Altitude Plane Booleans

This section describes the control strategies and supporting functional logic used in each of the regions of the speed-altitude plane.

5.2.1.4.1   Steady, Level Flight (Region 7)

Region 7 is the most highly used region because it represents the aircraft at or near steady, level flight. The aircraft is close enough to a desired state that our linear controller can capture that state without excessive control inputs. Both the lift coefficient and the thrust are controlled. The control law is given by equations (5.32) and (5.33) for IAS-based and Mach-based control, respectively. The desired altitude rate is given by equation (5.34) and the desired speed is given by equations (5.36) and (5.37) for IAS-based and Mach-based control, respectively.

5.2.1.4.2   Accelerating (Region 2)

In Region 2, the aircraft is slow enough to be *lowenergy*, but it may be above or below its commanded altitude. Because the aircraft is *lowenergy*, the throttle is advanced to full throttle. The system uses the lift coefficient to capture and maintain the desired altitude rate while accelerating into Region 7. The control law is given by equation (5.29) with the desired altitude rate given by equation (5.34) (the same as for Region 7).

5.2.1.4.3   Descending & Accelerating (Region 25)

Region 25 is an energy trade region. Throttle is set to idle and the desired altitude rate is a constant multiple of the altitude error. , The control law is given by equation (5.29) with the desired altitude rate given by equation (5.34). $K_{\dot{h}}$ must be large enough so that the desired descent rate is large enough to permit acceleration with an idle throttle. If the descent rate is too small, the energy loss of a negative *(T-D)* (because of the idle throttle) will force a deceleration. A value of $K_{\dot{h}} = 1$ is suggested.

An alternative to setting a constant idle throttle is to set the throttle so that the thrust produced is equal to the drag. With no energy being lost, the aircraft would be forced to accelerate while capturing the desired descent rate. From equation (2.59), with *T=D*,

$$ \dot{V}_a = -g \sin \gamma = -g \frac{\dot{h}}{V_a} $$

The problem from a software engineering standpoint is that the drag is not readily available to the throttle controller. However, the above equation can be used to calculate a desired acceleration and a new throttle controller could be developed that captures that desired acceleration. This approach has shown promise in preliminary tests, but has not been implemented. It requires a dual controller, with lift coefficient controlling altitude rate and throttle controlling acceleration.

5.2.1.4.4 Decelerating (Region 5)

In Region 5, the aircraft is fast enough to be *not lowenergy*, but it may be above or below its commanded altitude. It has more energy than it needs so the throttle is reduced to idle. It is the same as Region 2 except for the throttle setting. The system uses the lift coefficient to capture and maintain the desired altitude rate while decelerating into Region 7. The control law is given by equation (5.29) with the desired altitude rate given by equation (5.34) (the same as for Region 7).

5.2.1.4.5 Climbing & Decelerating (Region 55)

Region 55 is a subset of Region 5 that uses a constant descent rate; that is, the greater of its current altitude rate and 500 fpm.

$$ \dot{h}_d = \max\left(\dot{h}, 500 \ fpm\right) $$

Region 25 is an energy trade region. Throttle is set to max full and the desired altitude rate is a constant multiple of the altitude error. , The control law is given by equation (5.29) with the desired altitude rate given by equation (5.34). $K_{\dot{h}}$ must be large enough so that the desired climb rate is large enough to permit deceleration with full throttle. If the climb rate is too small, the energy gain of a positive *(T-D)* (because of the full throttle) will force an acceleration. A value of $K_{\dot{h}} = 1$ is suggested.

An alternative to setting a constant full throttle is to set the throttle so that the thrust produced is equal to the drag. With no energy being lost, the aircraft would be forced to decelerate while capturing the desired climb rate. From equation (2.59), with *T=D*,

$$ \dot{V}_a = -g \sin \gamma = -g \frac{\dot{h}}{V_a} $$

The problem from a software engineering standpoint is that the drag is not readily available to the throttle controller. However, the above equation can be used to calculate

a desired acceleration and a new throttle controller could be developed that captures that desired acceleration. This approach has shown promise in preliminary tests, but has not been implemented. It requires a dual controller, with lift coefficient controlling altitude rate and throttle controlling acceleration.

5.2.1.4.6 Descending (Region 3)

In Region 3, the aircraft is high enough to be *not lowenergy*. It may be above or below its desired speed. Because the aircraft is *not lowenergy*, the thrust is set to idle. The aircraft uses lift coefficient control to capture its desired speed while descending into Region 7. The control law is given by equation (5.30) and equation (5.31) for IAS-based and Mach-based control, respectively. The desired speed is given by equations (5.36) and (5.37) for IAS-based and Mach-based control, respectively.

5.2.1.4.7 Climbing (Region 6)

In Region 6, the aircraft is low enough to be *lowenergy*. It may be above or below its desired speed. Because the aircraft is *lowenergy*, the thrust is set to full. The aircraft uses lift coefficient control to capture its desired speed while climbing into Region 7. The control law is given by equation (5.30) and equation (5.31) for IAS-based and Mach-based control, respectively. The desired speed is given by equations (5.36) and (5.37) for IAS-based and Mach-based control, respectively.

5.2.1.4.8 Climbing & Accelerating (Region 1)

In Region 1, the aircraft is low and slow and is, therefore, *lowenergy*. The throttle is set to full and the system uses altitude rate feedback to maintain a balance of airspeed acceleration and climb rate that is weighted towards acceleration. The control law is given by equation (5.29).

Since the system uses altitude rate feedback, we need to determine the desired altitude rate that will yield the balance of airspeed acceleration and climb rate mentioned above. With the throttle set to full, the aircraft's thrust is typically greater than its drag. This means that the aircraft's total energy is increasing. We need to determine how much of this energy increase goes towards accelerating and how much goes towards climbing. An equation relating acceleration and altitude rate is given by equation (2.59),

$$\dot{V}_a = \frac{T-D}{m} - g \sin \gamma = \frac{T-D}{m} - g \frac{\dot{h}}{V_a} \tag{2.59}$$

which can be written in the form of the changing energy.

$$\frac{(T-D)V_a}{m} = g\dot{h} + V_a \dot{V}_a \tag{5.45}$$

- 131 -

Note that this equation is presented in BADA as equation (3.1-1). Note also that this equation is the time derivative of equation (5.38). We can rewrite this equation to express an aircraft's desired altitude rate in terms of an **energy ratio**, *ER*.

$$\dot{h}_d = \frac{(T-D)V_a}{mg\left(1+\dfrac{V_a \dot{V}_a}{g\dot{h}}\right)} = \frac{(T-D)V_a}{mg\left(1+ER\right)} \tag{5.46}$$

The energy ratio, *ER*, is an expression of the ratio of changing kinetic energy to changing potential energy. We can use it to express how much of the changing energy (i.e., the thrust energy being added to the system) goes towards changing speed and how much goes towards changing altitude. BADA uses the same approach, but expresses equation (5.46) in terms of an **energy share factor** as a function of Mach number. For acceleration in climb, BADA recommends an energy share factor that corresponds to an energy ratio of *ER = 2.3*, and that is what we use for our controller. With the desired altitude rate determined by equation (5.46) we can use an altitude rate controller to capture that altitude rate.

5.2.1.4.9   Descending & Decelerating (Region 4)

In Region 4, the aircraft is high and fast and is, therefore, *not lowenergy*. The throttle is set to idle and the system uses altitude rate feedback to maintain a balance of airspeed deceleration and descent rate that is weighted towards the descent. The control law is given by equation (5.29).

Just as in Region 1, we need to determine the desired altitude rate that will yield the balance of changing airspeed and altitude. For deceleration in descent, BADA recommends an energy share factor that corresponds to an energy ratio of *ER = 2.3*; however, our tests have shown that an energy ratio of *ER = 1.0* is more suitable. To determine the desired altitude rate for Region 4, we use equation (5.46) with the throttle set to idle thrust and the energy ratio set to *ER = 1.0.*

5.2.1.5 Constant Vertical Speed (CVS) Maneuvers – (Formerly Region 8)

When a vertical speed is commanded, the aircraft is performing a constant vertical speed (CVS) maneuver. The maneuver is completed when the aircraft becomes *not fast* and *not slow*. There are three separate CVS maneuvers: idle-thrust CVS, max-thrust CVS, and dual-control CVS. If the speed error is within SP_{error}, the aircraft is in a dual-control CVS. Otherwise, if the altitude error is positive, the aircraft is in a max-thrust CVS maneuver and if the altitude error is negative, the aircraft is in an idle-thrust CVS maneuver.

5.2.1.5.1 Dual-Control CVS Maneuver

The control law is given by equation (5.32) and equation (5.33) for IAS-based and Mach-based control, respectively – the same as for Region 7. The desired speed is given by equations (5.36) and (5.37) for IAS-based and Mach-based control, respectively. The desired altitude rate is as commanded.

Once in a dual-control CVS, if the aircraft becomes *slow*, that means it is losing speed. It is expected that this can happen only in a climbing maneuver in which the aircraft does not have enough thrust or power to maintain airspeed and vertical speed concurrently. If left in the CVS climb, the speed will only continue to fall. In this case, the aircraft must break out of the CVS maneuver and into a Mach or CAS climb.

Once in a dual-control CVS, if the aircraft becomes *fast*, that means it is gaining speed. It is expected that this can happen only in a descent maneuver in which the aircraft does not have enough drag to maintain airspeed and vertical speed concurrently. In this case, there is an alternative to breaking out of the CVS maneuver: deploy speed brakes. If the speed error moves back within ½ the SP_{error} (i.e., five knots), speed brakes can be turned off. It is possible for the aircraft to get in a cycle of turning speed brakes on and off – an unrealistic scenario – but this should yield acceptable performance.

With speed brakes on, if the aircraft continues to gain speed (i.e., if the speed error exceeds 1 ½ times the SP_{error} - i.e., 15 knots), it shall break out of the CVS descent and into a Mach or CAS descent.

5.2.1.5.2 Idle-Thrust CVS Maneuver

In this maneuver, the aircraft is *not lowenergy* and is descending. The altitude error is necessarily negative (an entry condition) and the commanded vertical speed is negative. The speed is not controlled; the maneuver is entirely independent of speed behavior. The throttle is set to idle and the system uses altitude rate feedback to maintain the commanded vertical speed. The control law is given by equation (5.29).

This maneuver also needs a break-out condition. It is necessary for the success of this maneuver that the aircraft's energy rate is negative. This is the purpose of setting idle thrust. As an example, if the commanded descent rate is so high that the aircraft must accelerate to extreme speeds in order to capture the commanded descent rate, the aircraft's energy may actually be increasing, even though the throttle is at idle. Therefore, if the energy increment, as given by equation (5.40), is positive, the aircraft can first deploy speed brakes. If the energy increment is still positive, the aircraft shall break out of the CVS descent and into a Mach or CAS descent.

5.2.1.5.3 Max-Thrust CVS Maneuver

In this maneuver, the aircraft is *lowenergy* and is climbing. The altitude error is necessarily positive (an entry condition) and the commanded vertical speed is positive. The speed is not controlled; the maneuver is entirely independent of speed behavior. The throttle is set to max climb thrust and the system uses altitude rate feedback to maintain the commanded vertical speed. The control law is given by equation (5.29).

This maneuver also needs a break-out condition. It is necessary for the success of this maneuver that the aircraft's energy rate is positive; this is the purpose of setting max climb thrust. As an example, if the commanded climb rate is so high that the aircraft must fall to dangerously low speeds in order to capture the commanded climb rate, the aircraft's energy may actually be decreasing, even though the throttle is at its maximum. Therefore, if the energy increment, as given by equation (5.40), is negative, the aircraft shall break out of the CVS climb and into a Mach or CAS climb.

5.2.2 Taking off

If an aircraft is initiated in the simulation as a take-off, the guidance module generates a sequence of legs that will take the aircraft to its low-altitude cruising speed and 6000 feet altitude. That sequence is the take-off ground run, rotation, lift-off, initial climb, and cruise at 6000 feet altitude. The take-off ground run, rotation, and lift-off legs are the "take-off" legs. An aircraft cannot enter either of these legs unless it is initiated as a take-off and it must successively satisfy the boundary conditions of each leg to progress into the initial climb. Additionally, these legs use their own controllers and are, therefore, given their own regions. The initial climb and level cruise legs use the region management of the speed-altitude plane.

5.2.2.1 Take-Off Ground Run (Region 12)

The take-off ground run region uses an open-loop controller to accelerate the aircraft until it is within ΔV_R of its rotation speed while keeping on the ground. The region specifies constant control inputs. A lift coefficient of zero is specified to keep the aircraft from lifting off during the ground run and take-off thrust is specified to give the aircraft its maximum acceleration.

$$
\begin{aligned}
C_L &= 0 \\
T &= C_{T_{TO}} T_{\max}
\end{aligned}
\tag{5.47}
$$

Boundary Condition: $\qquad V_{IAS} < V_R - \Delta V_R$

The constant ΔV_R is defined the same for all aircraft. It represents the speed at which the simulated aircraft enters the rotation region, region 13. Conceptually, it is intended to represent the increment below rotations speed at which the pilot begins to pull back on

the control stick to lift off the runway. Its value in NextGen is selected so as to provide ample time for the controller of region 13 to ramp up to the aircraft's rotation lift coefficient.

$$\Delta V_R = 20 \ knots$$

5.2.2.2 Rotation (Region 13)

The sole purpose of the rotation region is to ramp the lift coefficient up from zero to the aircraft's rotation lift coefficient as a function of speed. At first look, this requires an open-loop controller that ramps the lift coefficient between these two points as a function of time, but this would require a unique controller form. TGF programmers and engineers decided that it would be easiest to implement a controller of the same form as all the other controllers, i.e., of the form of equation (5.28). This requires the development of gains that cause the feedback controller to mimic our desired open-loop behavior.

Equation (5.28) is a shortened form of equation (4.2), which is rewritten here.

$$\mathbf{u}(t) = \mathbf{K_p}\mathbf{e}(t) + \int_0^t \mathbf{K_i}\mathbf{e}(t)\mathbf{dt} - \mathbf{K_b}\mathbf{y}(t) \tag{4.2}$$

We desire lift coefficient behavior that increases steadily. Since indicated airspeed increases with time during the ground run, we simplify our controller by selecting that output only. We also specify that the desired speed is the rotation speed throughout the region. The single input, single output (SISO) system is then,

$$C_L\left(V_{IAS}(t)\right) = k_{p_{11}}\left(V_R - V_{IAS}(t)\right) + \int_0^t k_{i_{11}}\left(V_R - V_{IAS}(t)\right)dt - k_{b_{11}}V_{IAS}(t) \tag{5.48}$$

The lift coefficient needed to lift the aircraft off the runway at rotation speed is dubbed the rotation lift coefficient.

$$C_{L_R} = \frac{W}{\frac{1}{2}\rho V_R^2 S}$$

We would like the lift coefficient to change from zero at the beginning of region 13 to the rotation lift coefficient when the aircraft reaches its rotation speed. At rotation speed, we want the rate of change of the lift coefficient with speed to flatten out so that we don't overshoot it and impose undo drag on the aircraft. We, therefore, specify the following conditions for our controller.

$$C_L(V_R - \Delta V_R) = 0$$

$$C_L(V_R) = C_{L_R}$$

$$\frac{d}{dV_{IAS}}\left(C_L\left(V_R\right)\right) = 0$$

The bound of region 13 is defined by aircraft speed only. Once the aircraft speed is greater than the rotation speed, control is passed to region 14. A lower bound is not specified; once control is passed from region 12, the aircraft stays within region 13 until the boundary condition is satisfied.

Boundary Condition: $\qquad\qquad V_{IAS} \leq V_R$

To simplify integration, we assume the indicated airspeed in region 13 has constant acceleration; i.e., it is of the following form.

$$V_{IAS} = \dot{V}_{IAS}t \quad \left(\dot{V}_{IAS} = constant\right) \tag{5.49}$$

We transform equations (5.48) and (5.49) into functions of the indicated airspeed.

$$dt = \frac{1}{\dot{V}_{IAS}}dV_{IAS}$$

$$C_L\left(V_{IAS}\right) = k_{p_{11}}\left(V_R - V_{IAS}\right) + \int_{V_R - \Delta V_R}^{V_{IAS}} k_{i_{11}}\left(V_R - V_{IAS}\right)\left[\frac{1}{\dot{V}_{IAS}}dV_{IAS}\right] - k_{b_{11}}V_{IAS}$$

$$C_L\left(V_{IAS}\right) = k_{p_{11}}\left(V_R - V_{IAS}\right) + \frac{k_{i_{11}}}{\dot{V}_{IAS}}\int_{V_R - \Delta V_R}^{V_{IAS}}\left(V_R - V_{IAS}\right)dV_{IAS} - k_{b_{11}}V_{IAS}$$

$$C_L\left(V_{IAS}\right) = k_{p_{11}}\left(V_R - V_{IAS}\right)$$
$$+ \frac{k_{i_{11}}}{\dot{V}_{IAS}}\left\{\left[V_R\left(\left(V_{IAS}\right) - \left(V_R - \Delta V_R\right)\right)\right] - \left[\frac{\left(V_{IAS}\right)^2 - \left(V_R - \Delta V_R\right)^2}{2}\right]\right\} - k_{b_{11}}V_{IAS}$$

We now have an equation relating the lift coefficient to the indicated airspeed.

$$C_L\left(V_{IAS}\right) = k_{p_{11}}\left(V_R - V_{IAS}\right) - \frac{k_{i_{11}}}{\dot{V}_{IAS}}\frac{\left(V_{IAS} - V_R\right)^2 - \Delta V_R^{\,2}}{2} - k_{b_{11}}V_{IAS} \tag{5.50}$$

The derivative of equation (5.50) is,

$$\frac{d}{dV_{IAS}}\left(C_L\left(V_{IAS}\right)\right) = -k_{p_{11}} - \frac{k_{i_{11}}}{\dot{V}_{IAS}}\left(V_{IAS} - V_R\right) - k_{b_{11}} \tag{5.51}$$

The initial conditions plugged into equations (5.50) and (5.51) yield the following equations.

$$C_L\left(V_R - \Delta V_R\right) = k_{p_{11}}\left(V_R - [V_R - \Delta V_R]\right) - \frac{k_{i_{11}}}{\dot{V}_{IAS}}\frac{\left([V_R - \Delta V_R] - V_R\right)^2 - \Delta V_R^2}{2} \cdot k_{b_{11}}\left[V_R - \Delta V_R\right] = 0$$

$$C_L\left(V_R\right) = k_{p_{11}}\left(V_R - [V_R]\right) - \frac{k_{i_{11}}}{\dot{V}_{IAS}}\frac{\left([V_R] - V_R\right)^2 - \Delta V_R^2}{2} \cdot k_{b_{11}}\left[V_R\right] = C_{L_R}$$

$$\frac{d}{dV_{IAS}}\left(C_L\left(V_R\right)\right) = -k_{p_{11}} - \frac{k_{i_{11}}}{\dot{V}_{IAS}}\left([V_R] - V_R\right) - k_{b_{11}} = 0$$

$$k_{p_{11}}\Delta V_R - k_{b_{11}}\left[V_R - \Delta V_R\right] = 0$$

$$\frac{k_{i_{11}}}{\dot{V}_{IAS}}\frac{\Delta V_R^2}{2} \cdot k_{b_{11}}V_R = C_{L_R}$$

$$-k_{p_{11}} - k_{b_{11}} = 0$$

This system yields the following solution for our region 13 controller.

$$
\begin{aligned}
k_{p_{11}} &= 0 \\
k_{i_{11}} &= \frac{2\dot{V}_{IAS}C_{L_R}}{\Delta V_R^2} \\
k_{b_{11}} &= 0
\end{aligned}
\tag{5.52}
$$

The region 13 controller is given by equation (5.48).

5.2.2.3 Lift-Off (Region 14)

When the aircraft reaches its rotation speed, the pilot pulls back on the control stick to lift off the runway, but maintains take-off thrust and take-off flaps. He uses this configuration until he reaches the maneuver altitude. NextGen operates similarly: control is passed to region 14 at rotation speed and the aircraft remains in region 14 control until it reaches its maneuver altitude, set to 400 feet AGL in NextGen. Therefore, we need a controller that returns take-off thrust and uses the lift coefficient to control speed. In this sense, region 14 is similar to region 6 (constant speed climbs) except that it uses take-off thrust.

$$T = C_{T_{TO}} T_{\max}$$
$$V_d = V_R$$

Boundary Condition: $\quad\quad\quad$ **h ≤ *400 ft AGL***

The controller is given by equation (5.30). Additionally, as soon as we enter this region, we can raise the landing gear, which amounts to removing the gear drag coefficient $C_{D_{gear}}$ from the drag equation.

5.2.3 Landing Region Management

An aircraft that has received the command to begin the landing sequence will remain in the speed-altitude plane regions until it reaches its glide slope. Once the aircraft reaches the glide slope, it begins the landing sequence and progresses through regions 9, 10, and 11. A new commanded altitude will move control back to the speed-altitude plane manager (i.e., landing is aborted). It is assumed that Mach-based control is not used for any landing maneuver, so Mach-based controllers are not considered.

5.2.3.1 Preparing for Approach

In many cases, an aircraft is instructed to begin preparations for approach. An unrestricted aircraft may begin bleeding off energy by decelerating on its own. In the real world, pilots will prepare for the approach in this way, particularly if they are familiar with the approach profile for their arrival airport. Tables Table 5.2 and Table 5.3 outline the desired speed profile as a function of altitude for an unrestricted aircraft that is on approach. The schedule comes from section 4 of the BADA User Manual. This schedule is used for aircraft before and on the glide slope. For intermediate altitudes, linear interpolation is used to determine the desired speed. In the table, $V_{des,1}$ is the aircraft's preferred descent speed below 10,000 feet altitude, available from BADA.

Altitude (ft)	Desired Speed, V_{IAS_d} (kts)
0	$1.3 V_{stall_{LD}}$
1000	$1.3 V_{stall_{LD}} + 5$
1500	$1.3 V_{stall_{LD}} + 10$
2000	$1.3 V_{stall_{LD}} + 20$
3000	$1.3 V_{stall_{LD}} + 50$
6000	*MIN($V_{des,1}$,220)*
10,000	*MIN($V_{des,1}$,250)*

Table 5.2 Desired Descent Speed Schedule for Jet and Turboprop Aircraft Preparing for Approach

Altitude (ft)	Desired Speed, V_{IAS_d} (kts)
0	$1.3V_{stall_{LD}}$
500	$1.3V_{stall_{LD}} + 5$
1000	$1.3V_{stall_{LD}} + 10$
1500	$1.3V_{stall_{LD}} + 20$
6000	$1.3V_{stall_{LD}} + 50$
10,000	$V_{des,1}$

Table 5.3 Desired Descent Speed Schedule for Piston Preparing for Approach

5.2.3.2 Approach (Region 9)

Because the aircraft is following the glide slope (a linear altitude profile) and a preferred speed profile, it needs a controller that feeds back speed and altitude rate. The control law is given by equation (5.32).

The only difference is in the development of the desired output. Region 9 specifies the aircraft's speed profile as a function of distance from the runway threshold. Alternatively, the aircraft can be speed restricted with a commanded speed. Either way, region 9 specifies a desired altitude rate that will have the aircraft descend along the glide slope.

The guidance module defines the altitude profile based on the aircraft's distance from the glide slope antenna of its assigned runway. The guidance module defines a distance, d_{GS}, as the distance parallel to the runway from the glide slope antenna to the aircraft. The aircraft's desired altitude is a function of that distance and the angle of the glide slope antenna's signal, γ_{GS}.

$$h_d = h_{GS} = d_{GS} \tan \gamma_{GS} \tag{5.53}$$

The aircraft's desired altitude rate must consider the local glide slope altitude as well as the aircraft's altitude relative to the glide slope. As in Region 7, equation (5.34) is used to determine the altitude that would correct the aircraft's altitude error, but we must also consider that the desired altitude is changing per equation (5.53). We add the derivative of equation (5.53) to equation (5.34) to get the desired altitude rate for Region 9.

$$\dot{h}_d = K_h \left(h_d - h \right) + \frac{d}{dt} \left(d_{GS} \right) \tan \gamma_{GS}$$

The time derivative of the aircraft's distance from the runway threshold is the aircraft's groundspeed projected into the plane of the localizer. If we assume that the aircraft captures the localizer at the same time as the glide slope, we needn't concern ourselves with the angle between the aircraft's ground path and the localizer. This is a reasonable assumption that makes the equation much simpler. Additionally, since the ground speed and the distance from the localizer are defined in opposite directions, a negative sign results.

$$\dot{h}_d = K_{\dot{h}}\left(h_d - h\right) - V_G \tan \gamma_{GS} \tag{5.54}$$

5.2.3.3 Landing Flare (Region 10)

When the aircraft is within 100 ft above the runway, it begins the landing flare. The landing flare region (region 10) is a region of heightened control sensitivity to match the desired flare profile. The desired profile is a quadratic relationship between height above the runway and desired altitude rate. It was designed to be tangent to a 3° glide slope at 100 ft above the runway and to touch down on the runway at 1 ft/s.

$$\dot{h}_d = 0.0011\left(h - h_{rwy}\right)^2 - 0.22\left(h - h_{rwy}\right) - 1$$

In this equation, height above the runway, $(h\text{-}h_{rwy})$, is in feet and the desired altitude rate, $\dot{h}_d$, is in ft/s. The desired speed is the aircraft's landing speed, V_{LD}. The control law is given by equation (5.32).

5.2.3.4 Landing Ground Run (Region 11)

Once the aircraft touches down, it enters the landing ground run region (region 11). In the landing ground run, the thrust is throttled back to idle, the lift coefficient is set to zero, and the drag coefficient is increased by the spoiler coefficient (to simulate the deployment of the spoiler). There is no feedback control in this region. When the speed is 20 knots below the landing speed, the aircraft is terminated from the simulation.

$$
\begin{aligned}
C_L &= 0 \\
T &= C_{T_{idle}} T_{\max}
\end{aligned}
\tag{5.55}
$$

5.3 Throttling in Regions 1 Through 6

When the thrust controller returns a thrust that differs from the current thrust, we must consider that the thrust difference may not be available in one time step; particularly when the difference is the full range from idle to max thrust, and particularly when the engine is a turbine engine. To account for this, a simple spooling lag has been added to the controller to limit the maximum amount that the thrust can change in a time step.

$$\Delta T_{\max} = \frac{T_{max}}{k_{lag}} \Delta t \tag{5.56}$$

The term k_{lag} is the lag factor. Conceptually, it is the time it takes the engine to spool from zero thrust to maximum thrust. While spooling is not applicable to piston engines, k_{lag} is still used, just at a much smaller value. The current values for the different engines are presented below.

<div align="center">

turbofans: k_{lag} = *20* sec

turboprops: k_{lag} = *5* sec

pistons: k_{lag} = *2* sec

</div>

We have chosen to model engine spooling in the longitudinal control logic rather than in the engine. Certainly, the real turbofan aircraft has spooling in the engine; however, spooling in the engine would introduce a troublesome nonlinearity into the open loop dynamics. Such nonlinearities would undoubtedly expand the control logic and increase the number of gains needed, and they would require extensive engineering effort to develop a sufficient control law. Furthermore, the location of the spooling has no bearing on the perceived motion of the aircraft.

THIS PAGE INTENTIONALLY LEFT BLANK

6. The Selection of Gains

In Section 5, we determined feedback control strategies for each of the regions in the speed-altitude plane. Furthermore, much effort was expended to develop a means to calculate acceptable gains for the different regions. The purpose for these computational methods was two-fold. First, there were many aircraft models to develop. Manually determining gains using root locus or bode techniques would be time consuming and would require a skilled controls engineer. Secondly, it was expected that each aircraft would need to have a schedule of gains to provide sufficient performance throughout the aircraft's flight envelope. Therefore, each aircraft would require gains to be calculated at many different reference conditions.

However, by carefully choosing the reference flight condition, it is possible to choose one set of gains that will work for the aircraft's entire flight envelope. This section documents the decision process that led to the final conclusion that gain scheduling would not be necessary.

6.1   The Aircraft's Flight Envelope

For a given aircraft weight, there are generally two parameters that define the aircraft's flight envelope: altitude and airspeed. The flight envelope, shown in Figure 6.1, illustrates how fast and slow the aircraft can fly and how high the aircraft can fly.
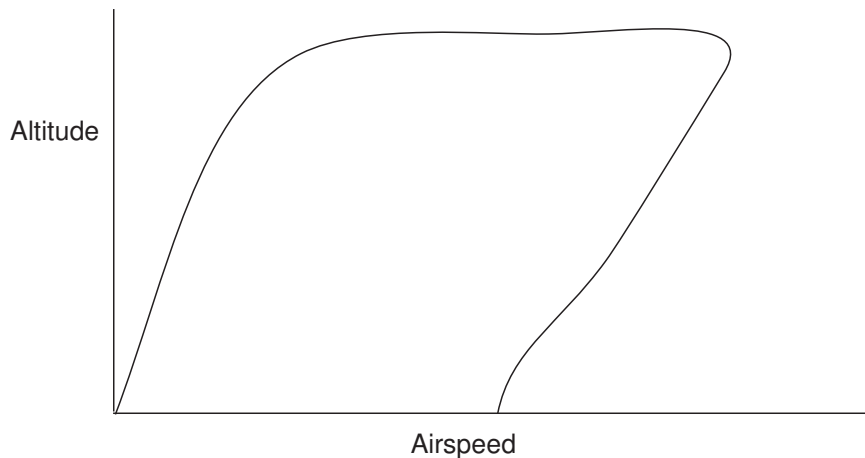
Figure 6.1. An example flight envelope

Of course, as the aircraft's weight changes, so do portions of the flight envelope of the aircraft; therefore, there are three parameters that affect the aircraft's dynamic condition.

In an effort to remove one of these parameters, Section 3 demonstrated that the flight envelope could be represented with true airspeed and lift coefficient rather than true

airspeed, altitude and weight. The phugoid dynamics could be represented exclusively in terms of lift coefficient and true airspeed if a trimmed aircraft is assumed. The only term that varied with weight was the thrust control derivative, which contributes to the forcing function of the system.

Therefore, the flight envelope can be modeled as shown in Figure 6.2. Only reasonable trim conditions are considered. Figure 6.2 shows the high-weight/high-altitude and low-weight/low-altitude stall condition boundaries, which encompass an area labeled as the useable range. This useable range represents all possible trim conditions for the aircraft. Outside of that range, the aircraft either must fly too fast, (i.e. faster than Mach 0.9) or must have air denser than sea level. Note that while the Region 7 controller may use this entire envelope, in the other regions, the envelope is bounded on the left by the max L/D lift coefficient. The interesting observation here is that the useable area is rather small when compared to the total range of viable lift coefficients and true airspeeds. One must ask the question, how much modal property variation can there be within this range?

To answer this question, the aircraft's flight envelope was represented in yet another way. The locus of all possible phugoid poles for the entire flight envelope was plotted on a single graph. The aircraft's speed, altitude, and weight were varied encompassing the entire range of reasonable trim conditions. The results are shown in Figure 6.3. From the locus we can see three extremes. Roughly, the points are:

- $-0.0011 \pm 0.056i$ $\omega_{n_p} = 0.057\,rad/sec$ $\xi_p = 0.19$ High lift coefficient at highest trimmable airspeed

- $-0.0074 \pm 0.042i$ $\omega_{n_p} = 0.043\,rad/sec$ $\xi_p = 0.17$ Low lift coefficient at highest trimmable airspeed

- $-0.0062 \pm 0.099i$ $\omega_{n_p} = 0.099\,rad/sec$ $\xi_p = 0.063$ High lift coefficient at lowest trimmable airspeed.

While there is considerable variation in frequency and damping, it is plain to see that the aircraft needs an increase in damping to have acceptable modal properties.
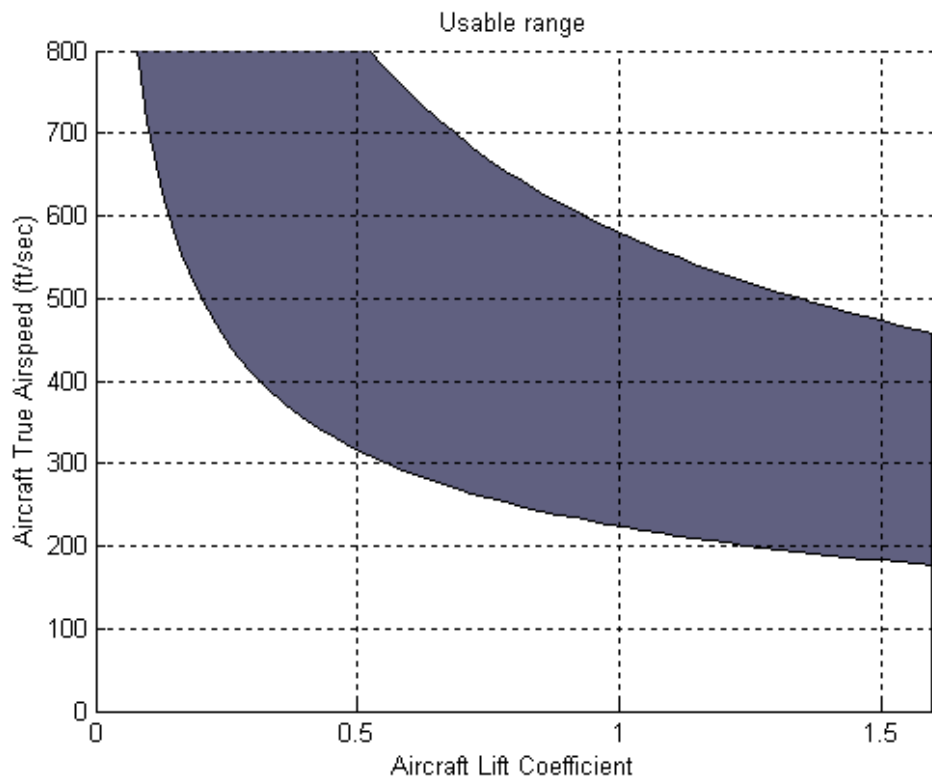
Figure 6.2. The flight envelope for a DC-9 in terms of CL and True Airspeed
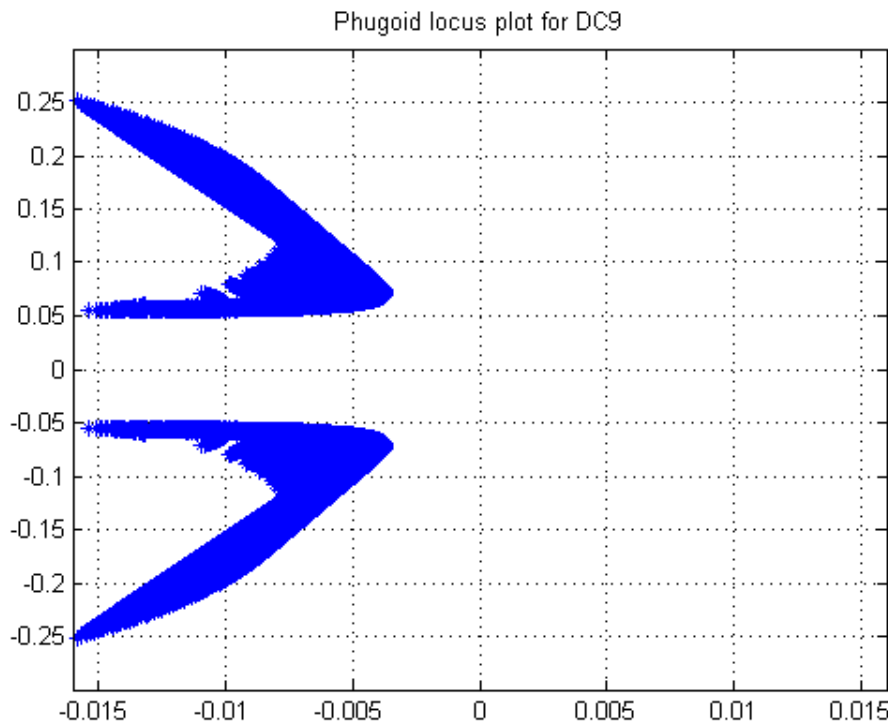
**Figure 6.3.** The locus of Phugoid poles for the entire flight envelope of a DC-9 in the clean configuration

6.2 Determining Acceptable Modal Properties

In previous sections of the document, a considerable effort was made to determine gains that would yield desirable transient responses for the aircraft's phugoid dynamics. Generally, determining what is desirable is easy. Most dynamic systems are considered to be well behaved if they have a damping ratio of 0.7 and a frequency sufficiently high enough to remove transients quickly. A harder question to answer however is what dynamic properties are sufficient. That is to say while it may be obvious what is desirable, it may not at all be obvious how to determine the range of acceptable values. Different types of operations may be more or less sensitive to poor uncontrolled dynamics. This section addresses the question of just how precisely the phugoid dynamics must be held to a specified set of modal properties.

There is no precise answer to this question. However, from observation of the aircraft flying with varied modal properties, one can conclude that a very wide range of properties is acceptable. First, consider the most important state variables in the longitudinal dynamics from the pilot's point of view: speed and altitude. The control system must be able to drive the aircraft to different speeds and altitudes. Consider changes in altitude. The feedback control systems don't use altitude explicitly, but rather feedback its derivative, altitude rate. Because of the integral relationship between the two, altitude tends to be insensitive to small transients in altitude rate. Furthermore, the careful design of the desired output vector minimizes large errors that would produce undesirable transients. In addition, the steady state error between the desired output vector and the actual output vector is of little concern until the desired output reaches the commanded output.. Zero steady state error is important only when the commanded output values have been reached. This is in contrast, of course, to a mission such as precise terrain following where the error in following a time-varying output vector would be critical.

While it is difficult to put a range on acceptable modal properties, we can state some general guidelines that are based purely on observation. These are:

- The damping ratio of the mode is more important than the frequency
- The damping ratio can vary from roughly 0.5 – 1.0 and achieve satisfactory performance
- The frequency can vary from $0.1\,^{rad}\!/_{sec}$ to $1.0\,^{rad}\!/_{sec}$ and still yield acceptable results.

This is a rather large range which suggests that a control system with even meager performance is likely to be acceptable. Most importantly, however, such a wide range suggests that a single set of gains, if chosen carefully, could accommodate the entire flight envelope of the aircraft.

6.3 Choosing a Single Reference Condition for Gain Calculation

To choose a single reference condition that would serve as representative of the whole flight envelope, several conclusions from Section 3 must be revisited. These conclusions are:

- $\zeta_p = \dfrac{1}{\sqrt{2}\left(\frac{L}{D}\right)};$ The damping of the mode is inversely proportional to the L/D ratio

- $\omega_p = \sqrt{\left(\dfrac{2g^2}{V_a^2}\right)};$ The frequency of the phugoid is inversely proportional to the true airspeed.

The lift coefficient that yields the highest L/D ratio, $C_{L_{(L/D)_{max}}}$, has the lowest damping.

This occurs at the bottom of the thrust curve, i.e., at the bucket speed. Any variation in the lift coefficient on either side of the thrust curve will yield a decrease in the L/D ratio and, therefore, an increase in phugoid damping.. Furthermore, the lowest true airspeed will have the highest phugoid frequency. Using this information the following reference condition was chosen.

- Choose the trim condition for the maximum L/D ratio
- Using the lift coefficient for maximum L/D, trim the aircraft with the lowest possible true airspeed. Generally this is done by choosing a low altitude and a low weight.

The rationale for gain selection is as follows:

- Since it is natural for the phugoid damping to increase, select gains at the reference condition that puts the damping near the lower bound of acceptable. As the lift coefficient varies, the damping will increase and fall within the acceptable range.
- Since the phugoid frequency decreases with increasing speed, select gains to put the frequency and the reference condition near the top of the acceptable frequency range. As the velocity increases, the frequency will come down and stay within the acceptable range.

Of course, in practice there is no guarantee that a system augmented with feedback control will maintain any of its open loop tendencies so the rationale as stated is merely a vague guideline. In reality different properties work better, however the stated reference condition did turn out to be a good choice.

6.4 Evaluating System Performance with Scheduled Gains

In practice, the aircraft dynamics did not vary as predicted when feedback control was applied; however, through some experimentation, the following modal properties were found to yield favorable results.

For jet (turbofan) and turboprop aircraft:
- Integrator pole locations: *-0.20, -0.25*
- $\omega_p = 0.25$ rad/sec, $\zeta_p = 0.9$

For piston aircraft:
- Integrator pole locations: *-0.20, -0.25*
- $\omega_p = 0.40$ rad/sec, $\zeta_p = 0.9$

Gains were calculated for the DC-9 aircraft in all control regions. Using these desired modal properties the loci of poles over the entire flight envelope are plotted in Figure 6.4 - Figure 6.7. A key to the figures is presented in Table 6.1. The poles are plotted only for the corners of the flight envelope as defined by the lift coefficient, altitude, and weight.

Table 6.1 Marker key to Figure 6.4 - Figure 6.7

Outer marker - Lift Coefficient		
	box	front-side
	circle	bucket
	diamond	back-side
Middle marker - Altitude		
	box	sea level
	circle	mid-range altitude
	diamond	service ceiling
Inner marker - Weight		
	+	empty weight
	x	mid-range weight
	dot	max take-off weight

Consider altitude-rate-only feedback. The locus of closed loop poles produced for the aircraft is in Figure 6.4. Notice that the lowest phugoid damping occurs on the back-side of the thrust curve, instead of at the bucket speed as predicted earlier. The highest phugoid frequencies occur at sea level, as predicted. One should note the location of the integral poles since they stray into the right-half-plane. This means that our analysis of the linear system is predicting instabilities near stall speed, particularly at low weights and low altitudes. We will have to validate this flight condition by analyzing the transient response of the non-linear system. It is useful to note that we should expect a significant difference between the non-linear system and our linear approximation outside of the

steady, level flight region because we stray more from the reference condition used for the linearization.

Figure 6.5 shows a similar locus for speed-only feedback. The trend is similar to that of Figure 6.4, except that the integral poles do not extend into the right-half-plane. While this region demonstrates greater stability, we should continue with an analysis of the non-linear transient response.

Figure 6.6 is a root locus plot for the steady, level flight region. We note similar trends as in Figure 6.4 and Figure 6.5: the lowest damping occurs on the back-side of the power curve and the highest phugoid frequencies occur at low weight and low altitude. However, inspection of the locus does show that the modal properties for the entire flight envelope do fall within the general guidelines set forth in Section 6.2.
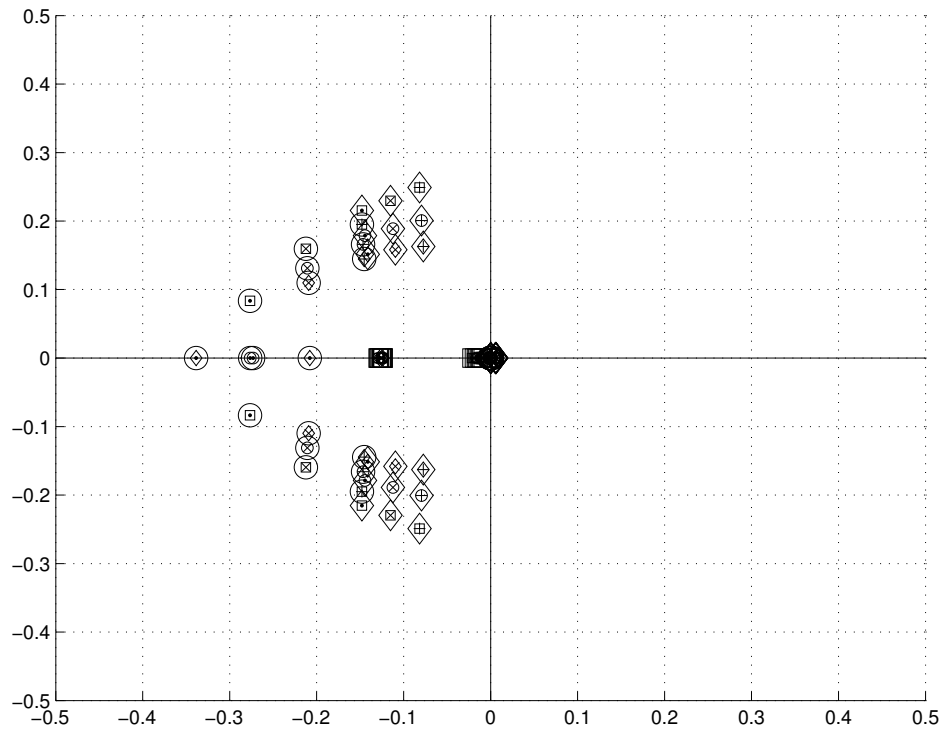
Figure 6.4. The locus of closed loop phugoid poles in for altitude-rate-only feedback for the entire flight envelope of a DC-9 in the clean configuration
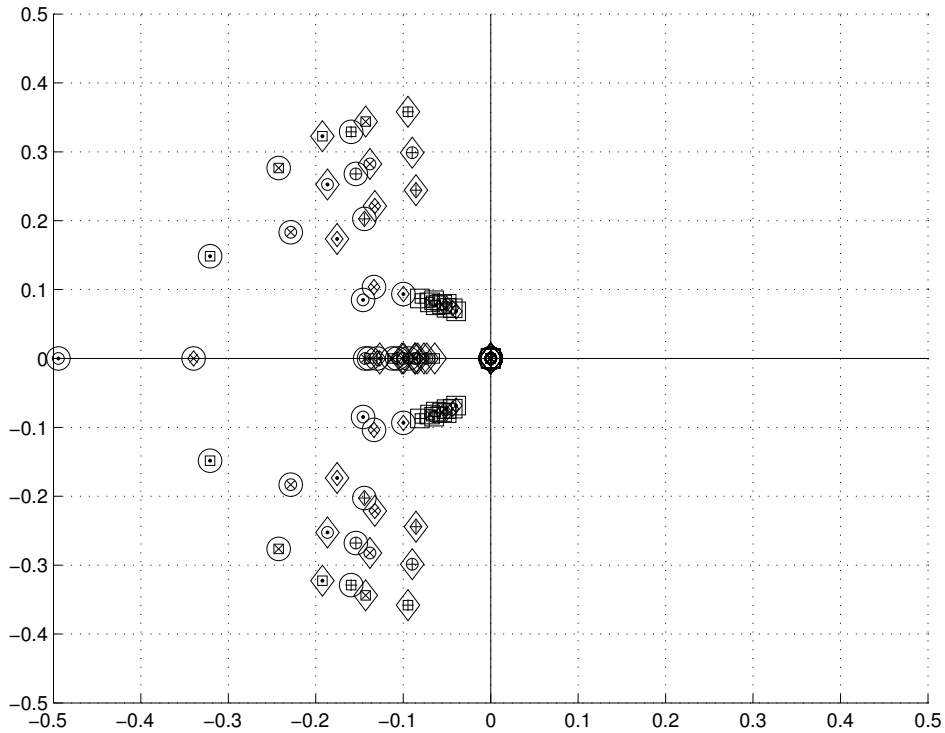
Figure 6.5. The locus of closed loop Phugoid poles for speed-only feedback for the entire flight envelope of a DC-9 in the clean configuration
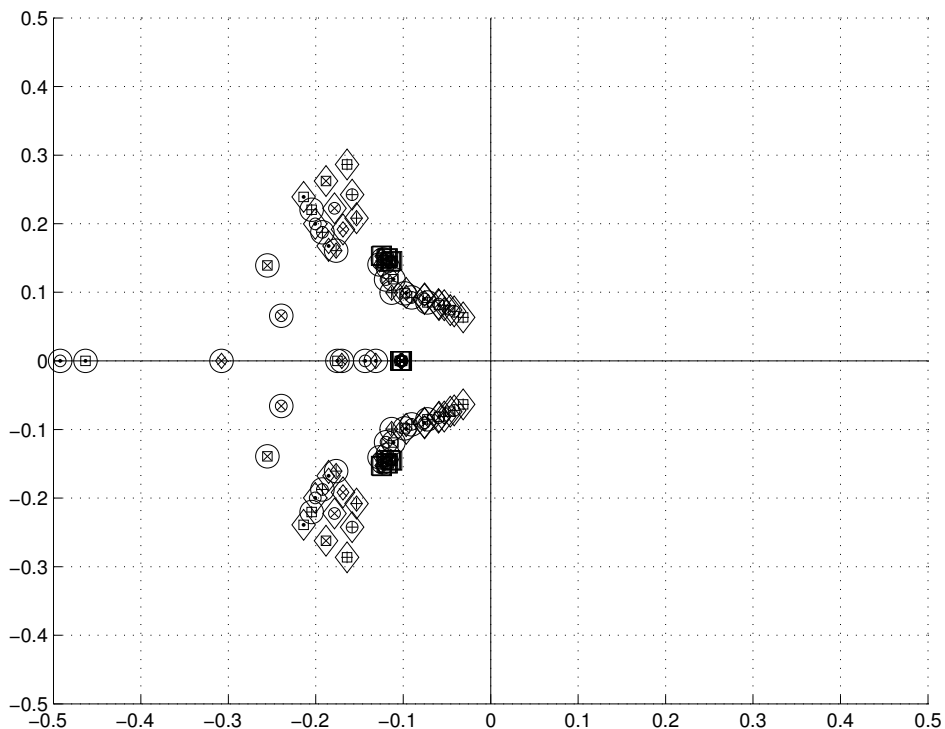
Figure 6.6. The locus of closed loop Phugoid poles in the steady, level flight region for the entire flight envelope of a DC-9 in the clean configuration

Unlike the other Regions, the steady, level flight controller may use the back-side of the thrust curve. There are two PI (proportional/integral) compensators at work and therefore there are two integral poles. In some parts of the envelope the integral poles become complex. This is seen in the locus of points grouped closer to the imaginary axis. (See Figure 6.7 as well). This still is not a concern because the integrator poles remain within the acceptable guidelines for modal property selection.

Finally, high lift devices are considered. If the aircraft can operate with a single set of gains when high lift devices are employed as well as during clean configuration, the number of required gains for the system can be cut by a factor of 5 (avoiding a different set of gains for each flap setting). To explore this possibility, the full flap case of the DC-9 is considered. Figure 6.7 shows the locus of points within the flight envelope under the full flap condition. As can be seen, the majority of flight conditions remain acceptable. However, in some cases, the integral poles become complex and are much slower than the Phugoid poles. This can cause a problem at low speed in that the aircraft may not capture the desired airspeeds as crisply and cleanly as it does at higher speeds.

This condition presents a bit of a dilemma. During most of the simulation development, it was assumed that low speed flight would require additional control laws and gains. Now we can see that one set of gains can fly the aircraft through its entire flight envelope; however, performance could be diminished in the low speed range. Here is a classic trade-off between precision and simplicity.
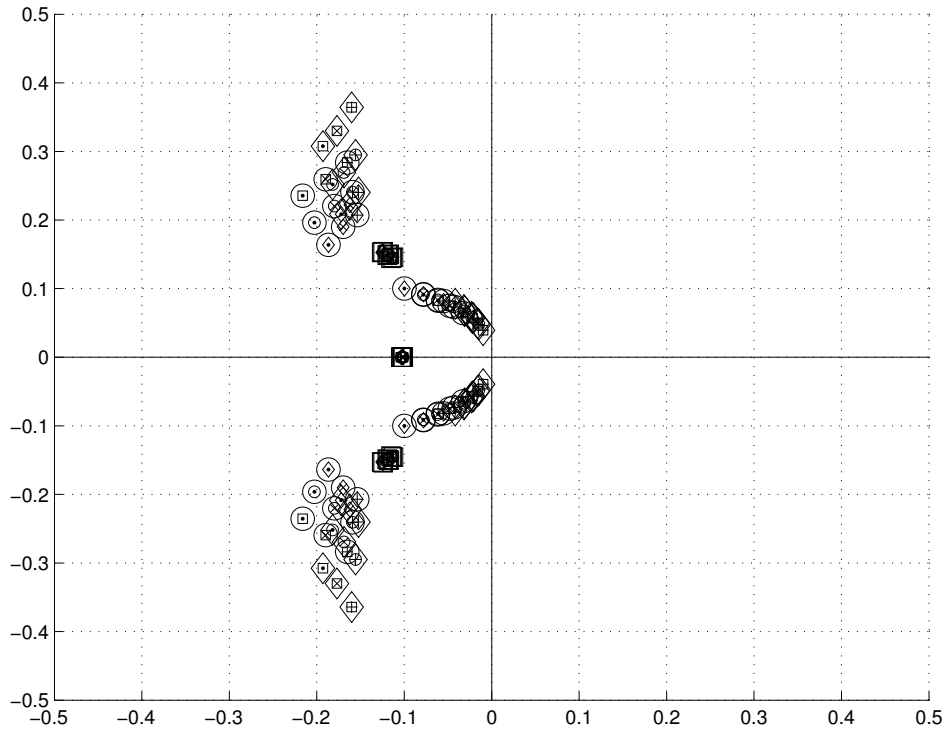
Figure 6.7. The locus of closed loop Phugoid poles in the steady, level flight region for the entire flight envelope of a DC-9 with full flaps deployed

A more sophisticated control law will fly the airplane more precisely; however, it would also require extra code, and more gains. For right now, since performance is still reasonably good in the low speed range, the decision has been made to capitalize on this unexpected result to simplify the control system. However, future requirements for other aircraft types may require a more complex control system to address the needs of low speed flight.

THIS PAGE INTENTIONALLY LEFT BLANK

7. The Lateral Directional Control Laws

The lateral directional control laws are considerably simpler than the control laws required to fly the aircraft longitudinally. The reason for the added simplicity is that one of the governing differential equations, the roll equation, can be modeled with a linear approximation. This approximation is used for two reasons. The first reason is that an accurate model of the full nonlinear roll dynamics is not essential to the modeling of accurate trajectories. The second is that the roll response is so heavily augmented by the pilot or autopilot that the dynamics of turn rate capture is much more dependent on control inputs than the actual roll dynamics.

The decision to approximate the speedy roll mode permits us to ease computational effort by selecting a half-second time step. Such a long time step is not adequate to capture the roll dynamics, though it is more than adequate to capture the slower phugoid dynamics.

Because our roll mode is linear, we can close feedback loops analytically without requiring the same detail that is done with the longitudinal dynamics. The main loop closures for the turning dynamics were already closed analytically in Section 2 and imbedded directly into the open loop dynamics making the desired bank angle, ϕ_{des}, the primary input to the roll equation.

The four topics for discussion are:

1. The bank angle capture algorithm
2. The heading capture algorithm
3. Using the Bank Angle Capture and Heading Capture Algorithms to execute a turn
4. Deciding which way to turn

7.1   The Bank Angle Capture Algorithm

The bank angle capture algorithm is the major kernel of the lateral directional control law. Consider the discretized bank angle system derived in Section 2.14. In general, the lateral state at the *(k+1)*th time step is a function of the lateral state at the *k*th time step and the desired bank angle.

$$\begin{bmatrix} p \\ \phi \end{bmatrix}_{k+1} = \mathbf{A} \begin{bmatrix} p \\ \phi \end{bmatrix}_k + \mathbf{B}\phi_{des}$$

The constant matrices, $\mathbf{A}$ and $\mathbf{B}$, are functions of the modal properties (ζ, ω_n) and the time interval.

Sometimes it is desirable to command a specific turn rate. Since the turn rate equation is very nearly a linear function of the roll angle, we simply choose to adjust our commanded bank angle rather than creating another feedback control loop to drive the system to a commanded turn rate. Calculating the required bank angle is done by rearranging equation (2.67).

$$\phi_d = \sin^{-1}\left(\frac{m\,\dot{\psi}V_aC_{\gamma_a}}{L}\right)$$
(7.57)

7.2   The Heading Capture Algorithm

The heading capture algorithm is designed to capture a specified heading. To capture a given heading, we feed back the desired heading to the bank angle using the control law shown in equation (7.58).

$$\phi_d = k_\psi\left(\psi_d - \psi\right)$$
(7.58)

To predict the effect of this feedback control law, we must first add the heading equation to our state space model. Consider the linearized version of the turn rate equation which finds its way into our state matrix.

$$\frac{d\dot{\psi}}{d\phi} = \frac{d}{d\phi}\left(\frac{LS_\phi}{mV_aC_{\gamma_a}}\right) = \left.\frac{LC_\phi}{mV_aC_{\gamma_a}}\right|_0 \Delta\phi$$
(7.59)

$$\frac{d\dot{\psi}}{dp} = 0$$
(7.60)

If we assign our reference condition for the linearization to be $\phi = 0.0$, then $\Delta\phi = \phi$. Furthermore, if we note that for the bulk of the flight the lift equals the weight and the flight path angle is near zero, we can simplify equation (7.59) to equation (7.61).

$$\frac{d\dot{\psi}}{d\phi} \cong \frac{g}{V_a}\phi$$
(7.61)

Arranging the system of equations in state space we have equation (7.62).

$$
\begin{bmatrix} \dot{p} \\ \dot{\phi} \\ \dot{\psi} \end{bmatrix} = \begin{bmatrix} L_p - L_{\delta_a} k_p & -L_{\delta_a} k_\phi & 0 \\ 1 & 0 & 0 \\ 0 & \dfrac{g}{V_a} & 0 \end{bmatrix} \begin{bmatrix} p \\ \phi \\ \psi \end{bmatrix} + \begin{bmatrix} L_{\delta_a} k_\phi \\ 0 \\ 0 \end{bmatrix} \phi_{des} \tag{7.62}
$$

When we close a proportional loop around the system with k_ψ as our feedback gain, as shown in Figure 7.1, we see that the new closed loop system is equation (7.63). There is an integral relationship between the heading and the roll angle so zero steady state error is achieved without the use of integral control.
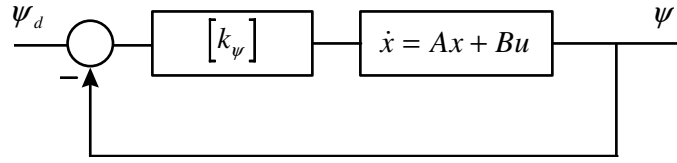
Figure 7.1. Block diagram for heading feedback

$$
\begin{bmatrix} \dot{p} \\ \dot{\phi} \\ \dot{\psi} \end{bmatrix} = \begin{bmatrix} L_p - L_{\delta_a} k_p & -L_{\delta_a} k_\phi & -L_{\delta_a} k_\phi k_\psi \\ 1 & 0 & 0 \\ 0 & \dfrac{g}{V_a} & 0 \end{bmatrix} \begin{bmatrix} p \\ \phi \\ \psi \end{bmatrix} + \begin{bmatrix} L_{\delta_a} k_\phi k_\psi \\ 0 \\ 0 \end{bmatrix} \psi_d \tag{7.63}
$$

Further verifying that integral control is unnecessary, we see that the transfer function that characterizes the relationship between ψ and ψ_d, equation (7.64), has a DC gain of 1.

$$
\frac{\psi}{\psi_d} = \frac{\dfrac{g}{V_a} L_{\delta_a} k_\phi k_\psi}{s^3 - \left(L_p - L_{\delta_a} k_p \right) s^2 + L_{\delta_a} k_\phi s + \dfrac{g}{V_a} L_{\delta_a} k_\phi k_\psi} \tag{7.64}
$$

7.3 Using the Bank Angle Capture and Heading Capture Algorithms to Execute a Turn

When turning, the heading capture algorithm cannot be used for large heading errors. The reason is that the heading capture algorithm will command a bank angle proportional to the heading error. If the heading error is large, the control law will command an unreasonably large bank angle such as 180 degrees. This bank angle would correspond to an inverted aircraft and certainly does not make the aircraft turn any faster. Therefore, the heading capture algorithm is used only when the heading error is less than 15 degrees.

For errors greater than 15 degrees, the bank angle control law is used to command a constant turn rate in the direction of minimizing the heading error. Nominally, a bank angle of 30 degrees is used. Consider the following simulation example. The simulation parameters are as follows:

- $V_a = 300 \, ft/sec$
- $L_p = -0.475$
- $L_{\delta_a} = 0.185$
- $k_p = 2.836$
- $k_\phi = 2.756$

Although the ADM uses $k_\psi = 1$, this simulation uses the following feedback gain, which accounts for variations in airspeed.

$$k_\psi = 0.005 \frac{V_a}{g} \qquad (7.65)$$

We simulate a turn to the right from a heading of 0 degrees to a heading of 100 degrees as shown in the simulation results in Figure 7.2. Initially, the aircraft rolls to the right to achieve a bank angle of 30 degrees. The aircraft holds the bank angle and steadily turns toward a heading of 100 degrees. When the aircraft is within 15 degrees of the desired heading, the heading capture algorithm takes over and drives the remaining heading error to zero.
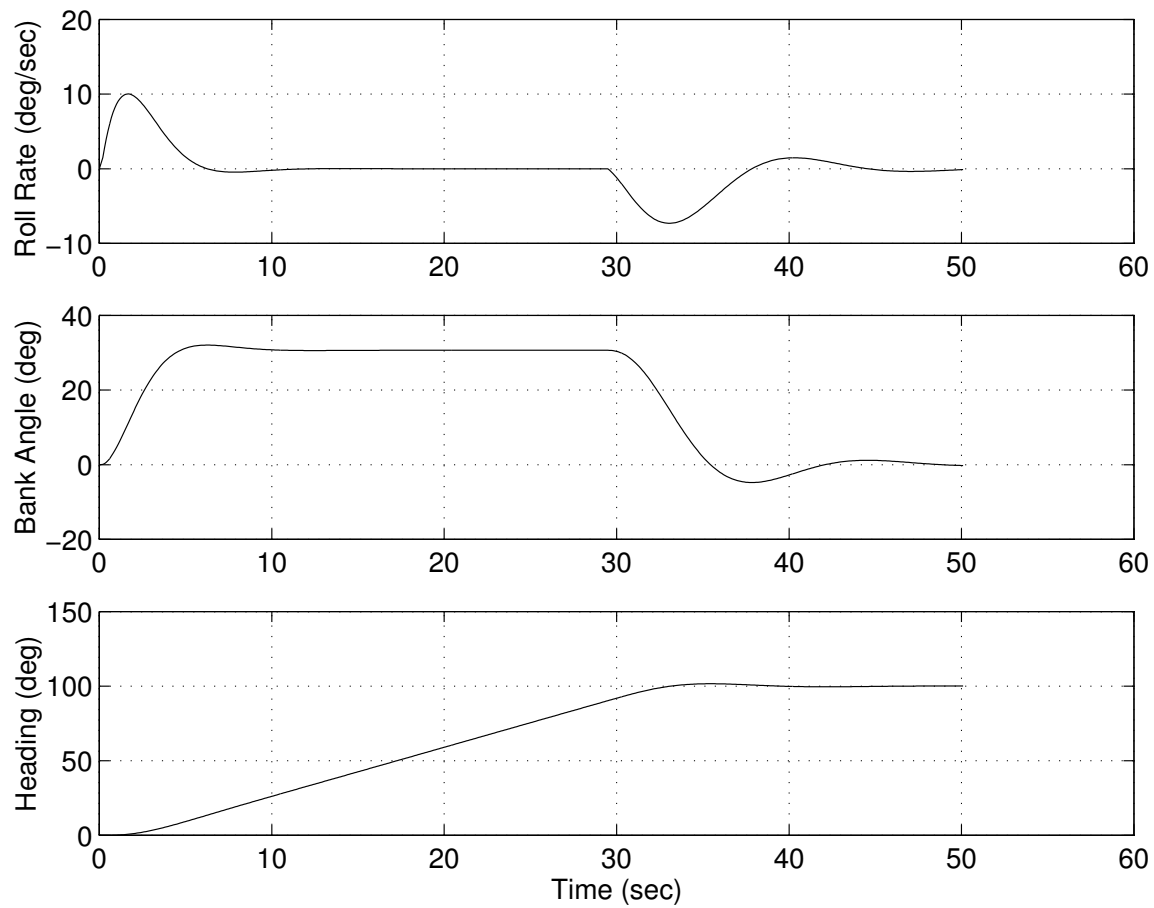
Figure 7.2. Simulation of Aircraft Executing a Turn

THIS PAGE INTENTIONALLY LEFT BLANK

8. Lateral Guidance and Navigation

The TGF Simulator's Lateral Guidance Manager breaks lateral instructions into a sequence of basic lateral maneuvers. These lateral maneuvers are described in this chapter along with descriptions of how they are flown using the lateral control laws already described.

It is the intent of the Lateral Guidance and Navigation System to follow the concepts and terminology of FAA Area Navigation (RNAV) procedures. The source for most of the RNAV concepts and procedures in this section is the web version of the FAA Aeronautical Information Manual (Federal Aviation Administration, 2010).

8.1   Route Legs and Waypoints

Routes are basic lateral paths. For the TGF simulator, routes are defined in accordance with RNAV processes and procedures. These definitions are provided here so that we can define route navigation procedures in the subsequent sections.

8.1.1   Path and Terminator Concept

A leg type describes the desired path preceding a route node. Leg types are identified by a two-letter code that describes the path (e.g., heading, course, track, etc.) and the termination point (route node). The "path and terminator concept" states that every leg of a route has a termination point and a path type into that termination point. Route legs in the TGF simulator are defined in this same way.

There are four leg types: direct-to-fix (DF), track-to-fix (TF), course-to-fix (CF), and radius-to-fix (RF). Only the TF leg type requires a preceding fix to define the path.
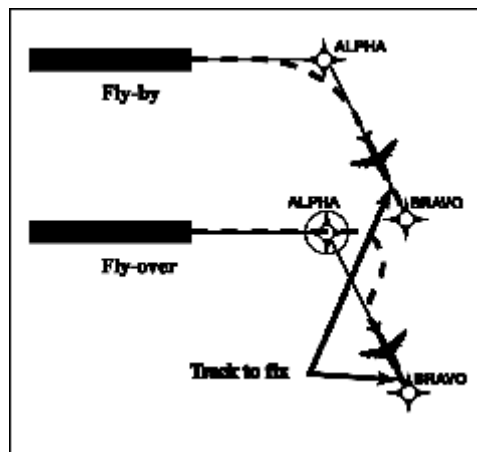
Figure 8.1: Fly-by and fly-over waypoints followed by track-to-fix legs (source: FAA AIM)

8.1.2 Leg Terminators – Geometric Nodes of a Route

Waypoints are geographic points on the surface of the Earth, defined by latitude/longitude coordinates. The TGF Simulator requires geographic representation of the leg termination points (route nodes), so waypoints are commonly used. In keeping with RNAV concepts, waypoints used as route nodes can be defined as "fly-over" or "fly-by." Fly-by waypoints are used when an aircraft should begin a turn to the next course prior to reaching the waypoint separating the two route segments. Fly-over waypoints are used when the aircraft must fly over the point prior to starting a turn. Fly-over and fly-by waypoints are illustrated in Figure 8.1.

8.1.3 Direct-To-Fix Leg

A Direct-to-fix (DF) leg type is the direct path from the aircraft's current position to the leg termination point (route node), regardless of course or track (see Figure 8.2). It is not a straight line or a geographically fixed path, but includes the path of the aircraft's turn towards the fix. The actual path flown will vary with aircraft type and speed. The path is defined by the aircraft's bearing to the termination fix.
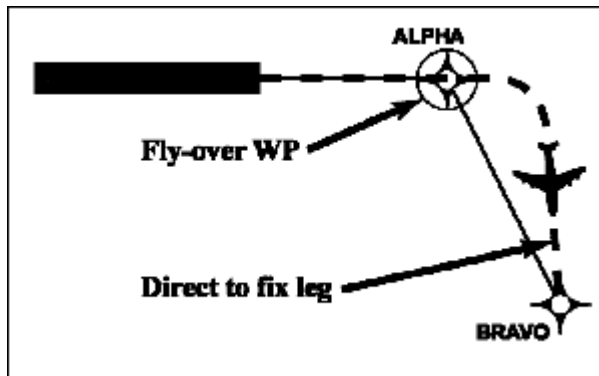
Figure 8.2: Fly-over waypoint followed by direct-to-fix leg (source: FAA AIM)

8.1.4 Track-To-Fix Guidance

A Track-to-fix (TF) leg type is defined as the constant course path (i.e., rhumb line) to the route node from a preceding route node. For this reason, track-to-fix legs are sometimes called point-to-point legs. The preceding route node is typically the termination fix of the previous leg. With the beginning and ending nodes of the track-to-fix leg defined, it is easy to calculate the rhumb line track (see Section 8.5), which is followed using Ground Track Guidance. Figure 8.1 illustrates a track-to-fix leg.

8.1.5 Course-To-Fix Guidance

A Course-to-fix (CF) leg type is defined as the constant course path (i.e., rhumb line) to the route node along the specified course (or heading). A course is assumed to be a magnetic course, unless otherwise specified. Course-to-fix and track-to-fix legs are similar in that they both define rhumb lines. The difference is that in a course-to-fix leg,

the rhumb line is defined by the termination fix (route node) and the specified course, and in a track-to-fix leg, the rhumb line is defined its end points. In both cases, the rhumb line is followed using Ground Track Guidance.
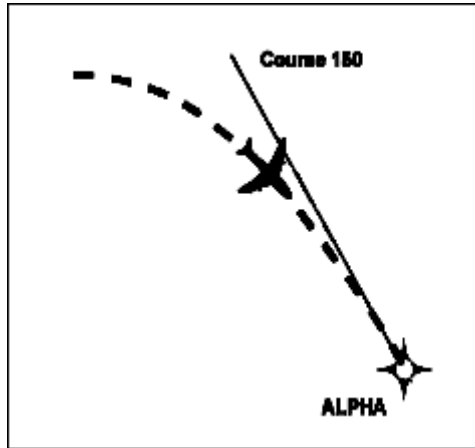
Figure 8.3: Course-to-fix leg showing the rhumb line and the aircraft's navigation to it (source: FAA AIM)

8.1.6 Radius-To-Fix Guidance

A Radius-to-fix (RF) leg is defined as a constant radius circular path around a defined turn center that terminates at a fix. In addition to the termination fix, the RF definition must include the turn center point and the turn direction (i.e., right turn or left turn). In the TGF Simulator, the start point of the RF leg is not defined so that any RF leg defines a complete circle. The aircraft navigates to the circular path and moves in the direction specified. The end condition for the RF leg is defined by the ending azimuth (regardless of tracking error), which is determined from the termination fix and the turn center. The circular path is a geometric path over the earth and is followed using Ground Track Guidance and Bank Angle Capture guidance. A radius-to-fix leg is illustrated in Figure 8.4. The parameters of a radius-to-fix leg are illustrated in Figure 8.9.
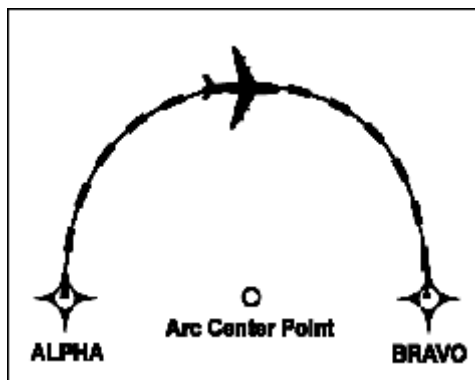
Figure 8.4: Radius-to-fix leg (source: FAA AIM)

8.2   Lateral Guidance

The purpose of the lateral guidance system is to steer the aircraft to follow routes or other lateral paths. There are three basic lateral maneuvers, which are used in combination to achieve lateral guidance. These are:

- Track a Geographic path
- Follow a Course Law
- Transition

Every lateral maneuver in the TGF Simulator is made up of these three basic maneuvers. The intent of this section is to describe these three basic maneuvers in terms of the two basic lateral control laws (heading control and bank angle control) described in Chapter 7. Once this description is completed, we will have a complete mapping of any lateral maneuver to the basic control laws of the simulator.

8.2.1   Tracking a Geographic Path

In this type of maneuver, an aircraft is intending to fly a specific geographic path over the surface of the earth. Currently, the TGF simulator is capable of navigating two types of geographic paths: circular arcs, and rhumb lines. The simulator must compare the aircraft's position on the surface of the earth to the desired geographic path and apply lateral control inputs to correct any lateral errors. This is accomplished using ground track guidance. The end condition of a Track Geographic Path maneuver is triggered by a distance from (or, capture halo around) the path's termination fix. For fly-by waypoints, this distance is adjusted to allow for the transition (described below).

The ground track guidance algorithm is the basic guidance algorithm used for navigating geographic paths (routes and fixes). These paths are translated into a ground track azimuth as a function of some independent variable and then tracked.

The ground track azimuth is the angle between the aircraft's ground track and true North. Under a zero wind condition, the ground track azimuth is the same as the aircraft's heading. In the presence of wind, the ground track azimuth will differ from the aircraft heading as illustrated in Figure 8.5. To navigate a geographic path, the aircraft must follow a given ground track azimuth rather than a specific heading; yet the lateral control system is designed only to turn to a desired heading. The lateral guidance must bias its heading commands to the lateral control system with a correction factor that accounts for winds. To accommodate this requirement, the lateral guidance measures the difference between the heading and the ground track azimuth, which we denote as $\Delta\psi$. Our tracking algorithm makes uses the following nomenclature:

- ψ: The aircraft's heading, in degrees.[2]
- ψ_{GT}: The aircraft's ground track azimuth, in degrees.
- $\delta\psi_w$: The wind bias.
- ψ_d: The desired heading.
- ψ_{GT_d}: The desired ground track azimuth.
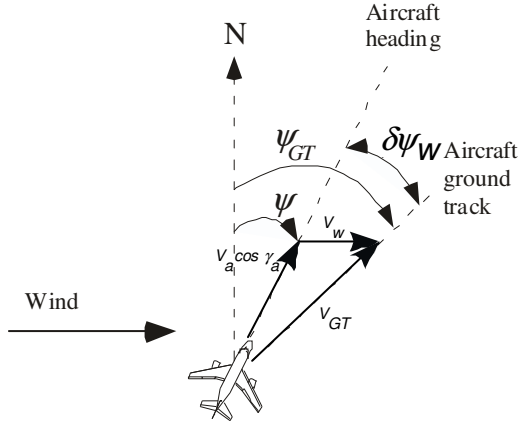
Figure 8.5. Illustration of the difference between ground track and heading

We define the wind bias as the difference between the aircraft's ground track azimuth and its heading.

$$\delta\psi_w \equiv \psi_{GT} - \psi \qquad (12.1)$$

The aircraft's ground track azimuth and heading are available from the aircraft dynamics. The wind bias, $\delta\psi_w$, is then used to adjust the desired ground track so that the aircraft will track properly. The result is the desired heading.

$$\psi_d = \psi_{GT_d} - \delta\psi_w \qquad (12.2)$$

Equation (3.212) is not intended as an accurate representation of the vector algebra graphically depicted in Figure 8.5; it merely shows the use of the wind bias as a correction factor. Its simplicity does not compromise its intent, which is to capture the desired ground track azimuth.

---

[2] Analysis of the wind bias requires a comparison of the azimuth of the aircraft's velocity vector, ψ_a, with the ground track azimuth, ψ_{GT}; but in Chapter 2, we stated the assumption that the aircraft is always trimmed for coordinated flight; i.e., the sideslip is always zero. This means that the azimuth of the aircraft's velocity vector, ψ_a, is coincident with the aircraft's heading, ψ. Therefore, for our purposes, the analysis is equally accurate in comparing ψ and ψ_{GT}.

8.2.1.1 Tracking a Rhumb Line

Track-to-fix and course-to-fix legs are composed of rhumb lines. When tracking a rhumb line, the tracking algorithm commands the ground track of the aircraft based on:

- the aircraft's lateral distance from the rhumb line,
- the rhumb line's bearing, and
- the aircraft's radius of turn.

This is illustrated in Figure 8.6. The intercept angle for the given segment is a function of how far the aircraft is laterally from the segment.
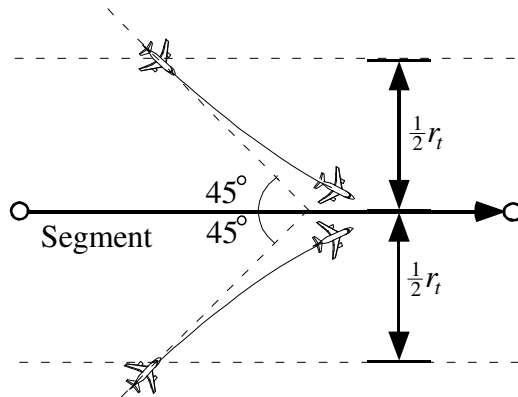
Figure 8.6. Illustration of the aircraft in route following mode

The intercept reaches a maximum of 45 degrees when the aircraft is one-half a turn radius away from the segment. The intercept angle is bounded at 45 degrees. Equations (12.3) and (12.4) are used to determine the aircraft's desired ground track. First, $\Delta\psi$ is calculated using Equation (12.3). If the result has a magnitude greater than 45 degrees, the answer is bounded at 45 degrees using Equation (12.4). The ratio $\delta/|\delta|$ is used to preserve the sign of the original value. Note that the lateral distance term, δ, maintains a sign convention of positive values on the right side of a segment and a negative value on the left side of the segment. This solution is adapted from the original System Segment Specification (Federal Aviation Administration, 1993).

$$\Delta\psi = 90\frac{\delta}{r_t} + \delta\psi_{FTE}, \quad |\Delta\psi| < 45^o \qquad (12.3)$$

$$\Delta\psi = 45\frac{\delta}{|\delta|}, \qquad |\Delta\psi| \geq 45^o \qquad (12.4)$$

$$\psi_{GT_d} = \psi_r - \Delta\psi \tag{12.5}$$

The terms are defined as follows:

- δ :   The aircraft's lateral distance from the capture segment (nm)
- ψ_r :   The capture segment's bearing. (degrees)
- r_t :   The aircraft's turn radius. (nm)
- ψ_{GT_d} : The aircraft's desired ground track (degrees)
- $\delta\psi_{FTE}$: The heading bias from flight technical error (degrees)

As with all other heading commands, the term ψ_{GT_d} needs to be adjusted to keep values within the 0 - 360 degree range. The logic for this operation is shown in Figure 8.7.

The flight technical error (Chapter 11) is sent to the heading-based course guidance in the form of a lateral offset, denoted as δr_{FTE}. The lateral error offset is then related to a heading bias using Equation (12.6).

$$\delta\psi_{FTE} = \frac{90}{r_t}\delta r_{FTE} \tag{12.6}$$
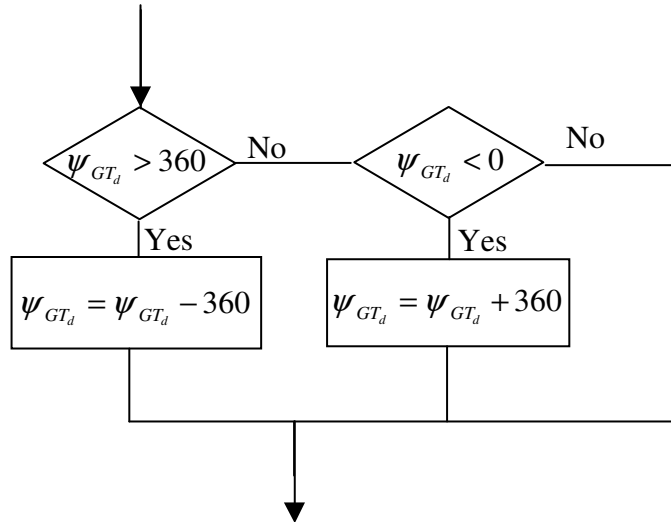
Figure 8.7. Logic for insuring desired ground track is within proper boundaries

The terms in the equation are defined as follows:

- $\delta\psi_{FTE}$: The heading bias created from flight technical error (degrees).
- r_t :   The turn radius for the aircraft at the current speed (nm).

- δr_{FTE} : The lateral offset from flight technical error (nm).

The flight technical error conversion from lateral distance to a heading bias mimics Equation (12.3) in form and causes the course guidance algorithm to produce the lateral offset error of δr_{FTE} in the flight path.
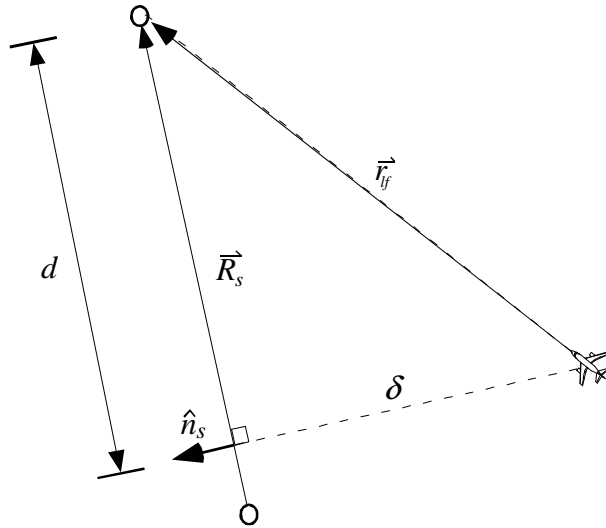
Figure 8.8. Illustration of distance calculation geometry

8.2.1.1.1   Determining Lateral Distance from a Rhumb Line

The aircraft's lateral distance from a rhumb line is calculated using vector operations. The dot product is taken of the position vector from the aircraft's location to the leading fix of the segment and a unit vector normal to the vector describing the segment itself. The expression is best represented mathematically in Equation (12.7) and Figure 8.8. To insure that the desired ground track for segment capture is correct, it is necessary for δ to be negative when on the left side of the segment and positive on the right side of the segment.

$$\delta = \mathbf{r}_{lf} \cdot \hat{n}_s \tag{12.7}$$

The unit normal is represented in Equation (12.8).

$$\hat{n}_s = \frac{R_{s_y}}{\|\mathbf{R}_s\|} \hat{x}_s - \frac{R_{s_x}}{\|\mathbf{R}_s\|} \hat{y}_s \tag{12.8}$$

The terms in the equations are defined as follows:
- δ: The lateral distance from the segment
- $\mathbf{r}_{lf}$: A vector from the aircraft's position to the leading fix

- $\hat{n}_s$: A unit vector normal to the segment
- $\mathbf{R}_s$: A vector representing the segment

8.2.1.2 Tracking a Circular Arc

When flying a radius-to-fix leg, an aircraft is tracking a circular arc path on the surface of the Earth. Tracking to this circular arc is performed similarly to the rhumb line tracking and the same approach is used here. Figure 8.6 applies equally to this discussion.

Because the aircraft is following a constant radius turn, it is assumed to be in a constant bank angle turn. While this assumption is a gross representation of the turn, the lateral correction term will handle any discrepancies.

The constant bank turn is followed using the Bank Angle Capture algorithm described earlier. The nominal bank angle for the turn, ϕ_t, is given by the parameters of the radius-to-fix leg. The heading adjustment, $\Delta\psi$, is calculated as with rhumb line tracking, using equations (12.3) and (12.4). The heading adjustment is then converted to a bank angle adjustment, using a heading gain, k_ψ, similar to that defined in equation (7.8). The nominal value for the heading gain is $k_\psi = 1$.

$$\Delta\phi = k_\psi \Delta\psi \qquad (12.9)$$

Then, similar to equation (12.5), the desired bank angle is given by…

$$\phi_d = \phi_t - \Delta\phi \qquad (12.10)$$

8.2.1.2.1 Determining Lateral Distance from a Circular Arc Route Leg

For the purposes of correcting the cross-track error when tracking a geographic circular path (i.e., a radius-to-fix leg), an aircraft's lateral distance, δ, from a circular arc is here defined as the difference between the arc's radius and the aircraft's distance from the turn center, as illustrated in Figure 8.9. To maintain the sign convention that lateral distance is positive when to the right of the path, a step function is defined here that is based on the turn direction specified in the RF definition.

$$f_{TD} = \begin{cases} +1, \ right\ turns \\ -1, \ left\ turns \end{cases} \qquad (12.11)$$

The lateral distance is then,

$$\delta = f_{TD}\left(r_t - d\right) \tag{12.12}$$

where r_t and d are defined as always positive. As stated earlier, circular paths are tracked using the Bank Angle Capture algorithm, which requires a desired bank angle. Using equation (12.12), the heading correction, $\Delta\psi$, is calculated using equations (12.3) and (12.4). The bank angle correction is calculated using equation (12.9), and the desired bank angle is calculated using equation (12.10).
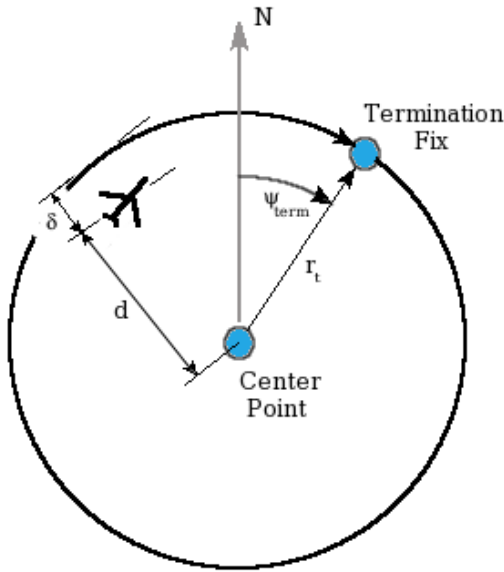
Figure 8.9: Parameters of a Right Turn Radius-To-Fix Leg

8.2.2 Following a Course Law

In this type of maneuver, an aircraft is intending to fly a specific compass course (heading) law. The course law may be constant (e.g., the aircraft is trying to maintain a magnetic heading of 190°) or a function of some independent variable, like position (e.g., a direct-to-fix leg is a course law that matches the aircraft's bearing to the fix, which is a function of the aircraft's position). The end condition of a course law may be time-based or position-based. A course law maneuver makes use of the Heading or Bank Angle control laws.

As described in Chapter 7, the lateral guidance manager must decide which direction to turn and whether or not bank angle control is needed to bring the heading error into a region in which linear heading capture can be used.

The strategy for deciding whether to use bank angle capture in the heading guidance is worth repeating. The heading capture algorithm is used only when the heading error is less than 15 degrees. For errors greater than 15 degrees, the bank angle control law is used to command a banked turn in the direction of minimizing the heading error.

8.2.2.1 Deciding Which Way to Turn

The TGF simulator's user interface allows for commanded left and right turns. Often, however the aircraft is left to make that decision itself. This may be the case for constant heading instructions and for direct-to-fix instructions. In this case, the aircraft must choose which direction of turn is the shortest. Either a left turn or a right turn will work, but one turn is shorter. The dilemma is illustrated in Figure 8.10. To the human, it is obvious that a right turn is appropriate for the situation; however, the logic required to make the autopilot come to the same conclusion is not trivial. The following logic determines the magnitude and the sign of the heading error, referred to as e_5 in the simulation code. The first task is to determine the magnitude of the heading errors to the left and right, symbolically represented as e_{left_turn} and e_{right_turn}.
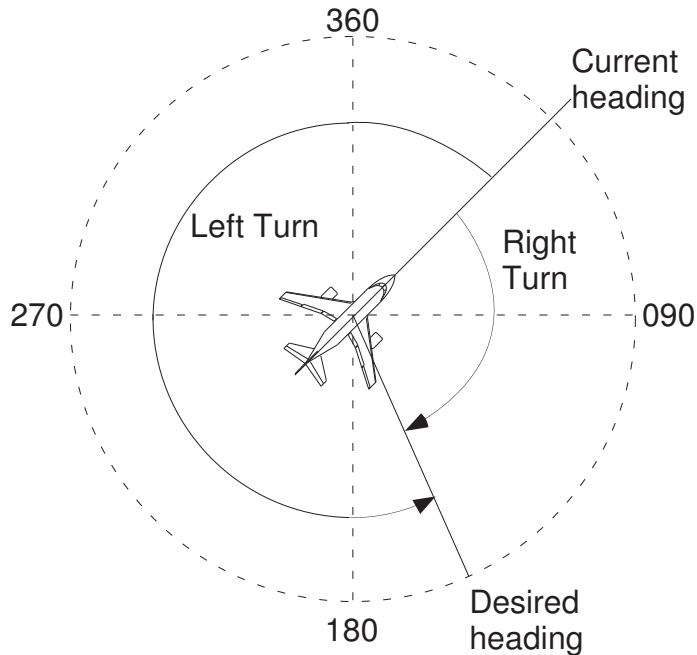
Figure 8.10. An illustration of the dilemma of whether to make a right of left turn to a heading

if $\psi_d > \psi$

$$e_{right\_turn} = (\psi_d - \psi)$$
$$e_{left\_turn} = (\psi_d - \psi) - 360$$

if $\psi_d < \psi$

-171-

$$e_{right\_turn} = (\psi_d - \psi) + 360$$
$$e_{left\_turn} = (\psi_d - \psi)$$

Next, the absolute value of e_{left_turn} and e_{right_turn} are compared to determine which is smaller. The actual heading error, e_5, is set equal to the smaller of these two errors. It is convenient to use the convention that turning errors to the left are always negative and turning errors to the right are always positive. This corresponds nicely to the bank angle convention where banks to the right are considered positive and banks to the left are negative. Therefore, there is no need to adjust the previously developed control laws to make sure that the aircraft turns in the desired direction when commanded.

8.2.2.2 Capturing a Heading when the Direction of Turn is Specified

The introduction of the left or right turn variability adds complexity to the system. When the aircraft is constrained to turn in only one direction, it will likely overshoot slightly and instead of turning back to the heading, it will continue turning in the specified direction for another 360 degrees. There needs to be a distinction made for the initial capture of the heading. Figure 8.10 shows the algorithm for determining whether or not a heading has been captured. Essentially, the aircraft turns in the specified direction until the heading error is within 5°, at which point the simulator uses the logic of the previous section to determine the turn direction on its own. The term e_5 is the error in heading.
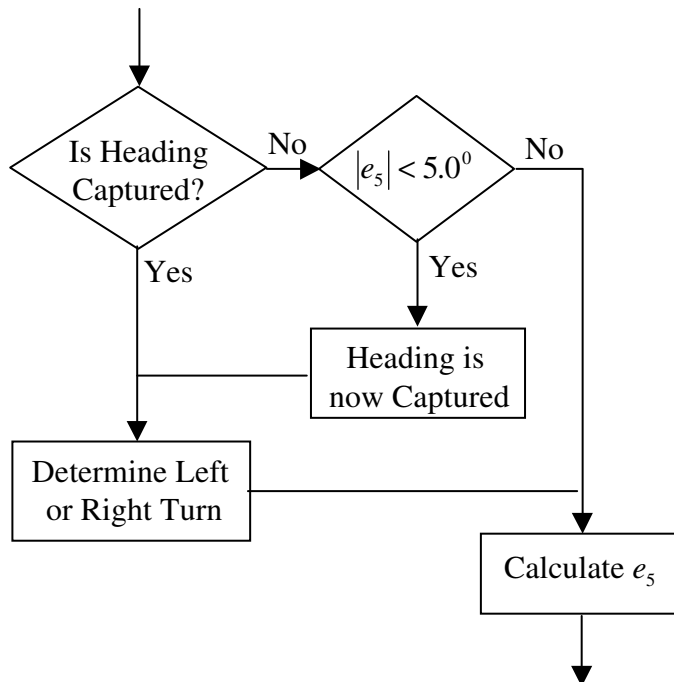
Figure 8.11. Algorithm for capturing a heading

8.2.2.3 Direct-To-Fix Guidance

Direct-to-fix guidance is used in several different super-maneuvers, including Fix Capture, Route Following, and Hold Maneuvers. To fly a direct-to-fix leg, it is necessary to know the aircraft's range and bearing to the fix. (Algorithms for calculating range and bearing to a fix are discussed later.) Once the bearing to the fix is known, the Course Law logic is used to turn the aircraft to that bearing. This control strategy is effective as long as the aircraft is sufficiently far away from the fix. This geometry is illustrated in Figure 8.12.
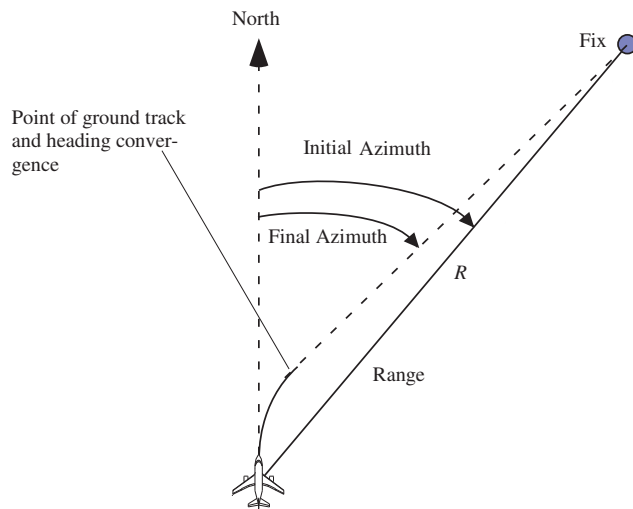
Figure 8.12. An aircraft turning to a fix
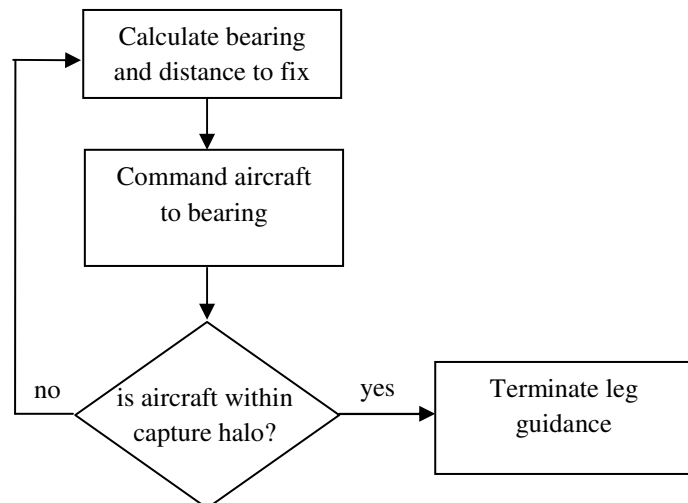
Figure 8.13. Guidance algorithm for Direct-to-fix leg with a fly-over termination point

The bearing to a fix changes constantly as the aircraft moves, except when it is flying directly at the fix. By using the aircraft's bearing to the fix as its desired heading, the aircraft is guaranteed to be flying to that fix. When the aircraft is a within a preset capture limit distance (nominally, 0.1 nm) of the fix, the fix is considered captured. Figure 8.13 illustrates the direct-to-fix algorithm.

When the capture "halo" around the fix is entirely within the turning circle of the aircraft, as illustrated in Figure 8.14, the aircraft cannot capture the fix. The simulation should perform a check to see if the capture halo is within the turning circle of the aircraft and, if so, to consider the fix captured.
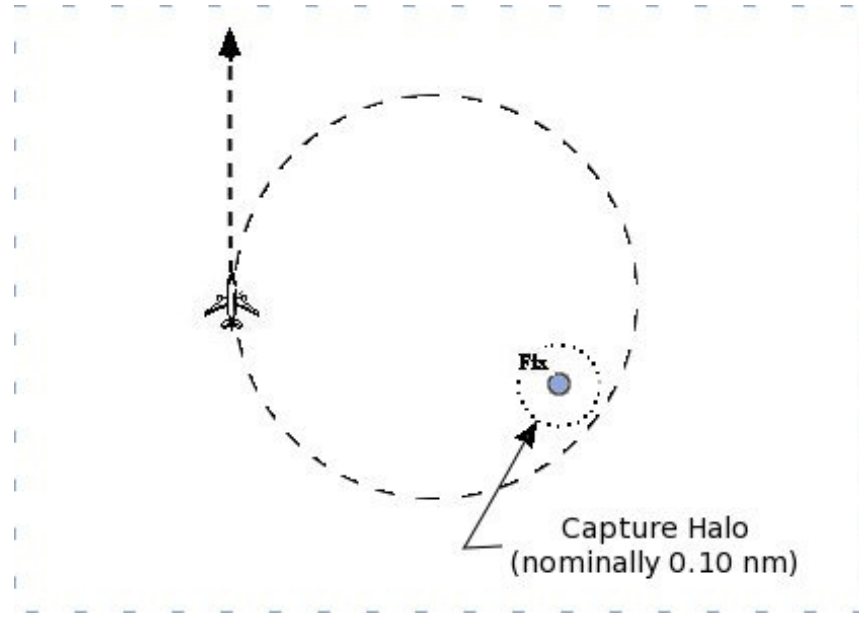
Figure 8.14 Aircraft Cannot Enter the Capture Halo

8.2.3 Transition

A transition maneuver is used to blend lateral maneuvers. The intent of the transition is to blend a lateral maneuver onto a subsequent geographic path. But the indicator used by the TGF Simulator for determining the need for a blended transition is the fly-by waypoint, not the subsequent path; and there is no requirement that the maneuver succeeding a fly-by waypoint is a geographic path. Nor is there a requirement that the fly-by waypoint lie on the geographic path defined in the succeeding maneuver. For this reason, the transition following a maneuver with a fly-by waypoint is defined by that same maneuver, and not by the subsequent geographic path that is to be blended. The unfortunate consequence of this approach is that it is possible to define transitions that do not actually blend the subsequent maneuver; however, this will not create lateral guidance anomalies, as the

lateral guidance system will simply correct to the current path, regardless of the size of the path error. Therefore, it is left to the route designer to ensure lateral path continuity.

There is one exception in which a transition is not indicated by a fly-by waypoint, and that is the constant course merge to route maneuver. This is a constant course law with an end condition defined by proximity to a route. In this case, the transition is <u>defined</u> by a subsequent geographic path. The Route Segment Selection algorithm is used to determine the route segment to be intercepted. As the aircraft approaches the route, the selected segment may change, so the selection algorithm repeats throughout the maneuver.
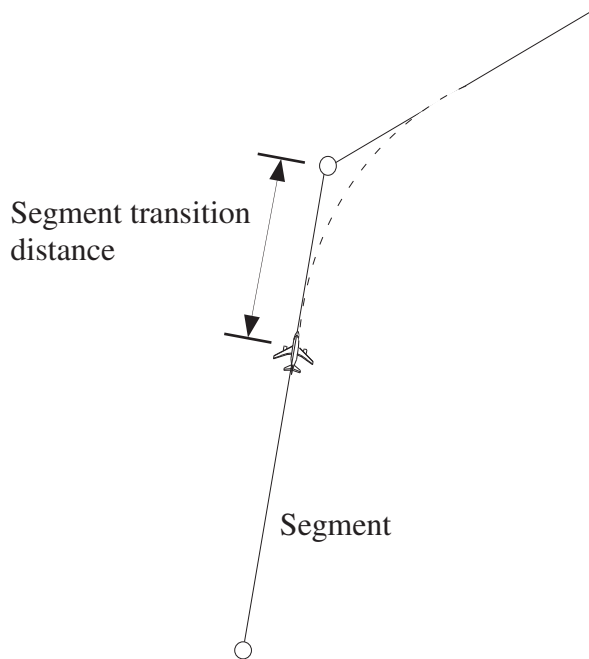
Figure 8.15. Illustration of segment transition distance

8.2.3.1 Fly-By Waypoint Transitions

A fly-by waypoint (as illustrated in Figure 8.1) indicates that the aircraft is to blend its path into a subsequent lateral maneuver. To accomplish this, the TGF guidance manager creates a "transition" phase during which the aircraft uses the bank angle capture algorithm to fly a constant bank angle (nominally 30°) until the aircraft is within an acceptable heading error (nominally, 5°) of the initial heading of the subsequent lateral maneuver.[3] This establishes the end condition of the transition phase. To accomplish this transition, the guidance manager needs to determine the point along the current segment at which the transition should begin. This point is defined by the distance from the

---

[3] If the initial heading of the subsequent maneuver is not defined, it is taken as the rhumb line bearing between the consecutive termination fixes. If a radius-to-fix leg is involved in the transition (preceding or trailing), the course vector at the beginning and terminating fixes should be used in determining the course difference, a.

termination fix. This distance is termed the segment transition distance and is illustrated by Figure 8.15. The magnitude of this distance is affected by the turning radius of the aircraft and hence the speed of the aircraft.

The transition is typically a constant bank angle law and its end condition is typically heading-based (e.g., a 30° bank until attaining the initial heading of the subsequent geographic path). A transition maneuver makes use of the Bank Angle control law.

We encounter a dilemma in choosing a bank angle for transition maneuvers. Standard procedures (Federal Aviation Administration, 2010) call for a 3 degrees/second turn, but experience and track data show that such turns are much sharper than is common. Turning with a 30 degree bank angle is not unrealistic but such turns are sharper than most turns seen in radar track data. The TGF has seen better correlation with track data when using 17 degree turns. Perhaps the choice of bank angle is better correlated to aircraft type or altitude of the turn. Currently, the TGF uses a constant default desired bank angle (nominally, 30°), but research may be necessary to determine a more suitable law.
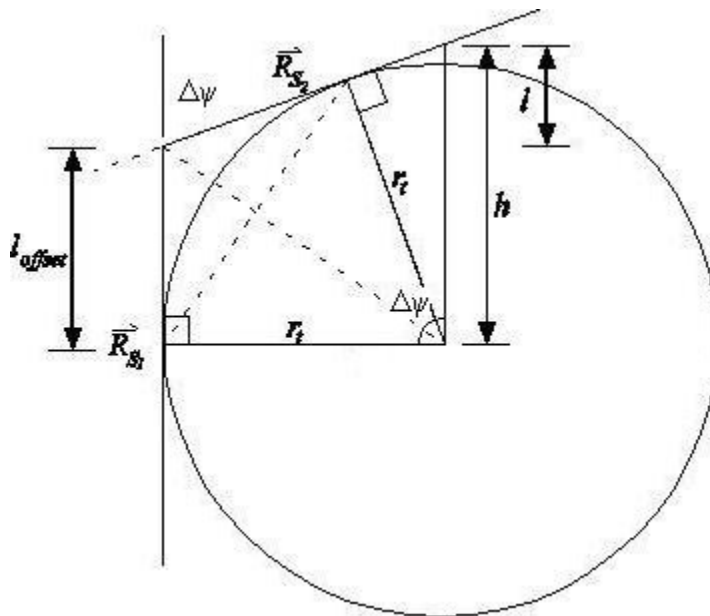
Figure 8.16. The geometry of segments that intersect at an obtuse angle

-176-
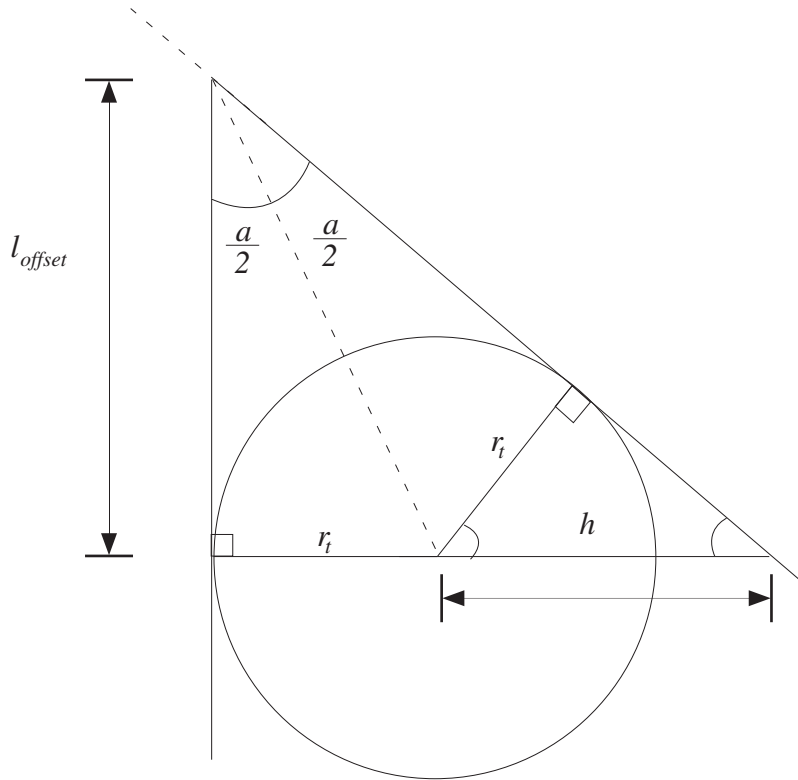
Figure 8.17. Geometric representation of segments adjoined at an acute angle

To determine the segment transition distance, two different drawings of the scenario are presented in Figure 8.16 and Figure 8.17. Figure 8.16 shows the more common case where segments intersect at obtuse angles. Figure 8.17 shows the less common case where segments intersect at acute angles. It will be shown that the equation for the segment transition distance is the same in both cases. The course (or heading) difference between the segments, $\Delta\psi$, can be calculated using the definition of the dot product of the course vectors and the angle, a (shown in Figure 8.17 but omitted from Figure 8.16), between them. The angles a and $\Delta\psi$ are supplementary angles (ie, they sum to 180°)

The segment transition distance, l_{offset}, is calculated by observing in Figure 8.16 that two isosceles triangles are formed creating a 'kite' like pattern. We can then bisect the angle and form two right triangles. Trigonometry can then be used to calculate the segment transition distance based on the difference of the headings of the two segments and the turn radius, r_t, of the aircraft. A lag factor, k, (suggested value, 1.3) is added to allow for a margin of error since turn dynamics are not instantaneous. The equation is valid for the acute angle case of Figure 8.17 as well.

$$l_{offset} = kr_t \, tan\left(\frac{\Delta\psi}{2}\right)$$ (12.13)

8.2.3.2 Merge to Route Transitions

When an aircraft is following a constant course law to intercept a route, it must gauge when it should start to turn to merge cleanly onto the route. Generally, the distance that is required is a function of the aircraft's speed and the intercept angle that the aircraft has with the segment. It is a very similar calculation to that used for fly-by waypoint transitions. Figure 8.18 illustrates the geometry of an aircraft merging onto a segment

The algorithm requires the aircraft's true airspeed and heading and a vector describing the segment.

- V_G: Aircraft's ground speed
- ψ: Aircraft's heading over the ground
- $\mathbf{R}_s$: A vector describing a segment.

First, a vector, $\mathbf{V}$, representing the aircraft's velocity is created from the aircraft's speed and heading. We can see from the geometry in Figure 8.18, that the problem is similar to the fly-by waypoint transition problem. We can also see that the distance at which the aircraft should turn, l_{turn}, is the projection of l_{offset} onto a line normal to the segment. Modifying equation (3.214), we get…

$$l_{turn} = kr_t \tan\left(\frac{\Delta\psi}{2}\right) sin(\Delta\psi) \tag{12.14}$$

Using trigonometric identities, equation (12.14) can be simplified to equation (12.15).
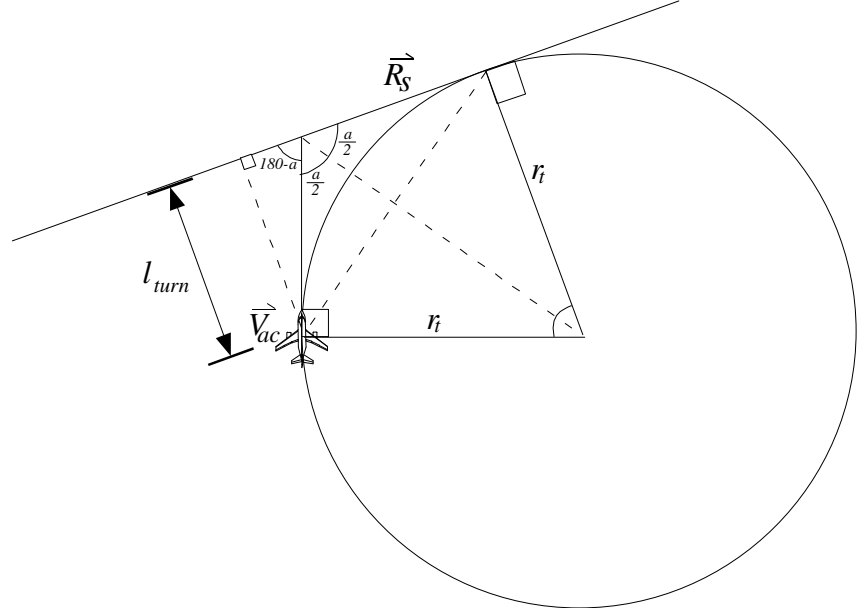
Figure 8.18. Illustration of geometry associated with an aircraft merging onto a segment when aircraft is heading in the direction of the segment
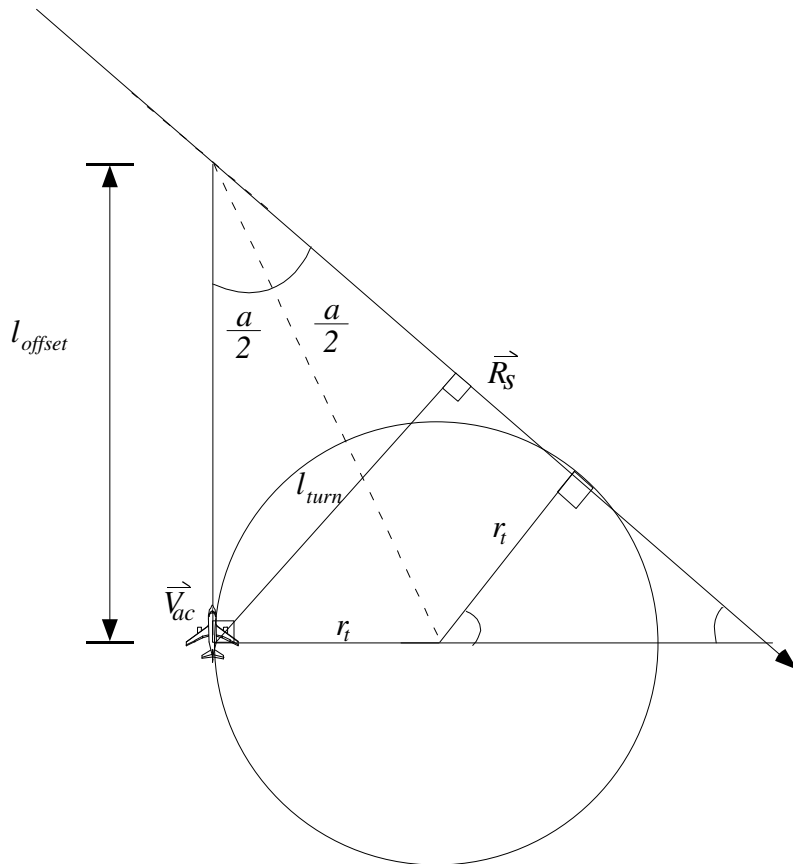
Figure 8.19. An aircraft merging onto a segment which is pointed in a direction opposite of the aircraft's current velocity

$$l_{turn} = kr_t\left(1 - cos\,\Delta\psi\right) \qquad (12.15)$$

When the aircraft is tending to head in the direction opposite the direction of the segment, more distance is needed to turn because the aircraft must completely change the direction of flight to fly along the segment. This case is illustrated in Figure 8.19. However, Equation (3.215) is still valid as can be verified from inspection of the geometry in Figure 8.19.

8.3 Lateral Guidance Manager

The Lateral Guidance Manager creates a sequence of the basic lateral maneuvers detailed above based on what are best described as "super-maneuvers." The Lateral Guidance Manager accepts the following super-maneuvers.

- Route Following
- Route Capture
- Heading Capture
- Hold
- Aircraft Following

- Aircraft Grouping

The Aircraft Following and Aircraft Grouping super-maneuvers are application-specific maneuvers and are not covered in this document.
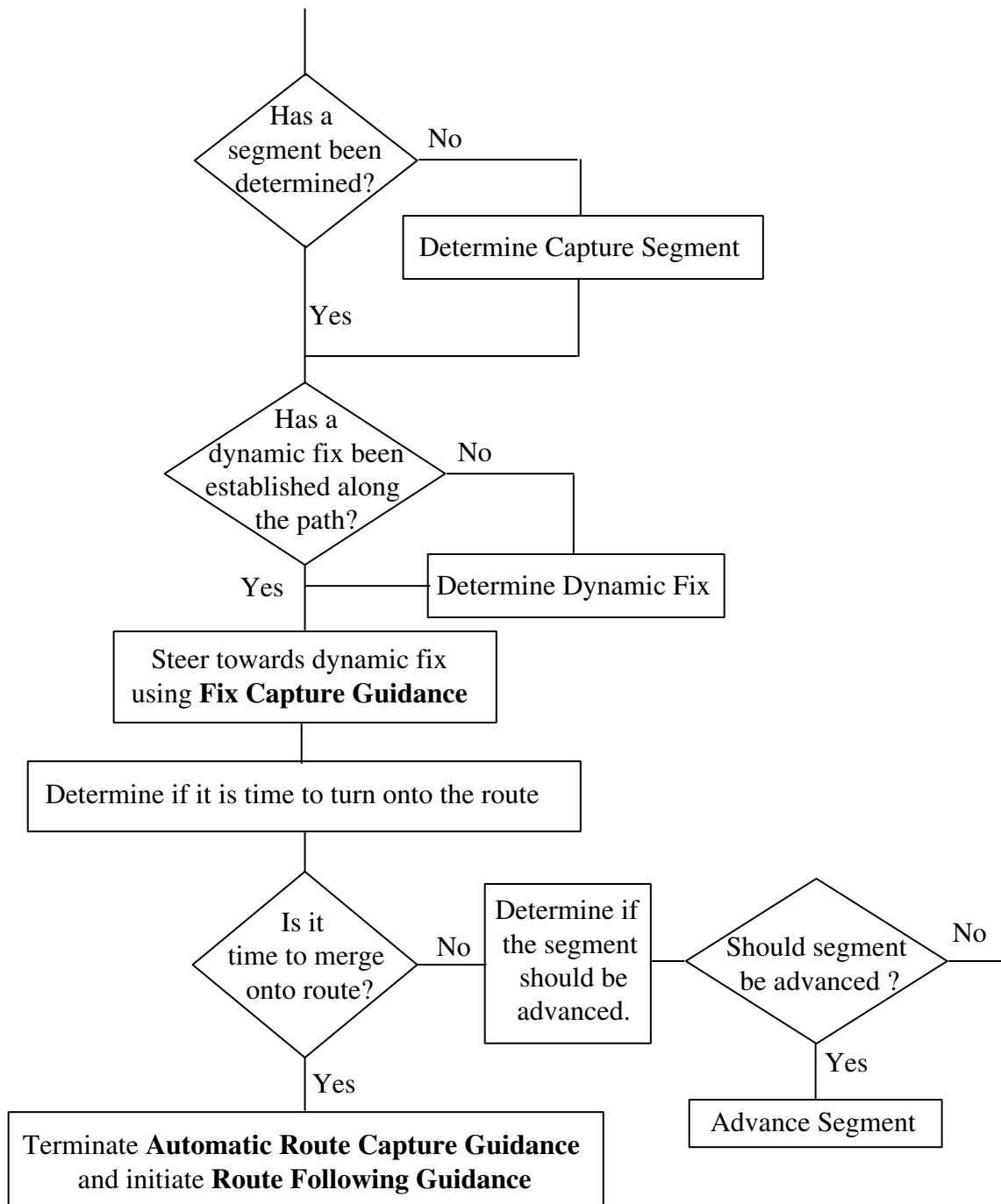
Figure 8.20. Logic for Automatic Route Capture Guidance

8.3.1 Route Following

Based on the aircraft's specified route, the Lateral Guidance Manager creates a sequence of maneuvers to guide the aircraft along that route. The most common route is a sequence of track-to-fix legs with fly-by waypoints. In accordance with the procedures of the preceding sections of this chapter, the Lateral Guidance Manager will create the rhumb lines defined by the legs and the transition maneuvers between them as well as the end conditions for each maneuver.

8.3.2 Route Capture

The Lateral Guidance Manager will define a path to the aircraft's specified route based on one of three capture types: Automatic, Direct, or Heading Intercept. It will also create the transition to the route, if necessary, and the maneuvers of the route itself.

8.3.2.1 Automatic Route Capture

For automatic route capture, the Lateral Guidance Manager must select a capture segment from the aircraft's route, then create a point on that segment to target for the capture. The route capture then becomes identical to a Direct Route Capture. The algorithm is described in the flow diagram illustrated in Figure 8.20. The procedure used in automatic route capture guidance involves determining a capture segment, determining a dynamic fix, and leg transition.

8.3.2.1.1   Selecting a Capture Segment

There are three criteria that are used to determine the appropriate segment to capture. These criteria use three parameters:

1. The Dot Products of the aircraft's location relative to the leading and trailing fixes and the segment's vector $\mathbf{R}_s$.
2. The lateral distance from the segment.
3. The closest trailing fix.

Criterion #1 is summarized as:

> If a segment's position vector, when dotted with a position vector from the aircraft's location to the leading fix, yields a positive value and if a segment's position vector, when dotted with a position vector from the aircraft's location to the trailing fix of the same segment, yields a negative value, then the aircraft should capture the segment.

$$\mathbf{r}_1 \cdot \mathbf{R}_{s1} < 0 \quad \mathbf{r}_2 \cdot \mathbf{R}_{s2} < 0 \quad \mathbf{r}_3 \cdot \mathbf{R}_{s3} > 0$$
$$\mathbf{r}_2 \cdot \mathbf{R}_{s1} < 0 \quad \mathbf{r}_3 \cdot \mathbf{R}_{s2} > 0 \quad \mathbf{r}_4 \cdot \mathbf{R}_{s3} > 0$$
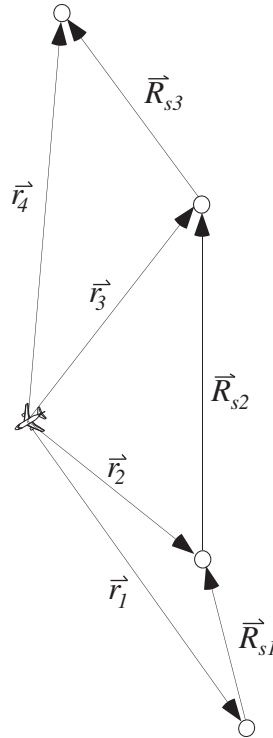
Figure 8.21. Scenario of an aircraft determining which segment to capture

Consider the following scenario shown in Figure 8.21. There are three segments in the route and the aircraft must determine which segment to capture. To do this the position vectors r_1 through r_4 are determined. These vectors are then dotted with the position vectors of each segment. If the dot product between a position vector from the aircraft location to the leading fix of a segment and the segment position vector is positive, then the aircraft tends to be behind the leading fix of a segment. Likewise, if the dot product is negative, the aircraft will be ahead of the fix. For a segment to be a good choice for capture, the aircraft should be behind the leading fix and in front of the trailing fix. In the scenario in Figure 8.21, we see that the dot products for the first segment are both negative. Therefore the aircraft is in front of the first segment. For the second segment, the dot product to the trailing fix is negative while the dot product to the leading fix is positive. The second segment would therefore be an acceptable choice for capture.

Looking at the third segment, both dot products are positive so the segment is in front of the aircraft. Initially, this test alone was thought to be sufficient to determine which segment should be captured; however, it is not.

Consider the next case shown in Figure 8.22. When the required dot products are calculated, it is shown that both segments meet the requirements for capture. Therefore criterion #2 calculates the lateral distance from every segment deemed acceptable by

criterion #1. The closest segment is captured. In Figure 8.22, the first segment is chosen because it is the closest to the aircraft.
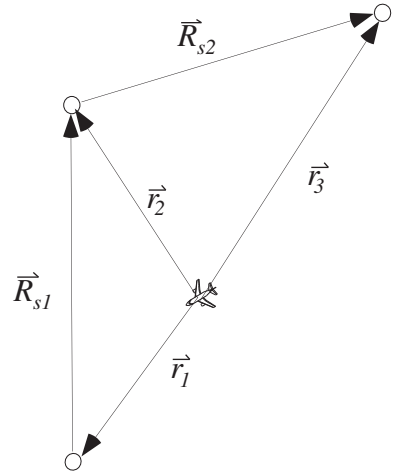
Figure 8.22. A scenario demonstrating the failure of criterion #1
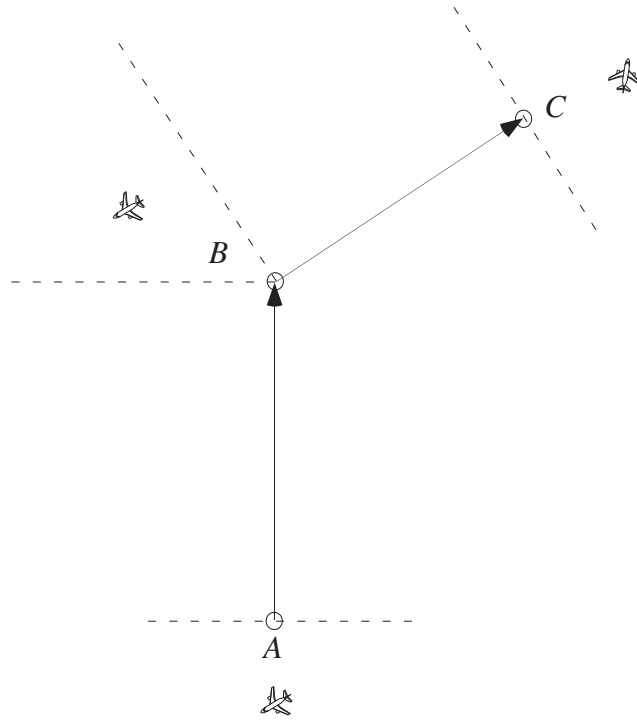
Figure 8.23. Regions where both criterion #1 and criterion #2 fail

These two criteria are not sufficient to handle all cases. Consider the cases where no segment is acceptable as defined by criterion #1. These cases are illustrated in Figure 8.23. Criterion #1 will fail to yield any segment for capture if its dot product

requirements are not met. This often occurs when the aircraft is sufficiently behind or in front of the route as shown in regions A and C of Figure 8.23. There is also another "dead" region where two segments meet as shown in region B. If an aircraft is in this region, criterion #1 will not find a segment. In this case, criterion #3 is used. Criterion #3 checks the aircraft's distance from every segment's trailing fix. It then chooses to capture the segment that is associated with the closest trailing fix. Figure 8.24 illustrates the segment determination logic.
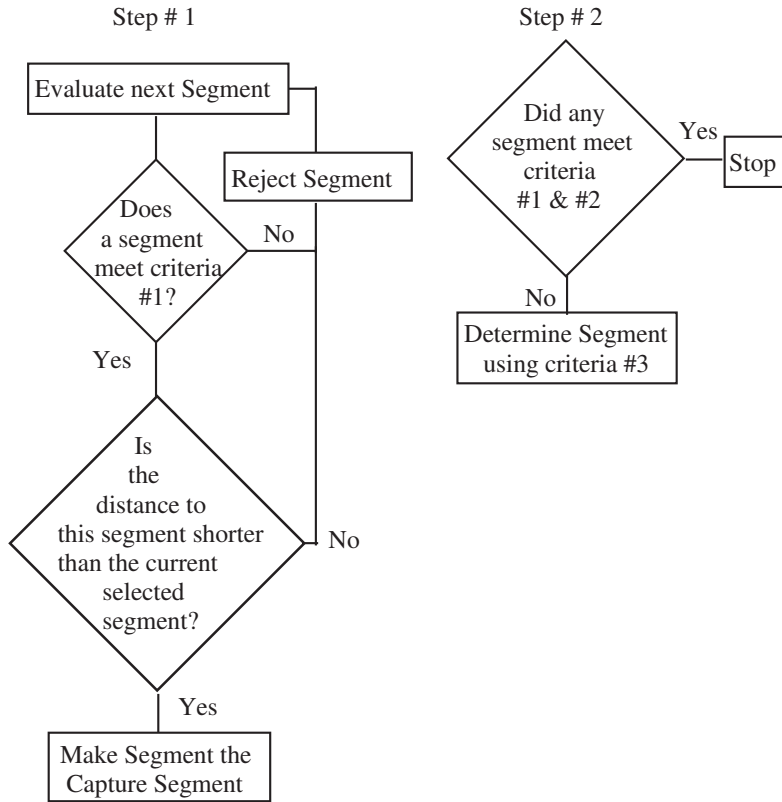
Figure 8.24. Flow chart detailing segment determination logic

8.3.2.1.2   The Dynamic Fix

The dynamic fix is an arbitrary fix that is created by the system at a convenient location along the selected capture segment to be used in a direct-to-fix maneuver. This is a more robust algorithm than an arbitrary intercept approach. For instance, once the capture segment is determined, the aircraft could be given an intercept heading of 45 degrees and intercept the segment. However, this method has some inherent limitations. First, the aircraft would always intercept using 45 degrees regardless of how far the aircraft was away from the segment. An aircraft far away from the capture segment might pass the segment before ever capturing it. This situation is illustrated in Figure 8.25.
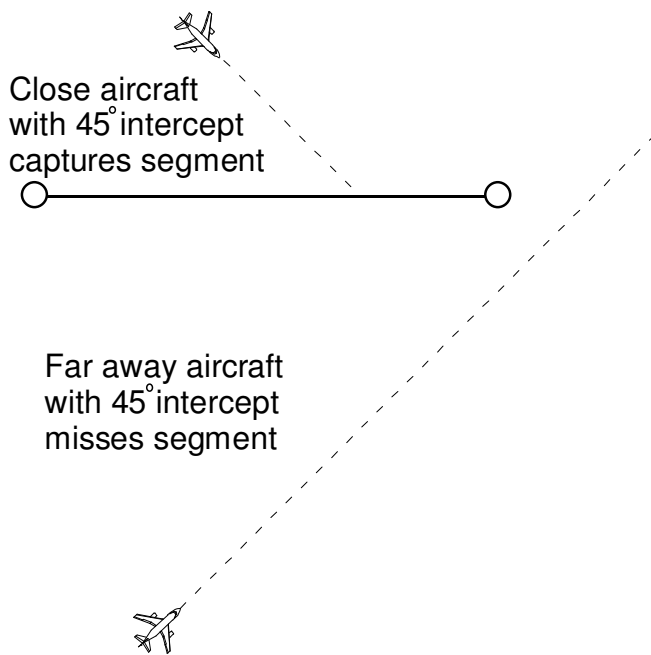
Figure 8.25. Illustration of aircraft using a 45 degree intercept

To avoid the problem of aircraft overshooting capture segments, a dynamic fix is placed on the segment to be captured, and the aircraft is commanded to fly toward the dynamic fix using direct-to-fix guidance. This situation is illustrated in Figure 8.26. In this case the further aircraft naturally uses a larger intercept angle. This system insures that the proper segment is captured and also provides some apparent variety in intercept angles so that all aircraft do not appear to behave the same. To calculate a dynamic fix, first consider the drawing in Figure 8.27.
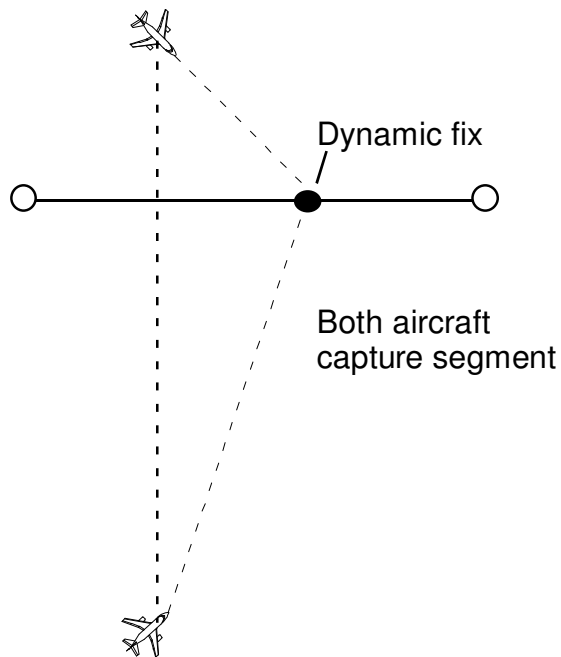
Figure 8.26. Illustration of two aircraft capturing a segment using a dynamic fix
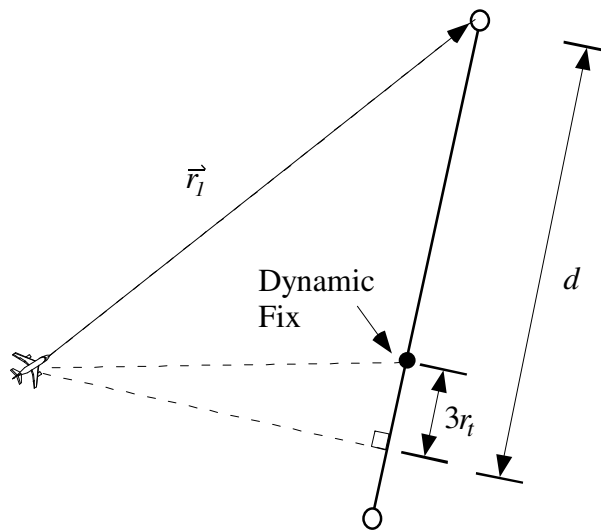
Figure 8.27. Determining an offset fix (dynamic fix) location

The distance, d, left to travel on a given segment is determined by dotting $\mathbf{r}_1$, the position vector from the aircraft to the leading fix, with a unit vector in the direction of the segment, $\hat{r}_s$. The dynamic fix distance from the leading fix, d_{offset}, is somewhat arbitrarily chosen to be three turn radii less than the distance d. The turn radius of the aircraft is notated, r_t.

The three-turn-radius distance was chosen to insure that the aircraft, regardless of its initial orientation or position, can capture the dynamic fix while still maintaining the proper general direction along the route. Generally, two turn radii would be sufficient, providing the aircraft does not speed up during the maneuver. However, three turn radii are used as a factor of safety just in case the aircraft increases its speed and hence its turn radius during the maneuver.

$$d = \mathbf{r}_1 \cdot \hat{r}_s \tag{12.16}$$

$$d_{offset} = d - 3r_t \tag{12.17}$$

We can create a vector, $\mathbf{R}_{offset}$, describing the location of the dynamic fix where $\hat{x}_s$ is a unit vector pointing true North and $\hat{y}_s$ is a unit vector pointing true East.

$$\mathbf{R}_{offset} = -d_{offset} \, cos\,\psi_r \hat{x}_s - d_{offset} \, sin\,\psi_r \hat{y}_s \tag{12.18}$$

However, to use the direct-to-fix guidance, the fix must be represented in terms of a latitude and a longitude. We can approximate the latitude of the fix by converting the $\hat{x}_s$ component of the $\mathbf{R}_{offset}$ vector to a degree value as done in Equation (12.19). Similarly, the longitude can be calculated in Equation (12.20).

$$\mu_{dyn} = \mu_{leading} - d_{offset} \, cos\,\psi_r \frac{360^o}{2\pi r_e} \tag{12.19}$$

$$l_{dyn} = l_{leading} - d_{offset} \, sin\,\psi_r \frac{360^o}{2\pi r_e \, cos\,\mu_{dyn}} \tag{12.20}$$

8.3.2.2 Direct Route Capture
In a Direct Route Capture, the capture point is known. The Lateral Guidance Manager builds a direct-to-fix maneuver to the capture point, a transition to the route, and the maneuvers of the route itself.

8.3.2.3 Heading intercept Route Capture
For a Heading Intercept Route Capture, the Lateral Guidance Manager builds a heading maneuver with a position-based end condition. This maneuver must constantly monitor the aircraft's position relative to the route and evaluate the selection of capture segment and the coincident transition maneuver. The Manager attaches the transition maneuver and the maneuvers of the route itself. It should be noted that the algorithm has no control over the initial heading, and so there is no guarantee that the course will intercept the

route. The Manager will, however, provide a warning if the aircraft is unlikely to intercept the route. Figure 8.28 shows the basic algorithm for the guidance law. It should be noted that even though the aircraft is being vectored, it is necessary to determine the capture segment so that the aircraft knows when to merge onto the route.
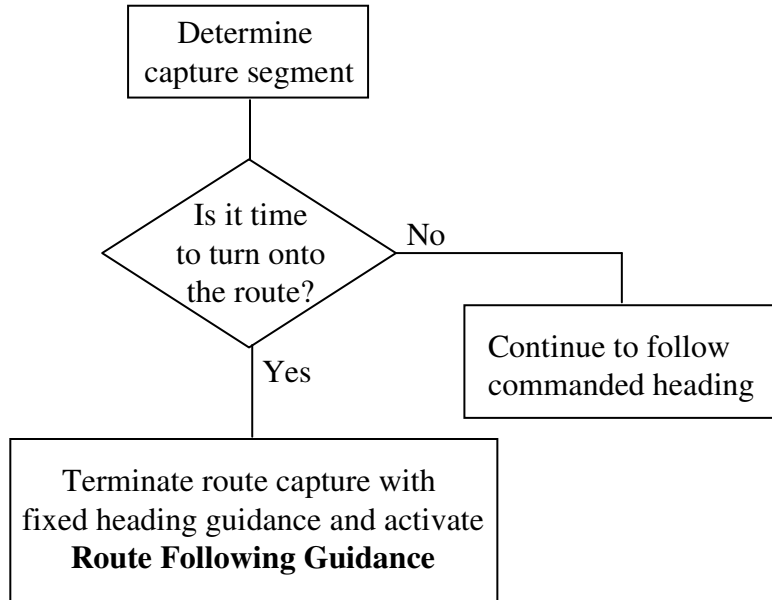
Figure 8.28. Route capture with fixed heading guidance

8.3.2.3.1   Determining Whether the Heading will Intercept a Route

While the algorithm has no control of the aircraft's initial heading, the algorithm will provide a warning if the heading chosen by the user is unlikely to intercept the given route. Basically, the algorithm measures whether or not the intercept angle crosses a segment and is related to the route following algorithm. The intercept angle ψ_t is calculated using Equation (3.216).

$$\psi_t = \psi_r - \psi_d \tag{12.21}$$

The terms are as follows:

- ψ_t: The intercept angle that the aircraft heading makes with the segment
- ψ_r: The bearing of the segment
- ψ_d: The desired heading

The resulting number is used in the logic presented in Figure 8.29

8.3.3   Hold

The Hold super-maneuver is used by the Lateral Guidance Manager when a hold is commanded or when the fix of a direct-to-fix command is not part of the aircraft's specified route. Holds in the TGF simulator are constructed in accordance with holding procedures in the AIM. The Lateral Guidance Manager builds a direct-to-fix maneuver followed by a hold entry (direct entry, parallel entry, or teardrop entry) and then a sequence of course-to-fix and radial legs. The reader is referred to the AIM for further information
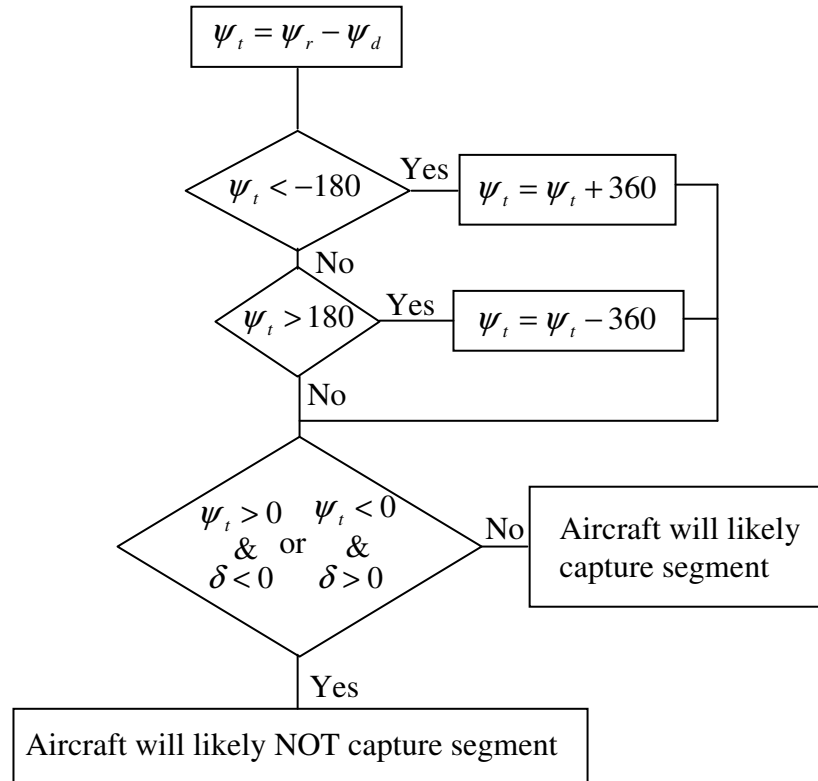
Figure 8.29. Logic for determining whether or not a heading will intercept a segment

8.3.4   Heading Capture

The Heading super-maneuver is simply a constant heading course law.

8.4   Basic Algorithms Required for Complete Functionality

To make the guidance system operate properly, some lower level functions are required. These functions are:

- Calculating the aircraft's turn radius
- Determining the lateral distance to a segment
- Determining the distance to go along a segment
- Determining the Rhumb line bearing and distance to a fix

-189-

8.4.1   Calculating the Aircraft Turn Radius

To calculate an aircraft's turn radius, r_t, a standard equation is used from Anderson (1989), Equation (12.22), where V is the aircraft's speed in the surface coordinate system, g is the gravitational acceleration, and n is the aircraft load factor.

$$r_t = \frac{V^2}{g\sqrt{n^2-1}} \qquad (12.22)$$

The load factor for the aircraft is calculated by considering Equation (12.23) where L is the lift of the aircraft, ϕ is the bank angle, and W is the weight of the aircraft. In the simulation, we will assume that the aircraft always will provide enough lift to maintain level flight which is implied by the equality of Equation (12.23).

$$L \cos\phi = W \qquad (12.23)$$

The load factor of an aircraft is defined as the lift over the weight. Assuming enough lift is provided to maintain level flight, the load factor can be determined as an exclusive function of bank angle.

$$n = \frac{L}{W} = \frac{L}{L\cos\phi} = \frac{1}{\cos\phi} \qquad (12.24)$$

Plugging equation (12.24) into equation (12.22), we get

$$r_t = \frac{V^2}{g\tan\phi} \qquad (12.25)$$

8.4.2   Determining Distance to go Along a Segment

Using the same nomenclature and geometry presented in Figure 8.8, the distance left to travel along the segment, d, can be calculated using Equation (12.26).

$$d = \mathbf{r}_{lf} \cdot \frac{\mathbf{R}_s}{\|\mathbf{R}_s\|} \qquad (12.26)$$

8.4.3   Rhumb Line Bearing

The rhumb line is a line of constant course, or heading. The distance between the two fixes using the rhumb line can be much greater than a great circle arc if the fixes are far apart.

For a spherical earth, a rhumb line is a straight line drawn between the two points on a Mercator projection of the earth's surface. The mercator projection separately maps latitude and longitude to a planar surface. The rhumb line is then the hypotenuse of the triangle formed by the projection of the latitude change and longitude change onto that planar surface. Our derived equations should be consistent with the Mercator transformation equations of Clarke (1995).
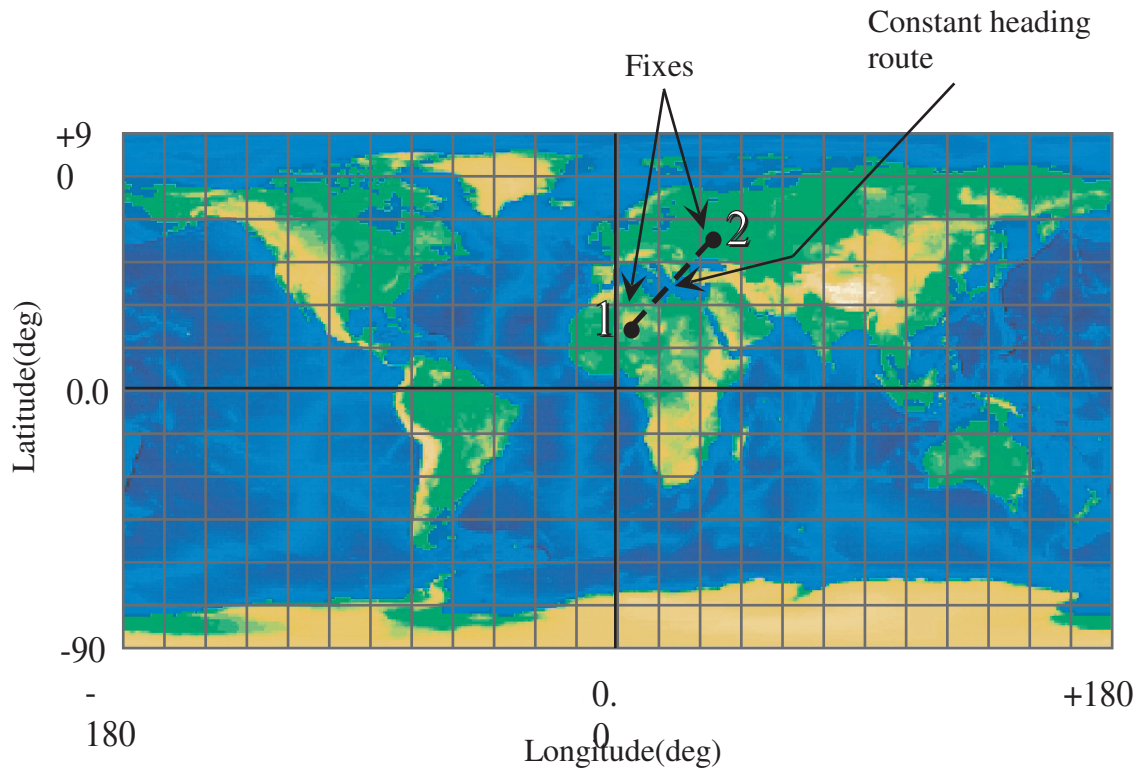
Figure 8.30. Cylindrical mapping of spherical Earth model. Shown are two fixes and the constant heading route between the fixes.
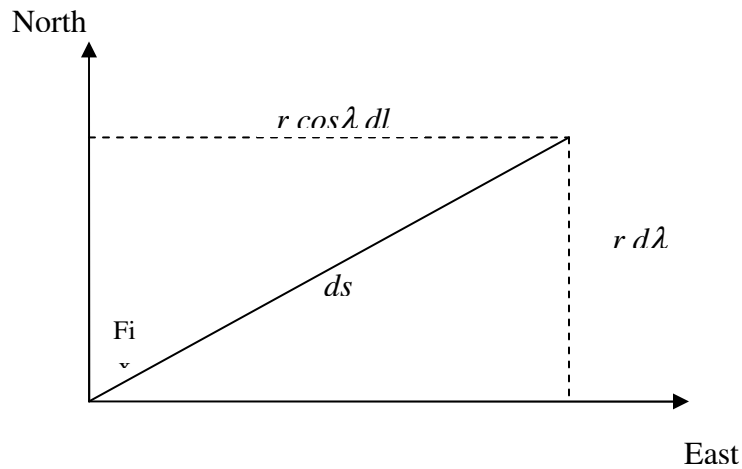
Figure 8.31 Geometry relating latitude, longitude, and bearing on a spherical earth

Referring to Figure 8.31, the changes in latitude and longitude along a rhumb line on a spherical earth are given by,

$$\tan\psi = \frac{r\cos\lambda\, dl}{r\, d\lambda}$$

$$\tan\psi = \frac{\cos\lambda\, dl}{d\lambda} \tag{12.27}$$

which can be rewritten as,

$$dl = \tan\psi\,\frac{d\lambda}{\cos\lambda}$$

Upon integrating, we get,

$$\int_{l_1}^{l_2} dl = \tan\psi\int_{\lambda_1}^{\lambda_2}\frac{d\lambda}{\cos\lambda}$$

$$l_2 - l_1 = \tan\psi\left[\ln\left|\sec\lambda + \tan\lambda\right|\right]_{\lambda_1}^{\lambda_2}$$

$$l_2 - l_1 = \tan\psi\left[\ln\left|\tan\left(\frac{\pi}{4}+\frac{\lambda}{2}\right)\right|\right]_{\lambda_1}^{\lambda_2}$$

$$l_2 - l_1 = \tan\psi\left[\ln\left|\tan\left(\frac{\pi}{4}+\frac{\lambda_2}{2}\right)\right| - \ln\left|\tan\left(\frac{\pi}{4}+\frac{\lambda_1}{2}\right)\right|\right] \tag{12.28}$$

Solving for the true heading, we get,

$$\tan\psi = \frac{\left(l_2 - l_1\right)}{\left[\ln\left|\tan\left(\frac{\pi}{4}+\frac{\lambda_2}{2}\right)\right| - \ln\left|\tan\left(\frac{\pi}{4}+\frac{\lambda_1}{2}\right)\right|\right]}$$

This is consistent with the equations for the equatorial Mercator projection as presented in Clarke (1995).

The longitudes must be analyzed so that the shorter path around the world is chosen. The following algorithm will normalize the longitude change for our purposes.

$$\Delta l = l_2 - l_1$$

$$\text{While} \quad |\Delta l| > 180° \quad \left\{ \Delta l = \Delta l + sign(\Delta l) * 360° \right\}$$

(12.29)

And the true heading equation becomes,

$$\tan \psi = \frac{\Delta l}{\left[\ln \left| \tan \left(\frac{\pi}{4} + \frac{\lambda_2}{2} \right) \right| - \ln \left| \tan \left(\frac{\pi}{4} + \frac{\lambda_1}{2} \right) \right| \right]}$$

(12.30)

Because the arctangent has a range *(-90°,90°)* and we want a heading in the range *(0°,360°)*, we need to be careful about how we solve this equation. We, therefore, develop the 360° arctangent function.

$$\psi = \arctan_{360} \left(\left[\ln \left| \tan \left(\frac{\pi}{4} + \frac{\lambda_2}{2} \right) \right| - \ln \left| \tan \left(\frac{\pi}{4} + \frac{\lambda_1}{2} \right) \right| \right], \Delta l \right)$$

(12.31)

8.4.3.1 360° Arctangent Function

In this section, we develop an algorithm for the arctangent of a ratio of Cartesian coordinates in the range *(0°,360°)*. Because the ratio is of the ordinate to the abscissa, we can adapt the range of the arctangent function per the quadrant of the coordinate pair.

Function $\theta = arctan_{360}(\delta_{abscissa}, \delta_{ordinate})$

    if $\delta_{abscissa} \geqslant 0$ and $\delta_{ordinate} \geqslant 0$

$$\theta = arctan \left| \frac{\delta_{ordinate}}{\delta_{abscissa}} \right|$$

    if $\delta_{abscissa} \geqslant 0$ and $\delta_{ordinate} \leqslant 0$

$$\theta = arctan \left| \frac{\delta_{ordinate}}{\delta_{abscissa}} \right| + 360°$$

    else

$$\theta = arctan \left| \frac{\delta_{ordinate}}{\delta_{abscissa}} \right| + 180°$$

    end

8.4.4   Rhumb Line Distance

Once again referring to Figure 8.31, the incremental distance along a rhumb line on a spherical earth is given by,

$$\cos \psi = \frac{r_e d\lambda}{ds}$$

$$ds = \frac{r_e d\lambda}{\cos \psi}$$

which integrates to,

$$s = \left| \frac{r_e \left(\lambda_2 - \lambda_1 \right)}{\cos \psi} \right| \tag{12.32}$$

Absolute value is used because we want a positive distance. Equation (12.32) does not apply for east-west rhumb lines. For these cases we use an alternate relation, also obtained from the geometry of Figure 8.31.

$$ds_{EW} = r_e \cos \lambda \, dl \tag{12.33}$$

Since the latitude is constant, this integrates to,

$$s_{EW} = \left| r_e \cos \lambda \, \Delta l \right| \tag{12.34}$$

The question arises as to what earth radius to use in the calculations. A good approximation to the spherical earth radius is to use the local radius of the first point in the WGS-84 earth model, which is given by using equations (2.107) and (2.108).

8.4.5   Creating Vectors Representing Segments

There is a need to represent segments as vectors. To create a vector, a magnitude and bearing are required. Generally, the rhumb line information is used. A segment's bearing is the rhumb line bearing between the two endpoint fixes that make up the segment, and the segment's length is the rhumb line distance between the two fixes. The vector components are represented in the surface frame as shown in Equation (12.35)

$$\mathbf{R}_s = s_s \cos \psi_s \hat{x}_s + s_s \sin \psi_s \hat{y}_s \tag{12.35}$$

The nomenclature is defined as follows:

- $\mathbf{R}_s$:   The vector representing the segment
- s_s: The rhumb line distance of the segment
- ψ_s: The rhumb line bearing between the trailing and leading fixes of the segment
- $\hat{x}_s, \hat{y}_s$: Unit vectors representing the x, y components of the surface frame.

THIS PAGE INTENTIONALLY LEFT BLANK

9. Navigation Error Modeling

The purpose of navigation error modeling is to model the variances which occur in aircraft flight paths as a result of imperfect information. Three different navigation systems are modeled: These are:

- VOR/DME navigation
- GPS navigation
- ILS navigation

The two navigation types generally used for en route types of operation are VOR/DME and GPS navigation. The ILS model is used only for approach to landing. All of the navigation error models perform similarly in that they create a perturbed estimate of the aircraft's location for the guidance system to use as an input. Therefore, the navigation error models all return a latitude-longitude pair which represents the aircraft's position as determined by imperfect navigation.

9.1   VOR/DME Navigation

Aircraft which use VOR/DME navigation are relying on a network of ground based VOR transmitters for bearing information and DME for distance information. The aircraft use range and bearing information from VOR/DME stations of known position to estimate the position of the aircraft. However, pure VOR/DME navigation puts more constraints on the problem in that aircraft usually always fly either to or from a VOR/DME station along a predetermined radial rather than using some area navigation (RNAV) technique. Therefore, not only does the aircraft's position need to be calculated, but also a technique to determine which VOR/DME is most appropriate for navigation must also be determined.

The process of VOR/DME navigation can be broken into two parts. These are:
- Determining the aircraft position from a given VOR/DME station
- Determining which VOR/DME station is best used for navigation

9.1.1   Determining Aircraft Position from a VOR/DME Station
The VOR transmitters send a line-of-sight RF signal that provides a bearing of the airborne receiver with respect to magnetic north. In the following discussion, it is assumed that the magnetic bearing angle, has been corrected with the magnetic bearing correction, to yield the geodetic bearing angle, B: The VOR/DME navigation error model takes perfect information about the aircraft's position and corrupts it according to the range and bearing biases for a given VOR/DME. This corrupted aircraft position information is sent to the guidance system which guides the aircraft using the corrupted information.

Consider the illustration in Figure 9.1. The estimated aircraft position is in error from the actual aircraft position by a certain range error, $\Delta\rho$, and bearing error, ΔB. Generally, the range and bearing from the station to the aircraft is calculated using the rhumb line bearing and distance algorithms in Section 8.

- ρ: The range to the station (nm)
- B: The bearing from the station (deg)
- $\Delta\rho$: The total range error (nm)
- ΔB: The total bearing error
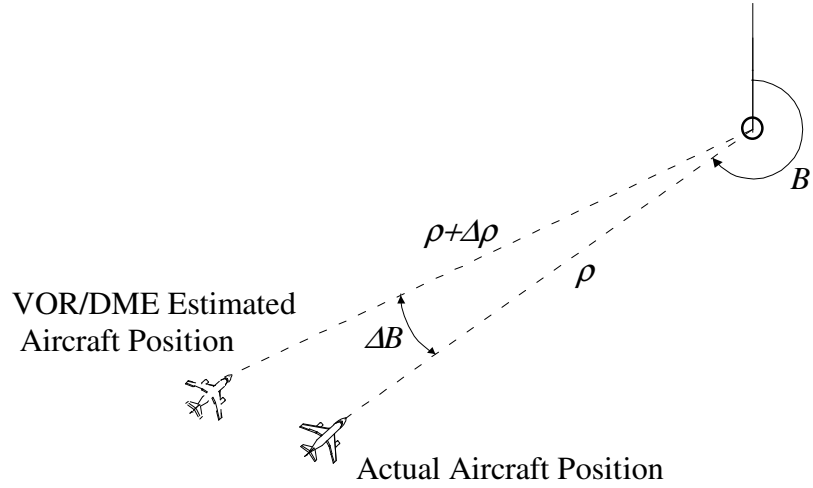
Figure 9.1. An illustration of the range and bearing from the station

The actual aircraft position in the NED or surface frame from the station is represented in (x,y) coordinates as defined in equations (3.210) and (3.212) where the terms x_{act} and y_{act} are the actual (x,y) locations for the aircraft.

$$x_{act} = \rho \cos B \tag{21.1}$$

$$y_{act} = \rho \sin B \tag{21.2}$$

The estimated location of the aircraft as determined from the range and bearing error is defined by equations (3.213) and (3.214).

$$x_{est} = (\rho + \Delta\rho)\cos(B + \Delta B) \tag{21.3}$$

$$y_{est} = (\rho + \Delta\rho)\sin(B + \Delta B) \tag{21.4}$$

The position error can be represented with Δx and Δy. Considering the x equation first, we can write

$$\Delta x = (\rho + \Delta \rho)\cos(B + \Delta B) - \rho \cos B \tag{21.5}$$

$$\Delta x = (\rho + \Delta \rho)(\cos B \cos \Delta B - \sin B \sin \Delta B) - \rho \cos B \tag{21.6}$$

$$\Delta x = \rho \cos B \cos \Delta B - \rho \sin B \sin \Delta B + \Delta \rho \cos B \cos \Delta B - \Delta \rho \sin B \sin \Delta B - \rho \cos B \tag{21.7}$$

Linearizing with respect to the error biases, we have equation (3.215).

$$\left. \frac{\partial \Delta x}{\partial \Delta B} \right|_{ref} \Delta B + \left. \frac{\partial \Delta x}{\partial \Delta \rho} \right|_{ref} \Delta \rho = -\rho \cos B \sin \Delta B \big|_{ref} \Delta B - \rho \sin B \cos \Delta B \big|_{ref} \Delta B$$
$$- \Delta \rho \cos B \sin \Delta B \big|_{ref} \Delta B - \Delta \rho \sin B \cos \Delta B \big|_{ref} \Delta B \tag{21.8}$$
$$+ \cos B \cos \Delta B \big|_{ref} \Delta \rho - \sin B \sin \Delta B \big|_{ref} \Delta \rho$$

Assuming a reference condition of $\Delta \rho = \Delta B = 0$, the linearized equation reduces to equation (21.9).

$$\Delta x = -\rho \Delta B \sin B + \Delta \rho \cos B \tag{21.9}$$

The y equation can be manipulated similarly.

$$\Delta y = (\rho + \Delta \rho)\sin(B + \Delta B) - \rho \sin B \tag{21.10}$$

$$\Delta y = (\rho + \Delta \rho)(\sin B \cos \Delta B + \cos B \sin \Delta B) - \rho \sin B \tag{21.11}$$

$$\Delta y = \rho \sin B \cos \Delta B + \rho \cos B \sin \Delta B + \Delta \rho \sin B \cos \Delta B + \Delta \rho \cos B \sin \Delta B - \rho \sin B \tag{21.12}$$

Linearizing, we have equation (21.13).

$$\left. \frac{\partial \Delta y}{\partial \Delta \rho} \right|_{ref} \Delta \rho + \left. \frac{\partial \Delta y}{\partial \Delta B} \right|_{ref} \Delta B = \sin B \cos \Delta B \big|_{ref} \Delta \rho + \cos B \sin \Delta B \big|_{ref} \Delta \rho$$
$$- \rho \sin B \sin \Delta B \big|_{ref} \Delta B + \rho \cos B \cos \Delta B \big|_{ref} \Delta B \tag{21.13}$$
$$- \Delta \rho \sin B \sin \Delta B \big|_{ref} \Delta B + \Delta \rho \cos B \cos \Delta B \big|_{ref} \Delta B$$

Assuming a reference condition of $\Delta\rho = \Delta B = 0$, the linearized equation reduces to equation (5.56).

$$\Delta y = \Delta\rho \sin B + \rho \Delta B \cos B \qquad (21.14)$$

Arranging in (21.9) and (5.56) in Matrix/Vector form, we have equation (12.14)

$$\begin{bmatrix} \Delta x \\ \Delta y \end{bmatrix} = \begin{bmatrix} \cos B & -\rho \sin B \\ \sin B & \rho \cos B \end{bmatrix} \begin{bmatrix} \Delta\rho \\ \Delta B \end{bmatrix} \qquad (21.15)$$

Generally, both the ground station and the airborne receiving equipment contribute to the range error and bias error. The terms $\delta\rho_{VD_A}$ and δB_{T_A} characterize the airborne receiver biases. These terms are randomly generated when the aircraft is initialized. The VOR/DME station has errors, $\delta\rho_{VD_G}$ and δB_{T_G}, which need to be obtained from the VOR/DME station itself. Depending on what quadrant the aircraft is in with respect to the VOR/DME, the bias can be different. A VOR/DME station needs some way of returning the correct bias information when prompted with the bearing from the station, B. Figure 9.2 illustrates the relationship between the VOR/DME and the four quadrants. For now, it may be easier to only have one bias per VOR/DME.
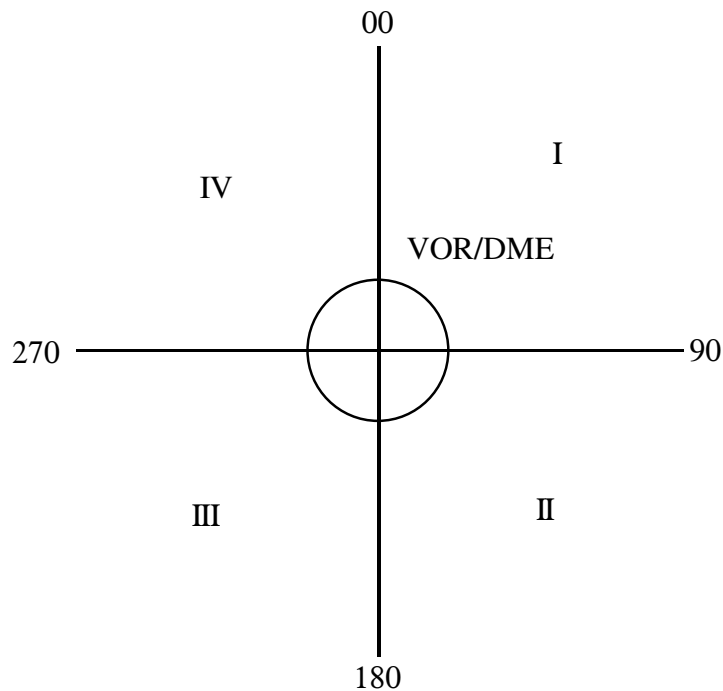
Figure 9.2. Illustration of the quadrants of the compass rose with respect to a VOR/DME station

When the airborne and ground station biases are summed, they can be inserted into equation (12.15) resulting in equation (12.3).

$$\begin{bmatrix} \Delta x \\ \Delta y \end{bmatrix} = \begin{bmatrix} \cos B & -\rho \sin B \\ \sin B & \rho \cos B \end{bmatrix} \begin{bmatrix} \left(\delta \rho_{VD_G} + \delta \rho_{VD_A} \right) \\ \left(\delta B_{T_G} + \delta B_{T_A} \right) \end{bmatrix} \tag{21.16}$$

However, the position of the aircraft is represented in terms of longitude and latitude. Therefore a conversion must be made. Two conversion factors are used. These are:

- $\frac{nm}{\deg_\mu}$: Nautical miles per degree of latitude
- $\frac{nm}{\deg_l}$: Nautical miles per degree of longitude

Equations (21.17) through (21.19) are used to calculate these conversion factors.

$$\frac{nm}{\deg_\mu} = \frac{2\pi r_e}{360} \tag{21.17}$$

$$r_l = r_e \cos \mu_{ac} \tag{21.18}$$

$$\frac{nm}{\deg_l} = \frac{2\pi r_l}{360} \tag{21.19}$$

The terms in the equations are defined as follows:

- r_e: The radius of the Earth in nautical miles
- r_l: The radius from the polar axis to the surface of the Earth at a given latitude
- μ_{ac}: The aircraft's current latitude

Finally, the aircraft's estimated (corrupted) position can be calculated using equations (3.216) and (21.21).

$$\mu_e = \mu_{ac} + \frac{\Delta x}{\frac{nm}{\deg_\mu}} \tag{21.20}$$

$$l_e = l_{ac} + \frac{\Delta y}{\frac{nm}{\deg_l}} \tag{21.21}$$

The terms in the equations are defined as follows:

- μ_{ac}: The aircraft's current actual latitude
- l_{ac}: The aircraft's current actual longitude
- μ_e: The aircraft's estimated latitude
- l_e: The aircraft's estimated longitude

The estimated values are the final return values.
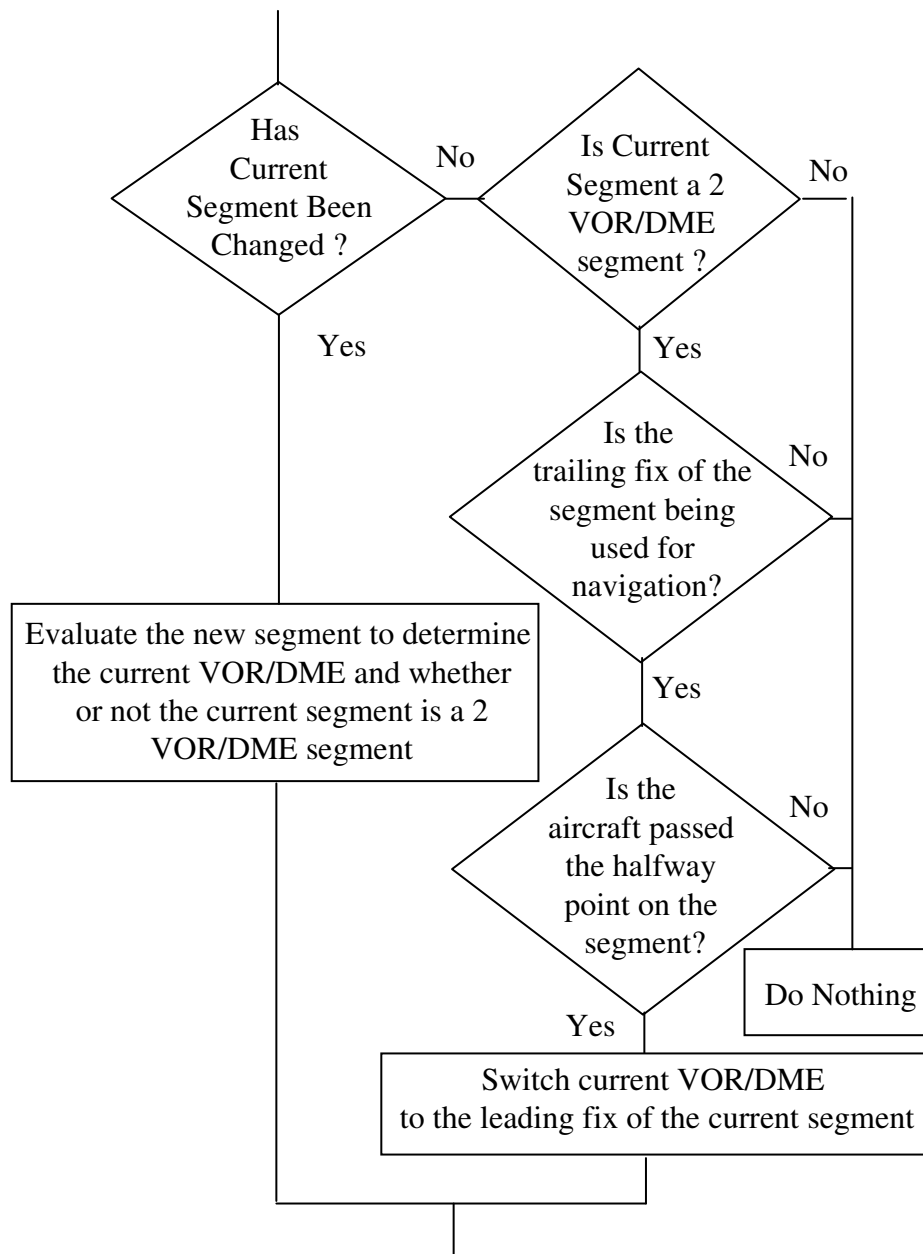
Figure 9.3. Logic for determining if the current VOR/DME used for navigation should be changed

-192-

The DME ground equipment accuracy is 0.05nm (1σ) while the airborne equipment accuracy is 0.25nm (1σ) or 1.5% (1σ) of range, whichever is greater (AC90-45A[4]). The accuracy of the VOR ground equipment is 0.95^0 (1σ) while the airborne equipment is 1.5^0 (1σ) (AC90-45A). By far, the greatest contributor to the navigation error is the bearing accuracy. The DME error plays a small role.

Slant range error is not accounted for explicitly in the model. This is because the altitude of each VOR/DME, which would need to be known to make the calculation, is not known. Furthermore, since the slant range error of a given situation can be estimated by the pilot, the pilot is likely to compensate for it when crossing fixes and capturing radials. Therefore, slant range error is unlikely to contribute greatly to the navigation error.

9.1.2 Determining the Proper VOR/DME Station to use for Navigation

When an aircraft is navigating using VOR/DME navigation, the pilot must tune in the VOR/DME which is associated with the particular segment which he/she is flying. The proper nav-aid information would be retrieved from the chart used for navigation. This level of realism does not exist explicitly in the TGF simulation because capturing every detail and nuance of the low altitude victor routes and high altitude jet routes would be prohibitively expensive to implement. Therefore, the victor and jet routes are not being explicitly followed. Rather, the aircraft only has knowledge of the fixes on the route and whether or not those fixes are VOR/DME stations or intersections. Because of this simplification, the navigation system must look at the available nav-aids along the route and determine which one would be most appropriate to use for navigation.

Figure 9.3 contains the logic which is used to determine whether or not the current VOR/DME should be switched. The logic can also be expressed as a set of the following rules:

- A fix is either a VOR/DME or an intersection
- A segment is defined by two fixes which are located at the endpoints of the segment
- If one of the fixes associated with the segment is a VOR/DME, that VOR/DME is used for navigation.
- If both fixes associated with the segment are VOR/DME's , then the VOR/DME closest to the aircraft is used for navigation.
- If neither fix is a VOR/DME, then a search is done to find the best VOR/DME along the route to use.

---

[4] AC90-45A: Advisory Circular "Approval of Area Navigation Systems for Use in the U.S. National Airspace System"

It is also worth noting that the navigation algorithms have nothing to do with switching segments. However, VOR/DME navigation needs to be aware of switches when they occur. If the current VOR/DME needs to be switched, the logic in Figure 9.4 must be used.
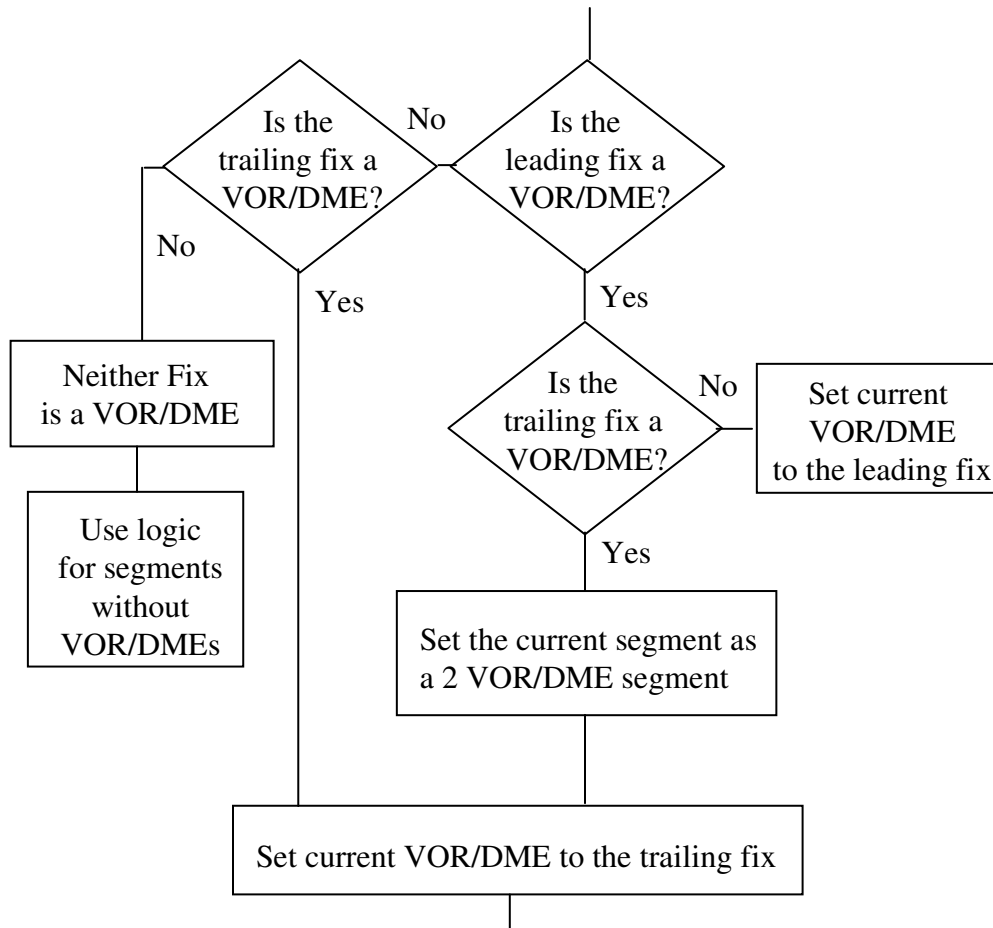
Figure 9.4. Logic for determining the appropriate VOR/DME for the next segment

Generally, there are either one or two VOR/DMEs on the segment. When there is only one VOR/DME, that VOR/DME is used. If there are two VOR/DMEs on the segment, the aircraft must use the closest one. When the segment does not have a VOR/DME associated with it, one must be determined. The algorithm must decide which of two VOR/DMEs is most appropriate. These two VOR/ DMEs are:

- The previous VOR/DME which was used for navigation on the last segment
- The next VOR/DME that lies along the route but not on the current segment

Such a scenario is illustrated in Figure 9.5. The aircraft lies on a segment which does not have a VOR/DME but it is in between two segments that do have a VOR/DME. From

-194-

inspection of the drawing, we can see that the next VOR/DME along the route is a much better choice because the current segment lies along a radial of the next VOR along the route.
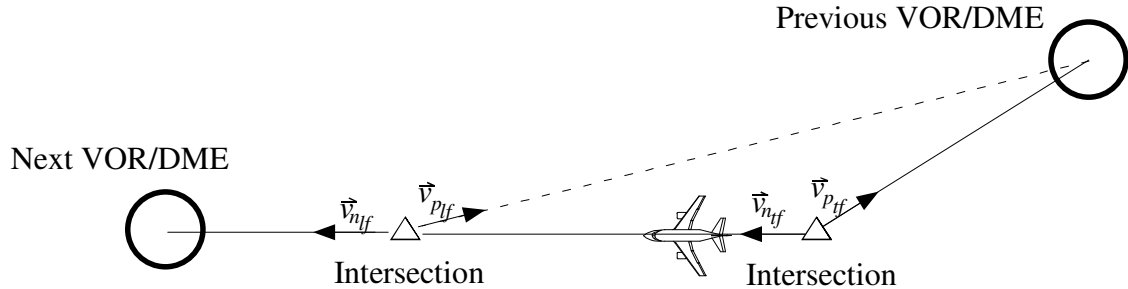
Figure 9.5. An illustration of the geometry used to determine which VOR/DME should be used for segments without a VOR/DME

To algorithmically draw the same conclusion, there are four unit vectors that must be calculated. The calculations can be made with a bearing calculation algorithm along with the vector tool of choice. It is imperative to the function of this algorithm that the vectors be unit vectors and not vectors of unequal magnitudes. These vectors are

- $\vec{v}_{n_{tf}}$: A unit vector from the trailing fix to the next VOR/DME
- $\vec{v}_{n_{lf}}$: A unit vector from the leading fix to the next VOR/DME
- $\vec{v}_{p_{tf}}$: A unit vector from the trailing fix to the previous VOR/DME
- $\vec{v}_{p_{lf}}$: A unit vector from the leading fix to the previous VOR/DME

The unit vectors associated with each VOR/DME are then dotted with each other. Ideally, the dot product is equal to unity for a perfect match between a VOR/DME and a segment. However, for the purposes of the algorithm, we choose the higher value of equations (21.22)and (12.35)as shown in Figure 9.6.

$$\vec{v}_{n_{tf}} \cdot \vec{v}_{n_{lf}} \tag{21.22}$$

$$\vec{v}_{p_{tf}} \cdot \vec{v}_{p_{lf}} \tag{21.23}$$

The higher value indicates that the vectors are pointing nearly in the same direction. This indicates that the segment lies along a radial to the VOR/DME in question which makes it a good candidate for navigation.

There will be cases when neither VOR/DME is appropriate for navigation. In this case, the algorithm still chooses the highest dot product; however, it can not really be said that the aircraft is following a radial To or From a VOR. The aircraft is area navigating

instead. This is not necessarily a realistic procedure for an aircraft that is flying using VOR/DME navigation; however, when such anomalies in the flight plan occur, it is best that the aircraft continue to fly rather than indicate an exception.

Determine the next VOR/DME along the route

Calculate
$$\vec{v}_{p_{tf}} \quad \vec{v}_{p_{lf}} \quad \vec{v}_{n_{tf}} \quad \vec{v}_{n_{lf}}$$

If
$$\left(\vec{v}_{n_{tf}} \cdot \vec{v}_{n_{lf}} \right) > \left(\vec{v}_{p_{tf}} \cdot \vec{v}_{p_{lf}} \right)$$

Use Previous VOR/DME

Use Next VOR/DME
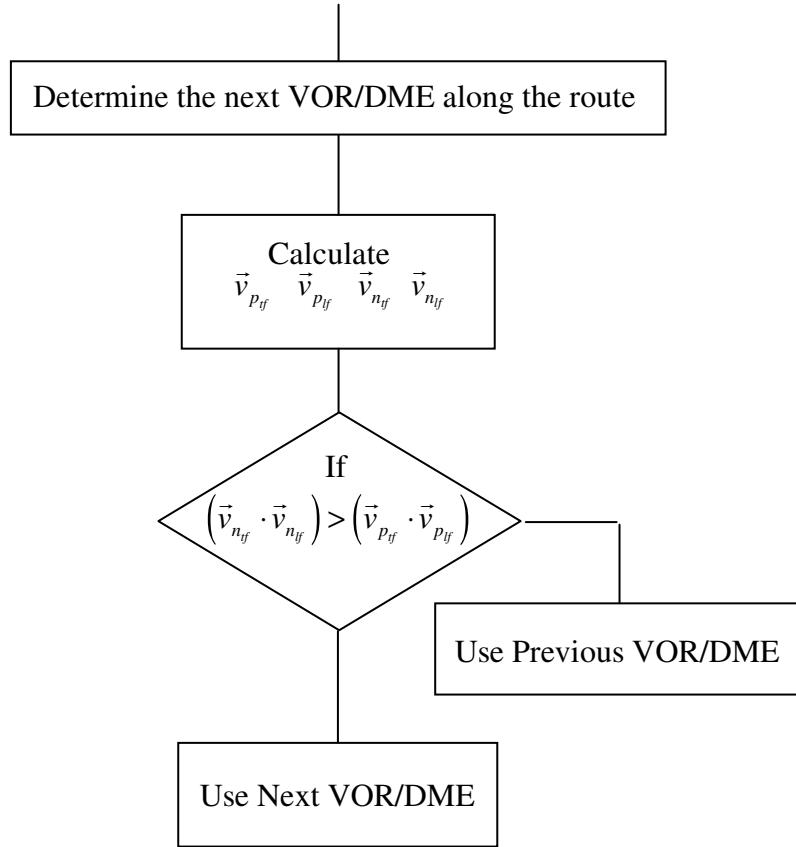
Figure 9.6. Logic For determining which VOR/DME to use when no VOR/DME lies along route

9.2   GPS Navigation

There are a number of error sources that contribute to the aircraft GPS position and velocity error. Up until 2000, the dominant error was the GPS satellite clock error.

GPS satellite clock error is an intentional degradation of the GPS signal called Selective Availability (SA). It was implemented in 1990 to deny full position and velocity accuracy to "unauthorized users" after initial testing of the GPS system revealed accuracies much better than anticipated.

In May of 2000, the United States stopped degrading GPS performance with SA.

The clock error of SA in GPS navigation was formerly modeled using a 2nd Order Gauss-Markov model. This is discussed in Appendix B. The analysis in Appendix B develops a closed-form 2nd order difference equation for 2nd Order Gauss-Markov process that forms the basis for implementing the process in code.

Other sources of GPS navigation error are so much less significant than that of GPS satellite clock error (from SA) that they do not merit inclusion in this model of Aircraft Dynamics.

9.3   ILS Localizer Error Model

For an ILS localizer, the measured lateral deviation is the angle, ΔB_I. This can be converted into a lateral position error as follows. The slant range, r_{IT} to the runway, is approximated using the rhumb line distance algorithm. Then the lateral position, r_{CT} is:

$$r_{CT} = r_{IT}\Delta B_I \qquad (21.24)$$

The deviation angle is comprised of errors from ground based equipment and airborne equipment as shown in equation (21.25) where $\Delta B_{I,G}$ is the ground based component and $\Delta B_{I,A}$ is the airborne component.

$$\Delta B_I \equiv \Delta B_{I,G} + \Delta B_{I,A} \qquad (21.25)$$

A number of references have determined that the ground-based component of the localizer error is not a simple random bias. Instead, it varies with the distance from the runway. A convenient model for this error source is to treat it as a spatial first-order Gauss Markov as shown in equation (21.26). By that is meant that the error does not vary with time but with the location of the receiver from the ILS localizer transmitter.

$$\frac{\partial}{\partial s}\Delta B_{I,G}(s) = -\beta_B(s)\Delta B_{I,G}(s) + n_B(s) \qquad (21.26)$$

where,

- $n_B(s)$: Scaled Gaussian white noise
- $\beta_B(s)$: Spatial damping factor

$$ds = \left(\frac{ds}{dt}\right)dt = v_{IT}(t)dt \qquad (21.27)$$

$$\beta_B(t) = v_{IT}(t)\beta_B(s) \qquad (21.28)$$

$$\Delta\dot{B}_{I,G}(t) = -\beta_B(t)\Delta B_{I,G}(t) + n_B(t) \qquad (21.29)$$

The actual ILS localizer beam bending errors for five different airports are illustrated in Figure 9.7. A set of five simulated ILS localizer beam bending errors using the above statistical model is presented in Figure 9.8.
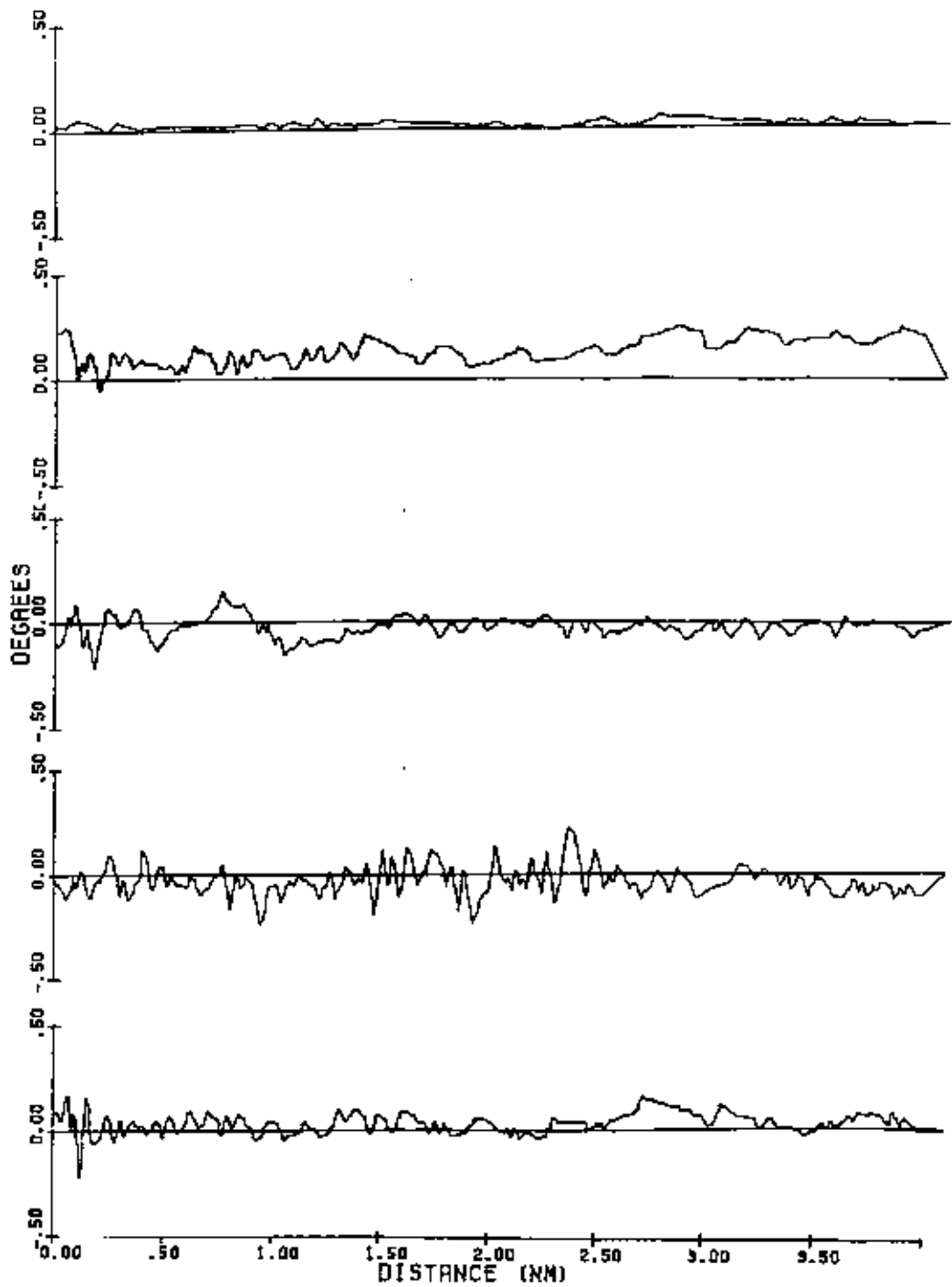

**Figure 9.7.** Measured ILS Localizer Bearing Deviation Angle Errors
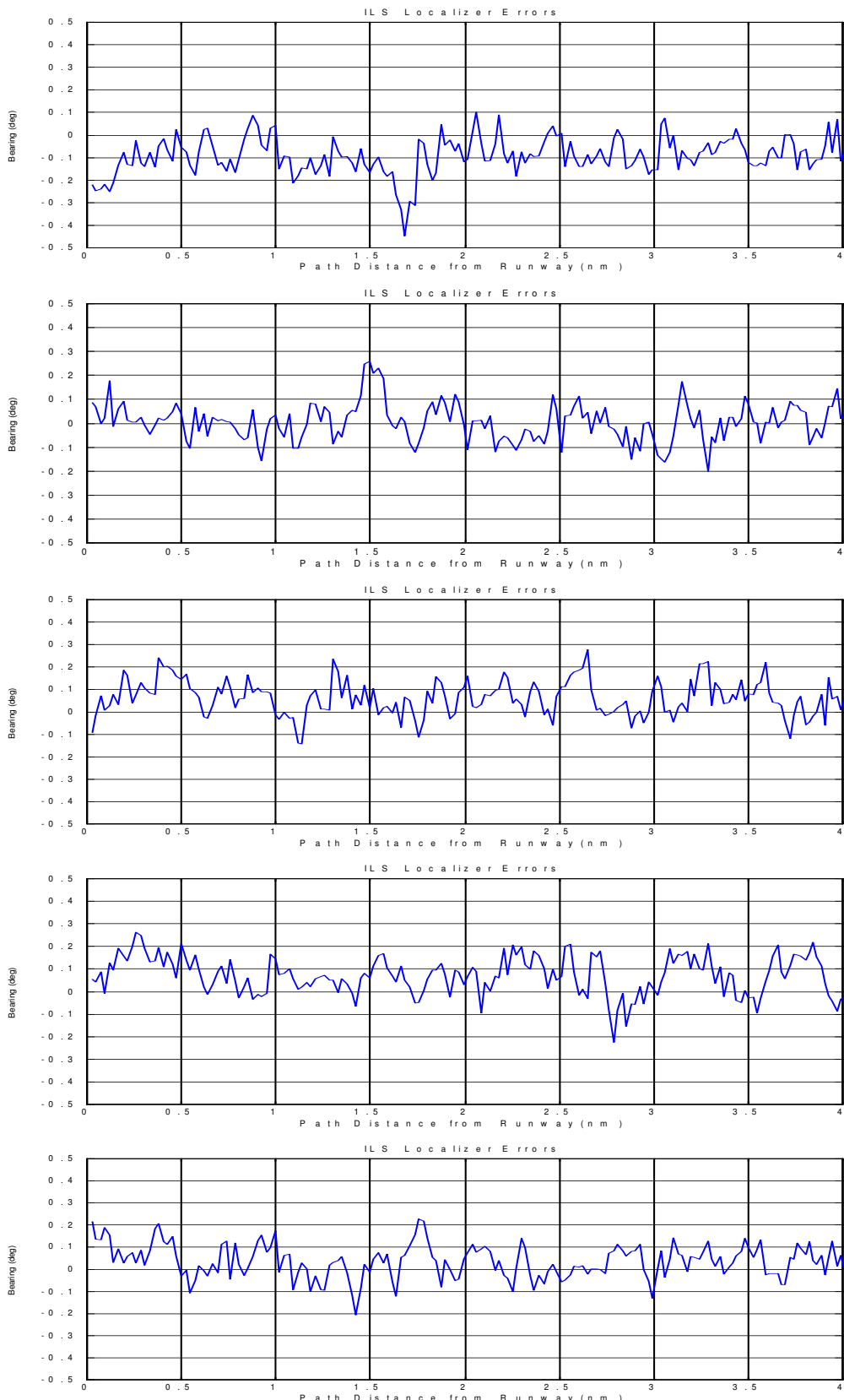
Figure 9.8. Simulated ILS Localizer Bearing Deviation Angle Errors

THIS PAGE INTENTIONALLY LEFT BLANK

10. The Longitudinal Guidance System

When an aircraft flies along a route it is often necessary to have the aircraft automatically meet speed and altitude constraints that are placed on fixes along the route. These are generally termed "crossing restrictions." One case where crossing restrictions are often used is when modeling flight along a Standard Arrival Route (STAR). When the flight plan contains a STAR for the pilot to follow, it is assumed that the pilot has at least a textual description of the STAR and will make appropriate speed and altitude changes as published.

This chapter describes procedures by TGF-simulated aircraft in meeting or preparing to meet longitudinal route restrictions. The procedures will involve the deployment of high-lift devices and targeting of desired speeds and altitudes.

10.1   Aircraft Device Deployment

Aircraft devices include high-lift devices (ie, wing flaps and slats) and landing gear. This section describes their deployment.

10.1.1 Flaps on Approach

For all aircraft, the flaps (or, more appropriately, high-lift devices) are modeled, as they are in BADA, with lift and drag coefficient values corresponding to the flap and slat deployment for the different wing configurations for the aircraft. The five configurations are cruise, initial climb, take-off, approach, and landing. We have changed the names to flaps0, flaps1, flaps2, flaps3, and flaps4, respectively, to remove the implication that a particular configuration is used in a particular phase of flight. Typically, piston aircraft have only 4 configurations, so flaps3 and flaps4 are identical. The standard flap schedule on approach is presented in Tables Table 10.1 and Table 10.2 . This is the schedule that is followed under standard approach. Once the aircraft's speed drops below the given flap set speed, that configuration is set. Flaps may be extended on a more aggressive schedule if the aircraft needs to lose energy more quickly, but never when the aircraft is above the flap limit speed. The flap limit speed is 30 knots above the flap set speed for jets and turboprops and 20 knots above the flap set speed for pistons.

Flap Configuration	Set Speed (kts)
flaps0	
flaps1	$1.3V_{stall_{LD}} + 80$
flaps2	$1.3V_{stall_{LD}} + 60$
flaps3	$1.3V_{stall_{LD}} + 30$
flaps4	$1.3V_{stall_{LD}} + 10$

Table 10.1 Flap Deployment Schedule for Jet and Turboprop Aircraft on Approach

Flap Configuration	Set Speed (kts)
flaps0	
flaps1	$1.3V_{stall_{LD}} + 50$
flaps2	$1.3V_{stall_{LD}} + 30$
flaps3	$1.3V_{stall_{LD}} + 10$
flaps4	$1.3V_{stall_{LD}} + 10$

Table 10.2 Flap Deployment Schedule for Piston on Approach

10.1.2 Flaps on Takeoff

The algorithm for the deployment of flaps in takeoff flight is presented in Figure 10.1. Basically, takeoff flaps are deployed for takeoff and retracted as the aircraft climbs. Flaps are not deployed in cruising flight.

10.1.3 Speed Brakes

Speed brakes are modeled in the simulator as an increment, $C_{D_{brakes}}$, to the profile drag coefficient. Speed brakes are deployed if an aircraft is asked to expedite its descent. Algorithms within the simulator guidance module will deploy speed brakes in the case that the aircraft is predicted to be unable to reach an altitude-fix restriction. Speed brakes may also be deployed in the landing sequence if the aircraft is well above the glide slope.
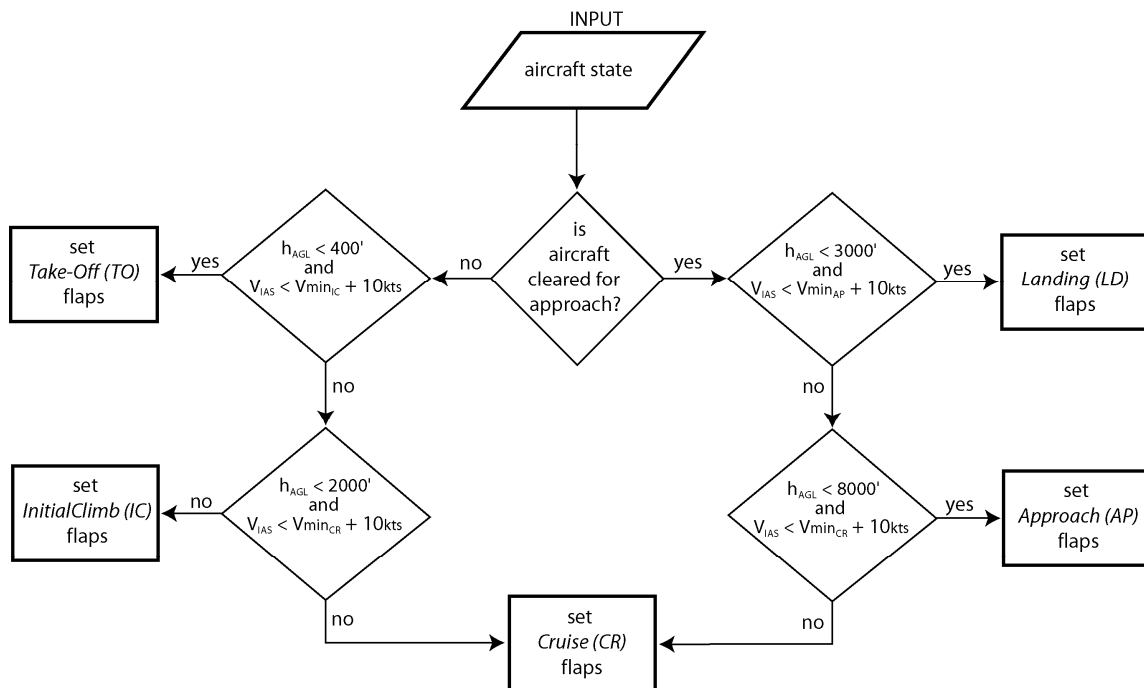

Figure 10.1: Flap Deployment Algorithm

10.1.4 Spoiler

The spoiler is modeled in the simulator as an increment, $C_{D_{spoiler}}$, to the profile drag coefficient and a complete loss of lift. It is used in the Touchdown region (Region 10) only and is deployed immediately when the aircraft's altitude is the same as the runway altitude. Region 10 uses an open-loop controller with the thrust set to touchdown thrust and the lift coefficient set to zero (a consequence of spoiler deployment).

10.1.5 Landing Gear

Landing gear are modeled in the simulator as an increment, $C_{D_{gear}}$, to the profile drag coefficient. They are extended for the takeoff sequence and retracted once the aircraft reaches 400 feet AGL. They are also extended during the landing sequence once the aircraft has passed the outer marker of its assigned runway.

10.1.6 Ground Braking

When the braking function was initially conceived, it was thought that some number from a data file would be read into the airframe model, and an increase in drag would result from some static braking force. However, the aircraft data files did not have any information regarding braking force. Equation (5.1) is a proposed ground breaking model that assumes that the braking force is 30% of the aircraft's weight. This approximation is convenient because it does not rely on an independent ground braking parameter in the aircraft data files. However, ground breaking is not currently implemented in the TGF simulator.

$$D_{brake} = 0.3 W_{ac} \tag{5.1}$$

10.2 Preparing for Approach and Landing

A pilot that is approaching a terminal airspace can infer certain details about his descent and deceleration. He may have flown in the airspace before and so he knows how controllers usually guide him in to the runway. He may have witnessed the paths of the aircraft in front of him. In either case, he knows that it would behoove him to begin either descending or decelerating or both within the implied constraints of the airspace or the constraints imposed on him by the controller.

These are details that are difficult to convey to a computer program that requires absolutes in the form of target speeds and altitudes. At the very least, we need to inform the simulator that the aircraft will soon begin its approach to the airport and that it may begin descending and decelerating within imposed constraints. This causes the aircraft to

make decisions on how quickly it needs to lose energy and whether or not to deploy drag increasing devices.

10.2.1 Energy Gradient

In reality, pilots do not make calculations comparing the energy gradient needed with the aircraft's ability to lose energy, but they do make intuitive judgments of this comparison. Our technique of modeling this judgment is to make those calculations. The simulator will calculate its current mechanical energy state (based on speed and altitude) and a target mechanical energy (based on a preferred speed and altitude upon crossing some fix, e.g., the outer marker) and divide the difference by the distance to the fix and compare that to its ability to lose energy. If the aircraft needs to increase its ability to lose energy, it can deploy a drag increasing device, such as speed brakes or flaps. This is referred to as "dirtying" the aircraft.

An aircraft's specific mechanical energy is the sum of its specific kinetic energy and specific potential energy, as defined by its speed and altitude. This was first shown in equation (5.11).

$$e = \frac{V_G^2}{2} + gh \tag{5.11}$$

We define an aircraft's energy gradient as the rate of change of specific mechanical energy per unit change in ground distance.

$$eg \equiv \frac{de}{dx} \tag{10.1}$$

The aircraft's actual energy gradient is a measure of its ability to lose energy. Combining equation (10.1) with equation (5.11), we get,

$$eg = V_G \frac{dV_G}{dx} + g \frac{dh}{dx} = V_G \frac{dV_G/dt}{dx/dt} + g \frac{dh/dt}{dx/dt}$$

$$eg = \dot{V}_G + g \frac{\dot{h}}{V_G} \tag{10.2}$$

Comparing this to equation (5.19) gives an equation for the aircraft's energy gradient in terms of thrust, drag, and mass.

$$eg = \frac{T - D}{m} \tag{10.3}$$

The energy gradient needed is defined as the difference between the target and current specific mechanical energies divided by the ground distance to the target. This can be represented in discrete notation.

$$eg_n = \frac{e_t - e_0}{\Delta x} \qquad (10.4)$$

An aircraft on approach will be descending and decelerating and will, therefore, have a negative energy gradient. An aircraft can decrease its energy gradient (i.e., make it more negative) by deploying drag increasing devices. A comparison of the energy gradient, eq. (10.3), with the needed energy gradient, eq. (10.4), will determine if this is necessary. If the needed energy gradient is less than the actual energy gradient, deployment of a drag increasing device may be necessary.

Under normal approach conditions, an aircraft's energy gradient will decrease (i.e., become more negative) as it slows down and deploys flaps in preparation for landing. Because the aircraft is typically in a clean configuration above about 8000 feet altitude, the needed energy gradient may be less than the actual energy gradient even though the aircraft is following a typical glide ratio and there is no urgency for dirtying the aircraft. The algorithm developed for drag device deployment must consider this. If the aircraft is on a normal glide ratio above 8000 feet, the aircraft will not increase its urgency.

The glide ratio is something that airline pilots normally consider on approach. A glide ratio of 3:1, distance:height, with distance to the runway measured in nautical miles and height measure in thousands of feet above ground level (AGL), is considered typical. For example, an aircraft that is 30 nm from the runway and at 10,000 feet has a glide ratio of 3:1. The equation for glide ratio is presented below.

$$glideRatio = \frac{\Delta x \, (nm)}{h_{AGL} \, (1000 \, ft)} \qquad (10.5)$$

If an aircraft is not on a normal glide ratio above 8000 feet and its needed energy gradient is less than its actual gradient, it will have trouble losing energy in its descent. The simulator will mark this aircraft as needing to increase its "urgency" in getting down. This can mean deploying flaps, speed brakes, or landing gear as appropriate. The simulator will respond to an increasing urgency by first trying to set the next increment of flaps (after checking to see that the aircraft is below the flap limit speed), then the speed brakes, then the landing gear. The algorithm for comparing the needed and actual energy

gradients for increasing urgency is presented in Figure 10.2. The algorithm for the deployment of drag devices is presented in Figure 10.3.
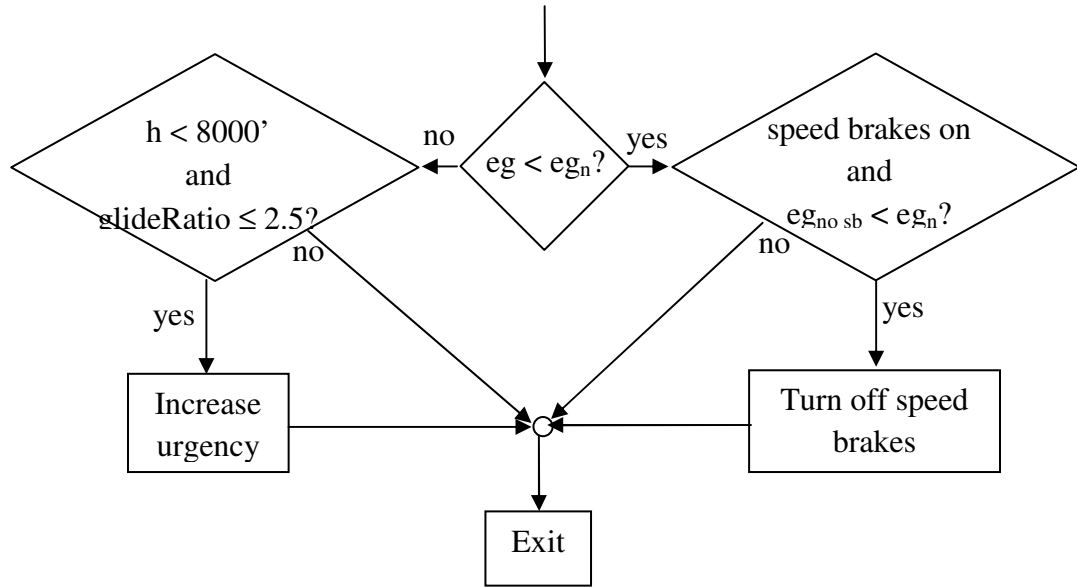

Figure 10.2: Comparing needed and actual energy gradients to determine urgency
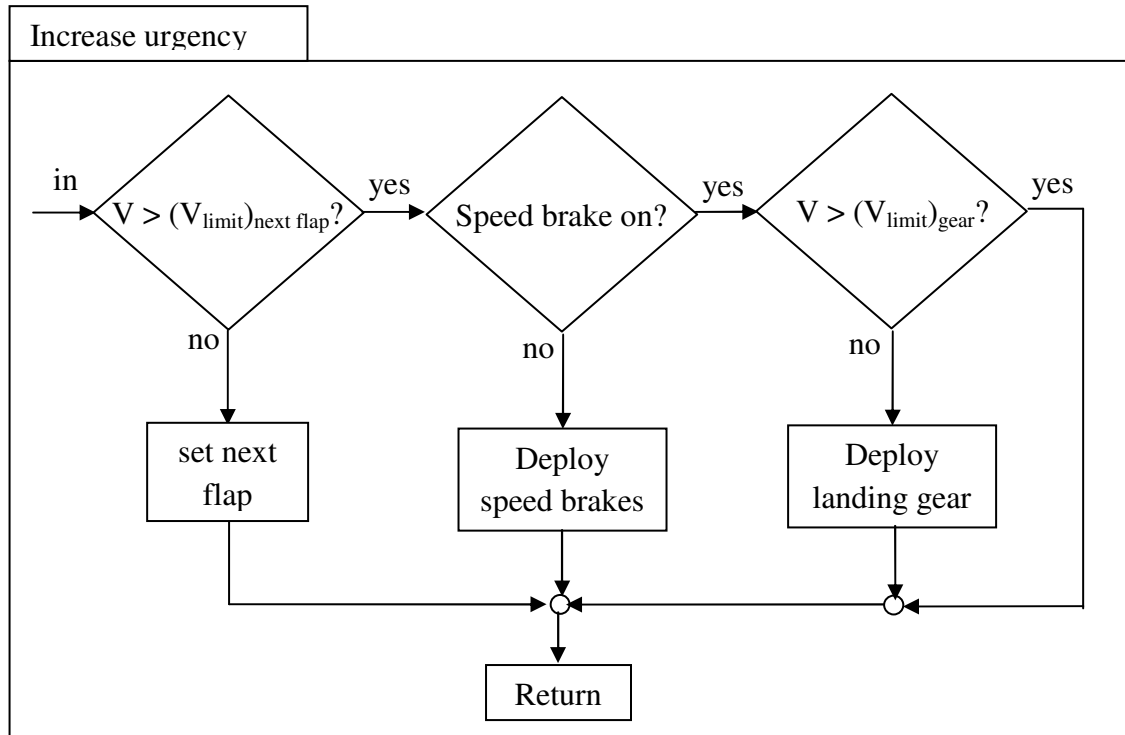
Figure 10.3: Procedure for increasing urgency (i.e., deploying drag devices)

Speed brakes are a convenient drag device used to increase an aircraft's ability to lose energy. When the speed brakes are deployed, they increase the aircraft's parasite drag coefficient by an increment given in the aircraft data file. Speed brakes typically work so well that after a period of use, they are no longer needed. If speed brakes are deployed and the actual energy gradient is less than the needed energy gradient, we can compare the needed energy gradient against the aircraft's energy gradient without speed brakes to see if they can be retracted.

The aircraft's mass and descent thrust are independent of speed brake deployment. From eq. (10.3), the aircraft's energy gradient without speed brakes is given by the following.

$$eg_{no\ sb} = \frac{T - D_{no\ sb}}{m}$$

The difference between the energy gradients with and without speed brakes is then calculated by subtracting eq. (10.3).

$$eg_{no\ sb} - eg = \frac{D - D_{no\ sb}}{m} = \frac{\frac{1}{2}\rho V_a^2\left[\left(C_{D_0} + KC_L^2\right) - \left(C_{D_0} + KC_L^2\right)_{no\ sb}\right]}{m}$$

The speed brakes affect neither the induced drag coefficient nor the lift coefficient.

$$eg_{no\ sb} - eg = \frac{\frac{1}{2}\rho V_a^2\left[\left(C_{D_0}\right) - \left(C_{D_0}\right)_{no\ sb}\right]}{m} = \frac{\frac{1}{2}\rho V_a^2 C_{D_{speedbrakes}}}{m}$$

So the difference in the energy gradient in the two configurations is a function of the parasite drag coefficient increment of the speed brakes. We can simplify this expression further by using an approximation for the lift coefficient. In a steady, wings-level descent, the lift is equal to the vertical component of weight.

$$L = W\ cos\ \gamma$$

$$C_L = \frac{W\ cos\ \gamma}{\frac{1}{2}\rho V_a^2}$$

Neglecting the flight path angle, γ, we get,

$$C_L = \frac{mg}{\frac{1}{2}\rho V_a^2} \ ,$$

a reasonable approximation for the lift coefficient. The energy gradient without speed brakes is then,

$$eg_{no\ sb} = eg + \frac{gC_{D_{speedbrakes}}}{C_L} \tag{10.6}$$

10.2.2 Distance Remaining to Runway

In order to calculate the needed energy gradient of equation (10.4) and the glide ratio of equation (10.5), we need to determine the distance remaining to the runway. This cannot be calculated simply as the distance between the aircraft's current position and the runway threshold because the aircraft may not be pointed at the runway. In the case of a simple approach, an aircraft is following a pre-determined route to the runway and so the distance to the runway is known. But in many cases, the aircraft does not know its directed route to the runway. If the aircraft is on a downwind leg, it could be vectored to the approach by the controller at any time. In this case, we have to make assumptions about the typical approach.

10.2.2.1   Distance Remaining to Runway along a Filed Route

If the aircraft's lateral guidance system is following a filed route and the last fix on the route is airport at which the aircraft is landing, then the distance remaining to the runway is the distance left along the route. If the airport is not the last fix, then the airport fix is appended to the filed route and the distance remaining to the runway is the distance left along the route. For the purpose of calculating the energy gradient on approach, the remaining route distance is typically limited to a maximum of 20 nm.

As discussed in Chapter 8, TGF routes are typically Track-to-Fix (TF) segments with fly-by waypoints. An estimate of the remaining route distance can be obtained by adding the distances, S, of the segments between the fixes, but this ignores that the segments are shortened by flying by the termination fixes when transitioning between segments. We can get a better estimate by predicting the aircraft's curved path in flying by the termination fixes.

Let us assume that the path flown by an aircraft in transitioning between TF segments with fly-by waypoints is a constant radius turn with a constant bank angle (ie, instantaneous bank dynamics). Using this assumption and referring to Figure 8.16, the length of the transition arc is given by, $r_t \Delta \psi$. (The assumed constant turn radius, r_t, is obtained from equation (8.25) using the speed in the route and a standard bank angle.)

For each transition, the route distance is shortened by twice the offset length and increased by the transition arc length. For n segments, our estimate of the route distance is…

$$RouteDistance = \sum_{i=1}^{n} S_i + \sum_{i=1}^{n-1}\left(r_t - 2l_{offset}\right)$$

Using equation (8.13) for l_{offset} and ignoring the lag factor, k, this becomes…

$$RouteDistance = \sum_{i=1}^{n} S_i + r_t\sum_{i=1}^{n-1}\left(\Delta\psi - 2\tan\left(\frac{\Delta\psi}{2}\right)\right) \qquad (10.7)$$

10.2.2.2   Distance Remaining to Runway for Vectored Aircraft

If the aircraft's lateral guidance system is following a vector, we have to make assumptions concerning the vectored approach. These assumptions are based on a typical vectored approach that meets Federal Air Regulations (FARs). They are as follows:

- Aircraft will merge onto the localizer bearing on a 30° intercept, and
- Aircraft will merge onto the localizer bearing at least 3 nm before the outer marker.

We assume that the aircraft will fly its current heading until crossing the 30° intercept, then follow the 30° intercept to the localizer bearing, then follow the localizer bearing to the runway. This approach is illustrated in Figure 10.4.

In order to develop an algorithm for the assumed vectored approach, the following variables are defined.

$\vec{P}$ a vector from a position 3 nm from the outer marker (along the localizer bearing) to the aircraft

$d_{P\text{-}rwy}$ the distance between a position 3 nm from the outer marker to the runway threshold

ψ_p the bearing from a position 3 nm from the outer marker (along the localizer bearing) to the aircraft

ψ_h the aircraft heading (Actually, the ground track heading is the accurate angle to use, but the aircraft heading will yield a suitable approximation.)

ψ_{loc} the localizer bearing

Note: all angles and angle differences are defined in the range [0,360].
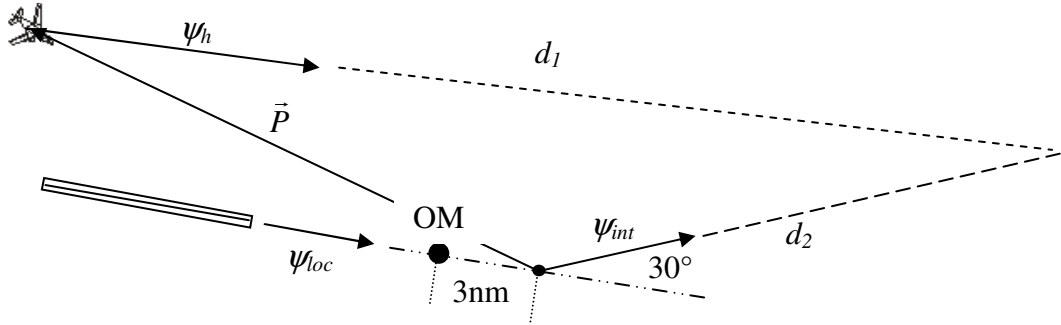
Figure 10.4: Illustration of Assumed Vectored Approach

By inspection of Figure 10.4, we write the following vector equation.

$$d_2 \angle \psi_{int} - d_1 \angle \psi_h = \vec{P} = P \angle \psi_P$$

Resolving into east - north components, we get,

$$d_2 \sin \psi_{int} - d_1 \sin \psi_h = P \sin \psi_P$$
$$d_2 \cos \psi_{int} - d_1 \cos \psi_h = P \cos \psi_P$$

In matrix form,

$$\begin{bmatrix} -\sin \psi_h & \sin \psi_{int} \\ -\cos \psi_h & \cos \psi_{int} \end{bmatrix} \begin{bmatrix} d_1 \\ d_2 \end{bmatrix} = P \begin{bmatrix} \sin \psi_P \\ \cos \psi_P \end{bmatrix}$$

Solving the matrix equation,

$$\begin{bmatrix} d_1 \\ d_2 \end{bmatrix} = P \begin{bmatrix} -\sin \psi_h & \sin \psi_{int} \\ -\cos \psi_h & \cos \psi_{int} \end{bmatrix}^{-1} \begin{bmatrix} \sin \psi_P \\ \cos \psi_P \end{bmatrix}$$

$$\begin{bmatrix} d_1 \\ d_2 \end{bmatrix} = \frac{P}{\sin \psi_{int} \cos \psi_h - \cos \psi_{int} \sin \psi_h} \begin{bmatrix} \cos \psi_{int} & -\sin \psi_{int} \\ \cos \psi_h & -\sin \psi_h \end{bmatrix} \begin{bmatrix} \sin \psi_P \\ \cos \psi_P \end{bmatrix}$$

$$\begin{bmatrix} d_1 \\ d_2 \end{bmatrix} = \frac{P}{\sin \psi_{int} \cos \psi_h - \cos \psi_{int} \sin \psi_h} \begin{bmatrix} \sin \psi_P \cos \psi_{int} - \cos \psi_P \sin \psi_{int} \\ \sin \psi_P \cos \psi_h - \cos \psi_P \sin \psi_h \end{bmatrix}$$

From the trigonometric identity,

$$sin\,a\,cos\,b - cos\,a\,sin\,b \equiv sin(a-b)$$

The solution for d_1 and d_2 becomes,

$$\begin{bmatrix} d_1 \\ d_2 \end{bmatrix} = \frac{P}{sin(\psi_h - \psi_{int})} \begin{bmatrix} sin(\psi_P - \psi_{int}) \\ sin(\psi_P - \psi_h) \end{bmatrix}$$

or
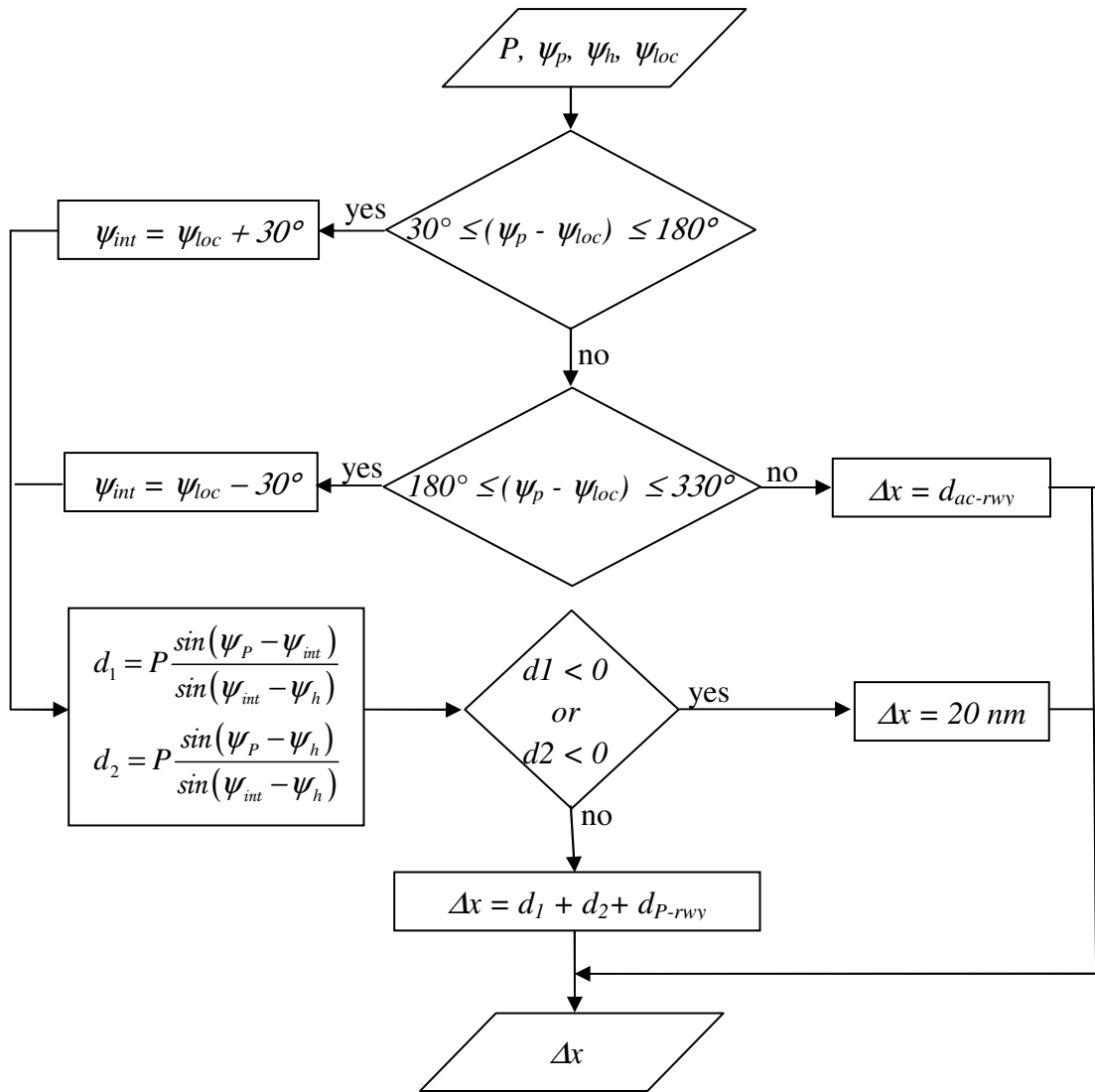
Figure 10.5: Algorithm for Determination of Distance Remaining to Runway

$$d_1 = P \frac{\sin(\psi_P - \psi_{int})}{\sin(\psi_{int} - \psi_h)}$$

$$d_2 = P \frac{\sin(\psi_P - \psi_h)}{\sin(\psi_{int} - \psi_h)}$$

(10.8)

And the distance remaining to the runway is given by

$$\Delta x = d_1 + d_2 + d_{P\text{-}rwy} \tag{10.9}$$

If either d_1 or d_2 is negative, then the heading will not intersect the localizer intercept. In this case, we assume $\Delta x = 20$ nm. If the aircraft is between the left and right localizer intercepts, we will assume that the distance remaining to the runway is the straight line distance. (This assumptions fails to consider that the aircraft may be between the intercepts and moving away from the runway, but that is an unlikely case.) Failing this case, if the aircraft is left of the localizer bearing, it is assumed that the aircraft will cross the left intercept, if right, then the right intercept. In any case, if the calculated value for the distance remaining to the runway is greater than 20 nm, then we set $\Delta x = 20$ nm. Figure 10.5 illustrates this algorithm.

10.3 Crossing Restrictions in Descent

When an aircraft is asked to descend and cross a fix at a specific altitude, normal procedure is for the aircraft to maintain the current altitude for as long as possible. This requires a calculation of the top of descent point. The reason for the delay in beginning the descent is that aircraft are more efficient at higher altitudes and so prefer to fly there. Conversely, there is no need to delay a climb if the crossing restriction is above the current altitude because the aircraft prefers to be at the higher altitude sooner rather than later.

Experience shows that aircraft in a constant CAS descent below the tropopause have very little variation in flight path angle. Our approach in the TGF model is to make a quick estimate of the top of descent point, apply a small margin of safety (i.e., make the glide slope shallower), and to fly with dual control along the calculated flight path angle in the same manner we fly along an ILS. We make consideration for alternate variations in true airspeed by estimating the energy ratio. Since we will have no prior knowledge of wind variation with altitude, we will neglect the effects of wind.

The first step is to make an estimate of the flight path angle. Equation (2.59) is rewritten here.

$$\dot{V}_a = \frac{T-D}{m} - g\sin\gamma_a \tag{2.59}$$

Once again, we re-write this in the form of changing energy, removing the subscript, a, referring to the airmass.

$$g\sin\gamma + \dot{V} = \frac{T-D}{m}$$

$$\sin\gamma\left(1 + \frac{\dot{V}}{g}\frac{V}{\dot{h}}\right) = \frac{T-D}{W}$$

$$\sin\gamma\left(1 + \frac{V\dot{V}}{g\dot{h}}\right) = \sin\gamma\left(1 + \frac{V}{g}\frac{dV}{dh}\right) = \frac{T-D}{W}$$

The energy ratio, ER, is defined as…

$$ER = \frac{V}{g}\frac{dV}{dh}$$

…and so the flight path angle is given by…

$$\sin\gamma = \frac{T-D}{W}\frac{1}{(1+ER)} \tag{10.10}$$

To make an estimate of the flight path angle, we first need an estimate of the energy ratio. We calculate the energy ratio averaged over the entire descent, from point 1 to point 2, using an average value for the velocity. Our approximation for the energy ratio over the entire descent is given by…

$$ER = \frac{\left(\dfrac{V_2+V_1}{2}\right)}{g}\frac{(V_2-V_1)}{(h_2-h_1)} = \frac{\left(V_2^2 - V_1^2\right)}{2g(h_2-h_1)} \tag{10.11}$$

Then we solve for the flight path angle using equation (10.10) and the top of descent values for thrust, drag, and weight. To allow for some margin of safety, the desired flight path angle 10% shallower.

$$\gamma_d = 0.9 \arcsin\left\{\frac{T-D}{W}\frac{1}{(1+ER)}\right\}$$ (10.12)

The next step is to obtain the distance to the crossing fix, d_{fix} and the top of descent distance, d_{TOD}. For aircraft flying a route, the distance to the crossing fix is the distance along the route to the fix. For aircraft on vectors, this is the rhumb line distance to the fix. The top of descent is the distance from the fix at which the flight path intersects the current altitude. The aircraft will maintain steady, level flight at the current altitude and distance until one nautical mile before the top of descent.

$$d_{TOD} = \frac{h_2 - h_1}{\tan \gamma_d}$$ (10.13)

Once in the descent, the desired altitude is the height of the desired flight path at a distance d_{fix} from the crossing fix.

$$h_d = h_2 - d_{fix} \tan \gamma_d$$ (10.14)

Recall that the control system needs a desired altitude rate, not a desired altitude. As in Region 7 for steady, level flight, equation (5.7) is used to determine the altitude rate that would correct the aircraft's altitude error, but we must also consider that the desired altitude is changing per equation (10.14). We add the derivative of equation (10.14) to equation (5.7) to get the desired altitude rate.

$$\dot{h}_d = K_{\dot{h}}\left(h_d - h\right) - \frac{d}{dt}\left(d_{fix}\right)\tan \gamma_d$$

The time derivative of the aircraft's distance from the fix is simply the negative of the aircraft's groundspeed, since the ground speed and the distance from the fix are defined positive in opposite directions.

$$\dot{h}_d = K_{\dot{h}}\left(h_d - h\right) + V_G \tan \gamma_d$$ (10.15)

.

The desired speed during the descent is given either by the preferred speed profile for the particular aircraft type in a descent or that given per the speed restriction and equation (5.9) or (5.10) for IAS-based or Mach-based speed control.

11. Flight Technical Error

The flight technical error (FTE) is the inability or inexactness of the pilot or autopilot to steer the aircraft perfectly along the desired course. If the aircraft is steered by an autopilot, it is the error in steering the aircraft perfectly along the intended course. The waypoint and navigation aid errors are independent of the FTE.

Field data indicate that there is a random lateral FTE component that exists along the route segments. For the FMS-guided aircraft, the random en route wander was found to be 0.13 nm. (1σ) while for the non-FMS-guided (piloted) aircraft, it was found to be 0.7 nm (1σ), with a period varying from roughly 4 to 8 minutes during the en route flight segment (Hunter, 1996).

A reasonable model for this random lateral position wander, δr_{FTE}, is described by a second order Gauss Markov process:

$$\begin{pmatrix} \delta \ddot{r}_{FTE} \\ \delta \dot{v}_{FTE} \end{pmatrix} = \begin{bmatrix} 0, & 1, \\ -\omega_0^2, & -2\beta\,\omega_0 \end{bmatrix} \begin{pmatrix} \delta r_{FTE} \\ \delta v_{FTE} \end{pmatrix} + c \begin{pmatrix} 0 \\ u_{FTE} \end{pmatrix} \tag{12.1}$$

The terms in the expression are defined as follows:

- δr_{FTE}: The lateral position error (nm)
- δv_{FTE}: The lateral position error velocity (nm/sec)
- c: The scale factor of the forcing function
- ω_0:   The natural frequency of the system
- β: The damping of the system
- u_{FTE}: The zero mean unity variance Gaussian white noise

For terminal flight segment during ILS localizer guidance, it was found that the lateral wander tended to increase linearly with the distance from the runway (Timoteo, 1990). This suggests that a FTE based on bearing deviation angle wander is more appropriate during the terminal flight phase. Therefore, a random wander of 0.24 degrees (1σ) with an approximate time constant of 90 seconds is appropriate. In the case of the ILS, the second order Gauss Markov process is written in terms of bearing deviation angle wander as shown in equation (21.13).

$$\begin{pmatrix} \delta \dot{B}_{ILS,FTE} \\ \delta \dot{\Omega}_{ILS,FTE} \end{pmatrix} = \begin{bmatrix} 0, & 1, \\ -\omega_0^2, & -2\beta\,\omega_0 \end{bmatrix} \begin{pmatrix} \delta B_{ILS,FTE} \\ \delta \Omega_{ILS,FTE} \end{pmatrix} + c \begin{pmatrix} 0 \\ u_{FTE} \end{pmatrix} \qquad (12.2)$$

The new terms in equation (3.212) are as follows:

- $\delta B_{ILS,FTE}$: The bearing deviation angle (deg)
- $\delta \Omega_{ILS,FTE}$: The bearing deviation rate (deg/sec)

11.1   Operational Details

The flight technical error is quite simple to implement using the Gauss Markov processes with valid error parameters. The three types of flight technical error only operate when the aircraft is operating under the route following guidance system. This guidance algorithm must prompt the particular flight technical error model being used for an update to the lateral position deviation, δr_{FTE}.

11.1.1 Piloted Flight Technical Error

The piloted flight technical error proceeds once the Gauss Markov process has been initialized. For each time step that the piloted flight technical error is used, the Gauss Markov process is advanced one time step and a value for δr_{FTE} is returned. The piloted flight technical error uses a Gauss Markov process with the following parameters:

- $\beta = 0.50$: The damping term.
- $\sigma_p = 0.7$ nm: The standard deviation of the 'position'
- $\sigma_v = 0.011944$ nm/sec: The standard deviation of the 'velocity'

11.1.2 FMS Flight Technical Error

The FMS flight technical error proceeds once the Gauss Markov process has been initialized. For each time step that the FMS flight technical error is to be used, the Gauss Markov process is advanced one time step and a value for δr_{FTE} is returned. The FMS flight technical error uses a Gauss Markov process with the following parameters:

- $\beta = 0.50$: The damping term.
- $\sigma_p = 0.13$ nm: The standard deviation of the 'position'
- $\sigma_v = 1.444 \times 10^{-3}$ nm/sec: The standard deviation of the 'velocity'

11.1.3 ILS Flight Technical Error

ILS flight technical error is more complex because the Gauss Markov process is set up to return an angular deviation from the path rather than a linear distance. Therefore the linear distance must be calculated from the angular deviation $\delta B_{ILS,FTE}$ which is returned

in degrees. To get the lateral offset, equation (3.215) is used where d_s is the distance to go to the localizer. Generally, the ILS is modeled as a two segment route, where the first capture segment is from some arbitrary initial approach fix to the final approach fix, and the second segment is from the final approach fix (the beginning of the glide slope for ILS approaches) to the localizer. Therefore, the distance that the aircraft is to the localizer can be calculated by using the rhumb line distance to a fix algorithm.

$$\delta r_{ILS,FTE} = d_s \sin\left(\frac{\pi}{180} \delta B_{ILS,FTE}\right) \tag{12.3}$$

The ILS flight technical error uses a Gauss Markov process with the following parameters:

- $\beta = 0.50$: The damping term.
- $\sigma_p = 0.3^\circ$: The standard deviation of the 'position'
- $\sigma_v = 0.06 \ ^{deg}\!/_{sec}$: The standard deviation of the 'velocity'

THIS PAGE INTENTIONALLY LEFT BLANK

12. Model Verification and Validation

Verification and validation of the algorithms used to develop the TGF simulation was accomplished primarily by using a small JAVA tool that served as a testing platform for the algorithmic development. This tool, which is named TGF-test, allowed for real time manipulation of aircraft trajectories on the screen and also monitored many of the aircraft's state variables on the screen in the form of stripcharts. All algorithms that are coded in the main TGF simulation were first tested and evaluated in the TGF-test simulation. The main screen of the TGF-test algorithm is shown in Figure 12.1 where aircraft trajectories are superimposed over an electronic map of fixes and routes. The aircraft icon, which represents the flying aircraft, shows the heading orientation so the difference between ground track and heading can also be viewed visually.
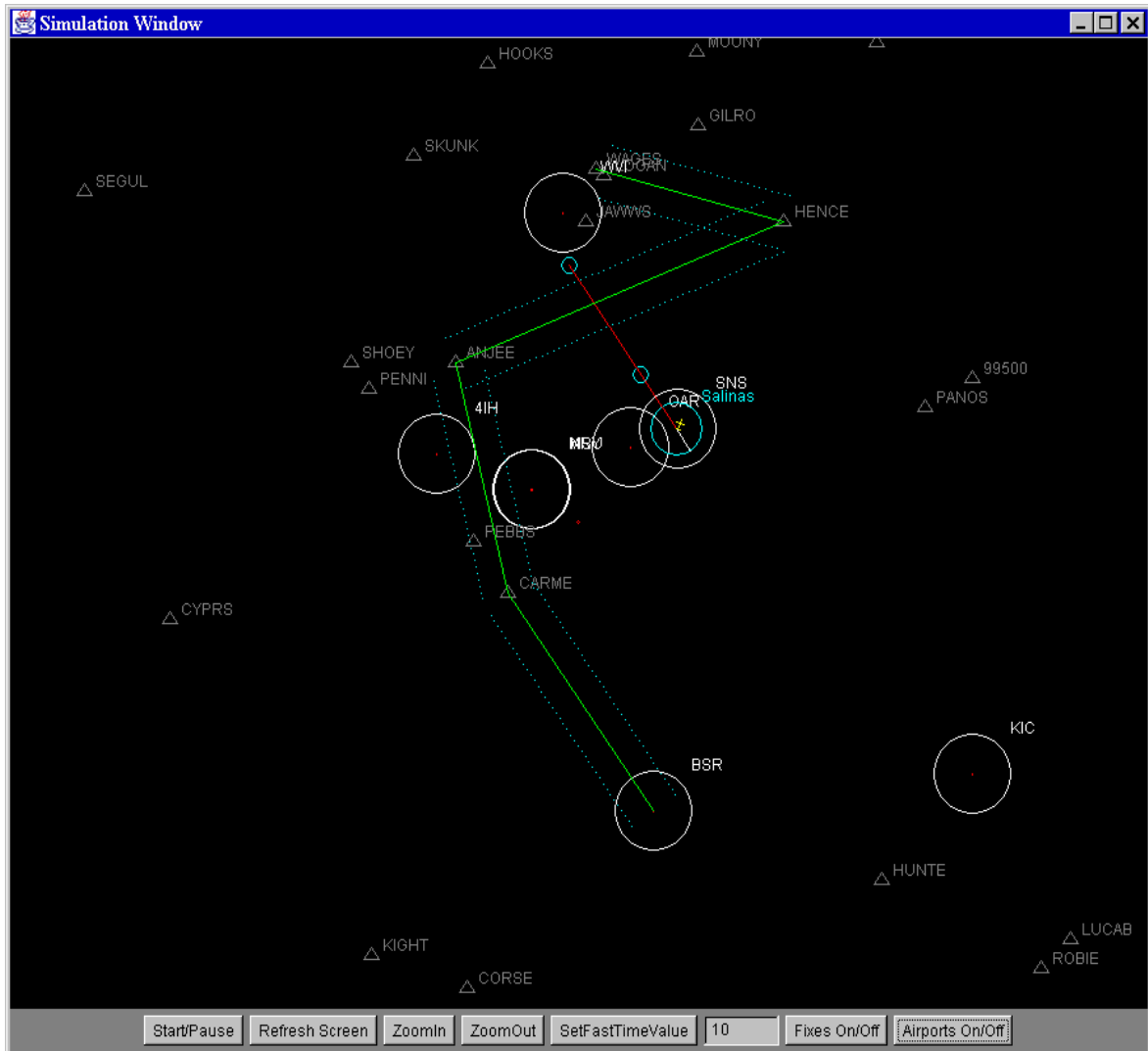
**Figure 12.1.** Simulation Window for TGF-test

The aspects of the TGF simulation that needed verification are as follows:

- Constant airspeed climbs and descents
- Mach/CAS descents and CAS/Mach climbs
- Speed changes during climbs and descents
- Automatic route capture
- Vectored route capture
- Initial fix route capture
- Segment transition
- Flight technical errors
- Navigation errors
- Take-off and landing

When appropriate, the TGF simulation model was compared to Pseudocontrol, the aircraft dynamics kernel of PAS. PAS, the NASA tool for trajectory generation, has been considered as an acceptable baseline for aircraft performance. Such cases include the verification of climb and descent performance as well as speed changes. For other operations, such as route capture and route following, visually inspecting the maneuvers is sufficient to insure proper operation.

12.1   Constant Airspeed Climbs and Descents

The PAS model in Pseudocontrol uses much higher fidelity aircraft and engine models than what the TGF model uses, so it is expected that there would be some variation in performance. Generally, however, the difference in the actual trajectories generated by the simulations is negligible. While the trajectories are nearly identical, the TGF model does not produce fuel burn estimates which are as accurate as the PAS model because PAS uses many more coefficients in the model. Two comparisons of Pseudocontrol and TGF-test are presented in this section.

The first comparison between Pseudocontrol and TGF-test is shown in Figure 12.2. Figure 12.2 illustrates an MD-80 at 10,000 ft and 280kts as it initiates a constant indicated airspeed climb to 30,000ft. Four stripcharts are shown in the plot, each representing a different aircraft state variable. These are Mach, indicated airspeed, altitude, and the lift coefficient. The Pseudocontrol plots are represented with the dark line and the TGF-test plots are shown in gray. The simulation shows a good match between the two models. Initially, there is a small fluctuation in the indicated airspeed of both models while the climb is established. Once the climb is established, both models hold the appropriate 280kt airspeed. The aircraft climb nearly identically in terms of altitude tracking. This is very important since the air traffic controllers are sensitive to the changing rate at which altitude increases. The Mach plot shows that both models track
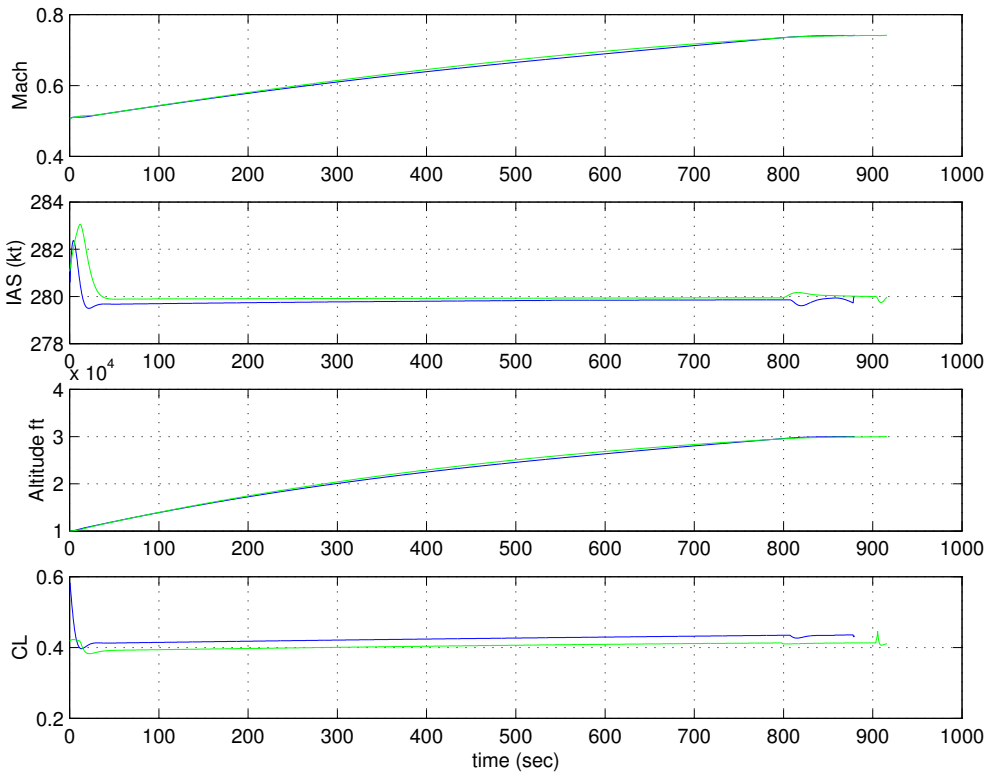
Figure 12.2. Comparison of Pseudocontrol (black) and TGF-test (gray) in a constant indicated airspeed climb and 280kt

Mach number identically as well. Considering the lower fidelity model represented in the TGF-test system, over Pseudocontrol, the data match is quite good.

A similar comparison is made in a descent. An MD80 weighing 130,000lbs is commanded to descend from 30,000ft to 10,000ft at an airspeed of 300kts. The descent is shown in Figure 12.3. When the aircraft initiate the descent, there is some fluctuation in the indicated airspeed. In this example, the TGF-test model has a larger fluctuation than the Pseudocontrol simulation, but the fluctuation is still only 1.5kts. This small fluctuation is acceptable. Once the descent is established, both aircraft hold the commanded airspeed well. The altitude profile of the TGF-test aircraft matches the Pseudocontrol aircraft well and the Mach number varies properly also.

12.2 Mach/CAS descents and CAS/Mach Climbs
The idle thrust Mach/CAS descent and full thrust CAS/Mach climb are important features of the aircraft simulation because jet airliners are most likely to use these types of maneuvers for climbs and descents. Because the maneuvers are similar, this section will considers as its only test case, the idle thrust descent. Full thrust CAS/Mach climbs are simply reverses of the descents.

When an idle descent is initiated, the throttle is pulled idle and the pilot descends at a rate so that the aircraft maintains the desired Mach of the desired Mach/CAS pair. At low speed and low altitude, convention dictates that the speed of aircraft be measured in terms of indicated airspeed. Therefore at some point during the descent, the pilot will capture the desired CAS of the Mach/CAS pair. As the pilot descends at a constant Mach, the indicated airspeed meter will show an 'increase' in speed. At some point during the descent, the indicated airspeed meter will read the desired indicated airspeed for the
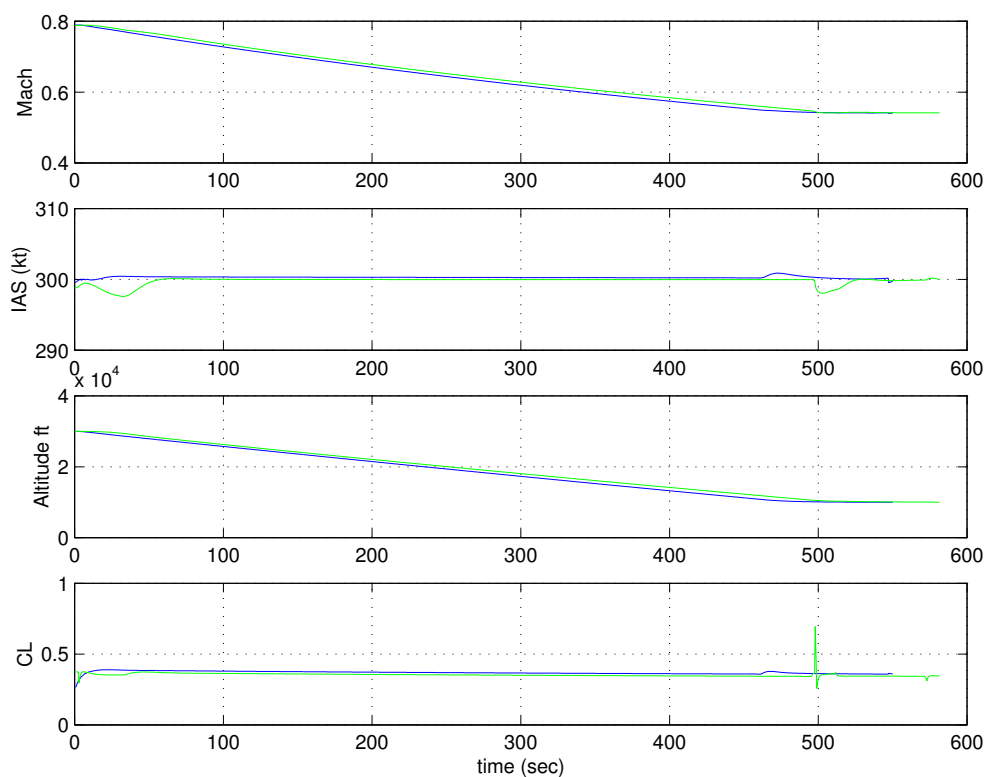

Figure 12.3. A comparison of Pseudocontrol (black) and TGF-test (gray) in a descent at a constant indicated airspeed of 300 kts

descent. At this point, the pilot tracks the desired CAS instead of the Mach. Typically there are four stages to a Mach/CAS descent. These stages are:

1. Change speed from the cruising Mach, M_1, to the descent Mach, M_2.
2. Descend at M_2. The aircraft descends at M_2 until reaching a predetermined CAS.
3. Descend at constant CAS. The aircraft descends at its constant descent CAS until it reaches the metering fix crossing altitude, where it levels off.
4. Decelerate to the metering fix crossing speed. Finally, the aircraft decelerates to 250 kt, the metering fix crossing speed of typically 250kt.

210

For this section's comparison between Pseudocontrol and TGF-test, we start with an MD80 at 30,000ft in cruise at M0.76. The aircraft initiates a Mach/CAS descent with the following speeds: (M0.76/320kt). The aircraft then levels out at 10,000 ft maintaining 320kts. Figure 12.4 shows the maneuver. The match between the Mach and indicated airspeeds is good and the transition between Mach and indicated airspeed is smooth without any undesirable transients. Similarly, the level off at 10,000 ft is smooth without any overshoot. Most importantly, the altitude profiles for both simulations match very well.
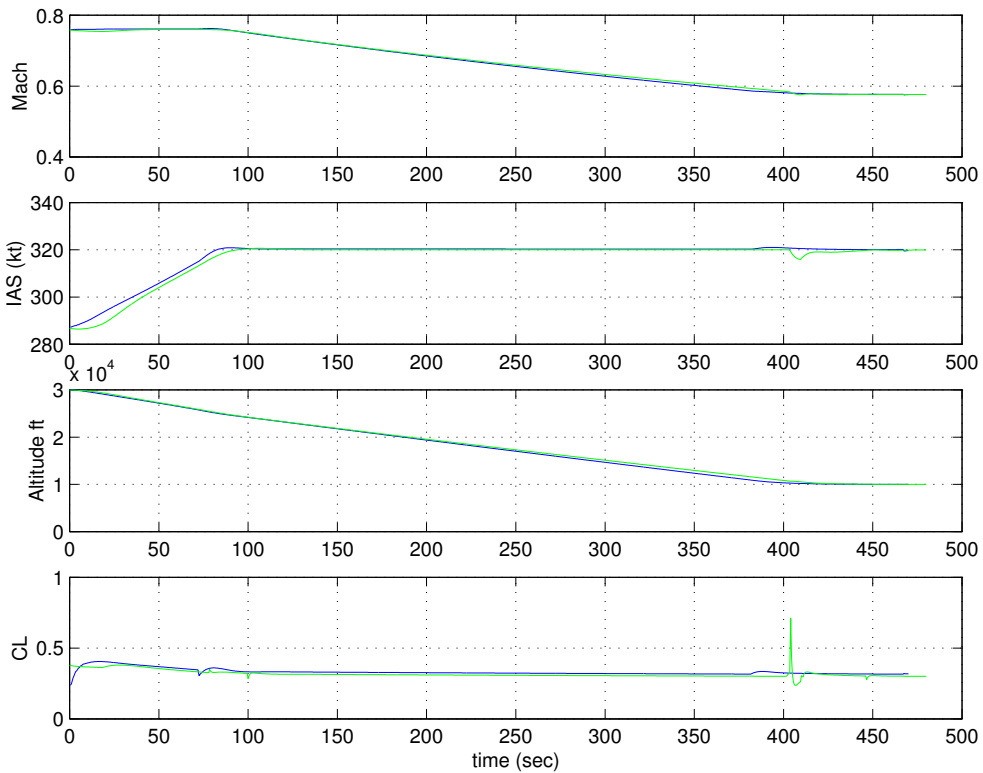

Figure 12.4. Comparison of Pseudocontrol (black) and TGF-test (gray) performing a Mach/CAS descent from 30,000 ft to 10,000ft using an MD80 at 130,000lb

12.3 Speed Changes

Speed changes, while they do not take much time in the course of a flight, do give a good indication of the model's fidelity in terms of drag and thrust. Consider an acceleration. For the aircraft to have the proper acceleration, in a speed up maneuver, the excess thrust must be correct. This excess thrust is a function of the total available thrust and the total drag. If either is off, the acceleration will not be right. However, errors in either could cancel each other out. For instance, a high drag number could be canceled by a high thrust value. Decelerations, because they are performed at idle thrust, tend to remove the thrust from the system so the primary deceleration factor is the aircraft's drag. If accelerations and decelerations are both studied,

generally conclusions about both the drag and thrust can be made. The deceleration gives insight into the fidelity of the drag
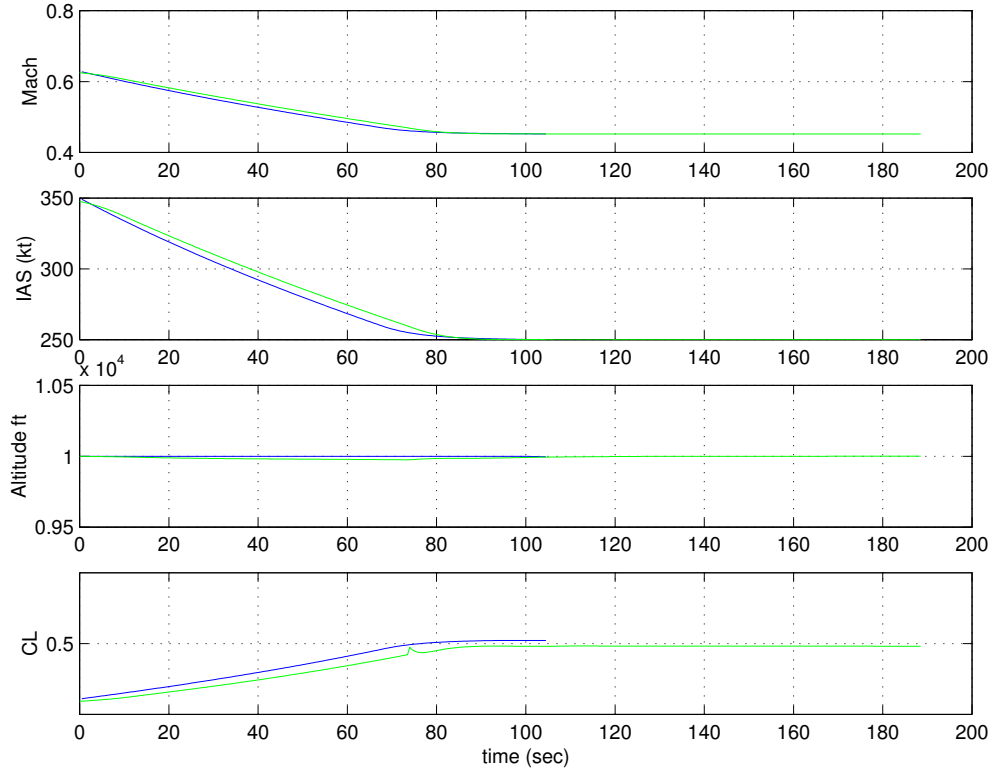

Figure 12.5. A deceleration of an MD80 from 350kts to 250kts while at 10,000ft using Pseudocontrol (black) and TGF-test (gray) simulation tools

model, and the acceleration gives insight into the thrust to drag ratio. Assuming drag information is known from the deceleration, thrust information can be derived from the acceleration.

First, a deceleration is considered. An MD80 at 130,000lbs cruising at 10,000 ft is slowed down from 350kts to 250kts. Figure 12.5 shows the deceleration maneuver. The two simulations show good agreement during the slowdown with no undesirable transients in either simulation. Furthermore, altitude is held constant at 10,000ft. From this plot we can assume that the drag information in the MD80 model is accurate.

Next, an acceleration is considered. The same MD80 is accelerated from a cruise condition of 250kts and 10,000ft to 350kts while maintaining altitude. The maneuver is shown in Figure 12.6. The slope of the speed curves for both simulations match very well, suggesting that the thrust model for the aircraft is working well. The altitude is held reasonably well; however, the TGF-test model does show a slight tendency to let the
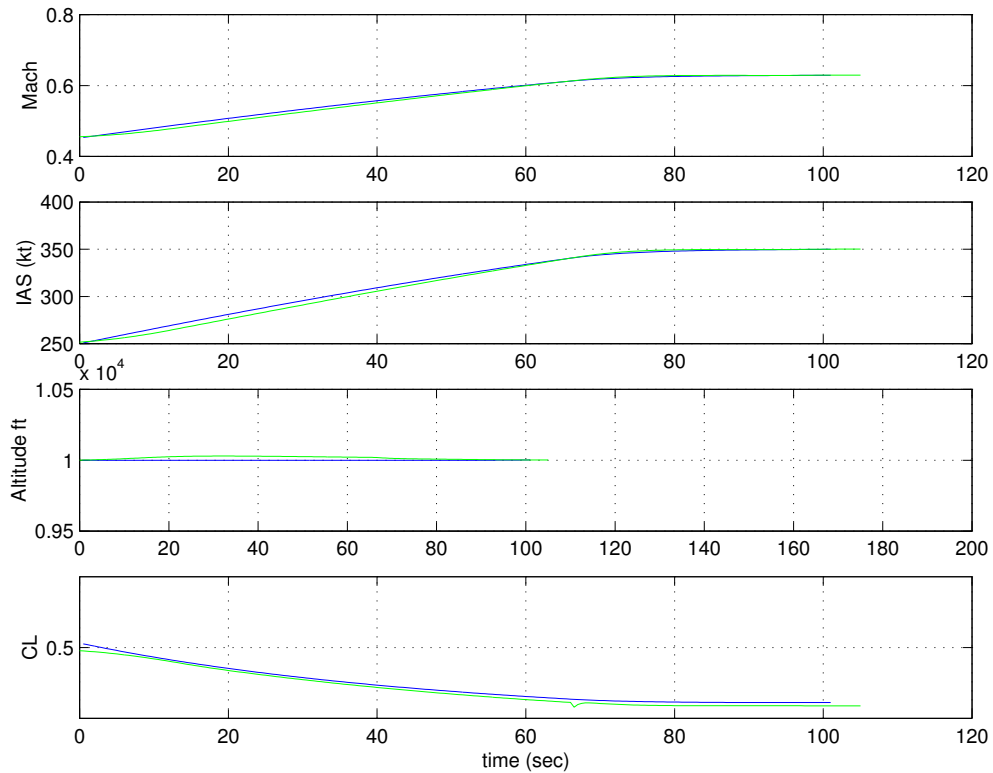
Figure 12.6. An MD80 accelerating from 250kts to 350kts while maintaining 10,000ft using Pseudocontrol (black) and TGF-test (gray) simulation tools

altitude drift slightly. The altitude variance shown on the plot is on the order of 10ft, so it is not a major concern. From the results in Figure 12.5 and Figure 12.6 we conclude that the thrust and drag models for this aircraft are good.

Speed changes are also performed at higher speeds to test the compressibility drag model. First a deceleration is considered as shown in Figure 12.7. An MD80 at 30,000ft and Mach 0.8 is decelerated to Mach 0.6. There is a slight discrepancy here between the Mach numbers of the two models. The TGF-test simulation takes longer to enter the deceleration whereas the Pseudocontrol model enters the deceleration immediately. One reason for this gentle initiation of the maneuver is that the TGF-test simulation models engine spooling whereas the Pseudocontrol model does not. Once the deceleration is established, notice that the two Mach lines are nearly parallel. This suggests that the rate of acceleration is very close but the slow initiation time on the part of TGF-test offsets the maneuver. The result is that the maneuver takes 7-10 seconds longer with TGF-test than it does with Pseudocontrol. Since the rate of acceleration is nearly the same, we know that the drag models are very close. The difference in initiation is explained by the differences in the spooling lags of the engines and some differences in control system design.

213

If the longer deceleration is a problem, the effectiveness of the spooling lags could be decreased. Presently this is not a concern.
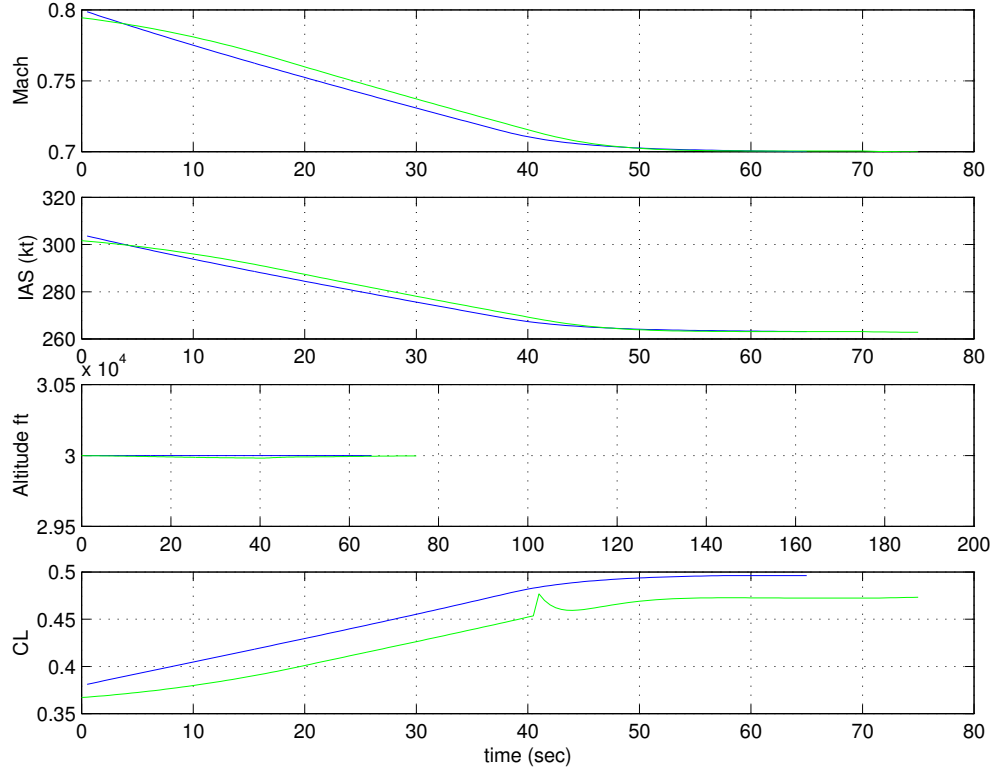

Figure 12.7. An MD80 decelerating from Mach 0.8 to Mach 0.6 while maintaining 30,000ft using Pseudocontrol (black) and TGF-test (gray) simulation tools

The Mach acceleration is shown in Figure 12.8, where the MD80 accelerates from Mach 0.6 to 0.8 while maintaining 25000 ft of altitude. Here we do not see the same spooling lags in the initiation of the maneuver. Since the spooling lags are the same for both increases and decreases in thrust level in the TGF-test model, there is no easy explanation for the discrepancy. At any rate, the two models are virtually identical in the Mach acceleration.

12.4   Speed Changes during Climbs and Descents

One of the more insidious problems encountered during the design of the longitudinal control system was the problem of changing speeds during climbs and descents. Section 4.2 of the longitudinal control system discusses the problem in depth and explains how the ultimate solution to the problem was the ramping of inputs. Generally, the problem centered around the fact that large speed changes while climbing or descending was not anticipated, and the feedback control system was only set up to handle small changes. This meant that the control system had

rather high gains to keep the speed errors small. When the high gains were applied to the large errors, the maneuvers became
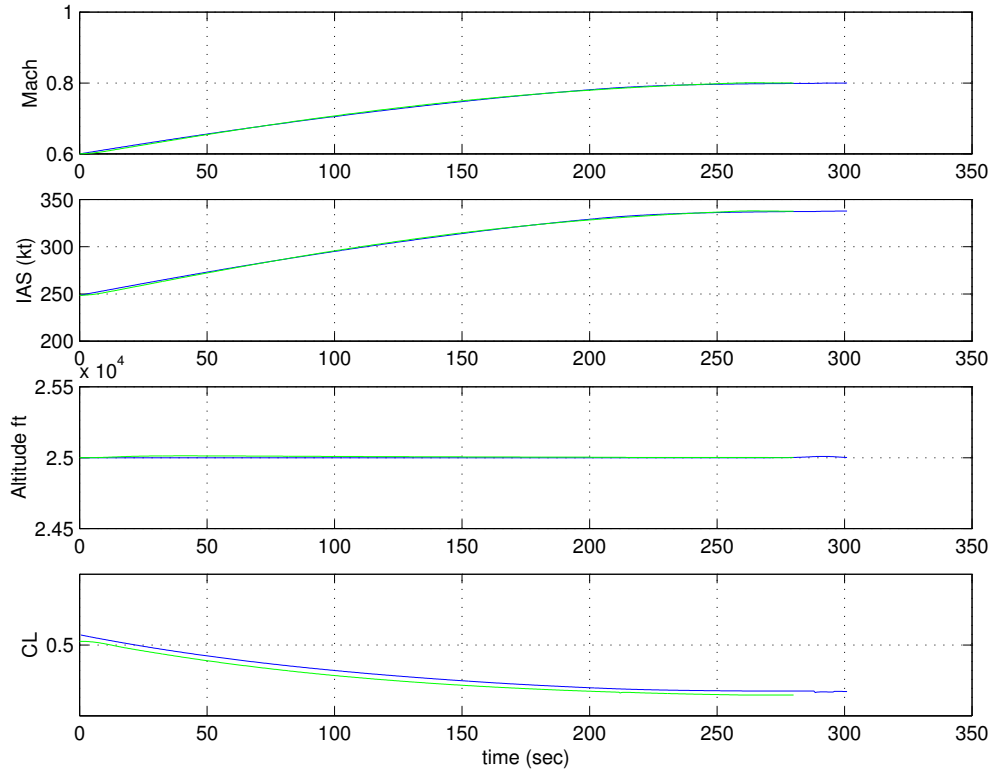

Figure 12.8. An MD80 accelerating from Mach 0.6 to Mach 0.8 while maintaining 25,000ft using Pseudocontrol (black) and TGF-test (gray) simulation tools

violent. It was easy to see what was happening. During climb and descent, the control stick rather than the throttle is used to control speed. Therefore, when the feedback control system saw large errors from a user, the control stick was moved violently to correct the situation. This section uses TGF-test to demonstrate the speed changes during climbs to illustrate the stability of the maneuvers using the ramped inputs.

Figure 12.9 illustrates an MD80 which is initially at 10,000ft and 250kts. A climb is initiated to 30,0000ft. During the climb, the speed of the aircraft is first increased to 320kts and then reduced to 280kts. Finally the speed is increased to 300kts where it is held until the aircraft completes the climb. The point of the plot is that speed changes are made gracefully and do not cause any unusual patterns in the altitude profile other than the normal affects associated with the change of speed during a climb. Furthermore, attention to the lift coefficient curve shows that the control system is well behaved and is not commanding unreasonable control inputs. There also isn't any chatter in the system.
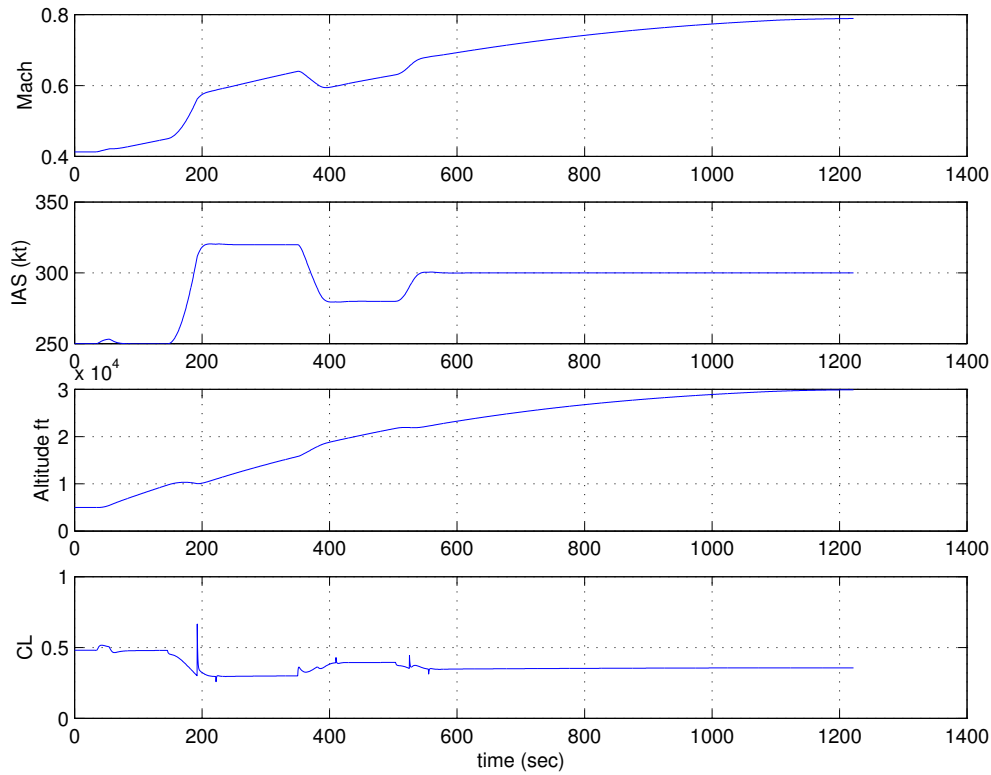
Figure 12.9. An MD80 in a climb with various speed changes using the TGF-test simulation

This is a direct result of the ramped inputs preventing large errors from occurring in Regions 3 and 6.

12.5 Automatic Route Capture

The TGF-test algorithm uses several route capture algorithms to capture routes. The first of these is the automatic route capture algorithm which captures a route regardless of the aircraft's location with respect to the route or its orientation. To verify this always works, many test cases were run. Generally, the key aspects which determine a good capture are whether or not the aircraft chooses a reasonable segment, and whether or not overshoot is excessive. Some of the more difficult test cases are presented in this section.

The first capture, shown in Figure 12.10, illustrates the case where the aircraft is very close to a segment along a route but headed in the wrong direction. When the route capture algorithm is initiated, the automatic route capture algorithm rightly chooses the segment which is closest to the aircraft. Then the algorithm calculates a dynamic fix for intercept along the route. However, because the aircraft is already so close to the segment, the aircraft penetrates the 1 turn radii boundary defining the route following algorithm
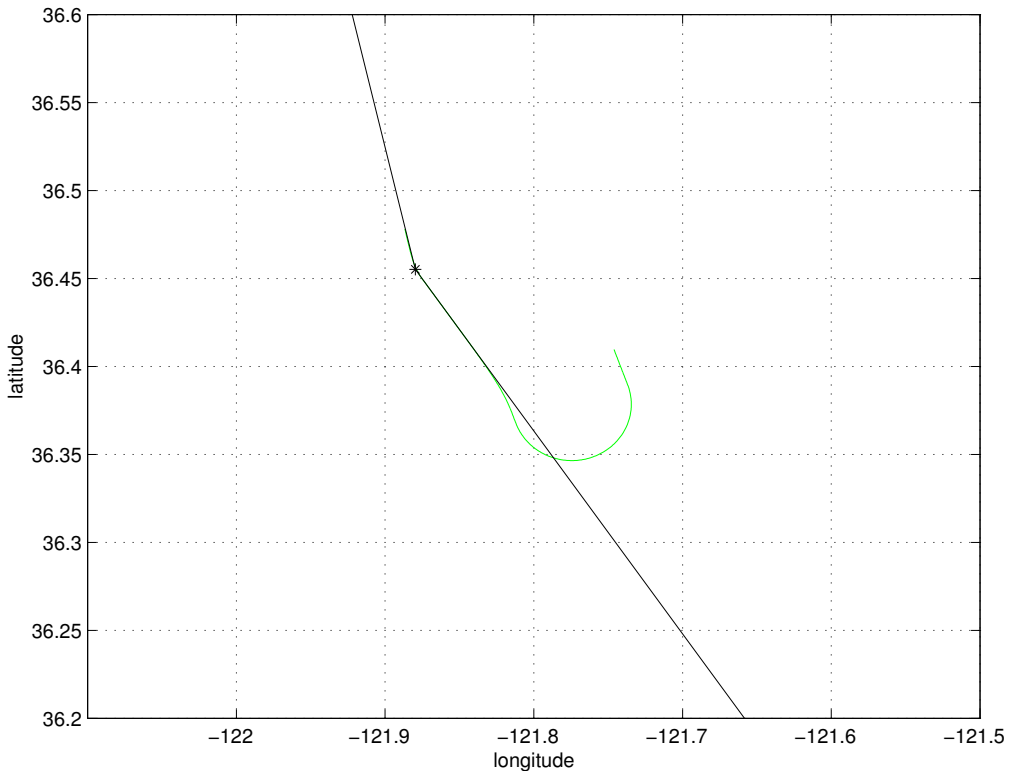
Figure 12.10. Automatic route capture with the aircraft close to the route but headed in the wrong direction

long before the aircraft is able to converge on a heading to the dynamic fix. Therefore, this particular scenario is a test of the route following algorithm more than it is a test of the automatic route capture algorithm. It demonstrates that the route following algorithm can handle large discrepancies in aircraft heading relative to the bearing of the segment. The aircraft makes a right turn towards the segment and then slightly overshoots the segment. This overshoot is unavoidable because the aircraft is well within 2 turn radii of the segment before the maneuver is initiated. The performance shown in Figure 12.10 is exactly what is desired.

The next route capture maneuver, shown in Figure 12.11, demonstrates the case where the aircraft is at a considerable distance from the capture segment. This route capture demonstrates the use of the dynamic fix. As stated in Section 8.4.3.1, the dynamic fix is an imaginary fix which is created by the system at some location along a segment and is used as a point of reference for capture. When the automatic route capture algorithm was first conceived, it seemed as though the most obvious method of capturing the route was to fly some intercept heading to the route. For instance, once the capture segment was determined, the aircraft could be given an intercept heading of 45 degrees and intercept the segment. However, this method seemed to have some inherent limitations. First, the aircraft would always intercept using 45

217
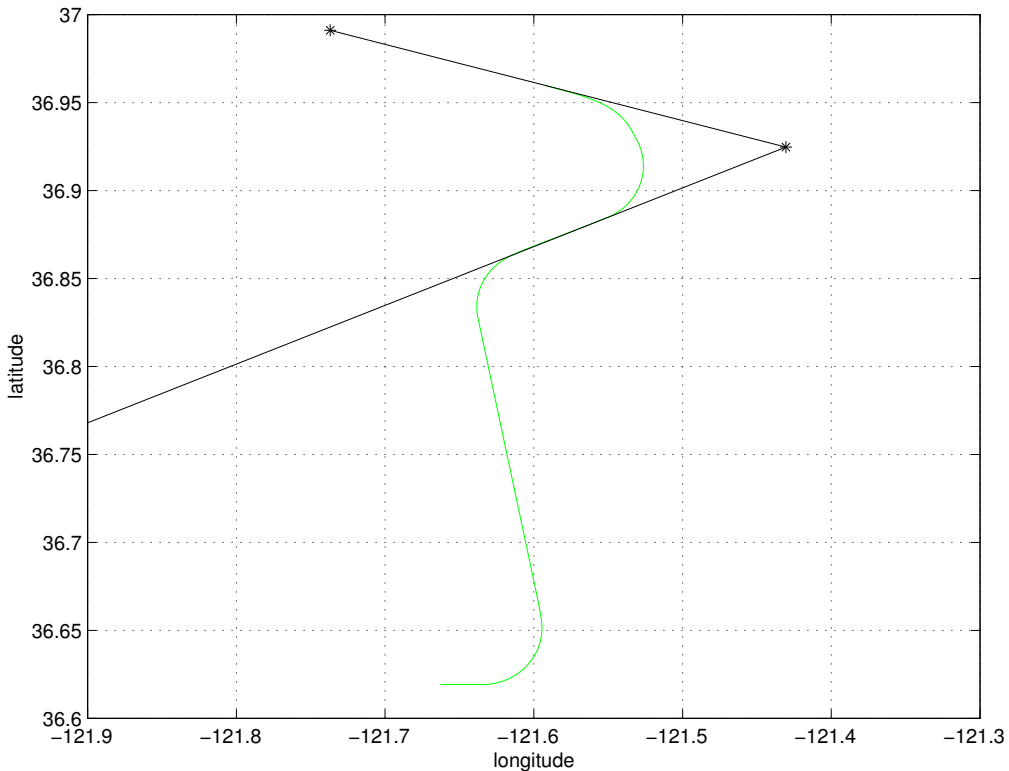
Figure 12.11. Automatic route capture with an aircraft far from the capture segment

degrees regardless of how far the aircraft was away from the segment. An aircraft far away from the capture segment might pass the segment before ever capturing it. Figure 12.11 illustrates an example of this type of capture situation.

To avoid the problem of aircraft overshooting capture segments, a dynamic fix is placed on the segment to be captured, and the aircraft is commanded to fly toward the dynamic fix. In this case the further aircraft naturally uses a larger intercept angle as seen in Figure 12.11. This system insures that the proper segment is captured and also provides some apparent variety in intercept angles so that all aircraft do not appear to behave the same. The capture algorithm does exactly what is expected. The automatic route capture guidance converges on a heading that leads directly to the dynamic fix, and then captures the route when the aircraft is within 1 turn radii of the segment. There is no overshoot because the aircraft is given enough space to maneuver in this example.

The track in Figure 12.11 also demonstrates one other important performance trait of the algorithm. The algorithm switches segments and captures the next segment along the route without overshoot in spite of the acute angle which joins the segments. This example demonstrates the effectiveness of the segment transition algorithms at assuring

218

smooth segment transition regardless of segment geometry. The case shown in Figure 12.11 is a more difficult segment transition maneuver.
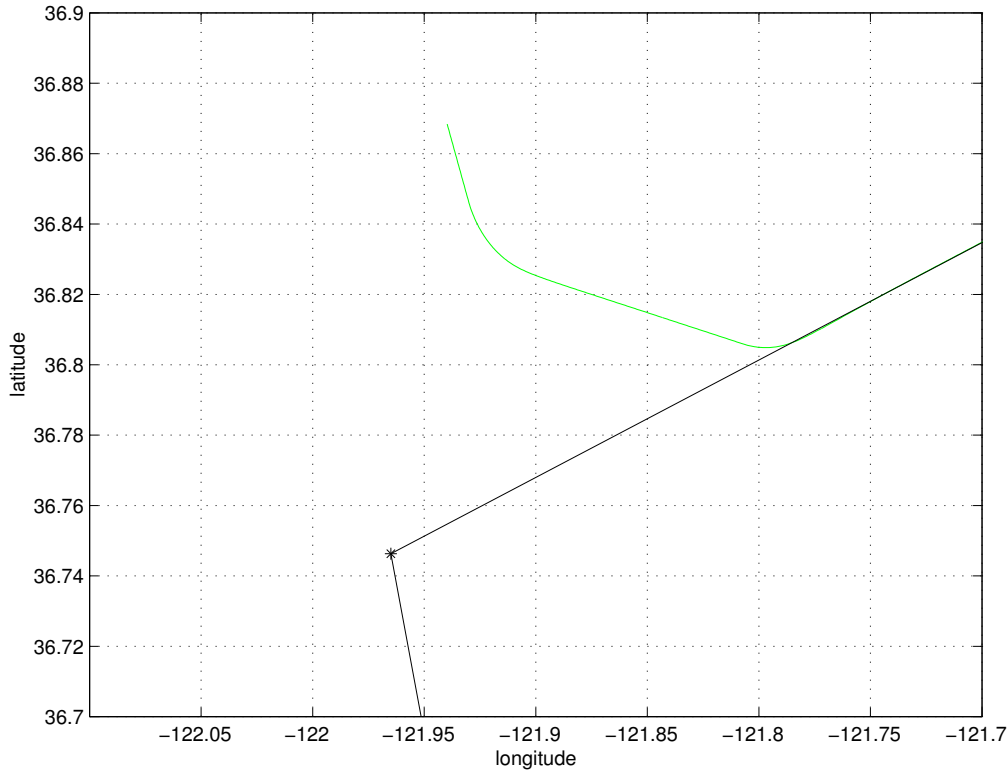

Figure 12.12. Automatic route capture with the aircraft headed perpendicular to route

Figure 12.12 is the least sensational of the capture examples in that it demonstrates a rather easy and likely scenario. The aircraft is relatively close to the capture segment and heading in the general direction of the segment. Therefore, the aircraft captures the segment with ease. This example does show how the dynamic fix does make the capture angles vary as a function of the distance that the aircraft is from the segment. Being relatively close in this example, the aircraft takes a smaller intercept angle which is apparent in the difference between the original heading and the intercept heading. Note that in this case, the original heading would have intercepted the segment as well. When the aircraft is well within 1 turn radii, the aircraft turns to intercept the segment without any overshoot. This is exactly what is desired.

The final automatic route capture example, shown in Figure 12.13, demonstrates the capture of a route from an ambiguous area relative to the route. As discussed in Section 8.4.1, there is a "dead" region where two segments meet as shown in Figure 12.13. If an aircraft is in this region, the normal segment determination algorithms will find that the aircraft is in front of the trailing

segment, behind the leading segment, and will not return a capture segment. In this case, another criteria is used which checks the aircraft's
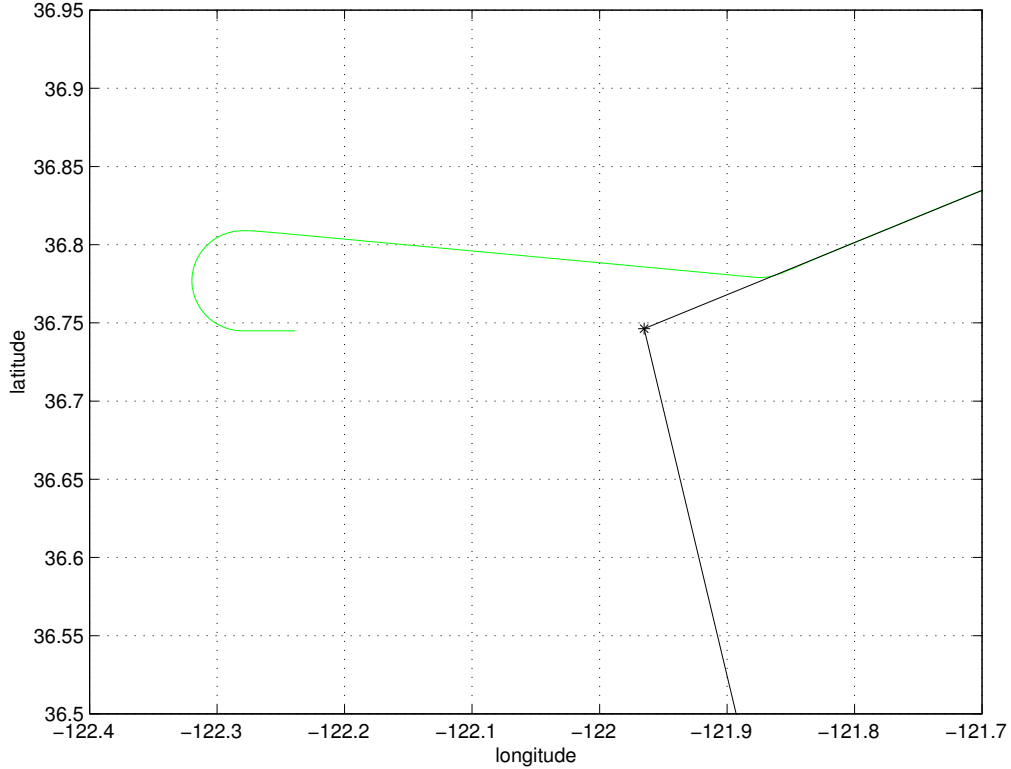

Figure 12.13. Automatic route capture with aircraft in an ambiguous region between segments

distance from every segment's trailing fix. It then chooses to capture the segment that is associated with the closest trailing fix. In Figure 12.13, the latter logic is used to determine the appropriate capture segment. Once the appropriate segment is determined, the aircraft is flown towards a dynamic fix and ultimately captures the segment with no overshoot.

12.6 Vectored Route Capture

The vectored route capture algorithm steers the aircraft along a user specified heading until the aircraft intercepts the route. Each time step, the algorithm determines which segment is best to capture and, each time step, the algorithm determines if it is time to merge onto the route. It should be noted that the algorithm has no control over the initial heading. Therefore, if the user supplied heading steers the aircraft away from the route, the guidance law is not able to do anything about it although it will provide a warning if the aircraft is unlikely to intercept the route. It is important that this algorithm work properly because it is the most heavily used capture algorithm.
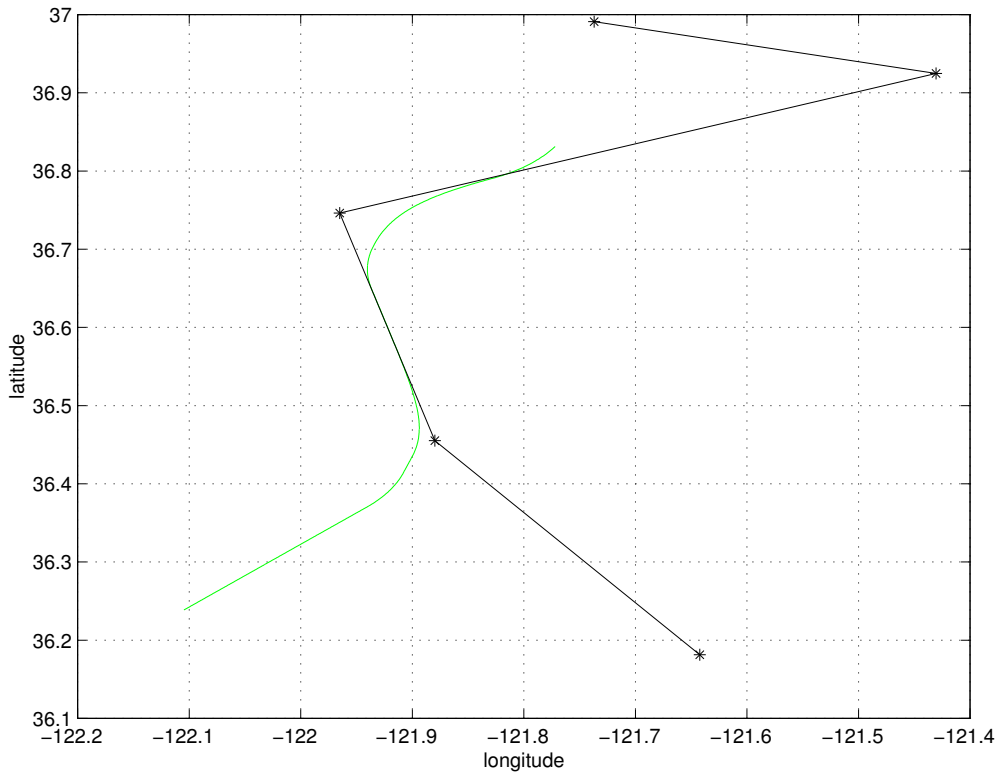
Figure 12.14. Vectored route capture from an ambiguous position

Because the vectored route capture algorithm does not choose the intercept heading, it must be prepared to work with all intercept headings, including those which may be poor choices. To test the vectored route capture algorithm several poor choices are provided. The first scenario, shown in Figure 12.14, demonstrates a vectored heading where the choice of capture segments is ambiguous. Because the algorithm can not control the heading of the aircraft, it is possible that the best capture segment could change depending on the aircraft's flight path. In our scenario, the aircraft is initially pointed so that the flight path will intercept the front end of the trailing segment; however, the best segment for capture is actually the next segment along the route. The aircraft realizes this and turns onto that segment without overshoot when the segment proximity permits.

Figure 12.14 also shows the aircraft transitioning to a new segment while on the route. This maneuver provides another example of the segment transition logic at work where the transition between segments occurs without any overshoot. This is good performance. Notice that the aircraft track is stopped just as the aircraft starts to make the turn onto the final segment at the route.

The final example of vectored route capture is shown in Figure 12.15. In this example, the aircraft is commanded to capture a route while being vectored on a heading which tends to be in the opposite direction of the route. This type of capture is particularly challenging because the aircraft must make such a large turn to capture the segment. As can be seen in Figure 12.15, the aircraft maintains the vectored heading until it is time
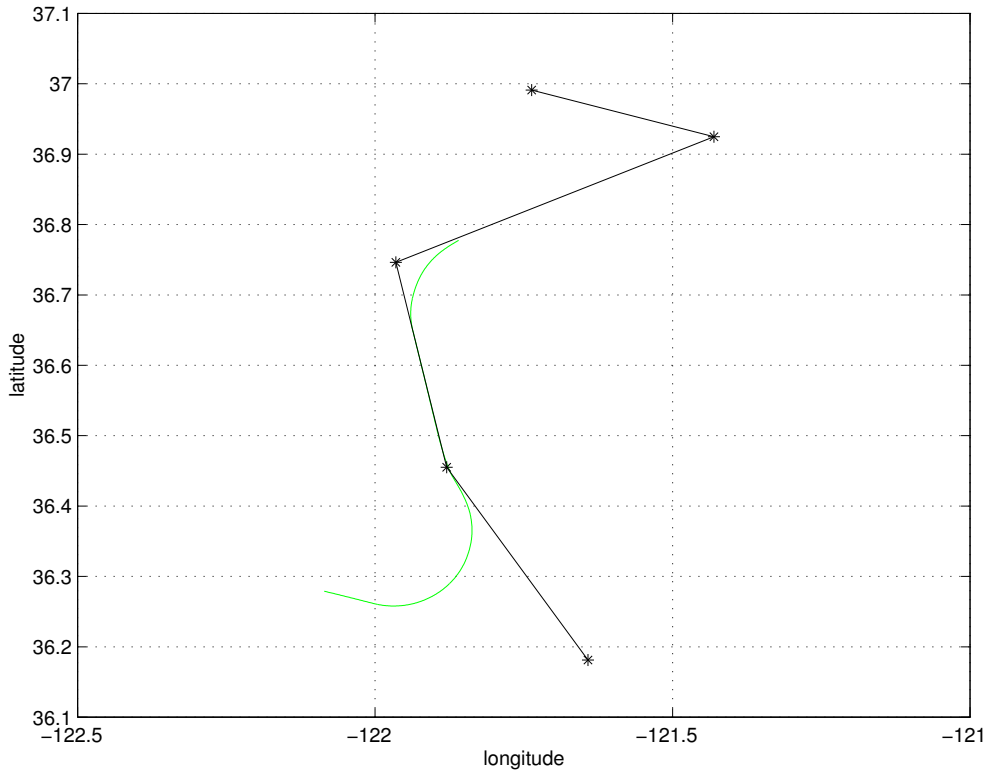
Figure 12.15. Vectored route capture when the vectored heading tends to be in the opposite direction of the route

to merge onto the route. Once the appropriate distance is reached, the aircraft merges with the route with no overshoot.

12.7   Initial Fix Route Capture

One requirement for the simulation was that the aircraft had to be able to start flying along a route by passing through the initial fix. This type of route capture algorithm is actually the least complicated because there is no need to determine a capture segment and there is no need to determine when to initiate route following. The route following is initiated as soon as the aircraft passes through the initial fix. Several examples of this maneuver are shown.

The first example, shown in Figure 12.16, illustrates the unlikely case where the aircraft is commanded to fly back to the beginning of the route from some location in front of the route. This maneuver turned out to be very handy for testing, but it is not likely to be used much in practice. It is interesting to see how this algorithm differs from the other capture algorithms. The

algorithm directs the aircraft to fly to the initial fix. However, unlike the automatic route capture algorithm, the initial fix capture flies the aircraft through the initial fix before capturing the route. This method guarantees overshoot when used in this
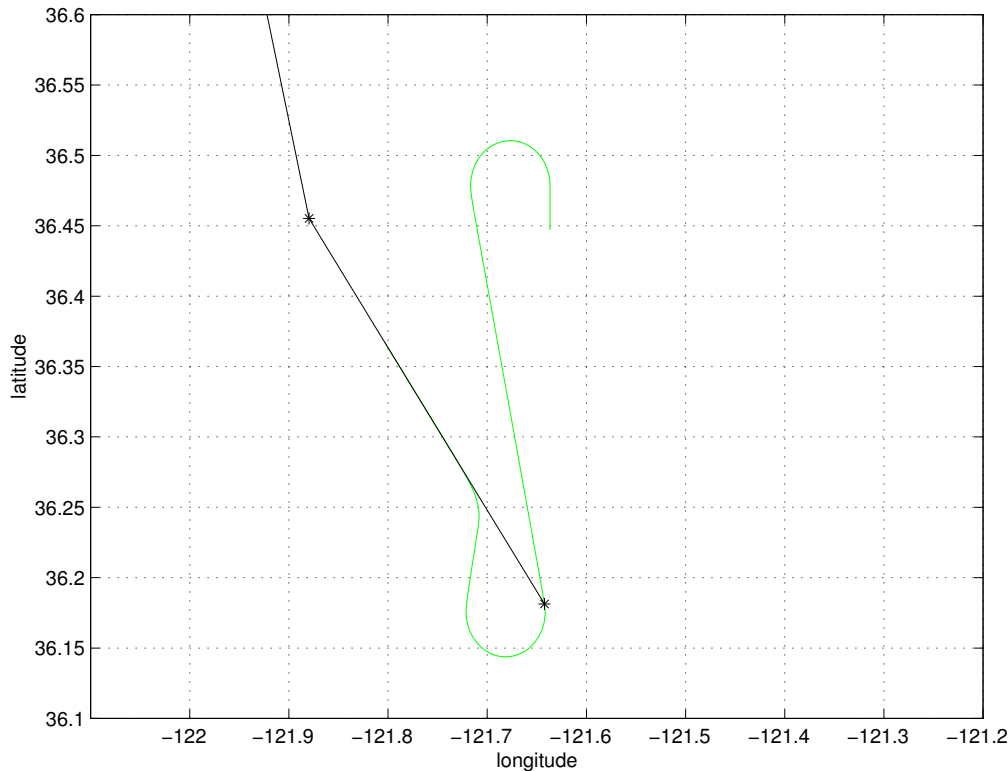

Figure 12.16. The initial fix capture algorithm being used to vector an aircraft back to the beginning of the route

fashion. Naturally, this algorithm is really designed to assure that an aircraft behind a route captures the route by flying through the first fix. This case is illustrated in Figure 12.17. Notice that when the algorithm is used as it is intended, the overshoot is minimized. However, there will usually be some overshoot because the algorithm is constrained to fly through the initial fix.

12.8 Segment Transition

The segment transition algorithm controls when the aircraft initiates a turn from one segment to another. The algorithm must initiate a turn with enough space to smoothly make the transition. Because so many examples of segment transition are contained in the plots dealing with route capture, no additional plots are presented here. The reader should observe the transitions in Figure 12.10, Figure 12.11, Figure 12.14, and Figure 12.15. Figure 12.10 shows a typical segment transition where the difference in bearing angle between segments is small. The aircraft manages these without difficulty. The other examples all deal with transitions between segments with large bearing differences. These are more complex because the amount of space allotted for the transition is
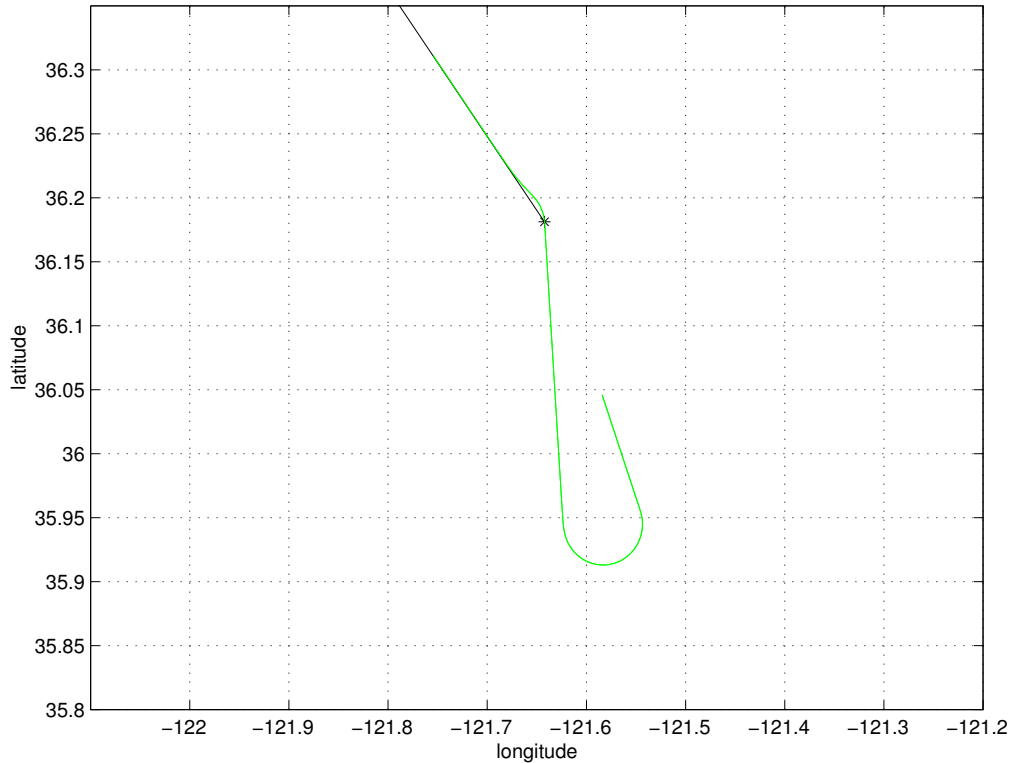
Figure 12.17. An aircraft capturing a route from behind using the initial fix capture algorithm

more constrained. Excessive overshoot occurs if the transition logic isn't designed to handle these cases. As can be seen from the plots, the current segment transition logic has no difficulty with these types of maneuvers.

12.9 Flight Technical Error

The flight technical error (FTE) is the inability or the inattention causing the pilot to steer the aircraft perfectly along the desired course. If the aircraft is steered by an autopilot, it is the error in steering the aircraft perfectly along the intended course. In terms of the previous navigation error sources, the FTE is considered to be the guidance and control error, where only the guidance error is included. The waypoint and navigation aid errors are not included. For the TGF simulation, there are two distinct flight technical errors modeled. The first flight technical error is the piloted flight technical error, the error associated with a human pilot following a route. The second error is the FMS error, the error associated with an FMS driven autopilot guiding the aircraft. Generally, the only difference between these errors is the magnitude of the standard deviation and the frequency of the mode. The statistics summary is reprinted in Table 12.1

Table 12.1 Error Statistics Summary

Error Source	Type	Bias (1σ)	Beta
FMS Enroute FTE	2nd Order	0.13 nm	0.7
	Gauss Markov	5.2 kts	
Piloted Enroute FTE	2nd Order	0.7 nm	0.5
	Gauss Markov	42 kts	

Generally, the only means of testing the final algorithms is to make sure that the lateral variation stays within the standard deviation requirements. This is difficult to do using graphical representation of trajectories, so generally tabulated data were used to verify the flight technical error. However, the trajectories provide a richer understanding of what the flight technical data does to the simulation.

Four plots are presented in this section demonstrating the en route flight technical error developed for the simulation. These plots were all created using a closed route so that an aircraft would fly around the same route creating a Monte-Carlo simulation. The route was flown at different speeds using both piloted and FMS flight technical error. Figure 12.18 shows an aircraft flying at 250kts and 5000ft. This is a relatively slow configuration so the trajectories show a considerable amount of 'wobbling' back and forth along the route. This is because the frequency of the lateral flight technical error is not a function of the aircraft's speed. Because the aircraft covers a greater distance per unit of time when moving faster, the flight technical error always appears to be more extreme in slower aircraft. This point is aptly demonstrated when Figure 12.18 is compared to
Figure 12.19 where a piloted aircraft is traveling at 300kts and 30,000ft. Even though the same flight technical error is in effect, the faster aircraft appears to have less 'wobble' in it trajectory, although the lateral offset of both plots is about the same.

The final two plots show the same aircraft using FMS. Figure 12.20 shows the aircraft moving at 250kts and 5000ft. Figure 12.9 shows the aircraft moving at 300kts and 30,000ft. Since the FMS has only about 20% of the lateral offset that the piloted flight technical error has, the aircraft trajectories are much tighter. This reduction in lateral offset over the piloted flight technical error is readily apparent; however, it is not impossible to get a sense for the 'wobble' of the aircraft along the route in either plot, with this scale of distance.
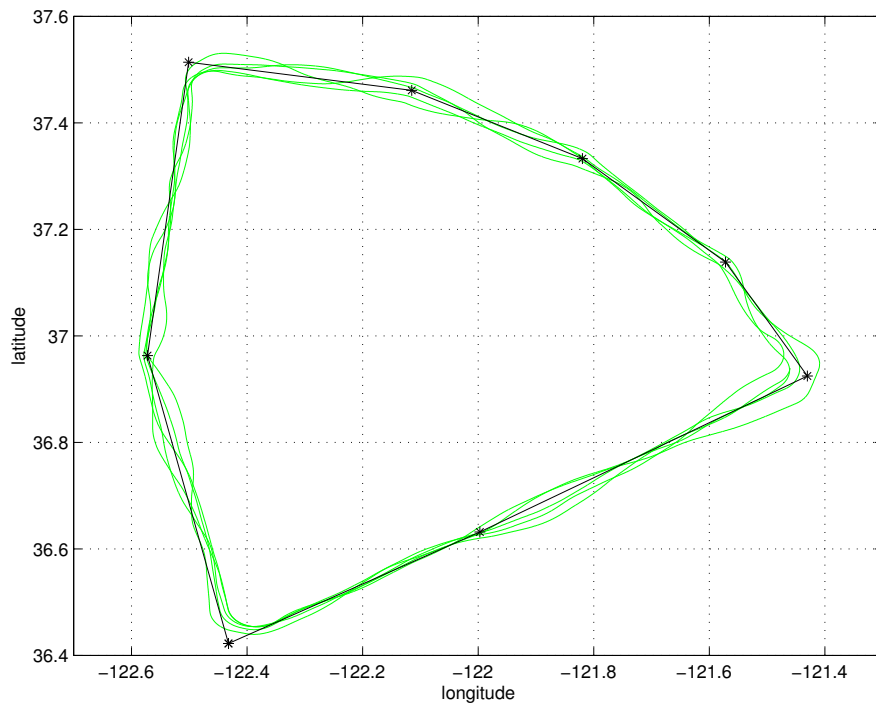
Figure 12.18. Piloted flight technical error of an MD80 traveling at 250kts and 5000ft
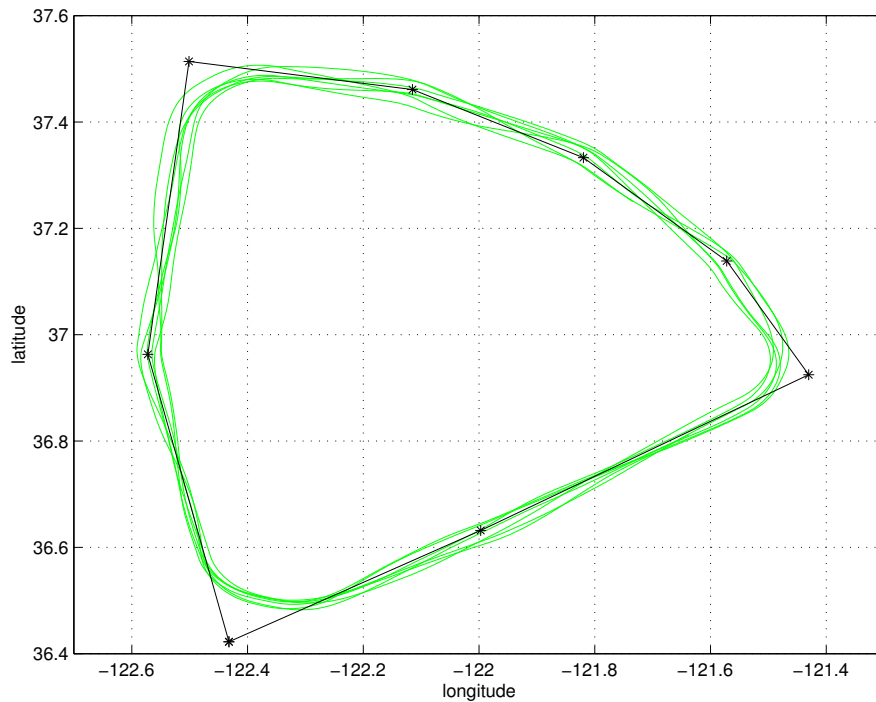

Figure 12.19. Piloted flight technical error of an MD80 traveling at 300kts and 30,000ft
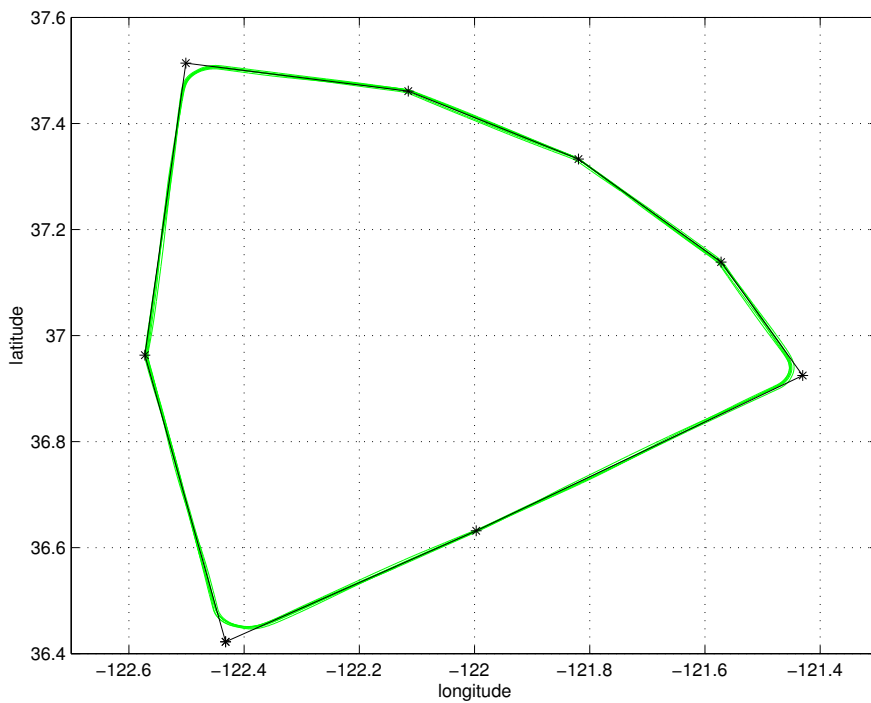
Figure 12.20. FMS flight technical error of an MD80 traveling at 250kts and 5000ft
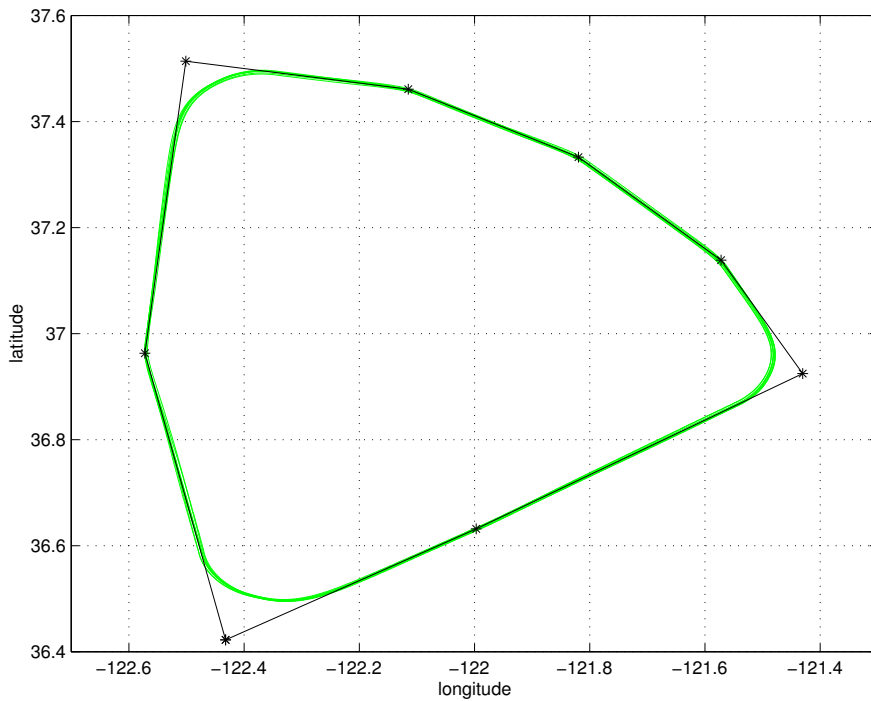
Figure 12.21. FMS flight technical error of an MD80 traveling at 300kts and 30,000ft

12.10 Navigation Errors

The purpose of navigation error modeling is to model the variances which occur in aircraft flight paths as a result of imperfect information. The two navigation types generally used within the simulation at this point for en route types of operation are VOR/DME and GPS navigation. All of the navigation models perform similarly in that they create a perturbed estimate of the aircraft's location for the guidance system to use as an input. Therefore, the navigation error models all return a latitude longitude pair which represents the aircraft's position as determined by imperfect navigation.

12.10.1 GPS Navigation Error

The GPS navigation error is so small that it is generally undetectable, for the typical scales used. For the purposes of completeness, a plot of GPS error over a route is generated, but for en route purposes, GPS error is small enough to warrant ignoring it completely. Figure 12.22 shows an aircraft flying a route. Unfortunately, there is no way of seeing the aircraft track because it is so superbly hidden by the route line itself. Even exploded views of this plot fail to reveal any interesting variation between GPS and the route.
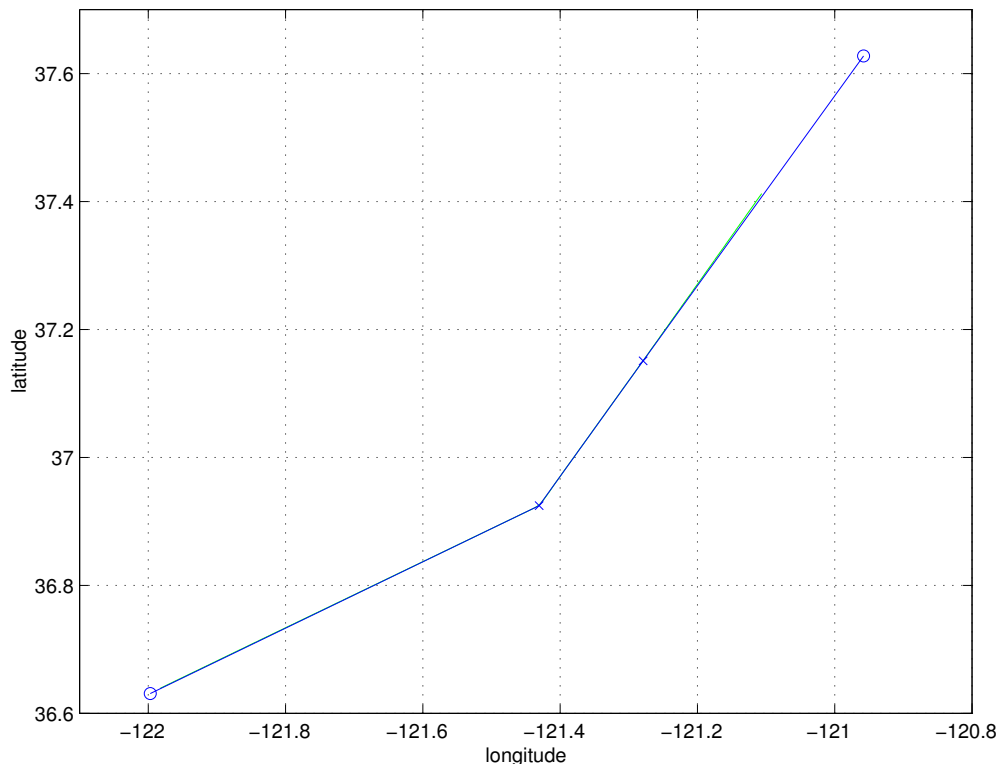
Figure 12.22. An aircraft trajectory using GPS navigation

12.10.2 VOR/DME Error

The navigation errors associated with VOR/DME error is much more interesting than those associated with GPS from a modeling point of view. Generally, VOR/DME navigation systems have biases in their angular measurements which tend to make lateral offset errors grow as a function of distance from the nav-aid. The errors also produce interesting quirks when VOR receivers are switched during navigation. For instance, an aircraft that is following one VOR for a portion of a segment may develop a lateral offset on one side of the segment and upon switching to the next VOR, immediately develop a lateral offset on the other side of the segment.

The first scenario considered is shown in Figure 12.23 where an aircraft is tracking a segment which has a VOR/DME at each endpoint. The northerly most station has a slight easterly bias which tends to make the aircraft track to the east of center. The southerly VOR/DME tends to have a slight westerly bias which makes the aircraft track to the west of center.
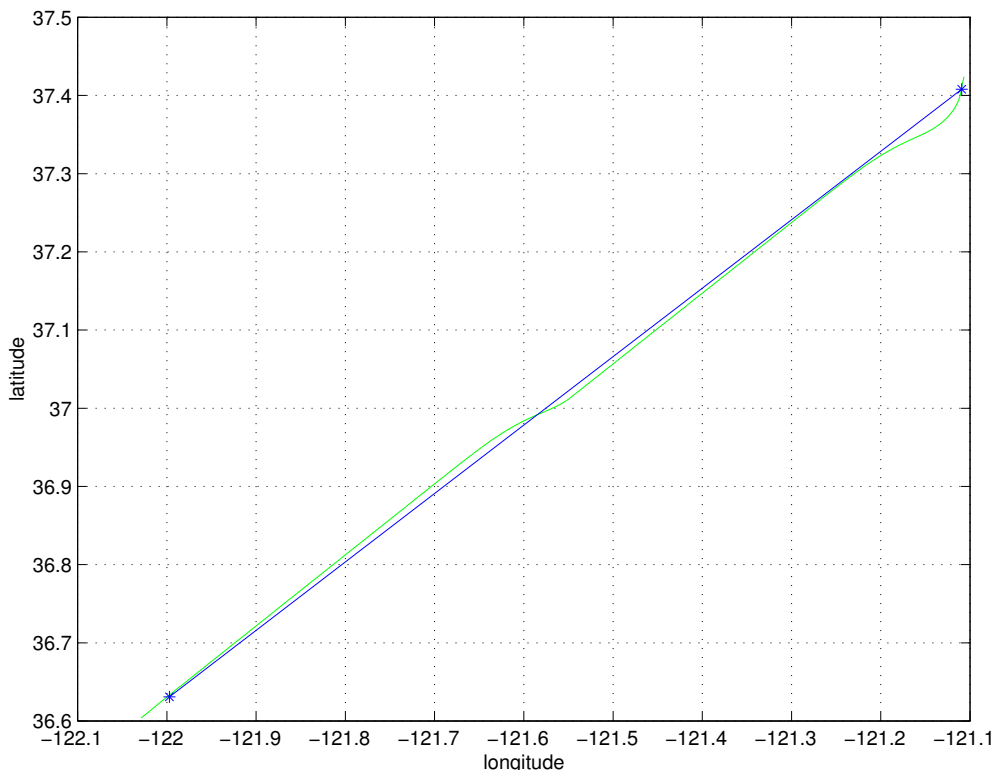
Figure 12.23. An aircraft flying a segment using VOR/DME navigation where both endpoints are VOR/DME stations

The aircraft is heading southwest along the segment, and it first captures the route shortly after passing the northerly VOR/DME. The aircraft then tracks the course using a signal from the northerly VOR/DME. As the aircraft progresses along the route, the aircraft drifts to the east slightly. When the aircraft passes the midpoint of the segment, the aircraft switches nav-aids and

uses the southerly VOR/DME instead. Upon tuning in this nav-aid, the aircraft crosses over the route and tracks on the other side because of the

slight westerly bias associated with the southern VOR/DME station. As the aircraft approaches the station, the error becomes smaller as would be expected.

The second scenario, shown in Figure 12.24, illustrates an aircraft following a route which has a VOR/DME station at each of its endpoints. However, there are two intersections in between the VOR/DME stations making three distinct segments. Because of this arrangement, the center segment does not have a VOR/DME station associated with it. In this situation, the algorithm must choose between the southerly VOR/DME and the northerly VOR/DME to determine which is most appropriate to use for navigation. From visual inspection, the human pilot would automatically choose the northerly most VOR/DME because the center segment is nearly perfectly aligned with a radial from that station. Using the southerly VOR/DME would require some sort of area navigation technique.
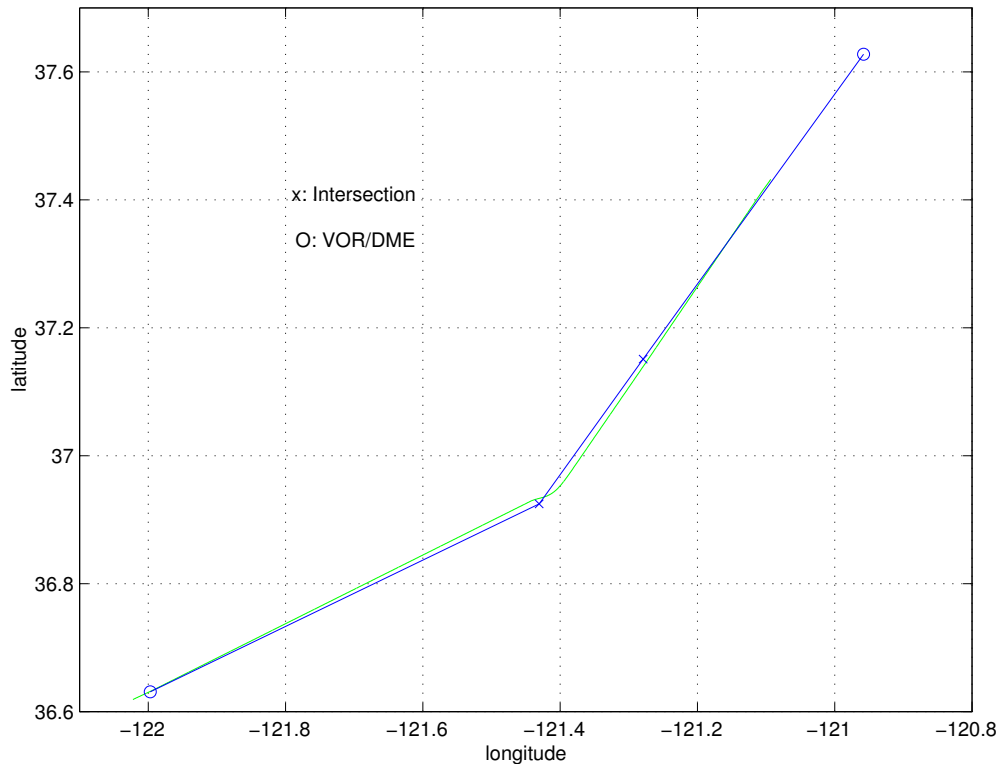

Figure 12.24. An aircraft flying a route comprised of 2 VOR/DME stations with 2 intersections between the VOR/DME stations

The aircraft is initially headed northeast on the first segment using the southerly VOR/DME for navigation. Because this is the only VOR/DME associated with the first segment, the aircraft does not switch nav-aids. However, when the aircraft switches to the middle segment, it must make a decision about which VOR/DME station to use. As discussed in the last paragraph, the northerly VOR/DME is the best one to use and in fact, we see that the northerly VOR/DME is the one chosen by the algorithm for navigation. We know this by observing the bias that the aircraft takes after switching between the first segment and the middle segment. The aircraft has an easterly bias which is associated with the northerly VOR/DME. This bias is continually decreased as the aircraft flies further towards the VOR/DME and crosses onto the final segment. Eventually, when the aircraft crosses the northern VOR/DME, the bias is reduced to zero.

There is one other characteristic to note regarding the crossing of segment 1 onto segment 2. Notice that the aircraft is using DME to determine the end of the route rather than the intersection of VOR/DME radials. If the intersection of VOR/DME radials was used to determine the fix location, the aircraft would have estimated the fix location to be northeast of the actual fix location. Rather, the aircraft estimates the end of the route with near perfection in spite of the VOR radial biases. This is a trait of an aircraft equipped with DME as opposed to one which only has VOR navigation. This segment transition phenomena is one of the distinguishing characteristics of VOR/DME navigation as opposed to VOR/VOR navigation which is not currently modeled in the system.

12.11 Terminal Flight Phases

The terminal flight phases for the aircraft consist of take off and landing. These maneuvers are different than any which have been considered so far because they require that the aircraft fly slowly and interact with the ground.

12.11.1 Take-Off

During take-off, the aircraft initially accelerates down the runway with the landing gear initially supporting all of the aircraft weight. This phase of take-off is referred to as the ground roll. The lift coefficient is held at zero. Since we assume coordinated flight, we do not concern ourselves with keeping the aircraft on the centerline. When the aircraft reaches rotation speed, the lift coefficient of the aircraft is increased until the aircraft leaves the ground and starts climbing. The landing gear is retracted as soon as the aircraft has climbed several hundred feet. Once the landing gear is retracted, the maximum available throttle is reduced to 90% of maximum possible throttle. Next, the aircraft accelerates to a new speed of 210 kt. While speeding up, the flaps are retracted as the proper speeds are obtained. Retraction of the flaps is the last commands issued by the navigator for take-off.

Figure 12.25 illustrates the take-off of an MD80 aircraft weighing 130,000lbs. The aircraft initiates the takeoff ground roll at 20 seconds into the strip chart recording. Roughly 40 seconds later, the aircraft has achieved sufficient speed for rotation. Looking at the lift coefficient plot,

we see the initial lift coefficient spike which is the control system executing the rotation. As the aircraft starts to lift off the ground we see the speed initially stabilize right around the rotation speed. Then, the aircraft starts to accelerate at a slower rate towards 210kts. Upon reaching 210kts, the aircraft holds a constant speed and
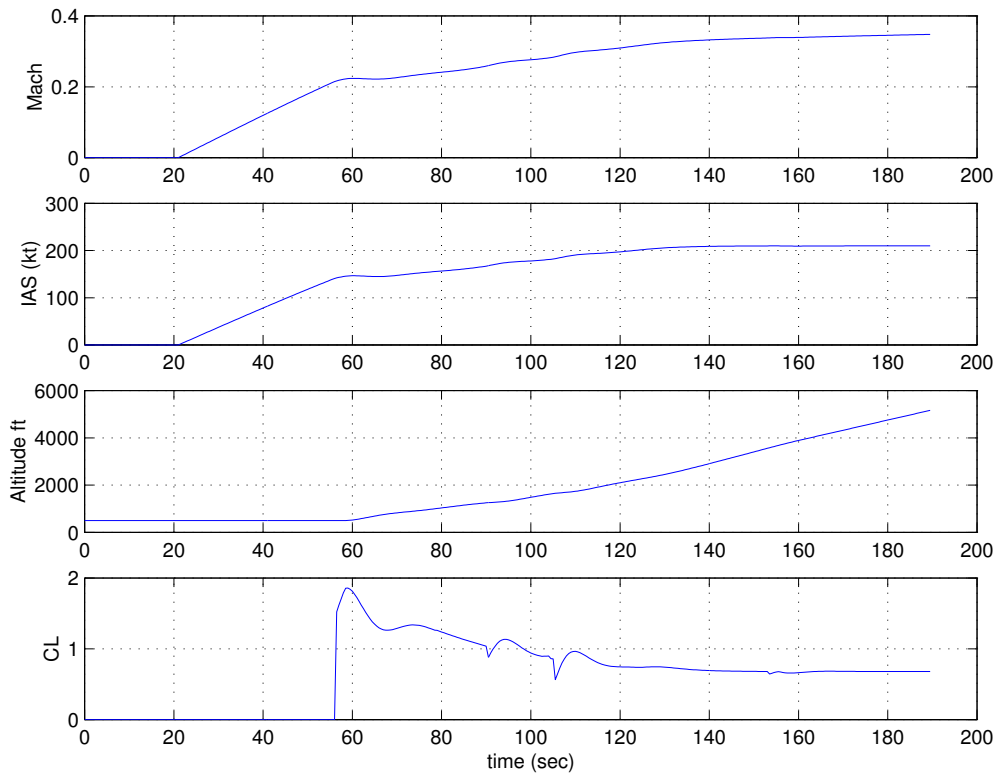
Figure 12.25. An MD80 at 130,000lbs taking off with a rotation speed of 150KIAS

continues to climb. Notice that the rate of climb increases when the aircraft stabilizes at 210kts.

One of the important features of this take-off example to notice is the simultaneous acceleration and climb between 60sec and 120sec. From Figure 12.1, we know that on takeoff the aircraft climbs and accelerates simultaneously. To cause this, special ramping of the speed input is performed as discussed in Section 12.4.3.

12.11.2 Landing

The final approach and landing is quite possibly the most difficult of all maneuvers to simulate. The aircraft must automatically follow an approach to an airport, maintaining the appropriate altitudes all along the path, and then capture the ILS localizer and glide slope for the final vertical descent. Finally, the aircraft must touchdown. All through the maneuver, the control logic must monitor and command the proper aircraft speed and make sure that the appropriate

232

flap settings are deployed. Furthermore, the entire final approach is flown on the back side of the thrust curve, the most difficult flight regime for the control logic.

The terminal flight phases are also the most difficult to verify. Pseudocontrol does not land aircraft so there is no acceptable baseline for insuring that the longitudinal dynamics are proper. Therefore, verification of the longitudinal performance on landing and take-off consisted of making sure that the aircraft performance conformed to the performance data which were used to create the algorithms. Such data are contained in Figures 12.1 and 12.2.

First, the longitudinal dynamics is considered. Figure 12.26 shows an MD80 on final approach and landing to an airport. By the time Figure 12.26 starts recording the approach, the aircraft has already slowed to 170kts and has captured the localizer. At roughly 55 seconds, the aircraft captures the glide slope. The aircraft simultaneously slows down to its final approach speed of 130kts. At roughly 180 seconds, the aircraft touches down and the brakes are applied. The speed reduces quickly and the aircraft is brought to a standstill by 210 seconds.
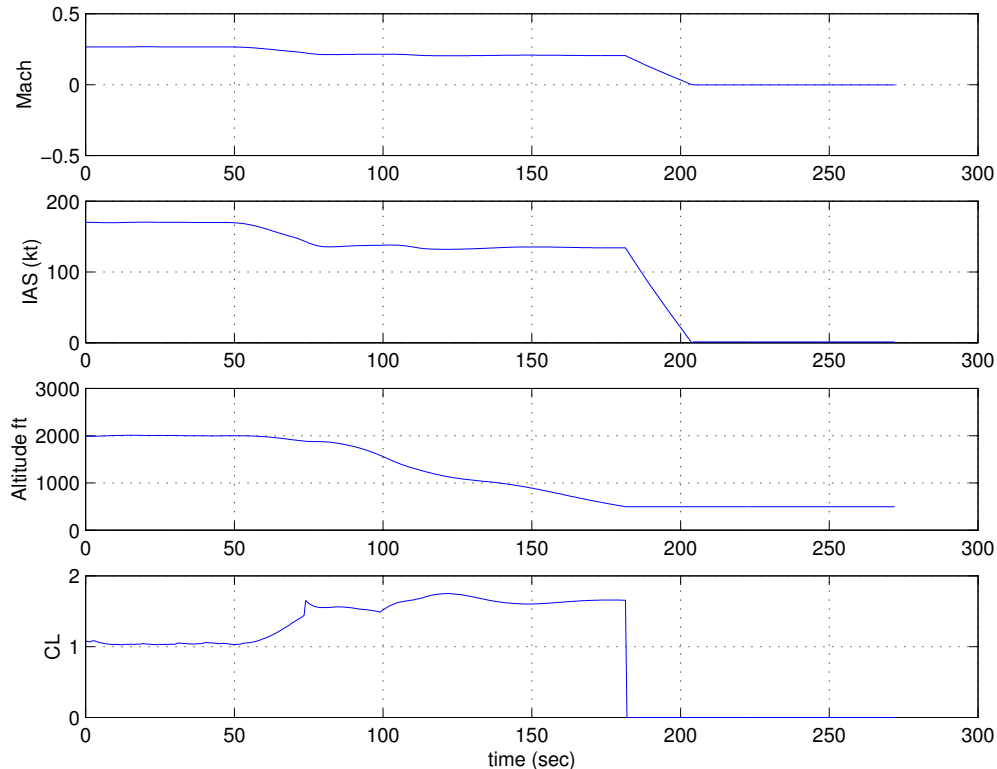
Figure 12.26. Longitudinal view of an MD80 on final approach and landing

233

Figure 12.27 illustrates the top view of the same MD80 from Figure 12.26. The aircraft has already captured the localizer when the track starts. The aircraft is heading southeast along the ILS. The first circle along the route is an initial approach fix located 20 miles from the airport threshold, which is marked by an 'X.' The second circle, which is 5 miles from the threshold, is the final approach fix for the ILS. For this example, both the flight technical error and the ILS beam bending model are in effect. However, as can be seen from the track in Figure 12.27, little variation is seen. This is expected considering the small standard deviations which are measured from actual data. The aircraft touches down near the threshold and stops moving about 3000 ft later.
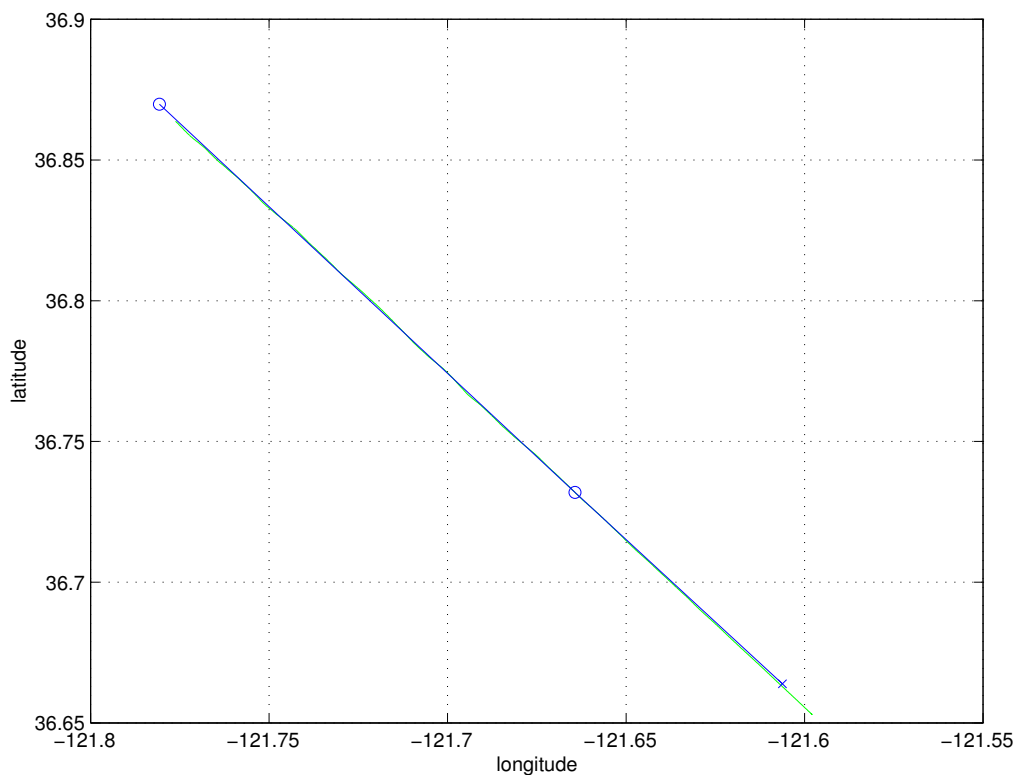
Figure 12.27. A top view of an MD80 on final approach to landing

12.12 Conclusions

The testing that was done to verify and validate the TGF simulation gives us a high degree of confidence that the models contained herein have sufficient fidelity for use as a target generating tool.

Generally, there were two means of verifying and validating the system. For the longitudinal dynamics, a quantitative measuring tool was needed to insure that the aircraft performance was

realistic. The tool used was Pseudocontrol, the aircraft dynamics kernel of PAS. PAS, the NASA tool for trajectory generation, has been accepted as an acceptable baseline for aircraft performance. For the guidance operations, such as route capture and route following, visually inspecting the maneuvers is sufficient to insure proper operation. Repeated testing of algorithms was done to insure that the route capture and route following algorithms would capture the route from all different initial conditions. Examples of the most difficult initial conditions have been discussed in this section.

Flight technical error and navigation error was validated by making sure that the modeled variances conformed to the real flight data statistics which were used to construct the models.

Terminal flight phases were the most difficult to verify because of the lack of information available for actual aircraft descents and landings. Information from flight handbooks and performance manuals was used to verify as best possible the aircraft performance on landing.

Appendix A - Analysis of the Transfer Functions of the Longitudinal Dynamics

In the original version of this document (in section 3.3), an analysis was conducted on the transfer function between a lift coefficient input and an altitude rate output for a single-input, single-output (SISO) system. This was intended to provide insight to the controllability of altitude rate using lift coefficient. There was concern about the right-half-plane zeros in the transfer function when the aircraft is flying on the back-side of the thrust curve. The analysis concluded that a control reversal occurred in this regime making it impossible to maintain stable flight when using lift coefficient to control altitude rate.

The analysis failed to consider that in steady, level flight on the back-side of the thrust curve, the system is not SISO; thrust is used to control speed while lift coefficient is used to control altitude rate. And in level acceleration where the system is SISO, the linearized system of equations (3.27) and (3.28) does not apply. The reader is reminded that the system is linearized about a steady, level reference condition in which thrust equals drag. In level acceleration, the throttle is advanced to full and is greater than drag and energy is being added to the system. A similar argument can be made for level deceleration.

To get an indication of the response of the altitude rate to lift coefficient input in steady, level flight, we can modify the LTD system of equations to absorb the thrust control and then analyze the system as a SISO, LTD system. The purpose of this appendix is to blend the optimized thrust control gains of Chapter 4 into the LTD system and then analyze the $\Delta \dot{h} / u_{P_{C_L}}$ transfer function. The analysis shows that, in this dual input, dual output system, thrust is adjusted to counteract the adverse effect of the changing lift coefficient on the speed so that the commanded altitude rate can be captured. Equations (4.26) are restated here.

$$
\begin{bmatrix} \dot{V}_a \\ \dot{\gamma}_a \\ \dot{I}_{C_L} \\ \dot{I}_T \end{bmatrix} = \begin{bmatrix} a_{11} & a_{12} & b_{11} & b_{12} \\ a_{21} & 0 & b_{21} & 0 \\ 0 & 0 & 0 & 0 \\ 0 & 0 & 0 & 0 \end{bmatrix} \begin{bmatrix} V_a \\ \gamma_a \\ I_{C_L} \\ I_T \end{bmatrix} + \begin{bmatrix} b_{11} & b_{12} & 0 & 0 \\ b_{21} & 0 & 0 & 0 \\ 0 & 0 & 1 & 0 \\ 0 & 0 & 0 & 1 \end{bmatrix} \begin{bmatrix} u_{P_{C_L}} \\ u_{P_T} \\ u_{i_{C_L}} \\ u_{i_T} \end{bmatrix}
$$

(4.26)

$$\mathbf{y} = \begin{bmatrix} \Delta M \\ \Delta \dot{h} \end{bmatrix} = \begin{bmatrix} c_{21} & 0 & 0 & 0 \\ 0 & c_{42} & 0 & 0 \end{bmatrix} \begin{bmatrix} V_a \\ \gamma_a \\ I_{C_L} \\ I_T \end{bmatrix}$$

The control law is reduced from equation (4.14).

$$\mathbf{u} = \begin{bmatrix} u_{P_{C_L}} \\ u_{P_T} \\ u_{i_{C_L}} \\ u_{i_T} \end{bmatrix} = - \begin{bmatrix} 0 & k_{p_{14}} \\ k_{p_{22}} & 0 \\ 0 & k_{i_{14}} \\ k_{i_{22}} & 0 \end{bmatrix} \begin{bmatrix} \Delta M \\ \Delta \dot{h} \end{bmatrix}$$

In order to incorporate the thrust control into the LTD system, the thrust and lift coefficient controls must first be separated. We also re-introduce the vectors as explicit functions of time.

$$\mathbf{u} = \begin{bmatrix} u_{P_{C_L}} \\ u_{P_T} \\ u_{i_{C_L}} \\ u_{i_T} \end{bmatrix} = \begin{bmatrix} u_{P_{C_L}} \\ 0 \\ u_{i_{C_L}} \\ 0 \end{bmatrix} + \begin{bmatrix} 0 \\ u_{P_T} \\ 0 \\ u_{i_T} \end{bmatrix} = - \begin{bmatrix} 0 & k_{p_{14}} \\ 0 & 0 \\ 0 & k_{i_{14}} \\ 0 & 0 \end{bmatrix} \begin{bmatrix} \Delta M \\ \Delta \dot{h} \end{bmatrix} - \begin{bmatrix} 0 & 0 \\ k_{p_{22}} & 0 \\ 0 & 0 \\ k_{i_{22}} & 0 \end{bmatrix} \begin{bmatrix} \Delta M \\ \Delta \dot{h} \end{bmatrix}$$

$$\mathbf{u}(t) \quad = \mathbf{u}_{\mathbf{C_L}}(t) + \mathbf{u}_{\mathbf{T}}(t) = -\mathbf{K}_{\mathbf{C_L}} \mathbf{y}(t) - \mathbf{K}_{\mathbf{T}} \mathbf{y}(t)$$

Then, assuming $\mathbf{K_T}$ is known.

$$\dot{\mathbf{x}}(t) = \mathbf{Ax}(t) + \mathbf{Bu}(t) = \mathbf{Ax}(t) + \mathbf{B}\left(\mathbf{u}_{\mathbf{C_L}}(t) + \mathbf{u}_{\mathbf{T}}(t)\right)$$

$$= \mathbf{Ax}(t) + \mathbf{Bu}_{\mathbf{C_L}}(t) + \mathbf{Bu}_{\mathbf{T}}(t) = \left(\mathbf{A} - \mathbf{BK}_{\mathbf{T}}\mathbf{C}\right)\mathbf{x}(t) + \mathbf{Bu}_{\mathbf{C_L}}(t)$$

$$\mathbf{y}(t) = \mathbf{Cx}(t) + \mathbf{Du}_{\mathbf{C_L}}(t)$$

$$\mathbf{u}_{\mathbf{C_L}}(t) = -\mathbf{K}_{\mathbf{C_L}} \mathbf{y}(t)$$

We arrive at the transfer function by converting to the laplace domain and solving the matrix algebra.

$$sx(s) = (A - BK_TC)x(s) + Bu_{C_L}(s)$$

$$\{sI - (A - BK_TC)\}x(s) = Bu_{C_L}(s)$$

$$x(s) = \{sI - (A - BK_TC)\}^{-1}Bu_{C_L}(s)$$

$$y(s) = \left(C\{sI - (A - BK_TC)\}^{-1}B + D\right)u_{C_L}(s) \tag{A.1}$$

We first solve for the closed-loop A matrix.

$$(A - BK_TC) = \left(\begin{bmatrix} a_{11} & a_{12} & b_{11} & b_{12} \\ a_{21} & 0 & b_{21} & 0 \\ 0 & 0 & 0 & 0 \\ 0 & 0 & 0 & 0 \end{bmatrix} - \begin{bmatrix} b_{11} & b_{12} & 0 & 0 \\ b_{21} & 0 & 0 & 0 \\ 0 & 0 & 1 & 0 \\ 0 & 0 & 0 & 1 \end{bmatrix}\begin{bmatrix} 0 & 0 \\ k_{p_{22}} & 0 \\ 0 & 0 \\ k_{i_{22}} & 0 \end{bmatrix}\begin{bmatrix} c_{21} & 0 & 0 & 0 \\ 0 & c_{42} & 0 & 0 \end{bmatrix}\right)$$

$$= \left(\begin{bmatrix} a_{11} & a_{12} & b_{11} & b_{12} \\ a_{21} & 0 & b_{21} & 0 \\ 0 & 0 & 0 & 0 \\ 0 & 0 & 0 & 0 \end{bmatrix} - \begin{bmatrix} b_{11} & b_{12} & 0 & 0 \\ b_{21} & 0 & 0 & 0 \\ 0 & 0 & 1 & 0 \\ 0 & 0 & 0 & 1 \end{bmatrix}\begin{bmatrix} 0 & 0 & 0 & 0 \\ k_{p_{22}}c_{21} & 0 & 0 & 0 \\ 0 & 0 & 0 & 0 \\ k_{i_{22}}c_{21} & 0 & 0 & 0 \end{bmatrix}\right)$$

$$= \left(\begin{bmatrix} a_{11} & a_{12} & b_{11} & b_{12} \\ a_{21} & 0 & b_{21} & 0 \\ 0 & 0 & 0 & 0 \\ 0 & 0 & 0 & 0 \end{bmatrix} - \begin{bmatrix} b_{12}k_{p_{22}}c_{21} & 0 & 0 & 0 \\ 0 & 0 & 0 & 0 \\ 0 & 0 & 0 & 0 \\ k_{i_{22}}c_{21} & 0 & 0 & 0 \end{bmatrix}\right)$$

$$= \begin{bmatrix} a_{11} - b_{12}k_{p_{22}}c_{21} & a_{12} & b_{11} & b_{12} \\ a_{21} & 0 & b_{21} & 0 \\ 0 & 0 & 0 & 0 \\ -k_{i_{22}}c_{21} & 0 & 0 & 0 \end{bmatrix}$$

Then,

-239-

$$\{s\mathbf{I}-(\mathbf{A}-\mathbf{BK_TC})\}=\begin{bmatrix} s & 0 & 0 & 0 \\ 0 & s & 0 & 0 \\ 0 & 0 & s & 0 \\ 0 & 0 & 0 & s \end{bmatrix}-\begin{bmatrix} a_{11}-b_{12}k_{p_{22}}c_{21} & a_{12} & b_{11} & b_{12} \\ a_{21} & 0 & b_{21} & 0 \\ 0 & 0 & 0 & 0 \\ -k_{i_{22}}c_{21} & 0 & 0 & 0 \end{bmatrix}$$

$$=\begin{bmatrix} s-\left(a_{11}-b_{12}k_{p_{22}}c_{21}\right) & -a_{12} & -b_{11} & -b_{12} \\ -a_{21} & s & -b_{21} & 0 \\ 0 & 0 & s & 0 \\ k_{i_{22}}c_{21} & 0 & 0 & s \end{bmatrix}$$

Computation of the inverse of this matrix is not trivial. We arrived at the solution using the algebraic matrix inversion functions of MATLAB®.

$$\left\{s\mathbf{I} - \left(\mathbf{A} - \mathbf{BK_T C}\right)\right\}^{-1} = $$

$$\frac{\begin{bmatrix} s & a_{12} & \dfrac{b_{11}s + a_{12}b_{21}}{s} & b_{12} \\[2em] a_{21} & \dfrac{s^2 + \left(-a_{11} + b_{12}k_{p_{22}}c_{21}\right)s + b_{12}k_{i_{22}}c_{21}}{s} & \dfrac{b_{21}s^2 + \left(-a_{11}b_{21} + b_{12}b_{21}k_{p_{22}}c_{21} + a_{21}b_{11}\right)s + b_{12}b_{21}k_{i_{22}}c_{21}}{s^2} & \dfrac{a_{21}b_{12}}{s} \\[2em] 0 & 0 & \dfrac{s^2 + \left(-a_{11} + b_{12}k_{p_{22}}c_{21}\right)s + \left(b_{12}k_{i_{22}}c_{21} - a_{12}a_{21}\right)}{s} & 0 \\[2em] -k_{i_{22}}c_{21} & \dfrac{-a_{12}k_{i_{22}}c_{21}}{s} & -k_{i_{22}}c_{21}\dfrac{b_{11}s + a_{12}b_{21}}{s^2} & \dfrac{s^2 + \left(-a_{11} + b_{12}k_{p_{22}}c_{21}\right)s - a_{12}a_{21}}{s} \end{bmatrix}}{s^2 + \left(-a_{11} + b_{12}k_{p_{22}}c_{21}\right)s + \left(b_{12}k_{i_{22}}c_{21} - a_{12}a_{21}\right)}$$

Because of the form of the **C**-matrix, which pre-multiplies the $\left\{ s\mathbf{I} - \left(\mathbf{A} - \mathbf{BK_T C} \right) \right\}^{-1}$ matrix in the equation (A.1), the $\Delta \dot{h} \Big/ u_{P_{C_L}}$ transfer function is concerned only with second row of the $\left\{ s\mathbf{I} - \left(\mathbf{A} - \mathbf{BK_T C} \right) \right\}^{-1}$ matrix. (Note: transposed notation is used to conserve page space.)

$$\left\{ s\mathbf{I} - \left(\mathbf{A} - \mathbf{BK_T C} \right) \right\}^{-1}_{(2,:)} = \frac{\begin{bmatrix} a_{21} \\ \dfrac{s^2 + \left(-a_{11} + b_{12}k_{p_{22}}c_{21} \right)s + b_{12}k_{i_{22}}c_{21}}{s} \\ \dfrac{b_{21}s^2 + \left(-a_{11}b_{21} + b_{12}b_{21}k_{p_{22}}c_{21} + a_{21}b_{11} \right)s + b_{12}b_{21}k_{i_{22}}c_{21}}{s^2} \\ \dfrac{a_{21}b_{12}}{s} \end{bmatrix}^T}{s^2 + \left(-a_{11} + b_{12}k_{p_{22}}c_{21} \right)s + \left(b_{12}k_{i_{22}}c_{21} - a_{12}a_{21} \right)}$$

Post-multiplying the **B**-matrix, we get,

$$\left\{ s\mathbf{I} - \left(\mathbf{A} - \mathbf{BK_T C} \right) \right\}^{-1}_{(2,:)} \mathbf{B} = \frac{\begin{bmatrix} a_{21}b_{11} + \dfrac{s^2 + \left(-a_{11} + b_{12}k_{p_{22}}c_{21} \right)s + b_{12}k_{i_{22}}c_{21}}{s} b_{21} \\ a_{21}b_{12} \\ \dfrac{b_{21}s^2 + \left(-a_{11}b_{21} + b_{12}b_{21}k_{p_{22}}c_{21} + a_{21}b_{11} \right)s + b_{12}b_{21}k_{i_{22}}c_{21}}{s^2} \\ \dfrac{a_{21}b_{12}}{s} \end{bmatrix}^T}{s^2 + \left(-a_{11} + b_{12}k_{p_{22}}c_{21} \right)s + \left(b_{12}k_{i_{22}}c_{21} - a_{12}a_{21} \right)}$$

and pre-multiplying the **C**-matrix, we get,

$$\mathbf{C}\left\{s\mathbf{I}-\left(\mathbf{A}-\mathbf{B}\mathbf{K_T}\mathbf{C}\right)\right\}^{-1}_{(2,:)}\mathbf{B}=\begin{bmatrix}a_{21}b_{11}c_{42}+\dfrac{s^2+\left(-a_{11}+b_{12}k_{p_{22}}c_{21}\right)s+b_{12}k_{i_{22}}c_{21}}{s}b_{21}c_{42}\\[2em]a_{21}b_{12}c_{42}\\[1em]\dfrac{b_{21}s^2+\left(-a_{11}b_{21}+b_{12}b_{21}k_{p_{22}}c_{21}+a_{21}b_{11}\right)s+b_{12}b_{21}k_{i_{22}}c_{21}}{s^2}c_{42}\\[2em]\dfrac{a_{21}b_{12}c_{42}}{s}\end{bmatrix}^{T}\!\!\!\bigg/ s^2+\left(-a_{11}+b_{12}k_{p_{22}}c_{21}\right)s+\left(b_{12}k_{i_{22}}c_{21}-a_{12}a_{21}\right)$$

The $\Delta\dot{h}\big/u_{p_{C_L}}$ transfer function is element (2,1) of the $\mathbf{C}\left\{s\mathbf{I}-\left(\mathbf{A}-\mathbf{B}\mathbf{K_T}\mathbf{C}\right)\right\}^{-1}\mathbf{B}$ matrix.

$$\Delta\dot{h}\big/u_{p_{C_L}}=\frac{a_{21}b_{11}c_{42}+\dfrac{s^2+\left(-a_{11}+b_{12}k_{p_{22}}c_{21}\right)s+b_{12}k_{i_{22}}c_{21}}{s}b_{21}c_{42}}{s^2+\left(-a_{11}+b_{12}k_{p_{22}}c_{21}\right)s+\left(b_{12}k_{i_{22}}c_{21}-a_{12}a_{21}\right)}$$

$$\Delta\dot{h}\big/u_{p_{C_L}}=c_{42}\frac{b_{21}s^2+\left(-a_{11}b_{21}+a_{21}b_{11}+b_{12}b_{21}c_{21}k_{p_{22}}\right)s+b_{12}b_{21}c_{21}k_{i_{22}}}{s\left(s^2+\left(-a_{11}+b_{12}c_{21}k_{p_{22}}\right)s+\left(b_{12}c_{21}k_{i_{22}}-a_{12}a_{21}\right)\right)} \tag{A.2}$$

We verify that by setting $k_{p_{21}}=k_{i_{21}}=0$ and substituting in the matrix partial derivatives, we get equation (3.67).

$$\Delta\dot{h}\big/u_{p_{C_L}}=c_{42}\frac{b_{21}s+\left(-a_{11}b_{21}+a_{21}b_{11}\right)}{s^2-a_{11}s-a_{12}a_{21}}$$

$$a_{11}=\frac{\partial f_{V_a}}{\partial V_a},\quad a_{12}=\frac{\partial f_{V_a}}{\partial\gamma_a},\quad a_{21}=\frac{\partial f_{\gamma_a}}{\partial V_a},\quad b_{11}=\frac{\partial f_{V_a}}{\partial C_L},\quad b_{21}=\frac{\partial f_{\gamma_a}}{\partial C_L},\quad c_{42}=60\frac{\partial f_h}{\partial\gamma_a}$$

$$\Delta\dot{h}\big/u_{p_{C_L}}=60\frac{\partial f_h}{\partial\gamma_a}\frac{\dfrac{\partial f_{\gamma_a}}{\partial C_L}s+\left(-\dfrac{\partial f_{V_a}}{\partial V_a}\dfrac{\partial f_{\gamma_a}}{\partial C_L}+\dfrac{\partial f_{\gamma_a}}{\partial V_a}\dfrac{\partial f_{V_a}}{\partial C_L}\right)}{s^2-\dfrac{\partial f_{V_a}}{\partial V_a}s-\dfrac{\partial f_{V_a}}{\partial\gamma_a}\dfrac{\partial f_{\gamma_a}}{\partial V_a}} \tag{3.67}$$

But of course, we are concerned with analyzing the transfer function with the optimized thrust gains left in. For a B763 at stall speed and 30,000 ft. equation (A.2) becomes,

$$\Delta\dot{h}\Big/u_{p_{C_L}} = \frac{1640s^2 + 631s + 96.7}{s\left(s^2 + 0.406s + 0.0758\right)}$$

which has complex conjugate zeros at $z_{1,2} = -0.19 \pm 0.152$. In other words, thrust control of speed moves the $\Delta\dot{h}\Big/u_{p_{C_L}}$ transfer function zeros into the left-half plane, thereby eradicating the non-minimum phase system. The integral control transfer function, $\Delta\dot{h}\Big/u_{i_{C_L}}$, is the same as equation (A.2) except with an added integral pole at $s = 0$. The root loci of proportional and integral $\Delta\dot{h}\Big/C_L$ transfer functions with thrust control of speed are shown in Figure A.1. The figure shows that lift coefficient control of altitude rate is well-behaved as long as speed is controlled by thrust simultaneously. We do, however, have to be mindful of low damping in this area, as indicated by the locus moving up the imaginary axis of the integral control root locus plot.
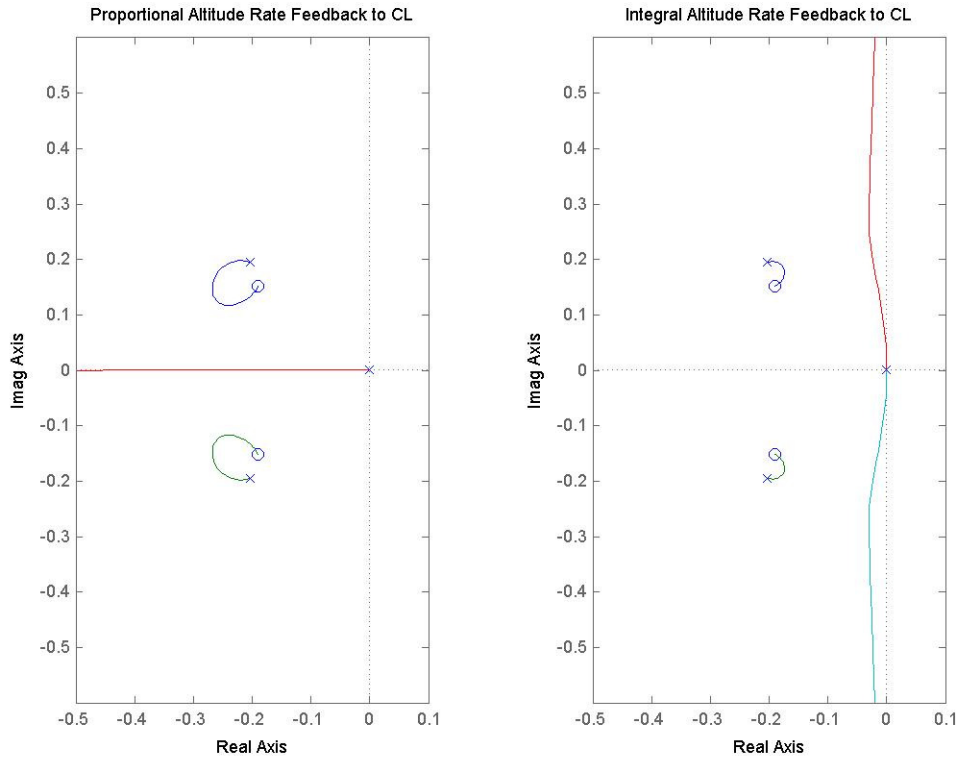

Figure A.1: The root loci of proportional and integral lift coefficient control of altitude rate considering the thrust control of speed

THIS PAGE INTENTIONALLY LEFT BLANK

Appendix B - 2nd Order Gauss-Markov model for GPS Clock Error due to Selective Availability

When GPS position and velocity error was first modeled, the dominant error was the GPS satellite clock error. **Figure B.1** illustrates the basic satellite geometry.

GPS satellite clock error is an intentional degradation of the GPS signal called Selective Availability (SA). It was implemented in 1990 to deny full position and velocity accuracy to "unauthorized users" after initial testing of the GPS system revealed accuracies much better than anticipated.

In May of 2000, the United States stopped degrading GPS performance with SA.

The analysis supporting the modeling of GPS satellite SA illuminates the implementation of the 2nd Order Gauss-Markov utility routines used to model other navigation errors, such as Flight Technical Error.

Since the exact model for GPS satellite SA clock error is classified, a number of authors have approximated it using a second order Gauss Markov model in the pseudorange domain (Parkinson & Spilker, 1996). These models can be used to determine the GPS receiver position and velocity errors as follows. Starting with the SA clock error model for each visible satellite, the SA clock pseudorange and range rate errors can be obtained. These errors can then be translated into a local coordinate frame, such as a local east-north-up (ENU) frame using the methodology described earlier.

An equivalent local coordinate system SA position and velocity error model can be formulated, to avoid the need to model the GPS satellite orbits which are required to determine the line-of-sight direction cosines. It also avoids the need for a Least Squares filter.
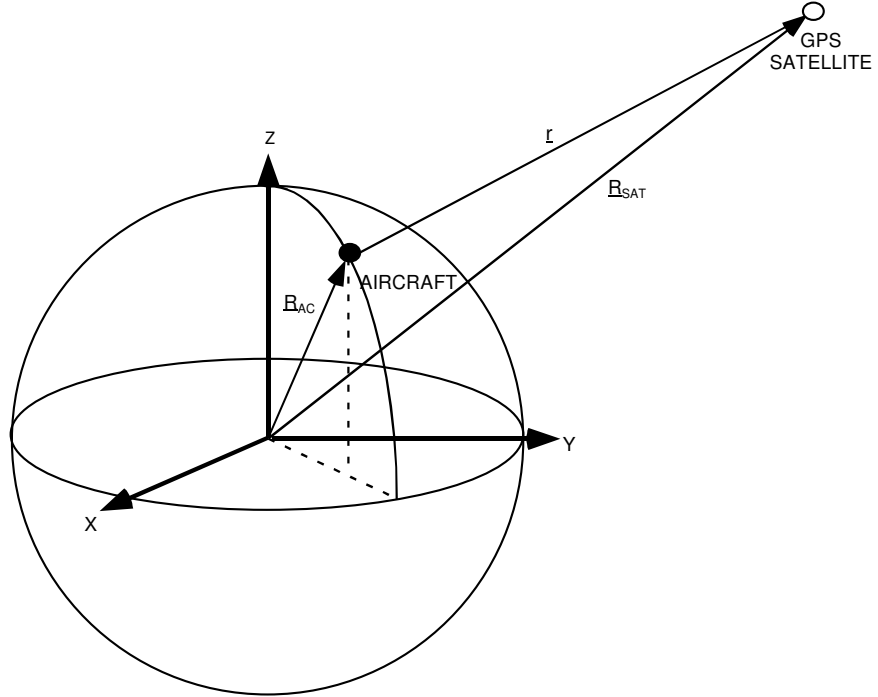
Figure B.1 GPS Receiver Measurement Geometry

The approach that is used is to start with a second-order Gauss Markov SA pseudorange model. Then, by adjusting the parameters of this model to match observed local coordinate SA position error statistics, it is possible to obtain a simplified SA position and velocity error model.

In general, when the uncorrelated SA pseudorange and range rate errors are translated into SA position and velocity errors, the resulting position and velocity errors are correlated. The fundamental simplifying assumption that will be used is to assume that these correlations are negligible. If the GPS satellites were located directly overhead and exactly on the horizon at the four cardinal directions, the correlations would indeed be zero.

Table B.1. Observed Local Coordinate Position Root-Mean-Square (rms) Errors

Coordinate	Position Error	Measured Average Daily Variations over 30 Days
East	32 m	15%
North	31 m	14%
Horizontal	41.5* m & 37.5** m	10%
Vertical	67 m	10%

* Based on observed horizontal position errors

** Based on observed steady state horizontal position time difference errors

The available field data, obtained from Timoteo (1992) consists of the position error statistics of Table B.1. In addition to the day-to-day variability, there is also a latitude dependence for the vertical error, particularly for latitudes greater than 60 degrees.

In addition, field data was abstracted from Timoteo (1992) to describe the horizontal temporal decorrelation.

A general second-order Gauss Markov model is described by the second-order differential equation (Gelb, 1974):

$$\ddot{x} + 2\beta\omega_0\dot{x} + \omega_0^2 x = cw \tag{B.1}$$

Expressed as a state-space equation, (B.1) becomes

$$\begin{pmatrix} \dot{x} \\ \dot{v} \end{pmatrix} = \begin{bmatrix} 0 & 1 \\ -\omega_0^2 & -2\beta\omega_0 \end{bmatrix} \begin{pmatrix} x \\ v \end{pmatrix} + \begin{pmatrix} 0 \\ c \end{pmatrix} w \tag{B.2}$$

where, x, v = error and error derivative ($v = \dot{x}$)

β = damping factor

ω_0 = *natural* frequency

w = Gaussian white noise

c = scale factor

equations (B.1) or (12.14) constitutes the simplified SA position and velocity error model. There is one set of these equations for each east, north, and vertical component.

Discretizing the Continuous 2nd Order Gauss Markov Process

To implement a 2nd order Gauss Markov process in code, it must be discretized. The corresponding closed-form 2nd order difference equation is shown in equation (B.3) (Parkinson & Spilker, 1996):

$$\begin{pmatrix} x \\ v \end{pmatrix}_{k+1} = \begin{bmatrix} \phi_{11} & \phi_{12} \\ \phi_{21} & \phi_{22} \end{bmatrix} \begin{pmatrix} x \\ v \end{pmatrix}_k + \begin{bmatrix} \gamma_{11} & \gamma_{12} \\ 0 & \gamma_{22} \end{bmatrix} \begin{pmatrix} w_1 \\ w_2 \end{pmatrix}_k \qquad \text{(B.3)}$$

The discrete input matrix has three terms and the state transition matrix has four terms within them that need to be calculated as shown in equations (B.4) and (B.5).

$$\Phi = \begin{bmatrix} \phi_{11} & \phi_{12} \\ \phi_{21} & \phi_{22} \end{bmatrix} \qquad \text{(B.4)}$$

$$\Gamma = \begin{bmatrix} \gamma_{11} & \gamma_{12} \\ 0 & \gamma_{22} \end{bmatrix} \qquad \text{(B.5)}$$

To calculate the state transition matrix variables, it is necessary to calculate some preliminary terms. These terms are defined in equations (B.6) and (B.7).

$$\omega_0 = \left(\frac{\sigma_v}{\sigma_p} \right) \qquad \text{(B.6)}$$

$$\omega_1 = \left(\frac{\sigma_v}{\sigma_p} \right) \sqrt{1 - \beta^2} \qquad \text{(B.7)}$$

The state transition matrix terms are then defined in equations (12.3) through (12.4).

$$\phi_{11} = e^{-\beta\omega_0\Delta t} \left[\cos(\omega_1\Delta t) + \beta(\omega_0 / \omega_1)\sin(\omega_1\Delta t) \right] \qquad \text{(B.8)}$$

$$\phi_{12} = (1 / \omega_1)e^{-\beta\omega_0\Delta t} \left[\sin(\omega_1\Delta t) \right] \qquad \text{(B.9)}$$

$$\phi_{21} = -\omega_0^2 \phi_{12} \qquad \text{(B.10)}$$

$$\phi_{22} = e^{-\beta\omega_0\Delta t} \left[\cos(\omega_1\Delta t) - \beta(\omega_0 / \omega_1)\sin(\omega_1\Delta t) \right] \qquad \text{(B.11)}$$

To calculate the discrete input matrix, an additional term is needed which is shown in equation (B.12).

$$c^2 = 4\beta\left(\frac{\sigma_v^3}{\sigma_p}\right)$$ (B.12)

The terms for the discrete input matrix are shown in equations (B.13) through (B.15)

$$\gamma_{11} = \sqrt{Q_{11} - Q_{12}^2 / Q_{22}}$$ (B.13)

$$\gamma_{12} = Q_{12} / \sqrt{Q_{22}}$$ (B.14)

$$\gamma_{22} = \sqrt{Q_{22}}$$ (B.15)

where the terms Q_{11}, Q_{12}, and Q_{22}, are terms of the white noise error covariance matrix and are defined in equations (B.16) through (B.18).

$$Q_{11} = \frac{c^2}{4\beta\omega_0^3}\left[1 - \left(\frac{\omega_0}{\omega_1}\right)^2 e^{-2\beta\omega_0\Delta t}\left[1 - \beta^2\cos(2\omega_1\Delta t) + \beta(\omega_1/\omega_0)\sin(2\omega_1\Delta t)\right]\right]$$ (B.16)

$$Q_{12} = Q_{21} = \frac{c^2}{4\omega_1^2}\left[e^{-2\beta\omega_0\Delta t}\left[1 - \cos(2\omega_1\Delta t)\right]\right]$$ (B.17)

$$Q_{22} = \frac{c^2}{4\beta\omega_0}\left[1 - \left(\frac{\omega_0}{\omega_1}\right)^2 e^{-2\beta\omega_0\Delta t}\left[1 - \beta^2\cos(2\omega_1\Delta t) - \beta(\omega_1/\omega_0)\sin(2\omega_1\Delta t)\right]\right]$$ (B.18)

The state variables of the process, x and v, are initialized using equations (B.19) and (B.20) where the terms w_1 and w_2 are unit variance discrete Gaussian white noise. (Gaussian random numbers).

$$x = \sigma_p w_1$$ (B.19)

$$v = \sigma_v w_2$$ (B.20)

Calibration of Parameters

The next step is to select the three unknown parameters, σ_p, σ_v, and β, to match the observed data statistics. The results are summarized in Table B.2. A one-hour sample history for all three local position and velocity SA error components is illustrated in Figure B.2 and Figure B.3.

Table B.2 Simplified vs. Observed SA Position and Velocity Model Parameters

Parameter	Symbol	Observed	Predicted
North Position Sigma	σ_{pN}	31 m	**31 m**
East Position Sigma	σ_{pE}	32 m	**32 m**
Vertical Position Sigma	σ_{pV}	67 m	**67 m**
North Velocity Sigma	σ_{vN}		**0.38 m/s**
East Velocity Sigma	σ_{vE}		**0.39 m/s**
Vertical Velocity Sigma	σ_{vV}		**0.82 m/s**
Damping Factor	β		**0.55**
Natural Frequency	ω_0		**0.0122**
	ω_1		**0.0102**
	c^2		**0.0021**
Horizontal Position Sigma	σ_{pH}	41.5* m & 37.5** m	37.3 m
Horizontal Position Correlation	ρ_{NE}	-0.13* & -0.29**	-0.3

* Based on observed horizontal position errors
** Based on observed steady state horizontal position time difference errors in Figure B.2.
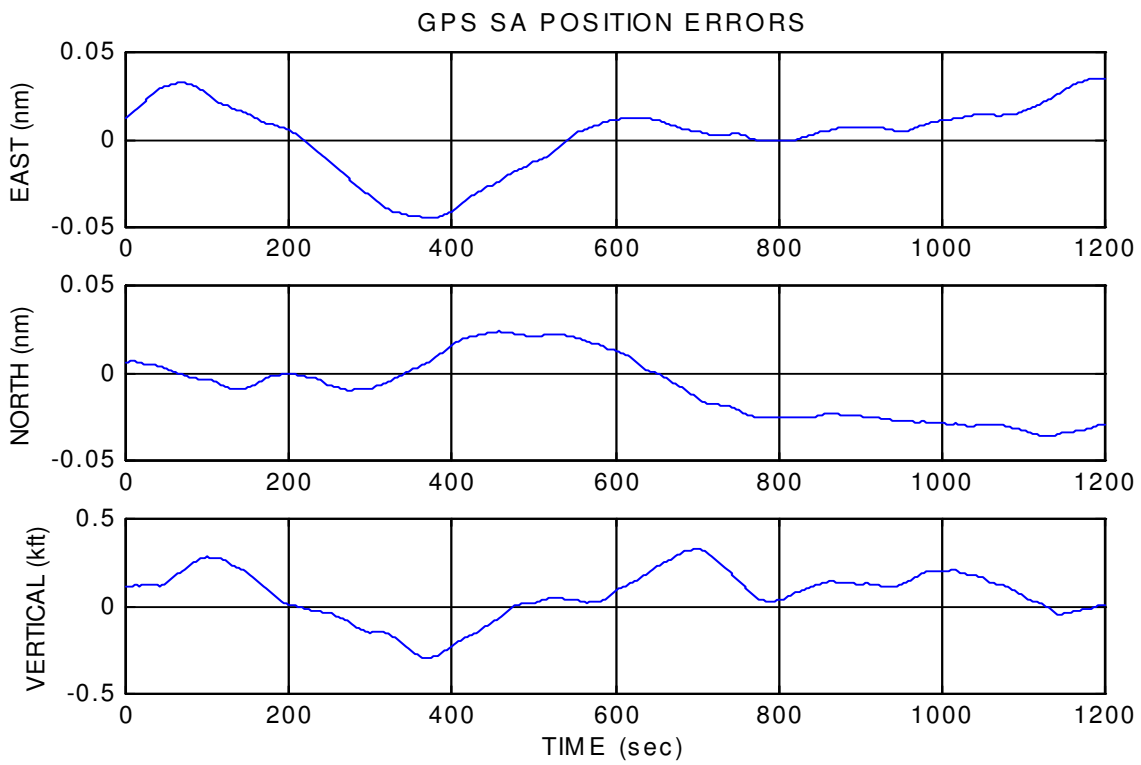
**Figure B.2.** Monte Carlo Simulated SA Position Errors
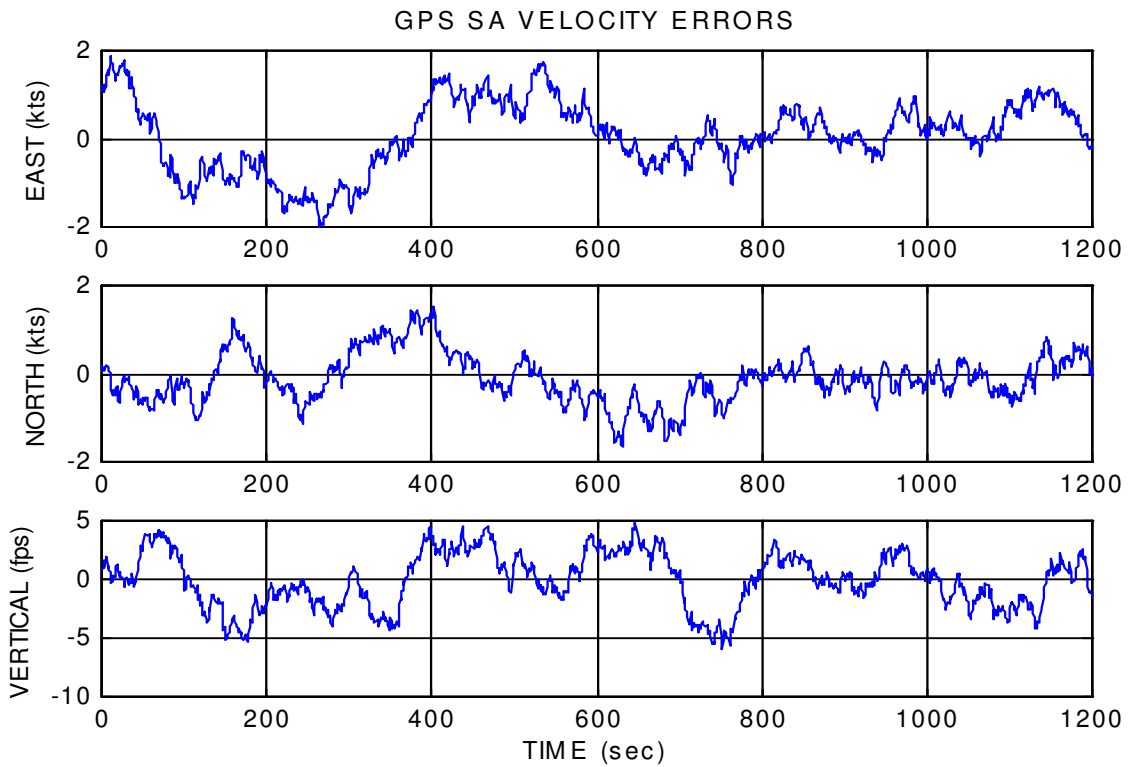
Figure B.3. Monte Carlo Simulated SA Velocity Errors

THIS PAGE INTENTIONALLY LEFT BLANK

Glossary

Azimuth   An angle measured relative to the ground-based coordinate system (i.e., true north).

Bearing   The azimuth direction of the position vector from one point to another (e.g., from an aircraft to a fix).

Drag   The component of aerodynamic force acting parallel to the aircraft's longitudinal axis and in a direction opposite the thrust. It is defined positive in the direction of the negative x-axis of the body axis system.

Dutch Roll Mode   A coupled roll and yaw motion that is often insufficiently damped.

Empty Weight   The weight of a fully operational aircraft without fuel or payload.

Flight Path Angle   The angle that the true airspeed vector makes with a horizontal plane.

Fuel Weight   The fuel capacity of the aircraft.

Geocentric Latitude   The angle between a line from center of the earth to the given point and the equatorial plane.

Geodetic Latitude   The angle between a line perpendicular to the surface of the ellipsoidal earth at the given point and the equatorial plane.

Ground Track Heading   The angle that the aircraft's ground speed vector makes with the ground-based coordinate system (i.e., true-north). This is the azimuth of the aircraft's velocity vector. The difference between ground track heading and true heading is due to the wind.

Ground Track Speed   The speed of the aircraft over ground. In other words, it is the magnitude of the aircraft's true airspeed projected to a horizontal plane.

Heading   The azimuth of the aircraft's nose (i.e., longitudinal axis).

Indicated Airspeed   This is the speed shown by an aircraft's airspeed indicator, as calculated from the measured local dynamic pressure. Its difference from true airspeed increases with altitude. (Also known as Calibrated Airspeed.)

Lift   The component of aerodynamic force acting normal to the plane formed by the true airspeed vector and the aircraft's lateral axis.

Mach Number   The ratio of the true airspeed to the local speed of sound.

Magnetic [Azimuth]   An azimuth angle (e.g., heading, bearing) measured relative to magnetic north.

Payload Weight	The payload capacity of the aircraft.
Phugoid Mode	An oscillatory mode of aircraft dynamics in which kinetic and potential energy are exchanged. The angle of attack is mainly unchanged.
Pitch Angle	The angle that the aircraft's longitudinal axis makes with the ground. (Also known as Elevation Angle)
Rhumb Line	A straight line on a Mercator projection of the earth. It is convenient in navigation because it yields the constant bearing to be followed for navigating between the two end points of the rhumb line.
Roll Angle	The angle that the aircraft's lateral axis makes with the ground. (Also known as Bank Angle)
Short Period Mode	An oscillatory motion in the axis of rotation of pitch. The angle of attack is constantly changing. This mode is typically much faster than the phugoid.
Thrust	The thrust force created by the aircraft's engines. Acts along the aircraft's longitudinal axis and is defined positive in the direction of the x-axis of the body axis system.
True [Azimuth]	An azimuth angle (e.g., heading, bearing) measured relative to true north.
True Airspeed	The actual speed of the aircraft relative to the surrounding air mass.

Acronyms

ADM	aircraft dynamics model
AGL	above ground level
AMT	aircraft modeling tool
ATC	air traffic control
ATM	air traffic management
BADA	Base of Aircraft Data
CAS	calibrated airspeed
DIS	Distributed Interactive Simulation (DIS provides a military standard earth coordinate system.)
DME	Distance Measure Equipment
DOF	degree of freedom
ECEF	earth-centered, earth-fixed
FAA	Federal Aviation Administration
FTE	flight technical error
GPS	Global Positioning System
IAS	indicated airspeed
LTD	linear, time-dependent
NAS	National Airspace System
NED	the North-East-Down coordinate system
RNAV	Radio Navigation
SISO	single input, single output
TGF	Target Generation Facility
VOR	VHF Omnidirectional Range navigation system

THIS PAGE INTENTIONALLY LEFT BLANK

References

Anderson, J.D. (1989). Introduction To Flight. New York: McGraw-Hill.

Federal Aviation Administration (1993), "System Segment Specification", TGF-SY01-Rev 1, ", William J. Hughes Technical Center, Atlantic City, NJ.

Borkowski, K. M. (1989). Accurate Algorithms to Transform Geocentric to Geodetic Coordinates. Bulletin Géodesique. 63, 50–56.

Brogan, W.L. (1991). Modern Control Theory. Englewood Cliffs, NJ: Prentice Hall, Inc.

Clark, K. C. (1995). Analytical and Computer Cartography. Englewood Cliffs, NJ: Prentice Hall, Inc.

Institute of Electrical and Electronics Engineers. (1993). IEEE Standard for Information Technology -- Protocols for Distributed Interactive Simulation Applications--Entity Information and Interaction, (IEEE 1278-1993), Washington, DC: IEEE.

Federal Aviation Administration. (2010). Aeronautical Information Manual (AIM). Washington, D.C.: U.S. Government Printing Office.

Gelb, A. (1974). Applied Optimal Estimation. Cambridge, MA: The M.I.T. Press.

Hoffman, J.D. (1992). Numerical Methods for Engineers and Scientists. New York: McGraw-Hill.

Hunter, G. (1996). CTAS Error Sensitivity, Fuel Efficiency, and Throughput Benefits Analysis, (Tech. Report 96150-02). Los Gatos, CA: Seagull Technology.

International Civil Aviation Organization. (2000). Manual of the ICAO Standard Atmosphere: extended to 80 kilometres(262 500 feet) (3rd ed., 1993, Doc 7488). Montreal: ICAO.

Kayton, M., Fried, W.R. (1997). Avionics Navigation Systems. New York: John Wiley & Sons, Inc.

Mukai, C. (1992). <u>Design and Analysis of Aircraft Dynamics Models for the ATC Simulation at NASA Ames Research Center</u> (Tech. Report 92119-02). Los Gatos, CA: Seagull Technology.

Nelson, R.C. (1989). <u>Flight Stability and Automatic Control.</u> New York: McGraw-Hill.

National Imagery and Mapping Agency (1997). <u>Department of Defense World Geodetic System 1984, Its Definition and Relationships With Local Geodetic Systems</u> (3rd ed., Technical Report TR8350.2). Washington, DC: NIMA.

Nuic, A. (2009). <u>User Manual for the Base of Aircraft Data (BADA)</u> (Rev. 3.7, Tech. Rep. No. 2009-003). Brétigny-sur-Orge, France: EUROCONTROL Experimental Centre.

Ogata, K. (1990). <u>Modern Control Engineering.</u> Englewood Cliffs, NJ: Prentice Hall.

Parkinson, B.W., Spilker, J.J. (1996). <u>Global Positioning System: Theory and Applications.</u> Washington, DC: American Institute of Aeronautics and Astronautics.

Raymer, D. P. (1999). <u>Aircraft Design: A Conceptual Approach</u> (3rd ed.). Reston, VA: American Institute of Aeronautics and Astronautics.

Stevens, B.L., Lewis, F. L. (1992). <u>Aircraft Control and Simulation.</u> New York: John Wiley & sons, Inc.

Thomas, J., Timoteo, D. (1990). <u>Chicago O'Hare Simultaneous ILS Approach Data Collection and Analysis</u> (DOT/FAA/CT-TN90/11). Atlantic City, NJ: Federal Aviation Administration William J. Hughes Technical Center.